NUREG/CR-5785
ORNL/TM-11950

Experimental Results of Tests to Investigate Flaw Behavior of Mechanically Loaded Stainless Steel Clad Plates

Prepared by
S. K. Iskander, G. C. Robinson, W. R. Corwin,
B. C. Oland, D. J. Alexander, K. V. Cook

Oak Ridge National Laboratory

Prepared for
U.S. Nuclear Regulatory Commission

AVAILABILITY NOTICE

Availability of Reference Materials Cited in NRC Publications

Most documents cited in NRC publications will be available from one of the following sources:

1. The NRC Public Document Room, 2120 L Street, NW., Lower Level, Washington, DC 20555
2. The Superintendent of Documents, U.S. Government Printing Office, P.O. Box 37082, Washington, DC 20013-7082
3. The National Technical Information Service, Springfield, VA 22161

Although the listing that follows represents the majority of documents cited in NRC publications, it is not intended to be exhaustive.

Referenced documents available for inspection and copying for a fee from the NRC Public Document Room include NRC correspondence and internal NRC memoranda; NRC bulletins, circulars, information notices, inspection and investigation notices; licensee event reports; vendor reports and correspondence; Commission papers; and applicant and licensee documents and correspondence.

The following documents in the NUREG series are available for purchase from the GPO Sales Program: formal NRC staff and contractor reports, NRC-sponsored conference proceedings, international agreement reports, grant publications, and NRC booklets and brochures. Also available are regulatory guides, NRC regulations in the *Code of Federal Regulations*, and *Nuclear Regulatory Commission Issuances*.

Documents available from the National Technical Information Service include NUREG-series reports and technical reports prepared by other Federal agencies and reports prepared by the Atomic Energy Commission, forerunner agency to the Nuclear Regulatory Commission.

Documents available from public and special technical libraries include all open literature items, such as books, journal articles, and transactions. *Federal Register* notices, Federal and State legislation, and congressional reports can usually be obtained from these libraries.

Documents such as theses, dissertations, foreign reports and translations, and non-NRC conference proceedings are available for purchase from the organization sponsoring the publication cited.

Single copies of NRC draft reports are available free, to the extent of supply, upon written request to the Office of Administration, Distribution and Mail Services Section, U.S. Nuclear Regulatory Commission, Washington, DC 20555.

Copies of industry codes and standards used in a substantive manner in the NRC regulatory process are maintained at the NRC Library, 7920 Norfolk Avenue, Bethesda, Maryland, for use by the public. Codes and standards are usually copyrighted and may be purchased from the originating organization or, if they are American National Standards, from the American National Standards Institute, 1430 Broadway, New York, NY 10018.

NUREG/CR-5785
ORNL/TM-11950
RF

Experimental Results of Tests to Investigate Flaw Behavior of Mechanically Loaded Stainless Steel Clad Plates

Manuscript Completed: November 1991
Date Published: April 1992

Prepared by
S. K. Iskander, G. C. Robinson, W. R. Corwin,
B. C. Oland, D. J. Alexander, V. V. Cook

Oak Ridge National Laboratory
Operated by Martin Marietta Energy Systems, Inc.

Oak Ridge National Laboratory
Oak Ridge, TN 37831-6285

Prepared for
Division of Engineering
Office of Nuclear Regulatory Research
U.S. Nuclear Regulatory Commission
Washington, DC 20555
RC FIN B0119
der Contract No. DE-AC05-84OR21400

EXPERIMENTAL RESULTS OF TESTS TO INVESTIGATE FLAW BEHAVIOR OF MECHANICALLY LOADED STAINLESS STEEL CLAD PLATES*

ABSTRACT

A small crack near the inner surface of clad nuclear reactor pressure vessels is an important consideration in the safety assessment of the structural integrity of the vessel. Four-point bend tests on large plate specimens, six clad and two unclad, were performed to determine the effect of stainless steel cladding upon the propagation of small surface cracks subjected to stress states similar to those produced by pressurized thermal shock conditions. Results of tests at temperatures 10 and 60° C below the nil-ductility transition temperature have shown that a tough surface layer composed of cladding and heat-affected zone has arrested running flaws in clad plates under conditions where unclad plates have ruptured. Furthermore, the load-bearing capacity of clad plates with large subclad flaws significantly exceeded that of an unclad plate with a much smaller flaw. More testing is necessary to unambiguously single out whether it is the cladding or the heat-affected zone that is primarily responsible for the observed enhanced load-bearing capacity of plates. The compressive stresses that limited the depth to which the flaw could propagate are absent in a repressurization event. Nonetheless, the experiments show that if the surface layer is sufficiently tough, it could prevent a flaw, near the surface, from propagating along the surface. The flaw could tunnel below the surface, but a sufficiently tough surface layer would reduce the maximum stress intensity factor. Considerable analytical work still remains to be done to quantify the amount of this reduction in order to transfer the results of these experiments to the integrity analysis of reactor pressure vessels.

*Research sponsored by the Office of Nuclear Regulatory Research, Division of Engineering, U.S. Nuclear Regulatory Commission under Interagency Agreement DOE 1886-8109-8L with the U.S. Department of Energy under Contract DE-AC05-84OR21400 with Martin Marietta Energy Systems, Inc.

CONTENTS

LIST OF FIGURES

Page

Page

Page

Page

Page

LIST OF TABLES

Page

FOREWORD

The work reported here was performed at Oak Ridge National Laboratory (ORNL) under the Heavy-Section Steel Technology (HSST) Program, W. E. Pennell, Program Manager. The program is sponsored by the Office of Nuclear Regulatory Research of the U.S. Nuclear Regulatory Commission (NRC). The technical monitor for the NRC is M. E. Mayfield.

This report is designated HSST Report 113. Prior and future reports in this series are listed below.

1. S. Yukawa, General Electric Company, Schenectady, N.Y., *Evaluation of Periodic Proof Testing and Warm Prestressing Procedures for Nuclear Reactor Vessels*, HSSTP-TR-1, July 1, 1969.

2. L. W. Loechel, Martin Marietta Corporation, Denver, Colo., *The Effect of Testing Variables on the Transition Temperature in Steel*, MCR-69-189, November 1, 1969.

3. P. N. Randall, TRW Systems Group, Redondo Beach, Calif., *Gross Strain Measure of Fracture Toughness of Steels*, HSSTP-TR-3, November 1, 1969.

4. C. Visser, S. E. Gabrielse, and W. VanBuren, Westinghouse Electric Corporation, PWR Systems Division, Pittsburgh, Pa., *A Two-Dimensional Elastic-Plastic Analysis of Fracture Test Specimens*, WCAP-7368, October 1969.

5. T. R. Mager and F. O. Thomas, PWR Systems Division, Pittsburgh, Pa., *Evaluation by Linear Elastic Fracture Mechanics of Radiation Damage to Pressure Vessel Steels*, WCAP-7328 (Rev.), Westinghouse Electric Corporation, October 1969.

6. W. O. Shabbits, W. H. Pryle, and E. T. Wessel, Westinghouse Electric Corporation, PWR Systems Division, Pittsburgh, Pa., *Heavy-Section Fracture Toughness Properties of A533 Grade B Class 1 Steel Plate and Submerged Arc Weldment*, WCAP-7414, December 1969.

7. F. J. Loss, Naval Research Laboratory, Washington, D.C., *Dynamic Tear Test Investigations of the Fracture Toughness of Thick-Section Steel*, NRL-7056, May 14, 1970.

8. P. B. Crosley and E. J. Ripling, Materials Research Laboratory, Inc., Glenwood, Ill., *Crack Arrest Fracture Toughness of A533 Grade B Class 1 Pressure Vessel Steel*, HSSTP-TR-8, March 1970.

9. T. R. Mager, Westinghouse Electric Corporation, PWR Systems Division, Pittsburgh, Pa., *Post-Irradiation Testing of 2T Compact Tension Specimens*, WCAP-7561, August 1970.

10. T. R. Mager, Westinghouse Electric Corporation, PWR Systems Division, Pittsburgh, Pa., *Fracture Toughness Characterization Study of A533, Grade B, Class 1 Steel*. WCAP-7578, October 1970.

11. T. R. Mager, Westinghouse Electric Corporation, PWR Systems Division, Pittsburgh, Pa., *Notch Preparation in Compact Tension Specimens*, WCAP-7579, November 1970.

12. N. Levy and P. V. Marcal, Brown University, Providence, R.I., *Three-Dimensional Elastic-Plastic Stress and Strain Analysis for Fracture Mechanics, Phase I: Simple Flawed Specimens*, HSSTP-TR-12, December 1970.

13. W. O. Shabbits, Westinghouse Electric Corporation, PWR Systems Division, Pittsburgh, Pa., *Dynamic Fracture Toughness Properties of Heavy Section A533 Grade B Class 1 Steel Plate*, WCAP-7623, December 1970.

14. P. N. Randall, TRW Systems Group, Redondo Beach, Calif., *Gross Strain Crack Tolerance of A533-B Steel*, HSSTP-TR-14, May 1, 1971.

15. H. T. Corten and R. H. Sailors, University of Illinois, Urbana, Ill., *Relationship Between Material Fracture Toughness Using Fracture Mechanics and Transition Temperature Tests*, T&AM Report 346, August 1, 1971.

16. T. R. Mager and V. J. McLoughlin, Westinghouse Electric Corporation, PWR Systems Division, Pittsburgh, Pa., *The Effect of an Environment of High Temperature Primary Grade Nuclear Reactor Water on the Fatigue Crack Growth Characteristics of A533 Grade B Class 1 Plate and Weldment Material*, WCAP-7776, October 1971.

17. N. Levy and P. V. Marcal, Brown University, Providence, R.I., *Three-Dimensional Elastic-Plastic Stress and Strain Analysis for Fracture Mechanics, Phase II: Improved Modelling*, HSSTP-TR-17, November 1971.

18. S. C. Grigory, Southwest Research Institute, San Antonio, Tex., *Tests of 6-in.-Thick Flawed Tensile Specimens, First Technical Summary Report, Longitudinal Specimens Numbers 1 Through 7*, HSSTP-TR-18, June 1972.

19. P. N. Randall, TRW Systems Group, Redondo Beach, Calif., *Effects of Strain Gradients on the Gross Strain Crack Tolerance of A533-B Steel*, HSSTP-TR-19, June 15, 1972.

20. S. C. Grigory, Southwest Research Institute, San Antonio, Tex., *Tests of 6-Inch-Thick Flawed Tensile Specimens, Second Technical Summary Report, Transverse Specimens Numbers 8 Through 10, Welded Specimens Numbers 11 Through 13*, HSSTP-TR-20, June 1972.

21. L. A. James and J. A. Williams, Hanford Engineering Development Laboratory, Richland, Wash., *Heavy Section Steel Technology Program Technical Report No. 21, The Effect of Temperature and Neutron Irradiation upon the Fatigue-Crack Propagation Behavior of ASTM A533 Grade B, Class 1 Steel*, HEDL-TME 72-132, September 1972.

22. S. C. Grigory, Southwest Research Institute, San Antonio, Tex., *Tests of 6-Inch-Thick Flawed Tensile Specimens, Third Technical Summary Report, Longitudinal Specimens Numbers 14 Through 16, Unflawed Specimen Number 17*, HSSTP-TR-22, October 1972.

23. S. C. Grigory, Southwest Research Institute, San Antonio, Tex., *Tests of 6-Inch-Thick Tensile Specimens, Fourth Technical Summary Report, Tests of 1-Inch-Thick Flawed Tensile Specimens for Size Effect Evaluation*, HSSTP-TR-23, June 1973.

24. S. P. Ying and S. C. Grigory, Southwest Research Institute, San Antonio, Tex., *Tests of 6-Inch-Thick Tensile Specimens, Fifth Technical Summary Report, Acoustic Emission Monitoring of One-Inch and Six-Inch-Thick Tensile Specimens*, HSSTP-TR-24, November 1972.

25. R. W. Derby et al., Oak Ridge Natl. Lab., Oak Ridge, Tenn., *Test of 6-Inch-Thick Pressure Vessels. Series 1: Intermediate Test Vessels V-1 and V-2*, ORNL-4895, February 1974.

26. W. J. Stelzman and R. G. Berggren, Oak Ridge Natl. Lab., Oak Ridge, Tenn., *Radiation Strengthening and Embrittlement in Heavy Section Steel Plates and Welds*, ORNL-4871, June 1973.

27. P. B. Crosley and E. J. Ripling, Materials Research Laboratory, Inc., Glenwood, Ill., *Crack Arrest in an Increasing K-Field*, HSSTP-TR-27, January 1973.

28. P. V. Marcal, P. M. Stuart, and R. S. Bettes, Brown University, Providence, R.I., *Elastic-Plastic Behavior of a Longitudinal Semi-Elliptic Crack in a Thick Pressure Vessel*, HSSTP-TR-28, June 1973.

29. W. J. Stelzman, R. G. Berggren, and T. N. Jones, Oak Ridge Natl. Lab., Oak Ridge, Tenn., *ORNL Characterization of Heavy-Section Steel Technology Program Plates 01, 02 and 03*, USNRC Report NUREG/CR-4092 (ORNL/TM-9491), April 1985.

30. Canceled.

31. J. A. Williams, Hanford Engineering Development Laboratory, Richland, Wash., *The Irradiation and Temperature Dependence of Tensile and Fracture Properties of ASTM A533, Grade B, Class 1 Steel Plate and Weldment*, HEDL-TME 73-75, August 1973.

32. J. M. Steichen and J. A. Williams, Hanford Engineering Development Laboratory, Richland, Wash., *High Strain Rate Tensile Properties of Irradiated ASTM A533 Grade B Class 1 Pressure Vessel Steel*, July 1973.

33. P. C. Riccardella and J. L. Swedlow, Westinghouse Electric Corporation, Pittsburgh, Pa., *A Combined Analytical-Experimental Fracture Study of the Two Leading Theories of Elastic-Plastic Fracture (J-Integral and Equivalent Energy)*, WCAP-8224, Octo' . 1973.

34. R. J. Podlasek and R. J. Eiber, Battelle Columbus Laboratories, Columbus, Ohio, *Final Report on Investigation of Mode III Crack Extension in Reactor Piping*, December 14, 1973.

35. T. R. Mager et al., Westinghouse Electric Corporation, Pittsburgh, Pa., *Interim Report on the Effect of Low Frequencies on the Fatigue Crack Growth Characteristics of A533 Grade B Class 1 Plate in an Environment of High-Temperature Primary Grade Nuclear Reactor Water*, WCAP-8256, December 1973.

36. J. A. Williams, Hanford Engineering Development Laboratory, Richland, Wash., *The Irradiated Fracture Toughness of ASTM A533, Grade B, Class 1 Steel Measured with a Four-Inch-Thick Compact-Tension Specimen*, HEDL-TME 75-10, January 1975.

37. R. H. Bryan et al., Oak Ridge Natl. Lab., Oak Ridge, Tenn., *Test of 6-Inch-Thick Pressure Vessels. Series 2: Intermediate Test Vessels V-3, V-4, and V-6*, ORNL-5059, November 1975.

38. T. R. Mager, S. E. Yanichko, and L. R. Singer, Westinghouse Electric Corporation, Pittsburgh, Pa., *Fracture Toughness Characterization of HSST Intermediate Pressure Vessel Material*, WCAP-8456, December 1974.

39. J. G. Merkle, G. D. Whitman, and R. H. Bryan, Oak Ridge Natl. Lab., Oak Ridge, Tenn., *An Evaluation of the HSST Program Intermediate Pressure Vessel Tests in Terms of Light-Water-Reactor Pressure Vessel Safety*, ORNL/TM-5090, November 1975.

40. J. G. Merkle et al., Oak Ridge Natl. Lab., Oak Ridge, Tenn., *Test of 6-In.-Thick Pressure Vessels. Series 3: Intermediate Test Vessel V-7*, USNRC Report ORNL/NUREG-1, August 1976.

41. J. A. Davidson et al., Westinghouse Electric Corporation, Pittsburgh, Pa., *The Irradiated Dynamic Fracture Toughness of ASTM A533, Grade B, Class 1 Steel Plate and Submerged Arc Weldment*, WCAP-8775, October 1976.

42. R. D. Cheverton, Oak Ridge Natl. Lab., Oak Ridge, Tenn., *Pressure Vessel Fracture Studies Pertaining to a PWR LOCA-ECC Thermal Shock Experiments TSE-1 and TSE-2*, USNRC Report ORNL/NUREG/TM-31, September 1976.

43. J. G. Merkle et al., Oak Ridge Natl. Lab., Oak Ridge, Tenn., *Test of 6-In.-Thick Pressure Vessels. Series 4: Intermediate Test Vessels V-5 and V-9 with Inside Nozzle Corner Cracks*, USNRC Report ORNL/NUREG-7, August 1977.

44. J. A. Williams, Hanford Engineering Development Laboratory, Richland, Wash., *The Ductile Fracture Toughness of Heavy Section Steel Plate*, USNRC Report NUREG/CR-0859, September 1979.

45. R. H. Bryan et al., Oak Ridge Natl. Lab., Oak Ridge, Tenn., *Test of 6-in.-Thick Pressure Vessels. Series 3: Intermediate Test Vessel V-7A Under Sustained Loading*, USNRC Report ORNL/NUREG-9, February 1978.

46. R. D. Cheverton and S. E. Bolt, Oak Ridge Natl. Lab., Oak Ridge, Tenn., *Pressure Vessel Fracture Studies Pertaining to a PWR LOCA-ECC Thermal Shock: Experiments TSE-3 and TSE-4 and Update of TSE-1 and TSE-2 Analysis*, USNRC Report ORNL/NUREG-22, December 1977.

47. D. A. Canonico, Oak Ridge Natl. Lab., Oak Ridge, Tenn., *Significance of Reheat Cracks to the Integrity of Pressure Vessels for Light-Water Reactors*, USNRC Report ORNL/NUREG-15, July 1977.

48. G. C. Smith and P. P. Holz, Oak Ridge Natl. Lab., Oak Ridge, Tenn., *Repair Weld Induced Residual Stresses in Thick-Walled Steel Pressure Vessels*, USNRC Report NUREG/CR-0093 (ORNL/NUREG/TM-153), June 1978.

49. P. P. Holz and S. W. Wismer, Oak Ridge Natl. Lab., Oak Ridge, Tenn., *Half-Bead (Temper) Repair Welding for HSST Vessels*, USNRC Report NUREG/CR-0113 (ORNL/NUREG/TM-177), June 1978.

50. G. C. Smith, P. P. Holz, and W. J. Stelzman Oak Ridge Natl. Lab., Oak Ridge, Tenn., *Crack Extension and Arrest Tests of Axially Flawed Steel Model Pressure Vessels*, USNRC Report NUREG/CR-0126 (ORNL/NUREG/TM-196), October 1978.

51. R. H. Bryan et al., Oak Ridge Natl. Lab., Oak Ridge, Tenn., *Test of 6-in.-Thick Pressure Vessels. Series 3: Intermediate Test Vessel V-7B*, USNRC Report NUREG/CR-0309 (ORNL/NUREG-38), October 1978.

52. R. D. Cheverton, S. K. Iskander, and S. E. Bolt, Oak Ridge Natl. Lab., Oak Ridge, Tenn., *Applicability of LEFM to the Analysis of PWR Vessels Under LOCA-ECC Thermal Shock Conditions*, USNRC Report NUREG/CR-0107 (ORNL/NUREG-40), October 1978.

53. R. H. Bryan et al., Oak Ridge Natl. Lab., Oak Ridge, Tenn., *Test of 6-in.-Thick Pressure Vessels, Series 3: Intermediate Test Vessel V-8*, USNRC Report NUREG/CR-0675 (ORNL/NUREG-58), December 1979.

54. R. D. Cheverton and S. K. Iskander, Oak Ridge Natl. Lab., Oak Ridge, Tenn., *Application of Static and Dynamic Crack Arrest Theory to TSE-4*, USNRC Report NUREG/CR-0767 (ORNL/NUREG-57), June 1979.

55. J. A. Williams, Hanford Engineering Development Laboratory, Richland, Wash., *Tensile Properties of Irradiated and Unirradiated Welds of A533 Steel Plate and A508 Forgings*, USNRC Report NUREG/CR-1158 (ORNL/Sub-79/50917/2), July 1979.

56. K. W. Carlson and J. A. Williams, Hanford Engineering Development Laboratory, Richland, Wash., *The Effect of Crack Length and Side Grooves on the Ductile Fracture Toughness Properties of ASTM A533 Steel*, USNRC Report NUREG/CR-1171 (ORNL/Sub-79/50917/3), October 1979.

57. P. P. Holz, Oak Ridge Natl. Lab., Oak Ridge, Tenn., *Flaw Preparations for HSST Program Vessel Fracture Mechanics Testing: Mechanical-Cyclic Pumping and Electron-Beam Weld-Hydrogen Charge Cracking Schemes*, USNRC Report NUREG/CR-1274 (ORNL/NUREG/TM-369), May 1980.

58. S. K. Iskander, Union Carbide Corp. Nuclear Div., Oak Ridge, Tenn., *Two Finite Element Techniques for Computing Mode I Stress Intensity Factors in Two- or Three-Dimensional Problems*, USNRC Report NUREG/CR-1499 (ORNL/NUREG/CSD/TM-14), February 1981.

59. P. B. Crosley and E. J. Ripling, Materials Research Laboratory, Glenwood, Ill., *Development of a Standard Test for Measuring KIa with a Modified Compact Specimen*, USNRC Report NUREG/CR-2294 (ORNL/Sub-81/7755/1), August 1981.

60. S. N. Atluri et al., Oak Ridge Gaseous Diffusion Plant, Oak Ridge, Tenn., *NOZ-FLAW: A Finite Element Program for Direct Evaluation of Stress Intensity Factors for Pressure Vessel Nozzle-Corner Flaws*, USNRC Report NUREG/CR-1843, (ORNL/NUREG/CSD/TM-18), March 1981.

61. A. Shukla, W. L. Fourney, and G. R. Irwin, University of Maryland, College Park, Md., *Study of Energy Loss and Its Mechanisms in Homalite 100 During Crack Propagation and Arrest*, USNRC Report NUREG/CR-2150 (ORNL/Sub-7778/1), August 1981.

62. S. K. Iskander, R. D. Cheverton, and D. G. Ball, Oak Ridge Natl. Lab., Oak Ridge, Tenn., *OCA-I, A Code for Calculating the Behavior of Flaws on the Inner Surface of a Pressure Vessel Subjected to Temperature and Pressure Transients*, USNRC Report NUREG/CR-2113 (ORNL/NUREG-84), August 1981.

63. R. J. Sanford et al., University of Maryland, College Park, Md., *A Photoelastic Study of the Influence of Non-Singular Stresses in Fracture Test Specimens*, USNRC Report NUREG/CR-2179 (ORNL/Sub-7778/2), August 1981.

64. B. R. Bass et al., Oak Ridge Natl. Lab., Oak Ridge, Tenn., *OR-FLAW: A Finite Element Program for Direct Evaluation of K-Factors for User-Defined Flaws in Plate, Cylinders, and Pressure-Vessel Nozzle Corners*, USNRC Report NUREG/CR-2494 (ORNL/CSD/TM-165), April 1982.

65. B. R. Bass and J. W. Bryson, Oak Ridge Natl. Lab., Oak Ridge, Tenn., *ORMGEN-3D: A Finite Element Mesh Generator for 3-Dimensional Crack Geometries*, USNRC Report NUREG/CR-2997, Vol. 1 (ORNL/TM-8527/V1), December 1982.

66. B. R. Bass and J. W. Bryson, Oak Ridge Natl. Lab., Oak Ridge, Tenn., *ORVIRT: A Finite Element Program for Energy Release Rate Calculations for 2-Dimensional and 3-Dimensional Crack Models*, USNRC Report NUREG/CR-2997, Vol. 2 (ORNL/TM-8527/V2), February 1983.

67. R. D. Cheverton, S. K. Iskander, and D. G. Ball, Oak Ridge Natl. Lab., Oak Ridge, Tenn., *PWR Pressure Vessel Integrity During Overcooling Accidents: A Parametric Analysis*, USNRC Report NUREG/CR-2895 (ORNL/TM-7931), February 1983.

68. D. G. Ball et al., Oak Ridge Natl. Lab., Oak Ridge, Tenn. *OCA-II, A Code for Calculating Behavior of 2-D and 3-D Surface Flaws in a Pressure Vessel Subjected to Temperature and Pressure Transients*, USNRC Report NUREG/CR-3491 (ORNL-5934), February 1984.

69. A. Sauter, R. D. Cheverton, and S. K. Iskander, Oak Ridge Natl. Lab., Oak Ridge, Tenn., *Modification of OCA-I for Application to a Reactor Pressure Vessel with Cladding on the Inner Surface*, USNRC Report NUREG/CR-3155 (ORNL/TM-8649), May 1983.

70. R. D. Cheverton and D. G. Ball, Martin Marietta Energy Systems, Inc., Oak Ridge Natl. Lab., Oak Ridge, Tenn., *OCA-P, A Deterministic and Probabilistic Fracture-Mechanics Code for Application to Pressure Vessels*, USNRC Report NUREG/CR-3618 (ORNL-5991), May 1984.

71. J. G. Merkle, Martin Marietta Energy Systems, Inc., Oak Ridge Natl. Lab., Oak Ridge, Tenn., *An Examination of the Size Effects and Data Scatter Observed in Small Specimen Cleavage Fracture Toughness Testing*, USNRC Report NUREG/CR-3672 (ORNL/TM-9088), April 1984.

72. C. E. Pugh et al., Martin Marietta Energy Systems, Inc., Oak Ridge Natl. Lab., Oak Ridge, Tenn., *Heavy-Section Steel Technology Program -- Five-Year Plan FY 1983-1987*, USNRC Report NUREG/CR-3595 (ORNL/TM-9008), April 1984.

73. D. G. Ball, et al., Martin Marietta Energy Systems, Inc., Oak Ridge Natl. Lab., Oak Ridge, Tenn., *Stress Intensity Factor Influence Coefficients for Surface Flaws in Pressure Vessels*, USNRC Report NUREG/CR-3723 (ORNL/CSD/TM-216), February 1985.

74. W. R. Corwin, R. G. Berggren, and R. K. Nanstad, Martin Marietta Energy Systems, Inc., Oak Ridge Natl. Lab., Oak Ridge, Tenn., *Charpy Toughness and Tensile Properties of Neutron Irradiated Stainless Steel Submerged-Arc Weld Cladding Overlay*, USNRC Report NUREG/CR-3927 (ORNL/TM-9309), September 1984.

75. C. W. Schwartz et al., University of Maryland, College Park, Md., *SAMCR: A Two-Dimensional Dynamic Finite Element Code for the Stress Analysis of Moving Cracks*, USNRC Report NUREG/CR-3891 (ORNL/Sub/79-7778/3), November 1984.

76. W. R. Corwin et al., Martin Marietta Energy Systems, Inc., Oak Ridge Natl. Lab., Oak Ridge, Tenn., *Effects of Stainless Steel Weld Overlay Cladding on the Structural Integrity of Flawed Steel Plates in Bending, Series 1*, USNRC Report NUREG/CR-4015 (ORNL/TM-9390), April 1985.

77. R. H. Bryan et al., Martin Marietta Energy Systems, Inc., Oak Ridge Natl. Lab., Oak Ridge, Tenn., *Pressurized-Thermal-Shock Test of 6-in.-Thick Pressure Vessels. PTSE-1: Investigation of Warm Prestressing and Upper-Shelf Arrest*, USNRC Report NUREG/CR-4106 (ORNL-6135), April 1985.

78. R. D. Cheverton et al., Martin Marietta Energy Systems, Inc., Oak Ridge Natl. Lab., Oak Ridge, Tenn., *Pressure Vessel Fracture Studies Pertaining to the PWR Thermal-Shock Issue: Experiments TSE-5, TSE-5A and TSE-6*, USNRC Report NUREG/CR-4249 (ORNL-6163), June 1985.

79. R. D. Cheverton et al., Martin Marietta Energy Systems, Inc., Oak Ridge Natl. Lab., Oak Ridge, Tenn., *Pressure Vessel Fracture Studies Pertaining to the PWR Thermal-Shock Issue: Experiment TSE-7*, USNRC Report NUREG/CR-4304 (ORNL-6177), August 1985.

80. R. H. Bryan et al., Martin Marietta Energy Systems, Inc., Oak Ridge Natl. Lab., Oak Ridge, Tenn., *Test of 6-in.-Thick Pressure Vessels. Series 3: Intermediate Test Vessel V-8A -- Tearing Behavior of Low Upper-Shelf Material*, USNRC Report NUREG/CR-4760 (ORNL-6187), May 1987.

81. R. D. Cheverton and D. G. Ball, Martin Marietta Energy Systems, Inc., Oak Ridge Natl. Lab., Oak Ridge, Tenn., *A Parametric Study of PWR Pressure Vessel Integrity During Overcooling Accidents, Considering Both 2-D and 3-D Flaws*, USNRC Report NUREG/CR-4525 (ORNL/TM-9682), August 1985.

82. E. C. Rodabaugh, E. C. Rodabaugh Associates, Inc., Hilliard, Ohio, *Comments on the Leak-Before-Break Concept for Nuclear Power Plant Piping Systems*, USNRC Report NUREG/CR-4305 (ORNL/Sub/82-22252/3), August 1985.

83. J. W. Bryson, Martin Marietta Energy Systems, Inc., Oak Ridge Natl. Lab., Oak Ridge, Tenn., *ORVIRT.PC: A 2-D Finite Element Fracture Analysis Program for a Microcomputer*, USNRC Report NUREG/CR-4367 (ORNL-6208), October 1985.

84. D. G. Ball and R. D. Cheverton, Martin Marietta Energy Systems, Inc., Oak Ridge Natl. Lab., Oak Ridge, Tenn., *Adaptation of OCA-P, a Probabilistic Fracture-Mechanics Code, to a Personal Computer*, USNRC Report NUREG/CR-4460 (ORNL/CSD/TM-233), January 1986.

85. J. W. Bryson and B. R. Bass, Martin Marietta Energy Systems, Inc., Oak Ridge Natl. Lab., Oak Ridge, Tenn., *ORMGEN.PC: A Microcomputer Program for Automatic Mesh Generation of 2-D Crack Geometries*, USNRC Report NUREG/CR-4475 (ORNL-6250), March 1986.

86. G. D. Whitman, Martin Marietta Energy Systems, Inc., Oak Ridge Natl. Lab., Oak Ridge, Tenn., *Historical Summary of the Heavy-Section Steel Technology Program and Some Related Activities in Light-Water Reactor Pressure Vessel Safety Research*, USNRC Report NUREG/CR-4489 (ORNL-6259), March 1986.

87. C. Inversini and J. W. Bryson, Martin Marietta Energy Systems, Inc., Oak Ridge Natl. Lab., Oak Ridge, Tenn., *ORPLOT.PC: A Graphic Utility for ORMGEN.PC and ORVIRT.PC*, USNRC Report NUREG/CR-4633 (ORNL-6291), June 1986.

88. J. J. McGowan, R. K. Nanstad, and K. R. Thoms, Martin Marietta Energy Systems, Inc., Oak Ridge Natl. Lab., Oak Ridge, Tenn., *Characterization of Irradiated Current-Practice Welds and A533 Grade B Class 1 Plate for Nuclear Pressure Vessel Service*, USNRC Report NUREG/CR-4880 (ORNL/TM-10387), July 1988.

89. K. V. Cook and R. W. McClung, Martin Marietta Energy Systems, Inc., Oak Ridge Natl. Lab., Oak Ridge, Tenn., *Flaw Density Examinations of a Clad Boiling Water Reactor Pressure Vessel Segment*, USNRC Report NUREG/CR-4860 (ORNL/TM-10364), April 1987.

90. D. J. Naus et al., Martin Marietta Energy Systems, Inc., Oak Ridge Natl. Lab., Oak Ridge, Tenn., *Crack-Arrest Behavior in SEN Wide Plates of Quenched and Tempered A 533 Grade B Steel Tested Under Nonisothermal Conditions*, USNRC Report NUREG/CR-4930 (ORNL-6388), August 1987.

91. D. B. Barker et al., University of Maryland, College Park, Md., *A Report on the Round Robin Program Conducted to Evaluate the Proposed ASTM Standard Test Method for Determining the Plane Strain Crack Arrest Fracture Toughness, K_{Ia} of Ferritic Materials*, USNRC Report NUREG/CR-4966 (ORNL/Sub/79-7778/4), January 1988.

92. W. H. Bamford, Westinghouse Electric Corp., Pittsburgh, Pa., *A Summary of Environmentally Assisted Crack-Growth Studies Performed at Westinghouse Electric Corporation Under Funding from the Heavy-Section Steel Technology Program*, USNRC Report NUREG/CR-5020, (ORNL/Sub/82/21598/1), May 1988.

93. R. H. Bryan et al., Martin Marietta Energy Systems, Inc., Oak Ridge Natl. Lab., Oak Ridge, Tenn., *Pressurized-Thermal-Shock Test of 6-in.-Thick Pressure Vessels. PTSE-2: Investigation of Low Tearing Resistance and Warm Prestressing*, USNRC Report NUREG/CR-4888 (ORNL-6377), December 1987.

94. J. H. Giovanola and R. W. Klopp, SRI International, Menlo Park, Calif., *Viscoplastic Stress-Strain Characterization of A533B Class 1 Steel*, USNRC Report NUREG/CR-5066 (ORNL/Sub/87-SA193/1), September 1989.

95. L. F. Miller et al., Martin Marietta Energy Systems, Inc., Oak Ridge Natl. Lab., Oak Ridge, Tenn., *Neutron Exposure Parameters for the Metallurgical Test Specimens in the Fifth Heavy-Section Steel Technology Irradiation Series Capsules*, USNRC Report NUREG/CR-5019 (ORNL/TM-10582), March 1988.

96. Canceled.

97. D. J. Naus, J. Keeney-Walker, and B. R. Bass, Martin Marietta Energy Systems, Inc., Oak Ridge Natl. Lab., Oak Ridge, Tenn., *High-Temperature Crack-Arrest Behavior in 152-mm-Thick SEN Wide Plates of Quenched and Tempered A533 Grade B Steel*, USNRC Report NUREG/CR-5330 (ORNL/TM-11083), April 1989.

98. K. V. Cook, R. A. Cunningham, Jr., and R. W. McClung, Martin Marietta Energy Systems, Inc., Oak Ridge Natl. Lab., Oak Ridge, Tenn., *Detection and Characterization of Indications in Segments of Reactor Pressure Vessels*, USNRC Report NUREG/CR-5322 (ORNL/TM-11072), August 1989.

99. R. D. Cheverton et al., Martin Marietta Energy Systems, Inc., Oak Ridge Natl. Lab., Oak Ridge, Tenn., *Impact of Radiation Embrittlement on Integrity of Pressure Vessel Supports for Two PWR Plants*, USNRC Report NUREG/CR-5320 (ORNL/TM-10966), February 1989.

100. D. J. Naus et al., Martin Marietta Energy Systems, Inc., Oak Ridge Natl. Lab., Oak Ridge, Tenn., *SEN Wide-Plate Crack-Arrest Tests Using A533 Grade B Class 1 Material: WP-CE Test Series,* USNRC Report NUREG/CR-5408 (ORNL/TM-11269), November 1989.

101. D. J. Naus et al., Martin Marietta Energy Systems, Inc., Oak Ridge Natl. Lab., Oak Ridge, Tenn., *High-Temperature Crack-Arrest Tests Utilizing 152-mm-Thick SEN Wide Plates of Low Upper-Shelf Base Material: Tests WP-2.2 and WP-2.6,* USNRC Report NUREG/CR-5450 (ORNL/TM-11352), March 1990.

102. Canceled.

103. D. J. Naus et al., Martin Marietta Energy Systems, Inc., Oak Ridge Natl. Lab., Oak Ridge, Tenn., *Crack-Arrest Behavior in SEN Wide Plates of Low Upper-Shelf Base Metal Tested Under Nonisothermal Conditions (WP-2 Series),* USNRC Report NUREG/CR-5451 (ORNL-6584), August 1990.

104. T. L. Dickson, R. D. Cheverton, and D. K. Shum, Martin Marietta Energy Systems, Inc., Oak Ridge Natl. Lab., Oak Ridge, Tenn., *Inclusion of Unstable Ductile Tearing and Extrapolated Crack-Arrest Toughness Data in PWR Vessel Integrity Assessment,* USNRC Report NUREG/CR-5473 (ORNL/TM-11450), May 1990.

105. T. J. Theiss, Martin Marietta Energy Systems, Inc., Oak Ridge Natl. Lab., Oak Ridge, Tenn., *Recommendations for the Heavy-Section Steel Technology Program Shallow-Crack Fracture Toughness Testing Effort.* USNRC Report NUREG/CR-5554 (ORNL/TM-11509), September 1990.

106. J. G. Merkle, Martin Marietta Energy Systems, Inc., Oak Ridge Natl. Lab., Oak Ridge, Tenn., *An Overview of the Low Upper-Shelf Toughness Safety Margin Issue,* USNRC Report NUREG/CR-5552 (ORNL/TM-11314), August 1990.

107. D. K. Shum et al., Martin Marietta Energy Systems, Inc., Oak Ridge Natl. Lab., Oak Ridge, Tenn., *Analytical Studies of Transverse Strain Effects on Fracture Toughness for Circumferentially Oriented Cracks,* USNRC Report NUREG/CR-5592 (ORNL/TM-11581), April 1991.

108. J. D. Landes, *Extrapolation of the J-R Curve for Predicting Reactor Vessel Integrity,* USNRC Report NUREG/CR-5650 (ORNL/Sub/89-99732C/UO3/1) (to be published).

109. J. Keeney-Walker, B. R. Bass, and J. D. Landes, Martin Marietta Energy Systems, Inc., Oak Ridge Natl. Lab., Oak Ridge, Tenn., *An Investigation of Crack-Tip Stress-Field Criteria for Predicting Cleavage-Crack Initiation,* USNRC Report NUREG/CR-5651 (ORNL/TM-11692) (to be published).

110. G. R. Irwin, University of Maryland, College Park, Md., *Use of Thickness Reduction to Estimate Values of K,* USNRC Report NUREG/CR-5697 (ORNL/Sub/79-7778C/5) (to be published).

111. P. Albrecht, University of Maryland, College Park, Md., *Limit Pressure Analysis of PTSE-2 Vessel*, USNRC Report NUREG/CR-5698 (ORNL/Sub/79-7778C/6) (to be published).

112. J. W. Dally, W. L. Fourney, and G. R. Irwin, University of Maryland, College Park, Md., *Lower-Bound Initiation Toughness with a Modified-Charpy Specimen*, USNRC Report NUREG/CR-5703 (ORNL/Sub/79-7778C/7) (to be published).

ACKNOWLEDGMENTS

The authors wish to acknowledge the significant contributions made to this testing program by the following: Randy K. Nanstad, John G. Merkle, and Richard D. Cheverton for guidance; James F. King and James D. Hudson for the electron-beam welds used as crack initiation sites; Ronald L. Swain, Eric T. Manneschmidt, and Thomas D. Owings for testing the plates; Sam E. Bolt, E. Hubert Guinn, W. Fred Jackson, and Sandra Birch Kennedy, all of the Engineering Technology Division for instrumentation; Robert A. Cunningham, Earl V. Davis, and Bill E. Foster for nondestructive testing; Harry R. Livesey for making many of the drawings; Julia L. Bishop and Suzanne M. Wilson for manuscript preparation; Gerry C. Marsh for the metallographical examinations; Jay W. Nave and R. Lynn Freeny for all the photographs in this report; E. Hubert Guinn for strain gaging the clip gages; John G. Merkle and Janice Keeney-Walker for their helpful reviews. The authors would like to acknowledge John Merkle's significant input and help given during the preparation of this report, and the encouragement of Milton Vagins of the Nuclear Regulatory Commission during the initial phases of this project.

The heat-treatment and cladding for this program were performed at Combustion Engineering, and the authors wish to acknowledge the contributions of C. D. Hackett and C. Ted Ward.

The authors also appreciate the financial support from the Nuclear Regulatory Commission.

NOMENCLATURE

Acronyms

ASME	American Society of Mechanical Engineers
ASTM	American Society for Testing and Materials
CE	The Combustion Engineering Company
CMOD	crack-mouth-opening displacement
CP-*n*	clad plate number *n*
CVN	Charpy V-notch
DAS	data acquisition system
DBTT	ductile-to-brittle-transition temperature, as measured by the Charpy impact energy
EB	electron beam
FN	ferrite number
HRB	Rockwell B-hardness
HAZ	heat-affected zone
HSST	Heavy-Section Steel Technology
LVDT	linear variable displacement transformer
LWR	light water reactor
NDT	nil-ductility-transition (temperature) as determined by the drop-weight test according to ASTM E 208
NRC	U.S. Nuclear Regulatory Commission
ORNL	Oak Ridge National Laboratory
PTS	pressurized thermal shock
PTSE-*n*	pressurized thermal shock experiment *n*
PWHT	postweld heat treatment, also in this report refers to the combined tempering and PWHT given to the clad plates

RPV	reactor pressure vessel
RT	room temperature
RT_{NDT}	reference temperature nil-ductility-transition
SEM	scanning electron microscopy
TSE-*n*	thermal shock experiment *n*
UTS	ultimate tensile strength
USE	upper-shelf energy
WE	weld embrittled

Symbols

a'	depth of a point on the crack front of surface flaw, measured from the surface
a	length of the minor axis of a semielliptic crack
b	length of the major axis of a semielliptic crack
E	Young's modulus
K_a	value of the stress intensity factor shortly after arrest*
K_I	plane strain stress intensity factor
K_{Ia}	value of the crack-arrest fracture toughness, K_a, for a crack that arrests under conditions of crack front plane-strain*
J-R	a plot of crack-extension resistance, measured by the J-integral, as a function of stable crack extension
t	plate thickness
με	microstrain in units of 10^{-6} mm/mm
ν	Poisson's ratio
¼t, ½t, and 0.4t	depth, relative to plate thickness (t), from which specimens are machined

*Excerpted from ASTM E 1221-88.

Transducer Designations

The following abbreviations followed by a sequential number were used in the instrumentation shown in Figs. 2.6 through 2.9, and they denote the following types of gages:

TE thermocouple

XE foil strain gage

XD foil strain gage, used during dynamic data acquisition

ZE weldable strain gage or a clip gage used to measure CMOD

1. INTRODUCTION

1.1 REACTOR PRESSURE VESSEL SAFETY ISSUE

A small crack near the inner surface of a clad nuclear reactor pressure vessel (RPV) is an important consideration in the safety assessment of the structural integrity of the vessel. The behavior of such flaws is relevant to the pressurized thermal shock (PTS) scenario and to the plant life extension issue.

There is a dearth of information on the behavior of small flaws in the presence of cladding. This has led one RPV integrity study [1] to assume infinitely long flaws (although small flaws are certainly more credible). Long flaws were assumed in that study because considerable experimental results have shown that, *in the absence of cladding*, a small surface flaw in an embrittled material subjected to severe thermal shock will become a long flaw. This important consideration will be discussed in more detail later. Thus, the question remains about the role a tough surface cladding will play in preventing the propagation of small flaws along the surface. Furthermore, the flaw could tunnel beneath the cladding, in which case the residual strength of the structure needs to be estimated.

1.2 PREVIOUS WORK ON CLADDING AND SHORT FLAWS

As previously mentioned, in the absence of cladding, short flaws tend to become long. In this section a brief review of work in these areas is presented, and important experimental evidence will be cited to support the concept of short flaws becoming, under suitable conditions, long ones.

To date, it is difficult to predict the behavior of finite-length flaws. There are various reasons for this. An important one is that no criteria exist to predict the evolution of the flaw geometry and only general qualitative estimates could be made in such terms as "there is a tendency for the crack to propagate in the ...direction." Another reason is the analytical complexity introduced by the three-dimensional nature of finite-length flaws. Until recent advances in large main-frame computers, only a limited number of surface flaw geometries under specific loading could be studied analytically [2].

The purpose of the stainless steel cladding on the inner surface of RPVs is corrosion prevention. The thermal resistance and coefficient of thermal expansion are both higher than that of the underlying base metal. Often, the high thermal resistance of the cladding has been included in the thermal analysis, but perhaps because of its relatively small thickness (3 to 4% of wall thickness) its effect on the stress distribution during overcooling accidents has been omitted. A two-dimensional, linear elastic fracture mechanics study by Ahlstrand et al. [3] showed that the omission of the thermal stresses in the cladding can lead to a significant underestimation of the stress intensity factor, K_I, for a flaw that extends through the cladding. A study by Sauter et al. [4] indicated that a more realistic approach would be to neglect the effect of cladding in both thermal and stress analyses

The tendency of short flaws to extend on the surface was confirmed in an unexpected manner in Thermal Shock Experiment 5 (TSE-5) [5]. Figure 1.1 shows the developed inner

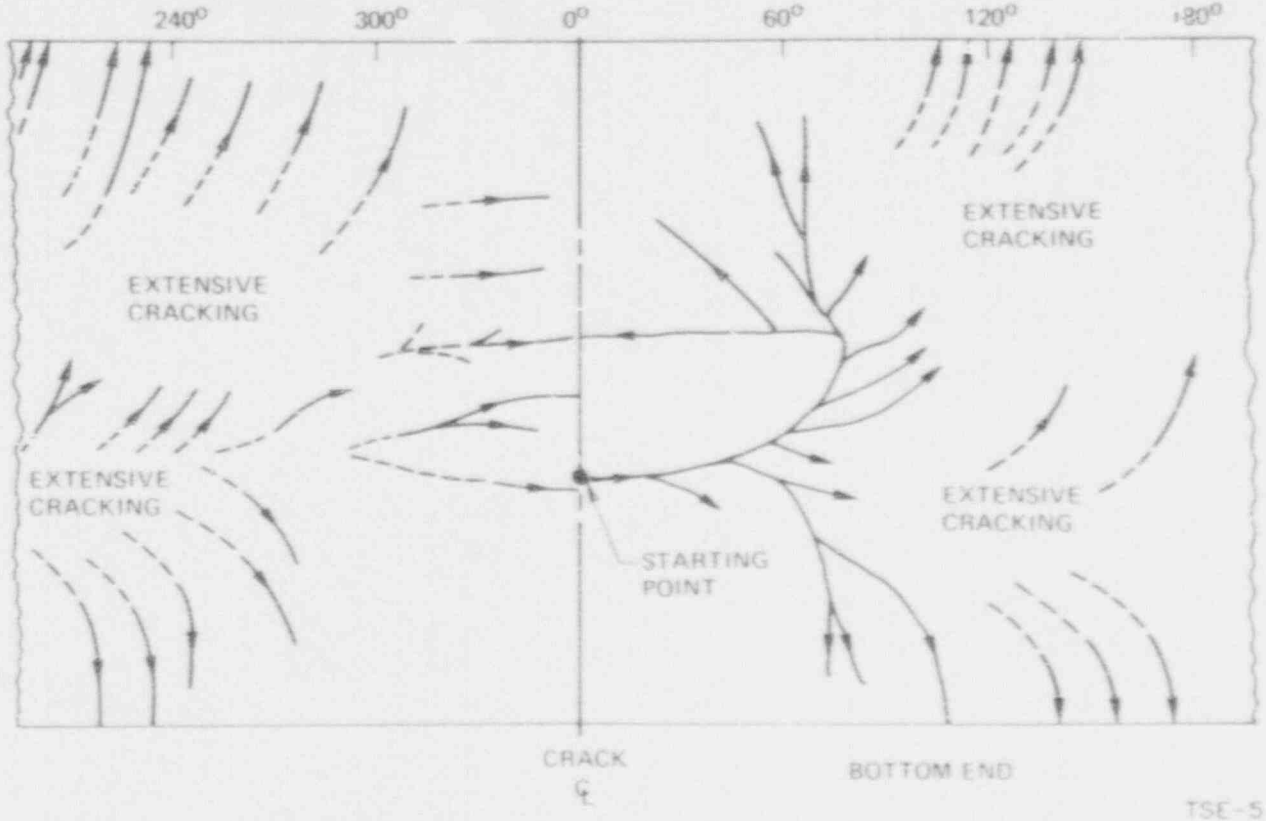

Fig. 1.1. Developed view of the inner surface of the TSE-5 cylinder in which a short cross flaw propagated on the surface during the test. *Source*: R. D. Cheverton, D. G. Ball, S. E. Bolt, S. K. Iskander, and R. K. Nanstad, Martin Marietta Energy Systems, Inc., Oak Ridge Natl. Lab., *Pressure Vessel Fracture Studies Pertaining to the PWR Thermal-Shock Issue: Experiments TSE-5, TSE-5A, and TSE-6*, USNRC Report NUREG/CR-4249 (ORNL-6163), June 1985.

surface of the TSE-5 cylinder, where a short cross flaw extended and covered the entire surface during testing. Since it was unexpected, it was not properly recorded. A separate, well-planned, and instrumented experiment, TSE-7, was performed to confirm this [6]. Figure 1.2 shows the

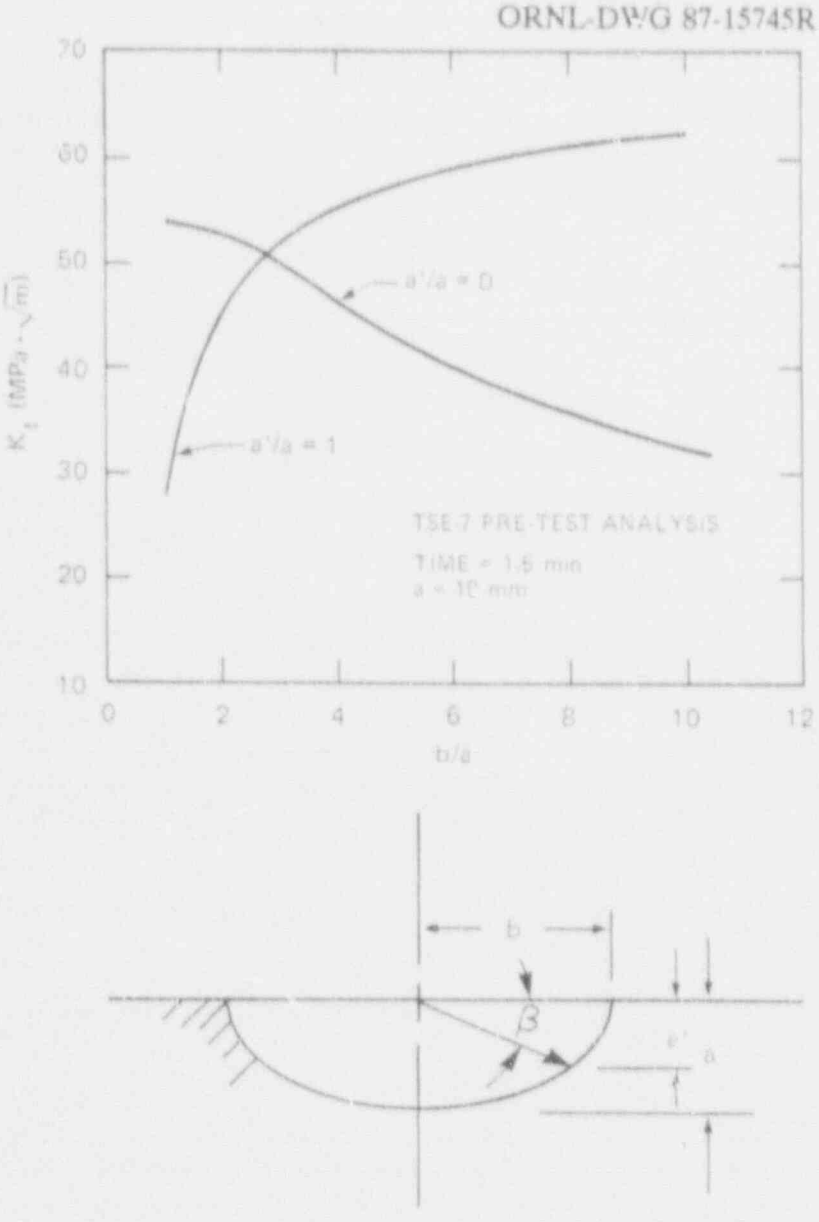

Fig. 1.2. Variation of the stress intensity factor, K_I, for an elliptic flaw as a function of the aspect ratio of the major-to-minor axes (b/a). *Source*: R. D. Cheverton, D. G. Ball, S. E. Bolt, S. K. Iskander, and R. K. Nanstad, Martin Marietta Energy Systems, Inc., Oak Ridge Natl. Lab., *Pressure Vessel Fracture Studies Pertaining to the PWR Thermal-Shock Issue: Experiment TSE-7*, USNRC Report NUREG/CR-4304 (ORNL-6177), July 1985.

variation of the stress intensity factor, K_I, for a semielliptic surface flaw as a function of the aspect ratio of the major to minor axes (b/a) for the conditions pertaining to the TSE-7 experiment. These curves show that for the initial 19-mm-radius, semicircular surface flaw used, b/a = 1, the stress intensity factor at the bottom of the flaw is less than that at the surface. If surface crack propagation occurs and the depth remains constant, K_I at the surface will exceed K_I at the deepest point until b/a exceeds 3. Thus, analysis indicates that such a flaw, once initiated, has a tendency to propagate on the surface before it can increase in depth. This has indeed been verified experimentally, as indicated by Fig. 1.3, which shows the extensive crack propagation and bifurcation on the surface of the TSE-7 cylinder, originating from a semicircular 19-mm surface flaw. The flaw also increased in depth to the values shown at selected locations in Fig. 1.3. Further experimental evidence from the Heavy-Section Steel Technology (HSST) Program was obtained in experiment PTSE-1, illustrated in Fig. 1.4. In this test, the 1000-mm-long axial flaw grew axially at each end by over 100 mm during the first crack jump [7]. A similar sequence of events occurred in PTSE-2 [8], in which the 1000-mm-long axial flaw grew to a length of 1340 mm. In both cases, the flaw was restrained from growing any further axially by manufacturing features of the cylinder.

The above examples illustrate why it is now generally assumed in the HSST Program that, in the absence of cladding, a short flaw in embrittled material subjected to a severe enough thermal shock will grow to become a long one before it grows deep.

1.3 OBJECTIVES OF THE PROGRAM AND PREVIOUS WORK IN THIS SERIES

The objective of the research program described here ("the clad plate program") is to determine the behavior of small flaws in or near cladding under stress fields similar to those occurring during a PTS scenario. The potential benefit to the U.S. Nuclear Regulatory Commission (NRC) is an improved capability to predict the fracture strength of an RPV with hypothetical flaws. The objectives of this research are achieved by comparing the load-bearing capacity of clad and unclad flawed plates. The clad plate program is conducted as part of the HSST Program.

The first series (Series 1) of such experiments indicated that the cladding employed may have had sufficient arrest toughness to stop running cracks [9]. The precise contribution of the stainless steel cladding to the arrest toughness was not determined.

1.4 PURPOSE OF THIS SERIES OF EXPERIMENTS

The central question to be investigated is whether a relatively thin layer of tough cladding, by maintaining its integrity, can redistribute the stresses in its immediate vicinity sufficiently to retard crack propagation that would have otherwise occurred. In particular, the question is whether cladding could arrest an initially short flaw that is propagating along the surface and keep it from becoming a long flaw. Should that occur, then the flaw cannot grow in depth to challenge the integrity of the plate without a significant increase of load beyond that needed to rupture unclad plates.

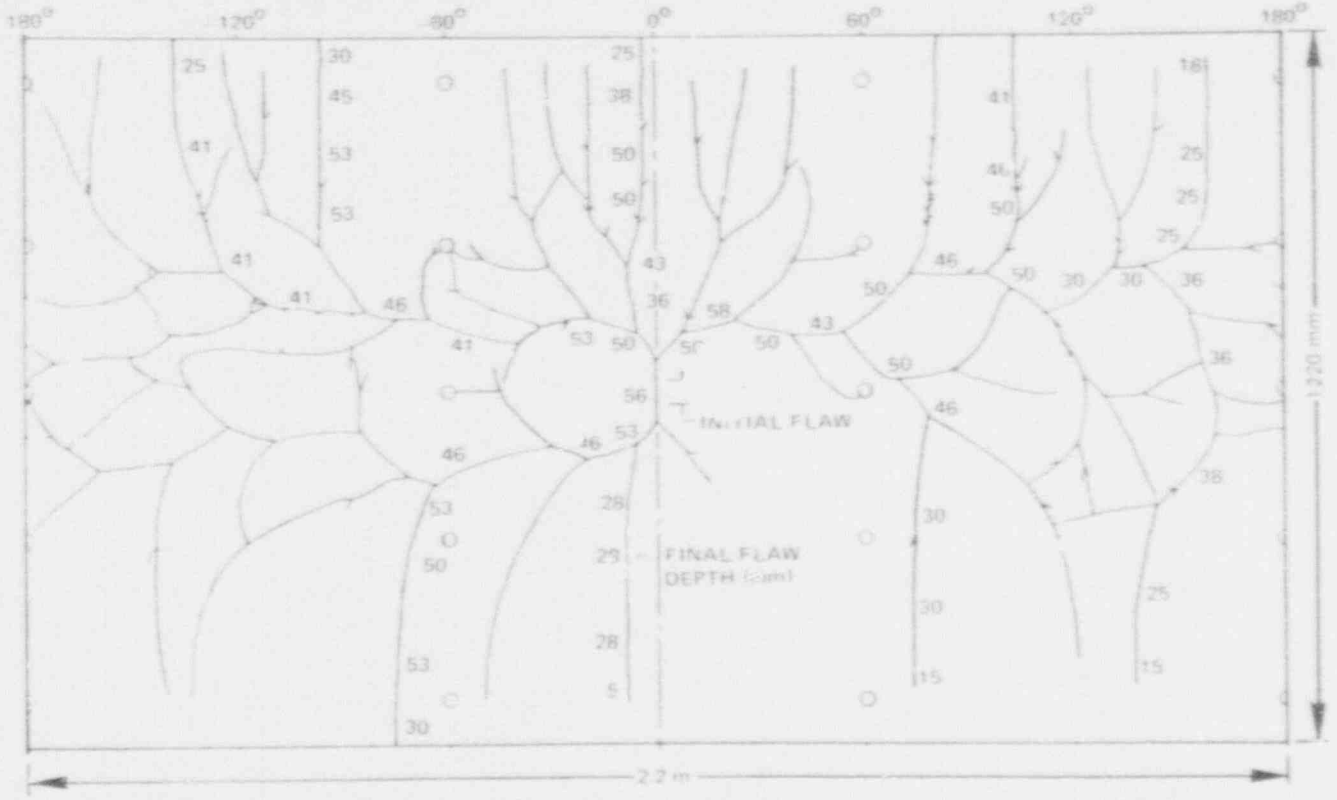

Fig. 1.3. Developed view of inner surface of the TSE-7 cylinder in which the 19-mm-radius semicircular flaw propagated on the surface to become a long flaw during the test. *Source*: R. D. Cheverton, D. G. Ball, S. E. Bolt, S. K. Iskander, and R. K. Nanstad, Martin Marietta Energy Systems, Inc., Oak Ridge Natl. Lab., *Pressure Vessel Fracture Studies Pertaining to the PWR Thermal-Shock Issue: Experiment TSE-7*, USNRC Report NUREG/CR-4304 (ORNL-6177), July 1985.

ORNL-DWG 82-6072CR ETD

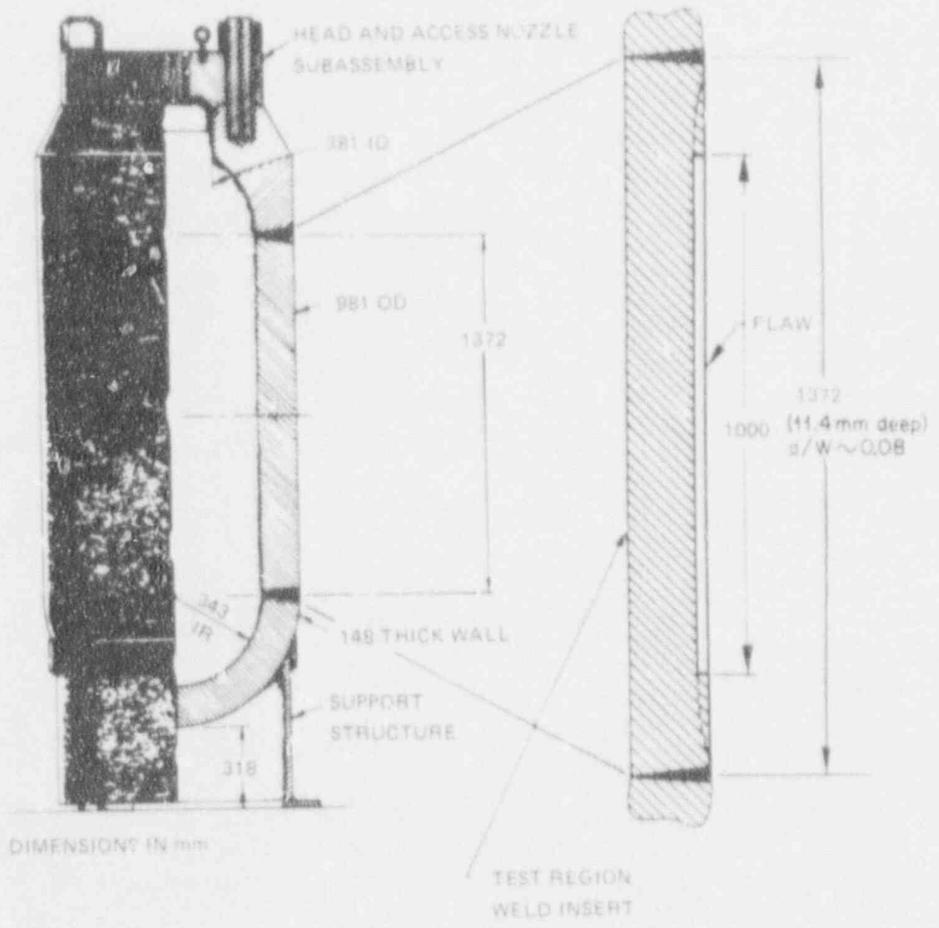

Fig. 1.4. The 1000-mm-long axial flaw on the outside of the PTSE-1 extended axially about 100 mm at each end during the thermal shock. *Source:* R. H. Bryan et al., Mart.. Marietta Energy Systems, Inc., Oak Ridge Natl. Lab., *Pressurized-Thermal-Shock Test of 6-in.-Thick Pressure Vessels. PTSE-1: Investigation of Warm Prestressing and Upper-Shelf Arrest*, USNRC Report NUREG/CR-4106 (ORNL-6135), April 1985.

A special plate specimen has been developed to investigate the effects of cladding on the behavior of flaws. The design avoided the specimen geometry problems encountered in Series 1. It was commercially clad using the three-wire, series-arc technique and types 308, 309, and 312 stainless steel weld wires. The three-wire, series-arc technique was used in some of the older vessels. An electron-beam (EB) weld is introduced into the base metal to provide a crack initiation site. The plate is loaded in four-point bending to approximate the stresses due to pressurized thermal shock.

To initiate the flaws, the EB weld zones of six of the test plates were each hydrogen charged while the loads were maintained constant, whereas, in the two other plates the flaw was initiated through hydrogen charging before the plate was loaded. The flaw, once it initiated from the EB weld region, either arrested or led to complete rupture of the plate. Plates which did not rupture were heat-tinted to define the arrested flaw shape and were then reloaded until either another pop-in or plate rupture occurred.

1.5 OUTLINE OF REPORT

In Chap. 2 of this report, the test specimens, their fabrication, and the method of inducing a flaw initiation site by means of an EB weld are described. The two different methods of testing used ("arrest" and "initiation") are also discussed in Chap. 2. This will be followed by a description of the instrumentation and the static and dynamic data acquisition systems used.

In Chap. 3, results of pretest and posttest material characterization are given. Material characterizations presented include Charpy V-notch impact energy, Young's modulus and stress-strain curves for the base metal, heat-affected zone (HAZ), and cladding, as well as results of room temperature tensile testing that had been performed on the HAZ from one of the broken halves of the first plate tested. The reference nil-ductility-transition temperature (RT_{NDT}) of the base metal, the variation of hardness across the thickness of the plate, some J-integral vs crack growth resistance (J-R) curves for cladding, and the results of metallographic examinations are also given.

The results of the tests performed on the eight plates are given in detail in Chap. 4 and include the fractography and scanning electron microscopy (SEM) of the fracture surface of one of the plates tested. Chapter 5 discusses the results in terms of the material properties and includes some very preliminary analytical work as well as some conclusions. One of the analytical methods used in these preliminary calculations is the semiempirical expression for partial through-surface cracks due to Merkle [10] and a summary of the method has been included as Appendix A. The Merkle expression gives the variation of the stress intensity factor, K_I, along the crack front of a semielliptic surface flaw. The position along the crack front can be given as either the fractional crack depth (a'/a) or as the angle β, see Fig. 1.2. The relationship between the fractional crack depth and the angle β is given in Appendix B. Photographs of the fracture surfaces of the clad plate are included in Chaps. 4 and 5, but the profiles of the cracks are sometimes difficult to discern from published photographs. Drawings of these crack profiles have been made from the original photographs as well as by referring to the fracture surfaces. The drawings of the crack profiles are given in Appendix C. Combustion Engineering (CE) performed the heat treatment of the base material of the clad plates and manufactured the cladding, and the report by CE has been reproduced in Appendix D.

REFERENCES

1. S. K. Iskander, "A Method of LEFM Analysis of RPV During SBLOCA," *Int. J. Pres. Ves. and Piping* 25, 279-98, 1986.*

2. G. R. Irwin, "Crack Extension Force for a Part-Through Crack in a Plate," *J. Appl. Mech., Trans. ASME*, 84, 651-4, December 1962.*

3. R. Ahlstrand, P. Päätiläinen, and H. Raiko, "Linear Elastic Fracture Analysis of Irradiated Nuclear Components having Welded Cladding," in *Transactions of the Sixth International Conference on Structural Mechanics in Reactor Technology*, Vol. G, Paper G1/4, August 1981.*

4. A. Sauter, R. D. Cheverton, and S. K. Iskander, , *Modification of OCA-I for Application to a Reactor Pressure Vessel with Cladding on the Inner Surface*, USNRC Report NUREG/CR-3155 (ORNL/TM-8649), Martin Marietta Energy Systems, Inc., Oak Ridge Natl. Lab., Oak Ridge, Tenn., May 1983.†

5. R. D. Cheverton, D. G. Ball, S. E. Bolt, S. K. Iskander, and R. K. Nanstad, , *Pressure Vessel Fracture Studies Pertaining to the PWR Thermal-Shock Issue: Experiments TSE-5, TSE-5A, and TSE-6*, USNRC Report NUREG/CR-4249 (ORNL-6163), Martin Marietta Energy Systems, Inc., Oak Ridge Natl. Lab., Oak Ridge, Tenn., June 1985.†

6. R. D. Cheverton, D. G. Ball, S. E. Bolt, S. K. Iskander, and R. K. Nanstad, *Pressure Vessel Fracture Studies Pertaining to the PWR Thermal-Shock Issue: Experiment TSE-7*, USNRC Report NUREG/CR-4304 (ORNL-6177), Martin Marietta Energy Systems, Inc., Oak Ridge Natl. Lab., Oak Ridge, Tenn., July 1985.†

7. R. H. Bryan et al., *Pressurized-Thermal-Shock Test of 6-in.-Thick Pressure Vessels. PTSE-1: Investigation of Warm Prestressing and Upper-Shelf Arrest*, USNRC Report NUREG/CR-4106 (ORNL-6135), Martin Marietta Energy Systems, Inc., Oak Ridge Natl. Lab., Oak Ridge, Tenn., April 1985.†

8. R. H. Bryan et al., *Pressurized-Thermal-Shock Test of 6-in.-Thick Pressure Vessels. PTSE 2: Investigation of Low Tearing Resistance and Warm Prestressing*, USNRC Report NUREG/CR-4888 (ORNL-6377), Martin Marietta Energy Systems, Inc., Oak Ridge Natl. Lab., Oak Ridge, Tenn., December 1987.†

---

*Available in public technical libraries.

†Available for purchase from National Technical Information Service, Springfield, VA 22161.

9. W. R. Corwin et al., *Effect of Stainless Steel Weld Overlay Cladding on the Structural Integrity of Flawed Steel Plates in Bending - Series 1*, USNRC Report NUREG/CR-4015 (ORNL/TM-9390), Martin Marietta Energy Systems, Inc., Oak Ridge Natl. Lab., Oak Ridge, Tenn., April 1985.*

10. J. G. Merkle, "Stress-Intensity Factor Estimates for Part-Through Surface Cracks in Plates Under Combined Tension and Bending," pp. 3-22 and 31-2 in *Quarterly Progress Report on Reactor Safety Programs Sponsored by the Division of Reactor Safety Research for July-September 1974*, Vol. II, ORNL-TM-4729, Union Carbide Corp. Nuclear Div., Oak Ridge Natl. Lab., Oak Ridge, Tenn., November 1974.*

---

*Available for purchase from National Technical Information Service, Springfield, VA 22161.

2. SPECIMEN DESIGN, EXPERIMENTAL PROCEDURE, AND INSTRUMENTATION

2.1 MATERIAL ALLOCATION, SPECIMEN FABRICATION, AND HEAT TREATMENT

The base metal used in the clad plate program was machined from segment "012B" of an approximately 7 by 3 m, 178-mm-thick steel plate, Fig. 2.1. It was manufactured by Lukens (Melt B8112) to ASTM Specification for Pressure Vessel Plates, Alloy Steels, Quenched and Tempered, Manganese-Molybdenum and Manganese-Molybdenum-Nickel, A 533 grade B class 1. The Oak Ridge National Laboratory (ORNL) identification for this plate is HSST Plate 012. The area of the plate designated for the six clad specimens, CP-15 through CP-20, was weld overlayed with stainless steel on both sides before the individual specimens were separated from the plate (lower half of Fig. 2.1).

Before the cladding was applied, the base metal was heat treated to raise its transition temperature so that it would be brittle at temperatures at which the cladding would be tough. The weld overlay cladding is a single layer of 308/309/312 stainless steel, made by the three-wire process. This process is more representative of the method used to manufacture some of the older RPVs. To avoid reducing the transition temperature, the plates were then given a slightly milder postweld heat treatment (593°C for 10 h) than typical for a clad reactor pressure vessel (607–635°C for 40 h).

Extensive studies were performed by CE in order to optimize the heat treatment required and to produce the necessary material properties; the CE report is included as Appendix D. Material characterization studies were also performed at ORNL (see Chap. 3) and agreed well with those reported by CE.

2.2 DESCRIPTION OF THE SERIES 2 PLATE TEST SPECIMEN

One of the problems encountered with the Series 1 plate specimens [1] was the unknown effect of a groove on the stress intensity factors. It was necessary to machine a groove through the stainless steel cladding that covered the entire surface of the plate in order to put an EB weld in the base metal, see Fig. 2.2.

The specimen used in Series 2 has been redesigned to avoid this problem by machining recesses in a large blank from Plate 012B thus providing a location for the stainless steel weld overlay, see Fig. 2.3. This configuration allowed the EB weld to be produced in the base metal surface protruding between the cladding strips, see Fig. 2.4. After cladding, both welded surfaces of the blank were machined to a smooth surface, and the specimens separated by sawing.

2.3 FLAWING PROCEDURE

The site for a sharp flaw in the base metal was produced in the plate specimens by means of an autogenous EB weld. When the sharp flaw was desired, the EB weld would be hydrogen charged [2,3]. The EB weld in the base metal was produced by a Leybold-Heraeus welder.

ORNL-DWG 88-14559

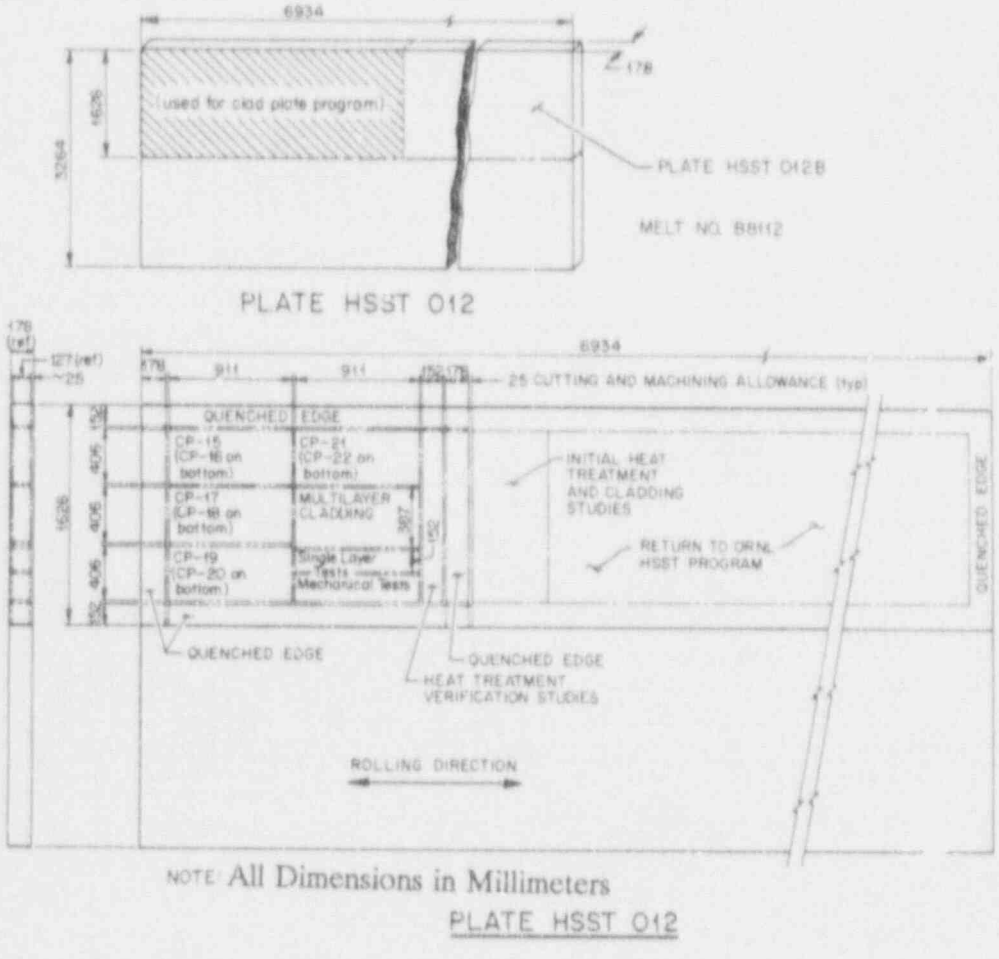

Fig. 2.1. Material allocation from HSST Plate 012 for the Clad Plate Program and cut-up diagram for the various specimens.

ORNL-DWG 88-14562

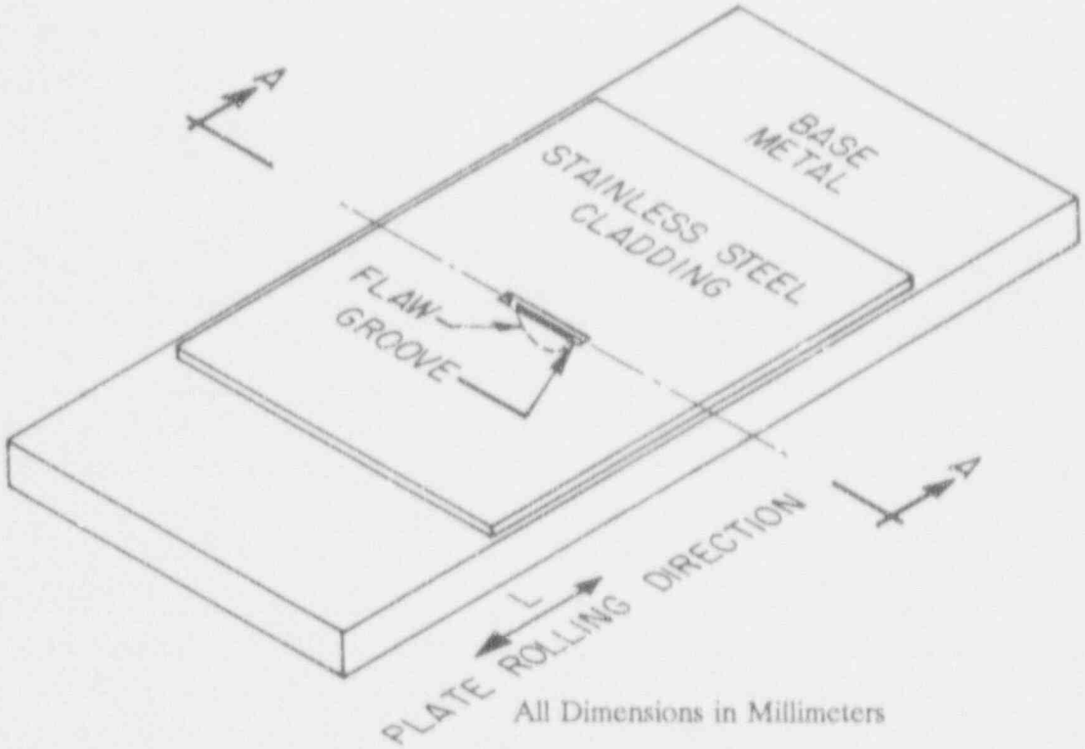

All Dimensions in Millimeters

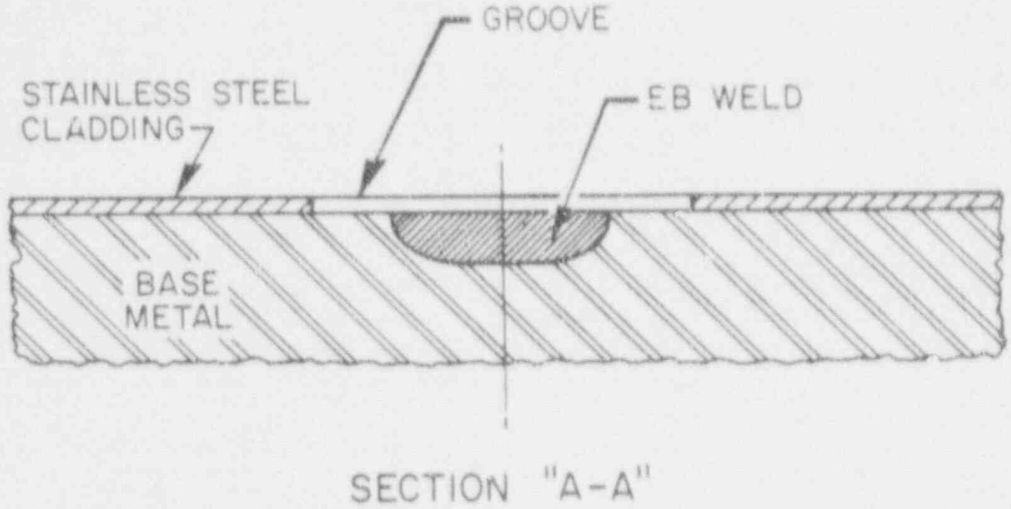

Fig. 2.2. The specimens of Series 1 had a groove in the stainless steel cladding to enable the placement of an electron beam weld to serve as a flaw initiation site.

ORNL-DWG 88-1456OR

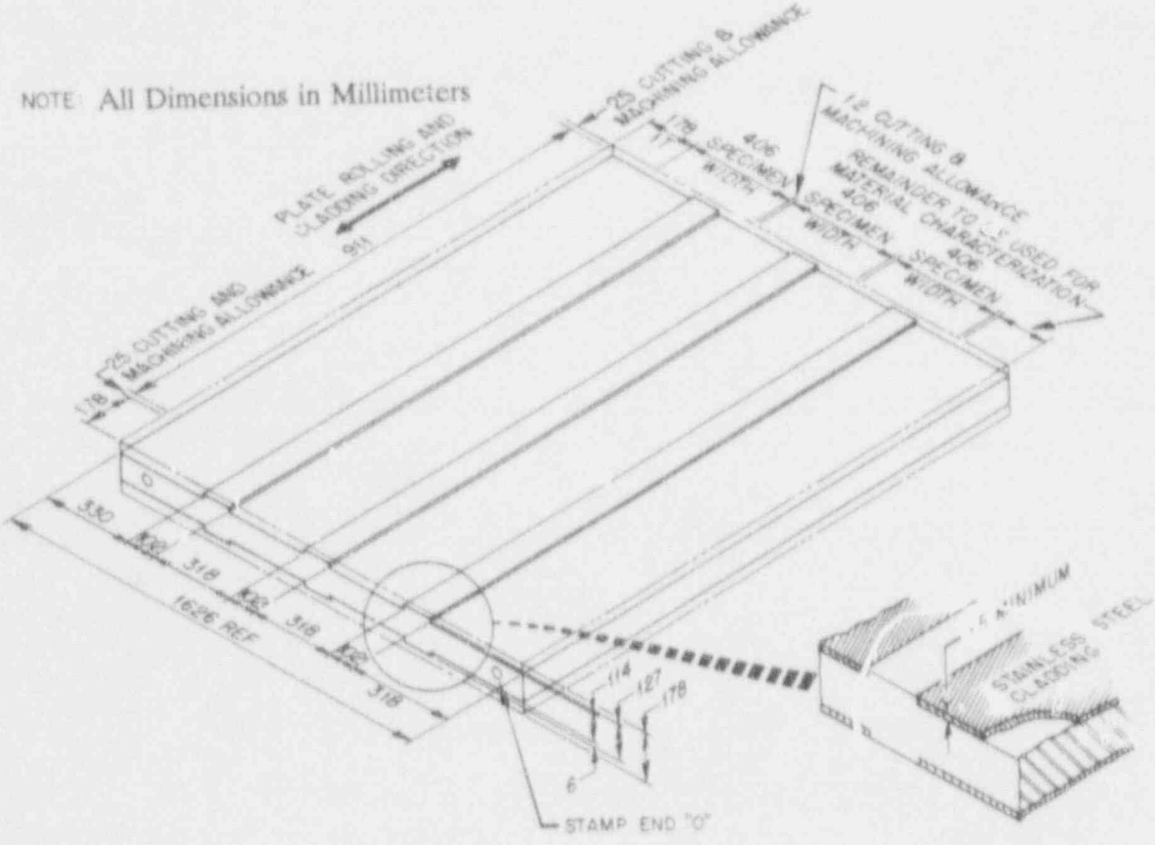

Fig. 2.3. Recesses machined on the surface of HSST Plate 012B to receive the stainless steel cladding for Series 2.

ORNL-DWG 88-14712

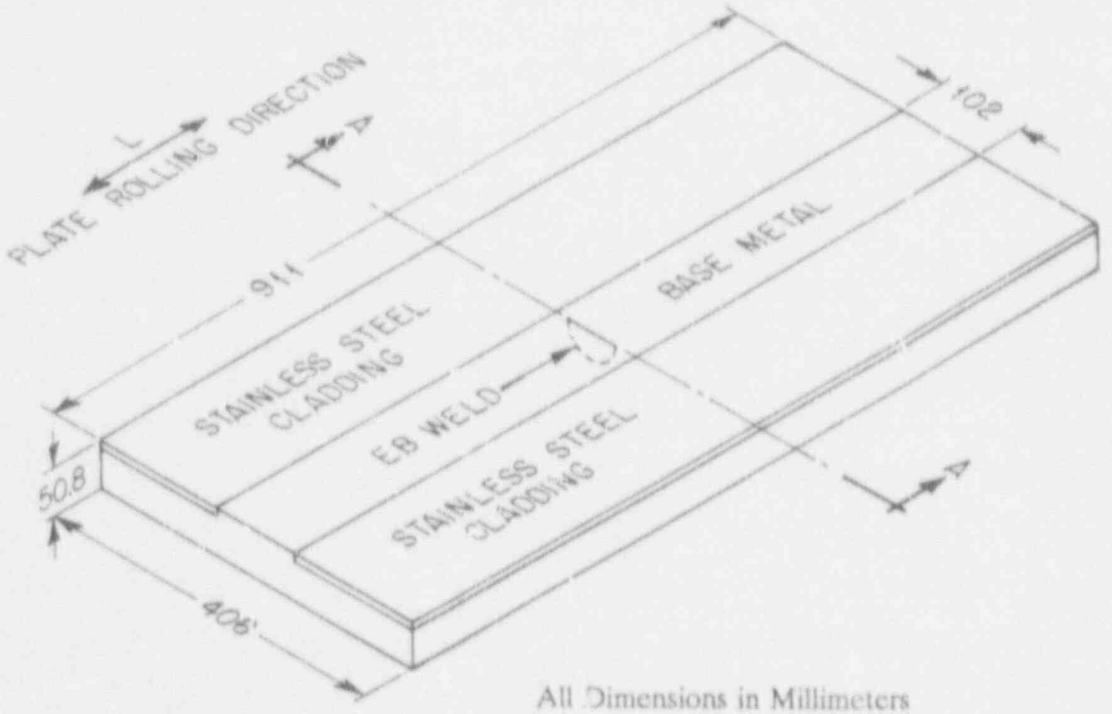

All Dimensions in Millimeters

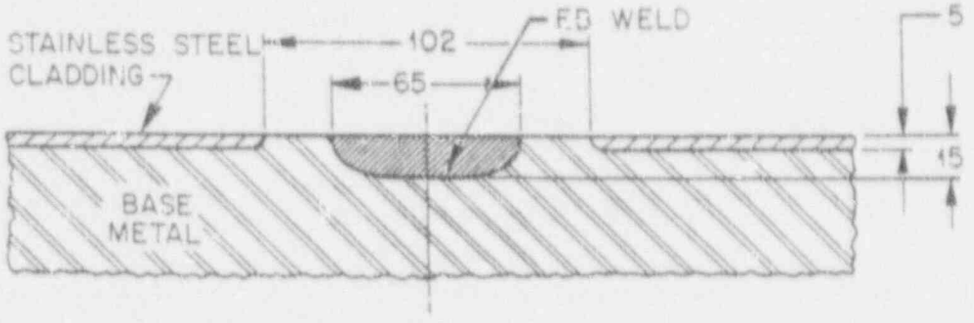

SECTION "A-A"

Fig. 2.4. Series 2 plate specimen. The cladding thickness is approximately 5 mm.

Computer control of the beam intensity resulted in an approximate semielliptical-shaped weld zone, 65-mm-long with the major axis along the surface, and 15-mm-deep, Fig. 2.4. The EB welding parameters used are given in Table 2.1. This flawing procedure was used on all eight plates tested in this program. A typical flaw produced by this method is shown later, and for brevity will be referred to as the "EB flaw."

Table 2.1. Parameters used in the electron beam welder to introduce a flaw initiation site in the clad plates

Distance from heat shield to plate surface	635 mm
Vacuum in chamber	6.0 mPa
Work table travel speed	250 mm/min
Accelerating voltage	150 kV
Beam current	17 mA
Filament current	4.2 A
Focus	Sharp at surface

2.4 GENERAL DESCRIPTION OF THE TEST

Eight plates have been tested in Series 2, and the general test procedure was essentially the same. The instrumented plate was mounted in a 1-MN Instron testing machine. For tests at other than room temperature, the plate was cooled to the specified temperature. The variation in temperature at various locations was kept within 3°C. The plates were loaded in four-point bending to induce a pure bending moment in the span containing the EB weld region, see Fig. 2.5, subjecting the flaw region to a stress gradient in the thickness direction. Six of the plates were loaded to induce a specified strain level on the surface of the base metal. The EB weld was then hydrogen charged, while the load was maintained constant using stroke control, until a flaw initiated. This type of test on an ***initially unflawed*** plate is thus essentially an ***arrest*** experiment the purpose of which is to study the effect of cladding on a brittle running flaw.

In the remaining two plates, a flaw was induced in the EB weld by hydrogen charging with no applied load. Each plate was then mounted in the testing machine and the load increased at a uniform rate under stroke control until this preexisting flaw either popped in and arrested, or the entire plate ruptured. Thus, the difference between the tests on these two plates and the six mentioned above is the presence of a flaw when the plates were first mounted in the test machine. These two tests, as well as those with an arrested flaw are designated as ***initiation*** tests. The objective of the tests performed on these two specimens was to determine the load-bearing capacity of the flawed clad plate.

In cases in which the flaw arrested, the plate is removed from the testing machine and heat-tinted at 250 to 350°C for 1 h to define the arrested flaw shape. For this type of low-alloy

ORNL-DWG 88-14561

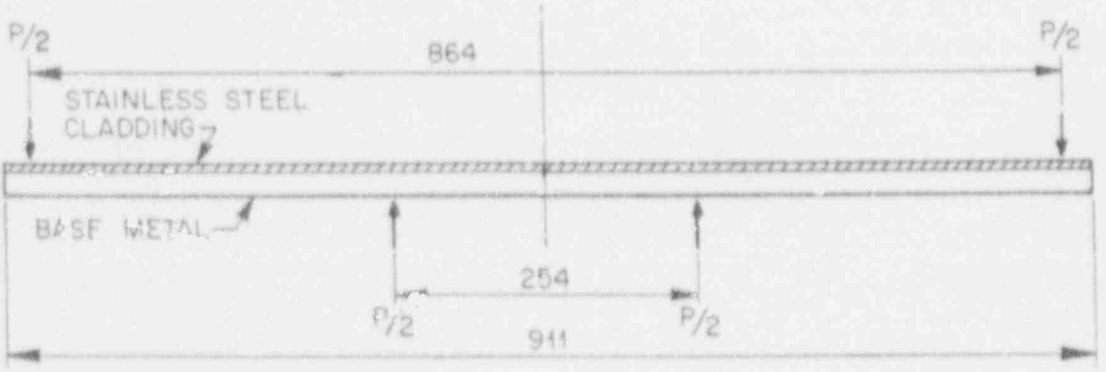

All Dimensions in Millimeters

Fig. 2.5. Location of loads used in testing the clad plates, subjecting the flaw to a pure bending moment. The plane of the flaw is at center of plate and normal to the plane of the figure

steel, no significant effects on the crack tip material properties are expected from heat-tinting in this temperature range. Some nondestructive examination was performed to determine the extent of flaw propagation. After partial reinstrumentation, the plate is put back into the testing machine and, in some cases, cooled to a specified temperature. The load is increased at a uniform rate until the plate either ruptures or further pop-in occurs. In the case of the latter, the process is repeated. The purpose of reloading the arrested flaw shapes is to obtain data on the residual load-bearing capacity of flawed clad plates. This portion of the experiment on an arrested flaw, as well as in tests on the two plates mentioned above, is designated an ***initiation*** test in contrast to the previously described ***arrest*** test.

Using an assumed flaw shape that corresponded approximately to the EB weld zone, the loading rate was chosen to be within the range specified in ASTM Test for Plane-Strain Fracture Toughness of Metallic Materials (E 399-83), 0.55 to 2.75 MPa$\sqrt{m}$/s.

For the first plate tested (CP-15), the surface strain was chosen to be approximately the yield strain of the base metal. As described in detail later, the crack arrested and the plate did not rupture. Therefore, the target surface strain was increased for the other plates tested at room temperature.

2.5 INSTRUMENTATION FOR ARREST–TYPE EXPERIMENTS

Typical instrumentation used for the initial arrest experiments on the six plates is shown in Fig. 2.6(a) and (b) for tests at room temperature (RT) and below RT, respectively. The gages

ORNL-DWG 87-3974R2 ETD

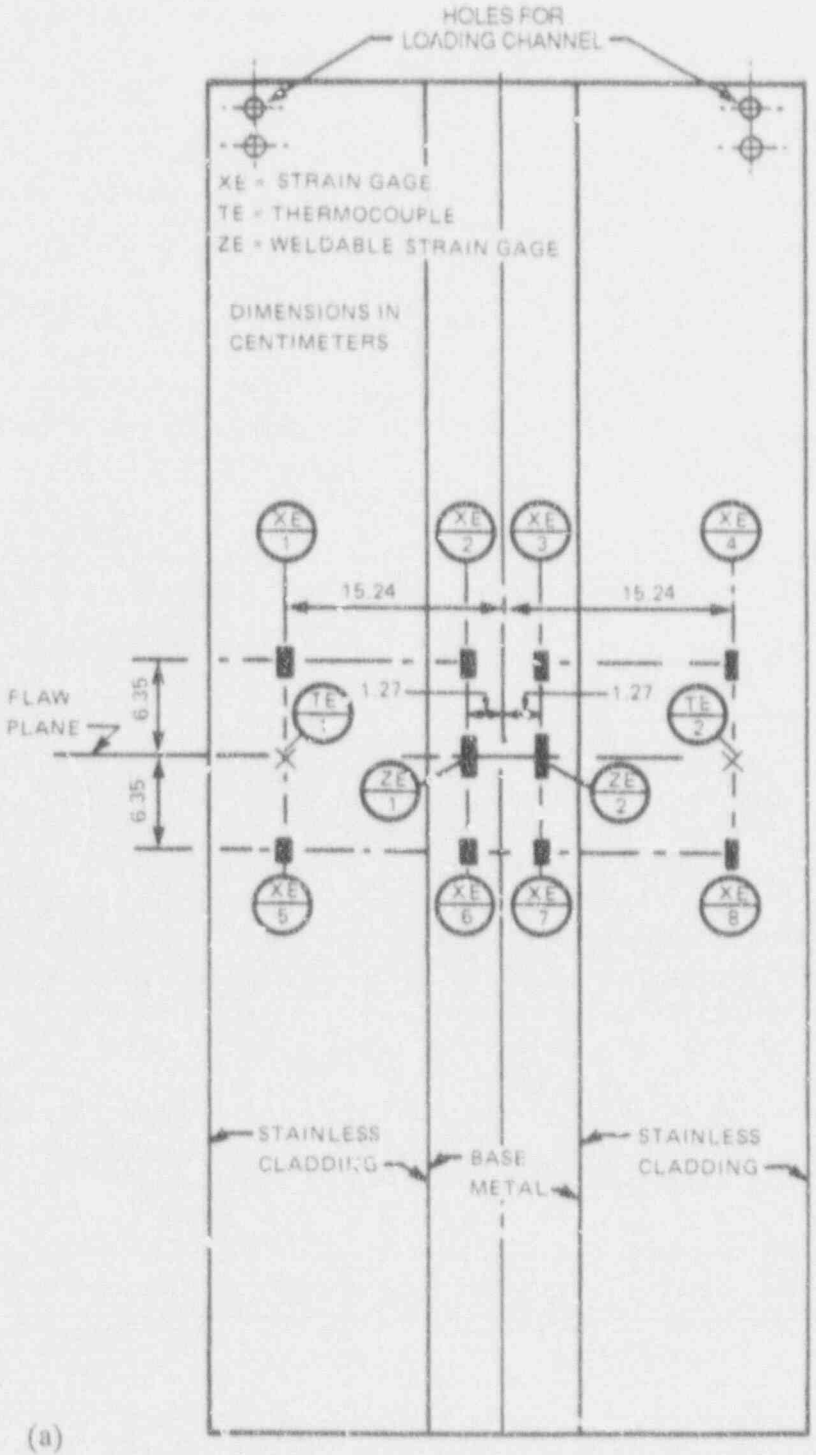

Fig. 2.6. Typical instrumentation used on six plates for the "arrest" portion of the test. (a) room temperature, (b) below room temperature

ORNL-DWG 90-15023

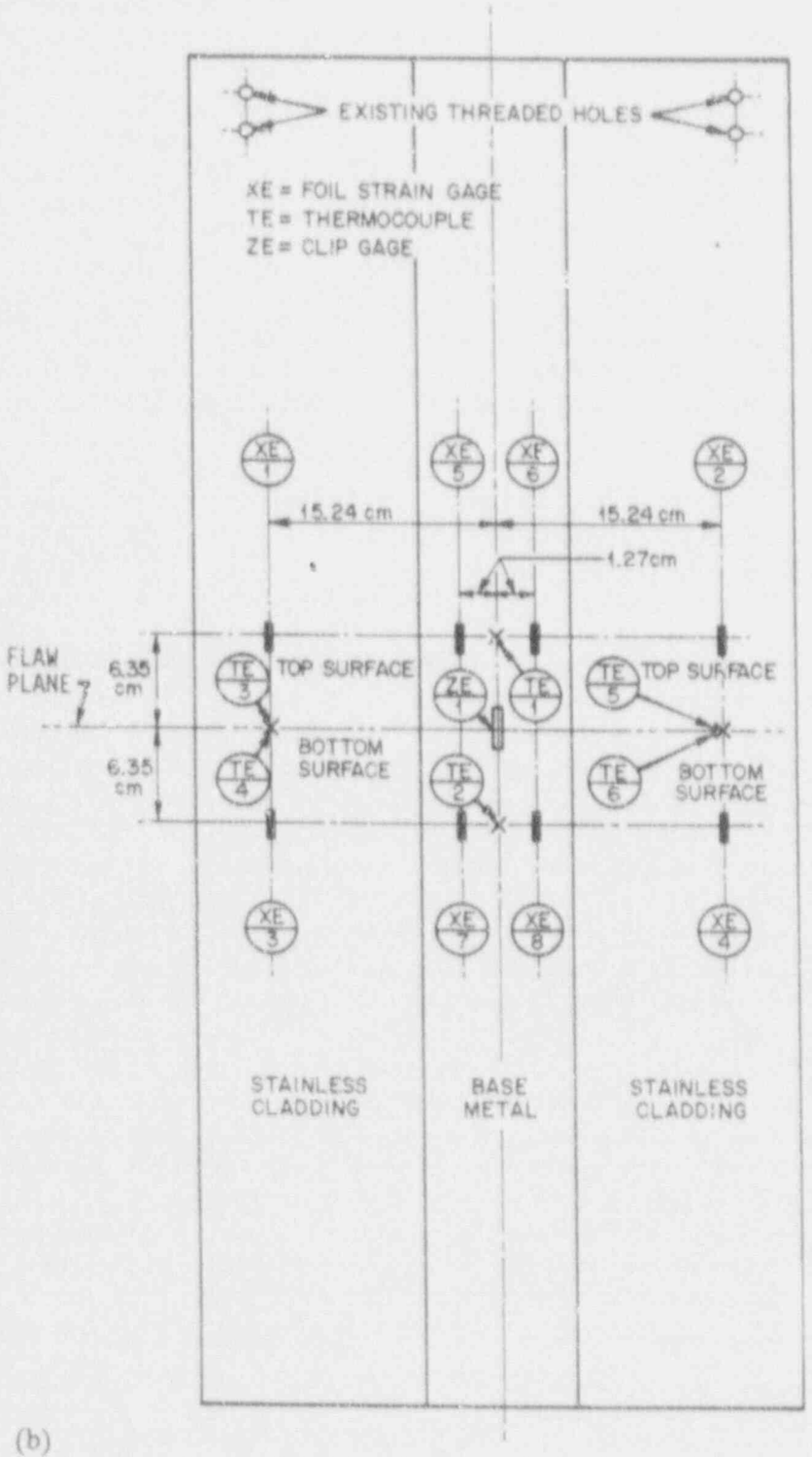

(b)

Fig. 2.6. (Continued)

designated ZE in Fig. 2.6(a) are weldable, stainless steel-sheathed strain gages that are used as crack mouth-opening displacement (CMOD) gages. Only the end portions of the gages are welded and a sufficient length is left unbonded such that the expected CMOD, when averaged over the unbonded length, is within the maximum strain capacity of the gage. These gages have been used successfully many times before in this manner by the HSST Program. For tests at RT, the top surface only was instrumented with two CMOD gages, four foil strain gages on each of the base metal and clad portions of the plate and two thermocouples. For tests below RT, two thermocouples were added on the bottom surface of the plate to ensure that the temperature through the plate thickness is uniform, and the CMOD was measured by means of a single clip gage, designated ZE-1, shown in Fig. 2.6(b), instead of the two weldable strain gages; the eight foil gages remained unchanged. Heat tinting destroyed the foil strain gages, and the plate was partially reinstrumented for the initiation test as shown in Fig. 2.7. After heat-tinting the first plate tested, an attempt was made to reuse the weldable strain gages with mixed success; subsequently a clip gage was used to measure the CMOD in tests after heat tinting.

A data acquisition system (DAS) was used to record the readings from the instrumentation on magnetic tape at suitable time and load intervals. In addition to the strain, CMOD and the temperature at various locations in the plate, the load and the displacement of the testing machine ram were also recorded.

2.6 INSTRUMENTATION FOR TWO INITIATION–TYPE EXPERIMENTS

The layout of the instrumentation used for the first initiation experiment on plates CP-16 and CP-22 was modified somewhat from that used with the previous six plates, and is shown in the upper portion of Fig. 2.8. Both plates were instrumented with four thermocouples, TE-1 through TE-4, one CMOD gage, ZE-1, and 12 strain gages, XE-1 to XE-12. Plate CP-16 carried extra instrumentation to capture the dynamic characteristics of crack propagation in the first initiation experiment. The extra instrumentation consisted of strain gages, XD-1 to XD-11, and two additional trigger strain gages. These were attached near the crack tip and in the path of possible crack propagation to trigger the DAS system described below. A closeup view of the flaw area (before clip gage installation) and the strain gages in the vicinity is shown in Fig. 2.9.

For plate CP-16 only, both a static and dynamic DAS were used. The static DAS recorded data every 6 min during the loading of the specimen, while the dynamic DAS recorded data from crack initiation to just after crack arrest. The static DAS recorded data from the four thermocouples, the CMOD gage, 12 strain gages, XE-1 to XE-12, the load cell and the stroke transducer. The dynamic DAS recorded signals from 11 strain gages, XD-1 to XD-11, the trigger gages and the load cell using four LeCroy and three Nicolet digital oscilloscopes that were simultaneously triggered when the crack initiated. A separate trigger circuit was used to ensure that the oscilloscopes triggered simultaneously. This circuit, which consisted of two trigger strain gages, a strain gage conditioner and a pulse generator, supplied a voltage spike of approximately 10 V when one of the trigger strain gages was fractured by the propagating crack. Each oscilloscope was set to trigger on a voltage change of 5 V. The LeCroy and Nicolet oscilloscopes were set to record data at a rate of 20 and 500-ns-per-point, respectively.

ORNL-DWG 88-3800R ETD

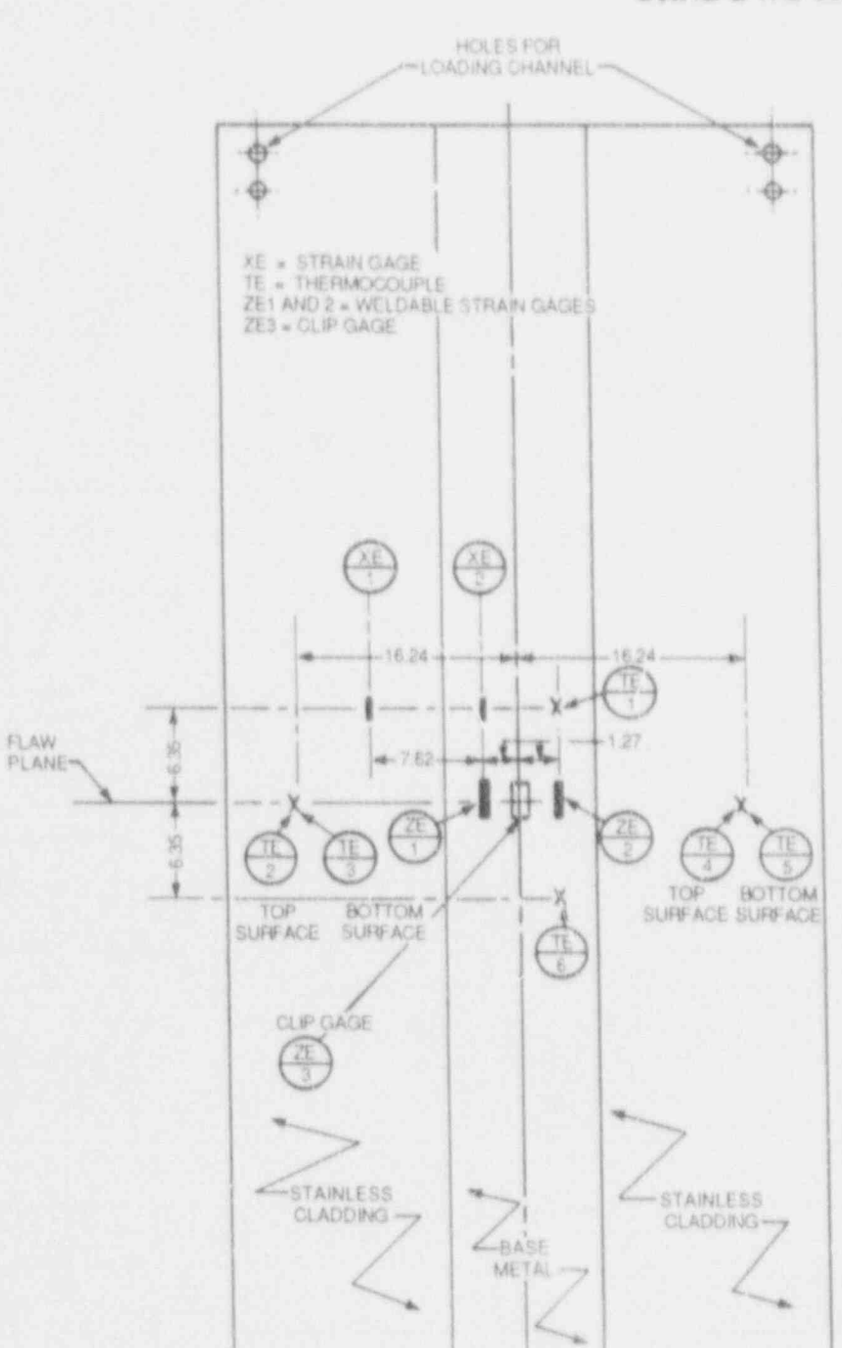

Fig. 2.7. Partial reinstrumentation of plates after some of the original gages were destroyed by heat tinting.

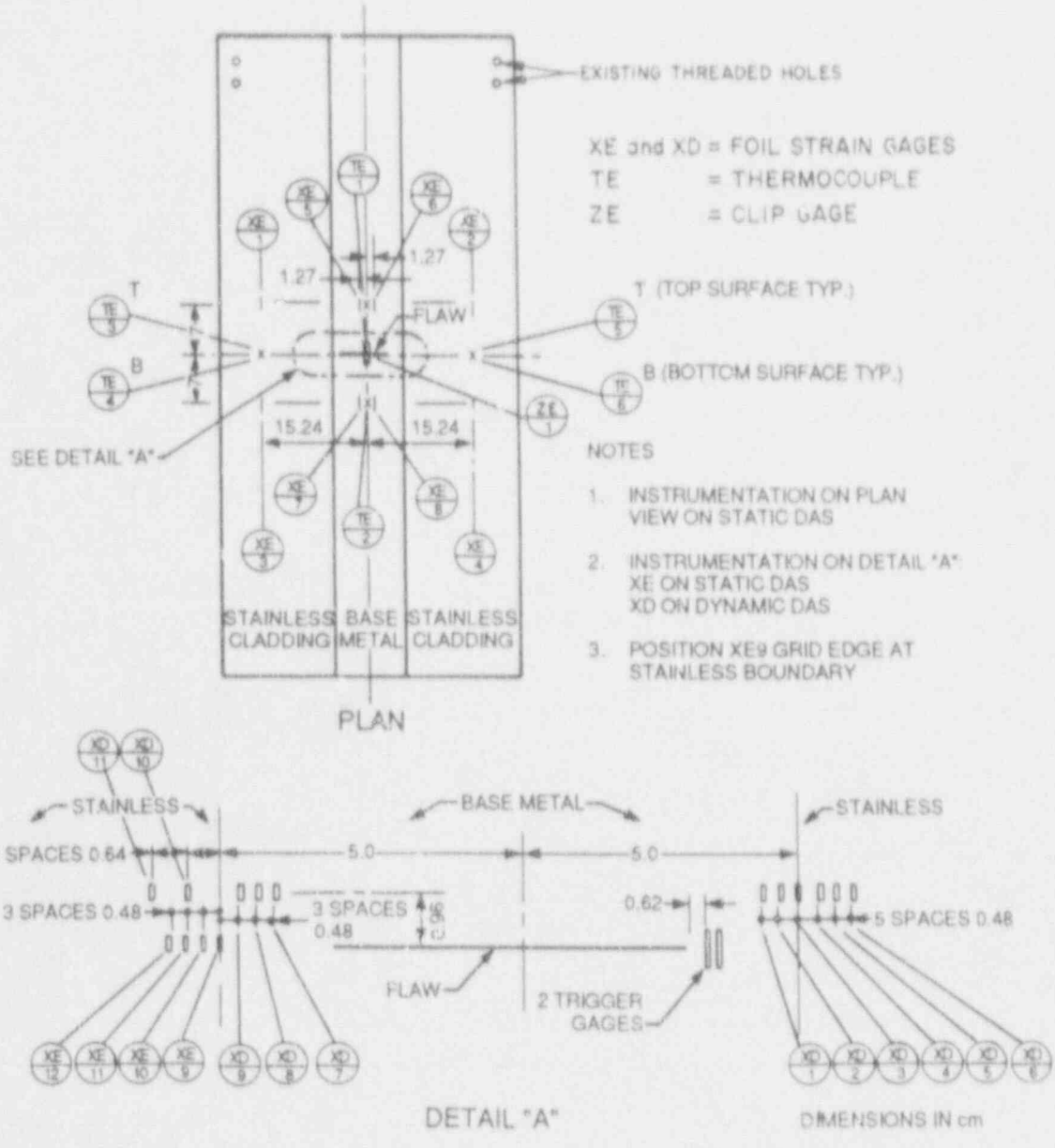

Fig. 2.8. Layout of instrumentation used for tests on plates CP-16 and CP-22. Gages shown in detail "A" were used only with the first phase of testing CP-16.

YP5186

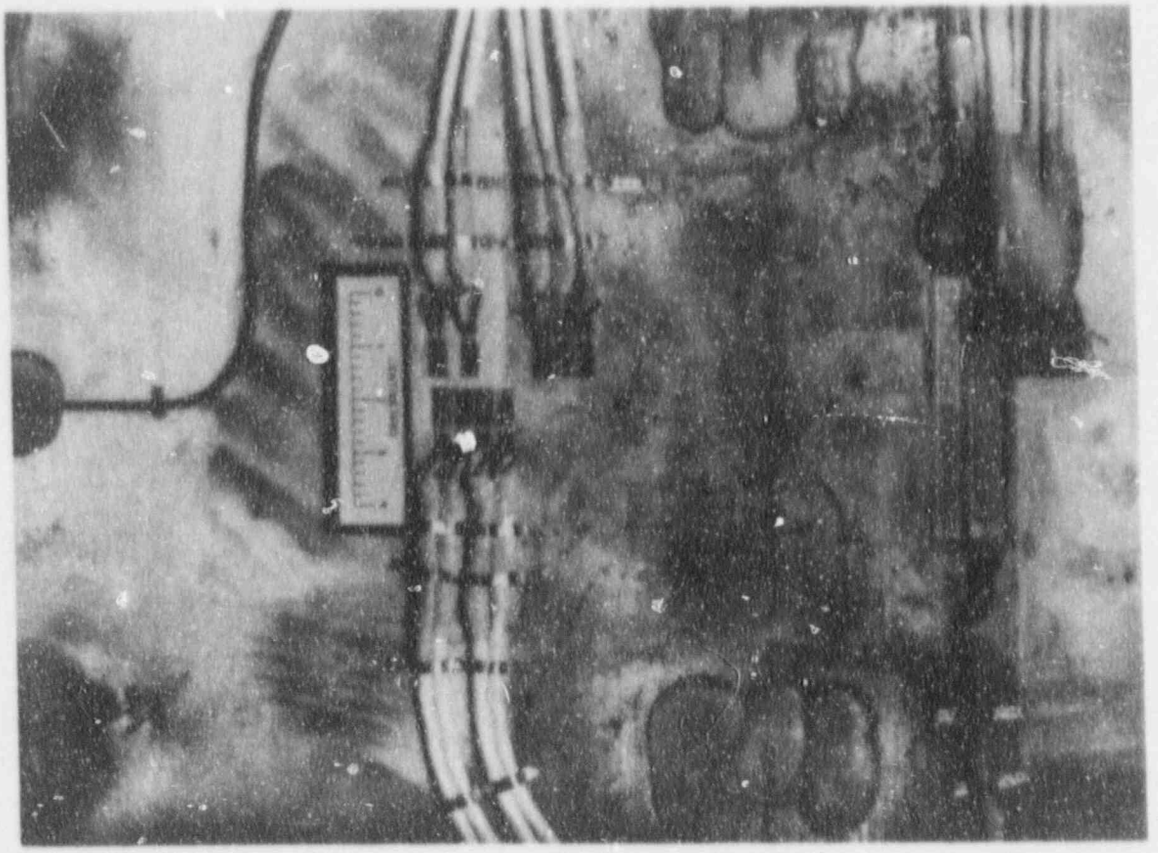

Fig. 2.9. Closeup view of the flaw and the strain gages in the vicinity for clad plate CP-16.

In all tests, the load and CMOD were also recorded on a strip chart and, additionally, the load was plotted against the signal from strain gage XE-1 (on the cladding) on an X-Y plotter. The loads reported for initiation and arrest events were taken from these plots.

REFERENCES

1. W. R. Corwin et al., Martin Marietta Energy Systems, Inc., Oak Ridge Natl. Lab., *Effect of Stainless Steel Weld Overlay Cladding on the Structural Integrity of Flawed Steel Plates in Bending - Series 1*, USNRC Report NUREG/CR-5015 (ORNL/TM-9390), April 1985.*

2. D. A. Canonico and J. D. Hudson, "Technique for Generating Sharp Cracks in Low-Alloy High Strength Steels," pp. 60-64 in *Heavy-Section Steel Technology Program Semiannual Progress Report for Period Ending February 28, 1971*, ORNL-4681, Union Carbide Corp. Nuclear Div., Oak Ridge Natl. Lab., Oak Ridge, Tenn., December 1971.*

3. P. P. Holz, *Flaw Preparations for HSST Program Vessel Fracture Mechanics Testing: Mechanical Cyclic Pumping and Electron Beam Weld-Hydrogen-Charge Cracking Schemes*, USNRC Report NUREG/CR-1274 (ORNL/NUREG/TM-369), Union Carbide Corp. Nuclear Div., Oak Ridge Natl. Lab., Oak Ridge, Tenn., May 1980.*

---

*Available for purchase from National Technic. Information Service, Springfield, VA 22161.

3. MATERIAL CHARACTERIZATION

3.1 PRETEST MATERIAL CHARACTERIZATION

The base metal and characterization blocks used in the clad plate project were machined from a single, 178-mm-thick plate of steel. It was manufactured by Lukens Steel (Heat B8112) to ASTM Specification for Pressure Vessel Plates, Alloy Steels, Quenched and Tempered, Manganese-Molybdenum and Manganese-Molybdenum-Nickel (A 533) grade B class 1, and is designated HSST Plate 012. The allocation of material for the clad plate program has been discussed in Chap. 2. The chemical composition according to analysis performed by ORNL on the material, from melt certification provided by Lukens, and from the ASTM specification is given in Table 3.1. The material used by ORNL for the chemical analysis was a broken Charpy V-notch (CVN) specimen (CP-23) machined from the 0.4t* depth of one of the broken halves of clad plate CP-15.

The cladding and heat treatment of the material used for the clad plate project was performed by CE. Prior to fabrication, CE performed extensive studies in order to optimize the heat treatment required and to produce the necessary properties; the CE report is included as Appendix D. Before cladding, the base metal plate was given a special heat treatment by CE to raise the transition temperature so that it would be brittle at temperatures at which the cladding would be tough. To meet this requirement, the base plate was first given a normalizing treatment in a gas-fired shop furnace at 1032°C (1890°F) for 2 h, followed by cooling in nominally still air with the plate suspended vertically above the shop floor. Prior to heat-treating the plate, an A 533 grade B "picture frame" buffer, 203-mm-thick and 127-mm-wide, had been fillet welded to the plate edges. The part of the base plate destined for the six clad specimens was machined into a large blank, and the cladding was then applied. The completed weldment was given a combined tempering and postweld heat treatment (PWHT) of 593°C (1100°F) for 10 h and then furnace cooled. As mentioned in the CE report (Appendix D), the practice of combining the tempering and PWHT "...is in accordance with paragraph NB 2170, Section III, American Society of Mechanical Engineers (ASME) Boiler and Pressure Vessel Code...," and for brevity the combined tempering and PWHT will be referred to simply as PWHT. The PWHT was milder than typically given a clad light water reactor (LWR) vessel, but produced cladding with Charpy properties similar to those obtained with a typical LWR PWHT [607°C (1125°F) for 40 h], see Fig. 3.1(a). Moreover, the Charpy impact ductile-to-brittle transition temperature (DBTT) of the base plate remained high enough to retain the material properties required by the program, Fig. 3.1(b). This special heat treatment was in addition to one generally performed when the plate is manufactured. The special heat treatment of the clad plates and, for reference, that generally performed in the course of manufacturing A 533 grade B class 1 plates about the time HSST Plate 012 was purchased have been summarized in Table 3.2(a). A PWHT given to a typical LWR pressure vessel [1] has been included in Table 3.2(b) for reference.

---

*The 0.4 refers to the approximate fractional depth in the original t = 178-mm-thick HSST Plate 012 (not of the clad plates) from which the CVN specimens were machined.

Table 3.1. Chemical composition of A 533 grade B Mn-Mo-Ni steel HSST Plate 012B used for clad plate specimens, as determined by ORNL, from Lukens certification for melt 8112, and as specified in ASTM A533B

Element	Composition (wt %)		
	ORNL[a]	Lukens	ASTM A533B-87
Carbon, max	0.25	0.22	0.25
Managanese	1.3	1.32	1.07-1.62
Phosphorus,[b] max	0.005[c]	0.007	0.015
Sulfur,[b] max	0.017	0.013	0.018
Silicon	0.25	0.27	0.13-0.45
Molybdenum	0.54	0.55	0.41-0.64
Nickel	0.43	0.63	0.37-0.73
Copper,[b] max	0.09		0.12
Vanadium,[b] max	0.02[c]		0.06
Aluminum[c]	< 0.002		
Antimony[c]	0.001		
Arsenic[c]	0.01		
Boron[c]	0.0003		
Chromium[c]	0.0150		
Cobalt[c]	0.02		
Niobium[c]	0.0005		
Nitrogen[c]	0.0116		
Oxygen[c]	0.0036		
Tin[c]	0.0005		
Titanium[c]	0.002		
Tungsten[c]	< 0.0003		
Zirconium[c]	< 0.0001		

[a]Performed using 0.4t depth (of original 178-mm-thick HSST Plate 012B) Charpy V-notch specimen CP-23 from clad plate CP-15. Precision of ORNL analysis is ± 5% unless otherwise noted.

[b]Nuclear reactor pressure vessel requirements.

[c]+100%, -50%.

ORNL-DWG 85-4350 ETD

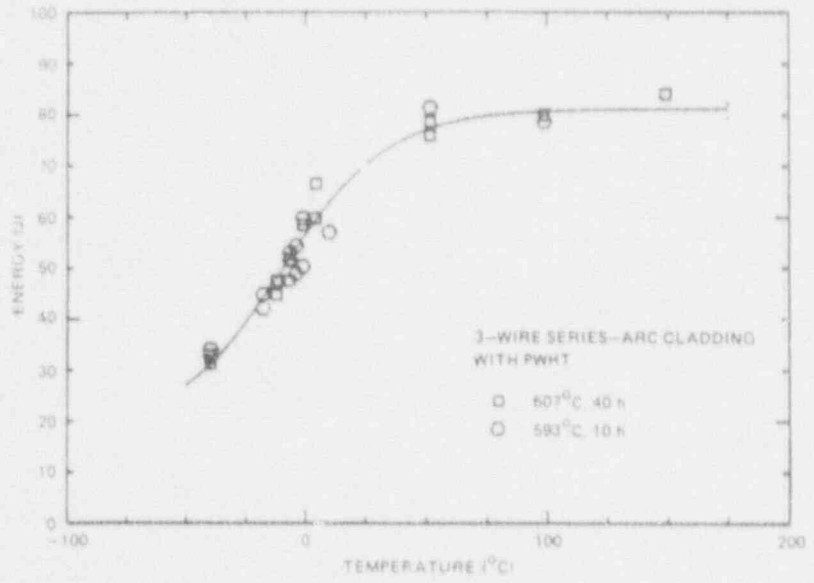

(a)

ORNL-DWG 85-4351 ETD

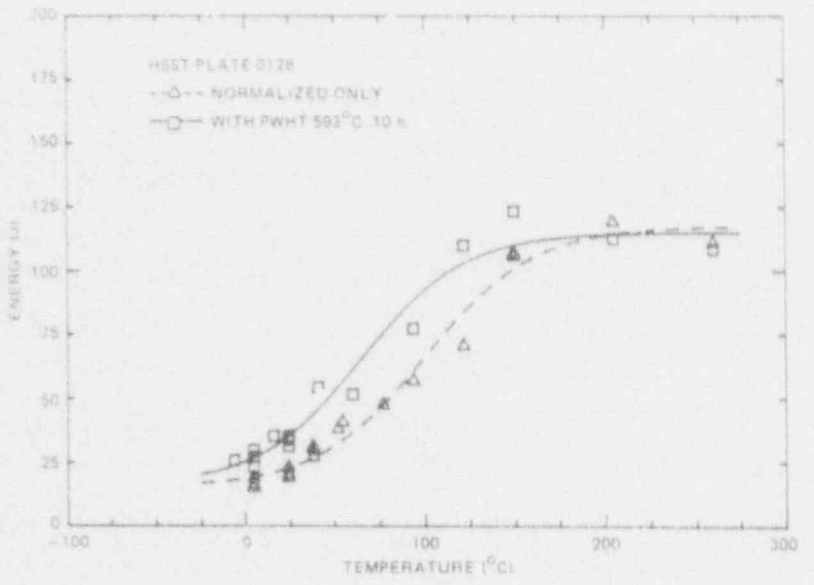

(b)

Fig. 3.1. (a) The milder (573°C/10 h) than typical (607°C/40 h) PWHT has not affected the Charpy V-notch energy of cladding and (b) has only slightly decreased the DBTT of the base metal.

Table 3.2(a). Special heat treatment of clad plate specimens performed by Combustion Engineering on "fabrication base plate" to raise transition temperature (in addition to that performed by Lukens Steel on A 533 grade B class 1 steel plate)

	Temperature, °C (°F)	Time (h)	Type of cooling
Normalizing	1032	2	Air cooled
Postweld heat treatment (PWHT) performed after one-layer three-wire series arc stainless steel weld overlay cladding	593 (1100)	10	Furnace cooled
Typical PWHT for LWR	607-635 (1125-1175)	40[a]	Air cooled

[a]The 40 h is intended to simulate not less than 80% of total time the plate will be subjected to later stress relief, see G. D. Whitman, G. C. Robinson, Jr., and A. W. Savolainen, "A Review of Current Practice in Design, Analysis, Materials, Fabrication, Inspection, and Test," pp. 553, *Technology of Steel Pressure Vessels for Water-Cooled Nuclear Reactors*, ORNL-NSIC-21, Union Carbide Corp. Nuclear Div., Oak Ridge Natl. Lab., Oak Ridge, Tenn., December 1967.

Table 3.2(b). Heat treatment by Lukens Steel for A 533 grade B class 1 material from a test certification dated 11-13-74 for a similar plate[a]

Heat treatment procedure - LS-102 DTD 2/21/69 Rev. 13 DTD 4/16/73 & Spec. Rev. 6/12/73
Plate and tests heated 1630 to 1650°F (888-890°C), held 7.5 h and water quenched (time in quench tank, 30 min), then tempered 1230 to 1250°F (666-677°C), held 8.5 h and water quenched (time in quench tank, 30 min)
Plate and tests stress relieved by heating 1035 to 1065°F (557-574°C), held 4 h and air cooled
Tests stress relieved by heating with a rate of 100°F/h (38°C/h) to 1150°F (621°C), held 50 h and furnace cooled at a rate of 100°F/h to 600°F (316°C)

[a]Two certifications, mechanical properties and heat treatment, by Lukens Steel are available for other melts of A 533 grade B class 1 material. The mechanical properties certification dated 9-26-74 for melt B8112 (HSST Plate 012) is available. The heat treatment certification is missing, but can be assumed that it is the same as the one given above. Both are included in Appendix E.

Pretest materials characterization included tensile, Charpy impact, and drop-weight testing. All specimens were taken from a specially prepared material characterization block. The block was fabricated concurrently with the clad plate specimens using the identical materials and procedures as the plates themselves. The only difference between the plates and the characterization block, other than size, was that the characterization block had three layers of cladding, as compared with only one on the plates, to allow the removal of tensile, Charpy impact, and 0.5TC(T) compact specimens from the cladding. The chemical and microstructural homogeneity and mechanical similarity among the layers was ensured with very careful controls during the fabrication process and verified by testing (see Appendix D).

All tensile specimens were oriented with their axes in the plate rolling direction. The long axis of the large clad plate specimens, the rolling direction of the base metal, and the welding direction in which the cladding was applied are all parallel. Therefore, the deformation in the tensile tests corresponds to the tensile and compressive deformation direction of the plate tests. The results of the tensile tests (Figs. 3.2 and 3.3 and Table 3.3) indicate that in the temperature range of the clad plate specimen, -25 to 25°C, the cladding is appreciably lower in tensile strength but somewhat more ductile (as indicated by the percent total elongation) than the undertempered base metal. Tests of HAZ specimens exhibited strength and tensile ductility properties like those of base metal taken at the quarter-thickness plate location. The agreement of the tensile properties between the quarter-thickness and HAZ locations is consistent with the hardness at both locations which exhibited values of 97 to 98 Rockwell B-hardness (HRB). It is of interest to convert these hardness values to the approximate ultimate tensile strength (UTS). One obtains values ranging from 715 to 750 MPa, which compare well with the measured average value of 727 MPa for base metal. The measured average UTS of HAZ (700 MPa) is somewhat lower than that inferred by the hardness measurement.

The percent total elongation and percent reduction of area of the clad plate materials have indicated an unusual relationship when considered as measures of ductility. As shown by the percent total elongation, the cladding is *more* ductile than either HAZ or base metal. However, when considered from the amount of percent reduction of area, the cladding is *less* ductile than HAZ or base metal. The explanation for this is not known.

The average base metal yield strength of 589 MPa at room temperature is 70% above the typical (quench and tempered) unirradiated A 533 grade B class 1 plate (345 MPa minimum) but is within the range of its postirradiation properties (610 MPa) and, therefore, provides a useful vehicle for performing structural testing applicable to service embrittled reactor pressure vessels. The tensile properties for the plate as delivered by Lukens, then the same material after normalization and PWHT, are given in Table 3.4. The tensile properties of A 533 grade B class 1, both unirradiated and irradiated to 1.8×10^{19} neutrons/cm^2 (> 1 MeV) from [2], and the ASTM specifications for A 533 grade B class 1, have also been included in Table 3.4 for comparison.

ORNL-DWG 86-4097R ETD

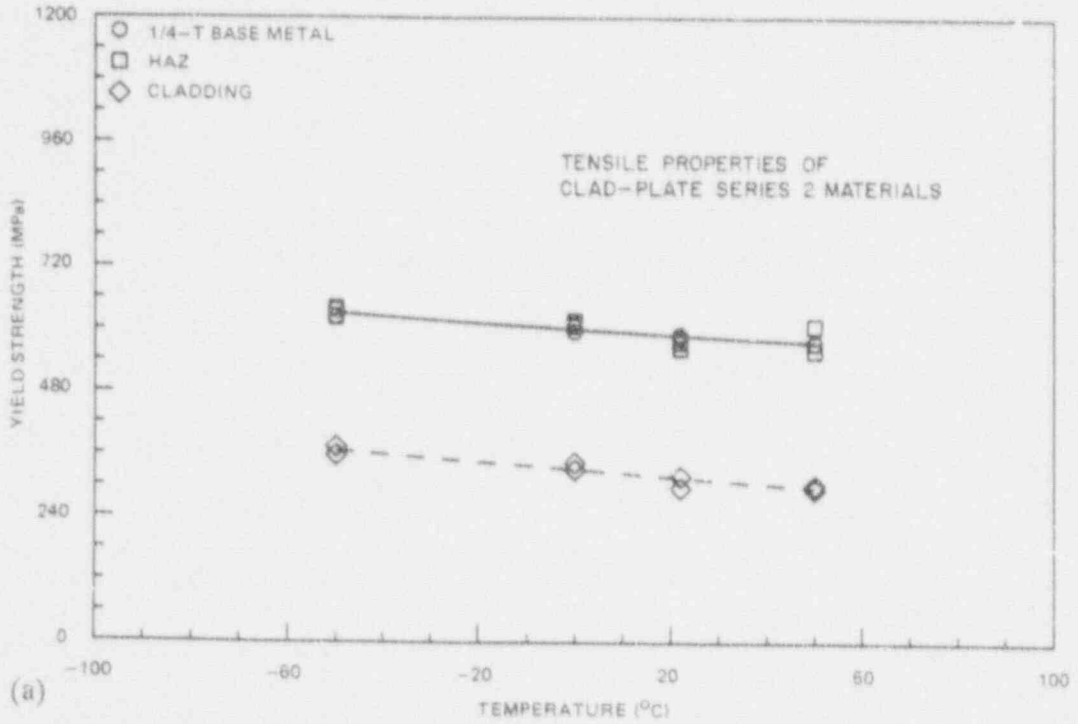

(a)

ORNL-DWG 86-4098R ETD

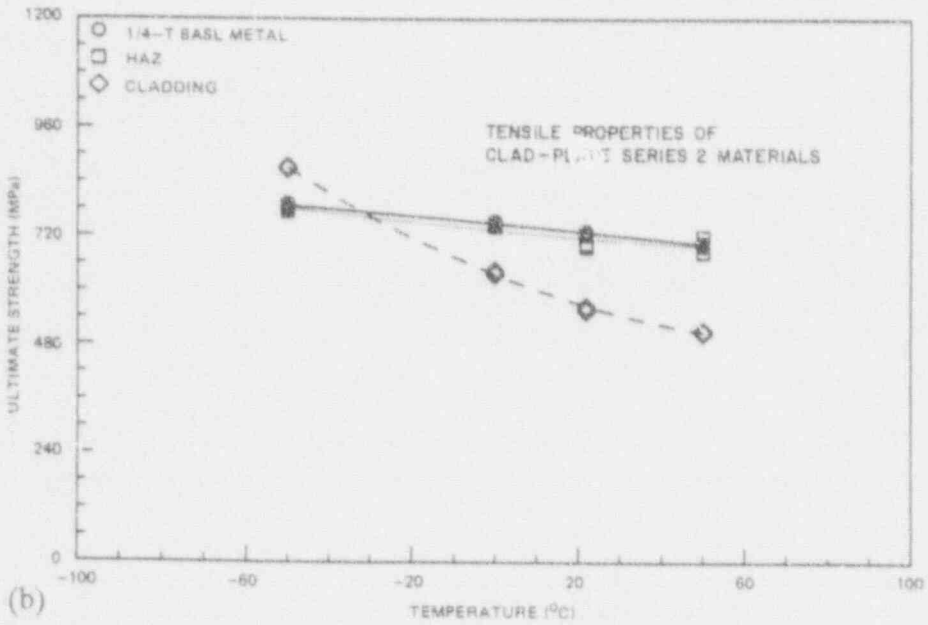

(b)

Fig. 3.2. (a) Yield strength and (b) ultimate strength, as a function of temperature for clad plate materials from the three-layer characterization block. Specimens were longitudinally oriented with respect to the rolling direction of the base metal of the clad plate specimen.

ORNL-DWG 86-4099R ETD

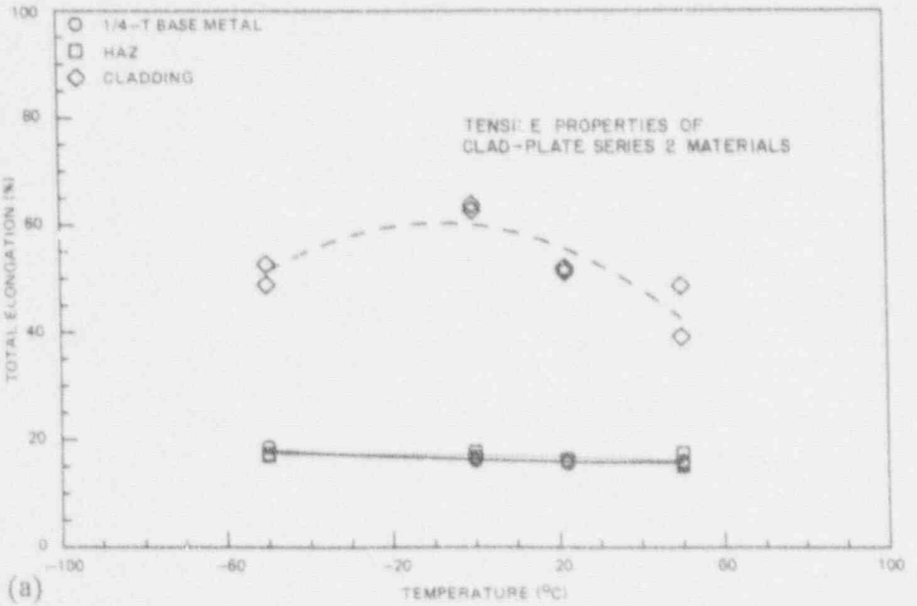

(a)

ORNL-DWG 86-4100R ETD

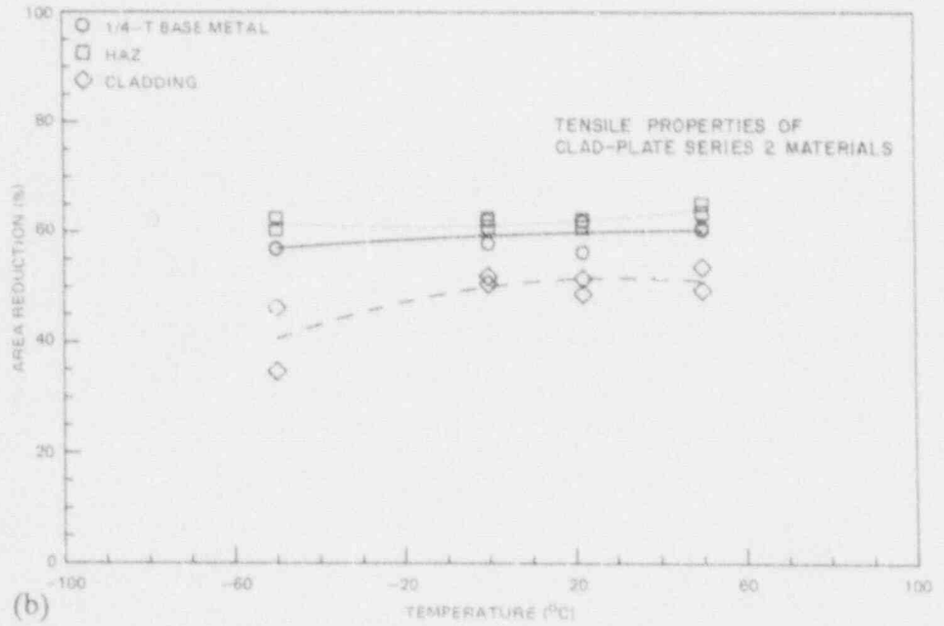

(b)

Fig. 3.3. (a) Elongation percent and (b) reduction of area as a function of temperature for clad plate materials from the three-layer characterization block. Specimens were longitudinally oriented with respect to the rolling direction of the base metal of clad plate specimen.

Table 3.3. Tensile properties of longitudinally oriented specimens of clad plate materials

Test temperature (°C)	Specimen	Strength (MPa)		Total elongation (%)	Reduction of area (%)
		Yield	Ultimate		
		Quarter-thickness base metal			
-50	WC04N	638	792	17	57
	WC15N	624	782	19	57
0	WC04L	608	753	16	58
	WC15L	597	743	17	62
22	WC04K	592	732	16	56
	WC15K	586	723	16	62
50	WC04M	575	699	16	61
	WC15M	575	706	16	61
		Heat-affected zone			
-50	WC04I	641	785	17	62
	WC15I	624	775	17	61
0	WC04G	610	743	18	61
	WC15G	617	748	18	63
22	WC04F	566	697	16	61
	WC15F	578	704	16	62
50	WC04H	608	719	15	64
	WC15H	561	686	17	65
		Weld metal			
-50	WC04D	359	873	53	46
	WC04B	375	868	49	35
0	WC04A	332	635	64	51
	WC04C	345	644	63	52
22	WC15D	297	556	52	52
	WC15B	320	565	51	49
50	WC15A	295	507	49	50
	WC15C	302	511	39	54

Table 3.4. Comparison of room temperature tensile properties of A 533 grade B class 1 steel used in the clad plates in the as-delivered condition, normalized and postweld heat treated with unirradiated/irradiated A 533 grade B class 1 and the ASTM specifications

	Strength (MPa)		Elongation (%)
	Yield	Ultimate	
As delivered (Lukens certification)	455	603	25
Normalized and postweld heat treated	589	709	16
HSST Plate 02:[a]			
Unirradiated	467	622	18
Irradiated[b]	609	749	18
ASTM A 533 grade B class 1 specifications	345[c]	550-690	18[c]

[a]J. J. McGowan, R. K. Nanstad, and K. R. Thoms, *Characterization of Irradiated Current-Practice Welds and A533 Grade B Class 1 Plate for Nuclear Pressure Vessel Service*, NUREG/CR-4880, Vol. 1 (ORNL-6484/V1), Martin Marietta Energy Systems, Inc., Oak Ridge Natl. Lab., Oak Ridge, Tenn., July 1988.

[b]Irradiated at 288°C to 1.8×10^{19} neutrons/cm^2 (> 1 MeV).

[c]Minimum.

Charpy V-notch impact testing of the cladding, HAZ, and base metal was performed on specimens machined in both the L-T and L-S orientations, corresponding to crack extension across and through the thickness of the clad plate specimens, respectively (see Tables 3.5 through 3.7 and Fig. 3.4). Tests to determine nil-ductility-transition (NDT), according to ASTM Test for Conducting Drop-Weight Test to Determine Nil-Ductility-Transition Temperature of Ferritic Steels (E 208-82) were also performed. The detailed results of the drop-weight testing are given in Table 3.8, and have resulted in an NDT of 36°C. The specimen type was P-3, and had a single-pass crack-starter weld bead.

The results show that the cladding has a substantially lower DBTT than base metal. The NDT in the base metal of 36°C corresponds well with the CVN 41-J transition temperatures of 32 and 41°C determined for the L-T and L-S orientations, respectively, of the base metal at the quarter-thickness location, see Table 3.9. These temperatures are in the region at which the upper knee of the CVN impact energy curve occurs for the cladding. Charpy V-notch impact testing of the cladding and base metal confirmed the data provided by CE (Appendix D).

Table 3.5. Charpy V-notch impact energy test results for specimens from the quarter-thickness depth of clad plate characterization block base metal (specially heat treated ASTM A 533 grade B class 1) in the L-T and L-S orientations

Specimen	Test temperature (°C)	Energy (J)	Lateral expansion (mm)	Fracture appearance (% shear)
		L-T orientation		
WC09-N	-100	2	0.013	0
WC09-M	-50	7	0.178	10
WC09-L	0	9	0.089	25
WC10-N	0	14	0.191	10
WC10-O	0	21	0.343	5
WC11-K	24	39	0.622	20
WC10-K	24	49	0.749	25
WC09-K	24	17	0.241	25
WC11-M	50	53	0.775	45
WC11-L	50	53	0.673	45
WC10-L	50	113	1.727	95
WC09-O	50	30	0.470	43
WC11-N	50	76	1.067	65
WC10-M	200	104	1.727	100
WC11-O	300	106	1.727	100
		L-S orientation		
WC02-N	-100	3	0.025	0
WC02-M	-50	11	0.102	1
WC03-N	0	22	0.305	5
WC02-L	0	19	0.241	0
WC02-K	24	25	0.267	5
WC03-K	24	20	0.216	0
WC05-K	24	26	0.305	0
WC03-O	50	51	0.787	40
WC02-O	50	42	0.635	35
WC05-L	75	73	1.041	50
WC05-M	75	81	1.344	60
WC03-L	100	115	1.435	100
WC05-O	100	99	1.499	85
WC03-M	200	105	1.397	100
WC05-N	300	81	1.778	100

Table 3.6. Charpy V-notch impact energy test results for specimens from the heat-affected zone of the three-layer clad plate characterization block in the L-T and L-S orientations

Specimen	Test temperature (°C)	Energy (J)	Lateral expansion (mm)	Fracture appearance (% shear)
		L-T orientation		
WC09-I	-100	3	0.025	0
WC09-H	-50	11	0.152	0
WC11-G	-25	18	0.356	10
WC10-J	-25	45	0.597	30
WC11-J	0	41	0.660	28
WC09-G	0	71	1.003	42
WC10-I	0	50	0.914	40
WC09-F	24	94	0.787	68
WC11-F	24	87	1.295	41
WC10-F	24	89	1.143	80
WC09-J	50	132	1.753	100
WC11-H	50	119	1.549	90
WC10-G	100	142	1.918	100
WC10-H	200	145	1.994	100
WC11-I	300	123	1.892	100
		L-S orientation		
WC02-H	-100	21	0.152	0
WC05-G	-50	60	0.749	23
WC02-N	-50	59	0.775	33
WC03-J	-25	41	0.559	14
WC05-J	0	56	0.686	23
WC02-I	0	77	0.826	42
WC03-I	0	101	1.410	47
WC02-F	24	92	0.965	53
WC05-F	24	97	1.245	67
WC03-F	24	100	1.270	67
WC02-J	50	122	1.702	75
WC05-H	50	96	1.321	70
WC03-G	100	128	1.219	100
WC03-H	200	140	1.918	100
WC05-I	300	121	1.448	100

Table 3.7. Charpy V-notch impact energy test results for three-wire, three-layer stainless steel weld overlay cladding specimens from the clad plate characterization block in the L-T and L-S orientations (L orientation corresponds to the welding direction and the rolling direction of the underlying base metal)

Specimen	Test Temperature (°C)	Energy (J)	Lateral expansion (mm)
L-T orientation			
WC09-E	-100	18	0.318
WC09-D	-50	26	0.546
WC11-D	-25	40	0.800
WC11-C	0	55	1.092
WC11-B	0	54	1.080
WC09-C	0	58	1.181
WC11-A	24	68	1.524
WC10-A	24	67	1.524
WC10-E	24	65	1.384
WC11-E	50	75	1.740
WC09-B	50	77	1.702
WC10-B	100	75	2.121
WC10-C	200	71	2.045
WC10-D	300	68	2.210
L-S orientation			
WC02-E	-100	16	0.140
WC02-D	-50	33	0.343
WC05-C	-25	47	0.699
WC05-B	-25	43	0.635
WC05-D	0	45	0.775
WC02-C	0	5[illegible]	0.673
WC05-E	0	59	0.826
WC02-A	24	65	0.838
WC03-A	24	70	0.775
WC05-A	24	68	1.118
WC02-B	50	71	0.775
WC03-E	50	79	1.864
WC03-B	100	83	0.914
WC03-C	200	72	0.927
WC03-D	300	68	1.105

ORNL-DWG 86-4102 ETDR2

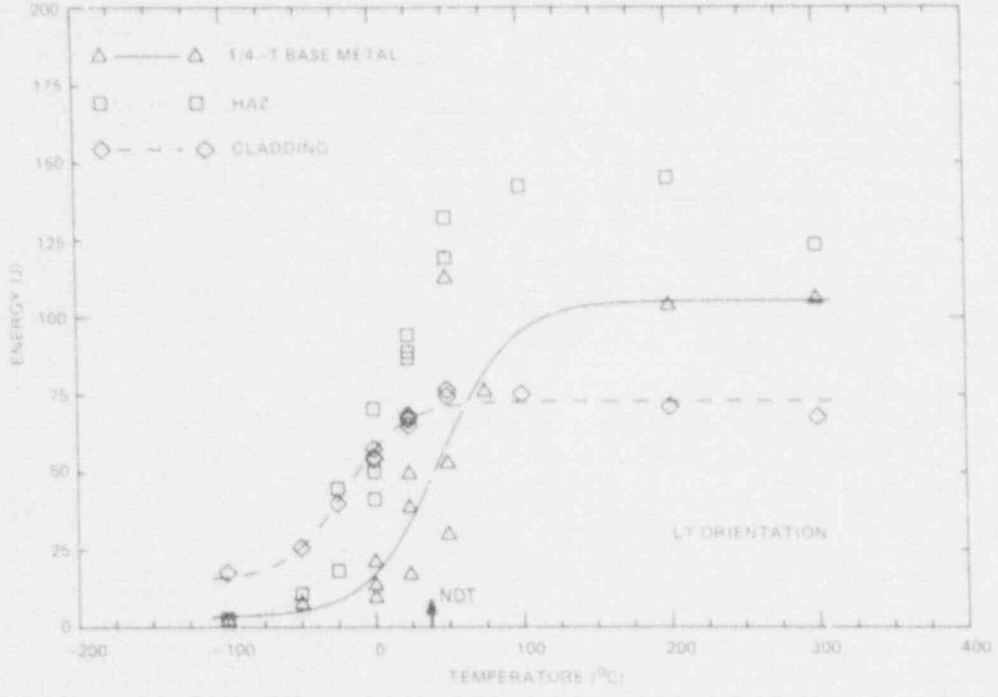

(a)

ORNL-DWG 86-4101 ETDR

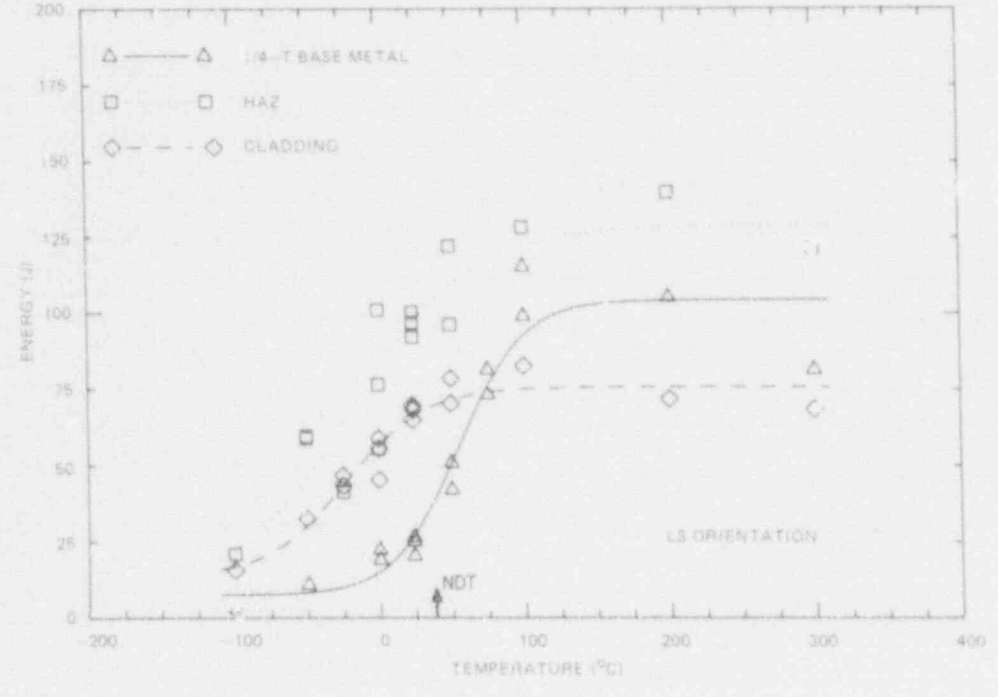

(b)

Fig. 3.4. Results of Charpy V-notch impact tests of clad plate materials in the (a) L-T orientation and (b) L-S orientation.

Table 3.8. Results of drop-weight testing on specially heat treated A 533 grade B, quarter-thickness base metal from the clad plate characterization block (nil-ductility-transition temperature, NDT, is defined in ASTM E 208-82 to be the highest temperature at which a specimen breaks and two tests at a temperature 5°C higher show no-break performance)

Specimen	Test temperature (°C)	Test results	
		Break	No break
3UAB1	25	X	
3UAB2	36	X	
3UAB3	58		X
3UAB4	53		X
3UAB5	47		X
3UAB6	41		X
3UAB7	41		X

NDT = 36°C

Table 3.9. Transition temperatures determined by Charpy V-notch impact tests on clad plate materials from the characterization block with three layers of cladding (drop-weight nil-ductility-transition temperature, NDT, of the quarter-thickness base metal is 36°C)

Material	Orientation[a]	Transition temperature criterion (°C)		
		41 J	68 J	0.889 mm
Cladding	L-T	-24	28	-19[b]
	L-S	-29	36	32[b]
Quarter-thickness base metal	L-T	32	59	51
	L-S	41	66	59
Heat-affected zone	L-T	-12	7	6
	L-S	-59	-19	-14

[a]With respect to the base metal.

[b]Lateral expansion of cladding in L-T orientation appreciably greater than in L-S orientation at all temperatures.

The Charpy transition of the HAZ is also noticeably lower than that of the bulk of the base metal. This is principally the result of the special heat treatment given to the base metal to raise the transition temperature. The base plate was first normalized at 1032°C for 2 h and air cooled. This produced a basically bainitic microstructure with a larger grain size than would be typical in a normally quenched-and-tempered A 533 grade B class 1 steel. This microstructure was needed to achieve a high transition temperature. The plate was then clad and given the mild PWHT at 593°C for 10 h, which tempered it only slightly. By comparison, material in the HAZ was transformed to martensite during the first welding pass and subsequently tempered during the deposition of the successive layers. As expected, this increased the toughness of the HAZ above that of the base metal in a similar manner as the toughness of the HAZ of a reactor pressure vessel is raised by its transformation and the full tempering that occurs during the cladding operation and subsequent normal PWHT of the vessel [3].

The transition temperature of the HAZ in the clad plates is expected to be somewhat higher than that determined from the characterization block because the plates received only one layer of cladding during fabrication. The HAZs have, therefore, not received the additional tempering from the subsequent weld layers that the HAZ of the characterization block received. As shown later in this chapter, the values obtained in posttest measurements of the hardness, yield, and UTS of one clad plate (CP-18) HAZ are indeed higher than those of the characterization block.

The Charpy and drop-weight results show that there is a temperature range from about room temperature down to at least -25°C within which the toughness of the cladding is relatively high and the bulk of the base plate is frangible. However, the HAZ is also tough and; as described in the following chapters, by arresting a running flaw, the HAZ prevented its propagation to the surface. Thus, the HAZ contributed significantly to the enhanced load-bearing capacity of clad plates as compared to unclad plates.

The cladding exhibited a ductile-to-brittle transition as a function of temperature in Charpy impact testing. To ascertain why a nominally austenitic material would exhibit transition behavior typical of a ferritic steel, Corwin et al. [4] examined the fracture path in broken CVN specimens of a single-wire, submerged-arc, oscillating-electrode 308/309 stainless clad deposit. Results showed that below the mid-transition, the fracture preferentially followed the small volume fraction of δ-ferrite present in the cladding. On the Charpy upper shelf, the fracture proceeds primarily through the matrix in a dimple rupture mode, and the ferrite then fails only coincidentally.

The three-wire, stainless steel, weld overlay clad used in this study also exhibited a ductile-to-brittle transition behavior similar to that exhibited by the single-wire, submerged-arc cladding described above. In order to ascertain whether fracture follows the same paths as in the single-wire cladding, two sets of broken CVN specimens of three-wire stainless steel weld overlay clad metal, each set containing two specimens, were examined metallographically. One set of specimens was in the L-T and the other in the L-S orientation. In each set of CVN specimens, one specimen was tested at -100°C and the other at 200°C. Figure 3.5 shows one of the L-T oriented CVN specimens tested at 200°C, and the general appearance of the fracture profile of specimens tested at this temperature. To reveal the fracture profile, all four specimens were sectioned longitudinally and normal to the machined notch whose root is visible in the upper left corner of Fig 3.5. After polishing, the four specimens were etched using Murakami's reagent.

Y212662

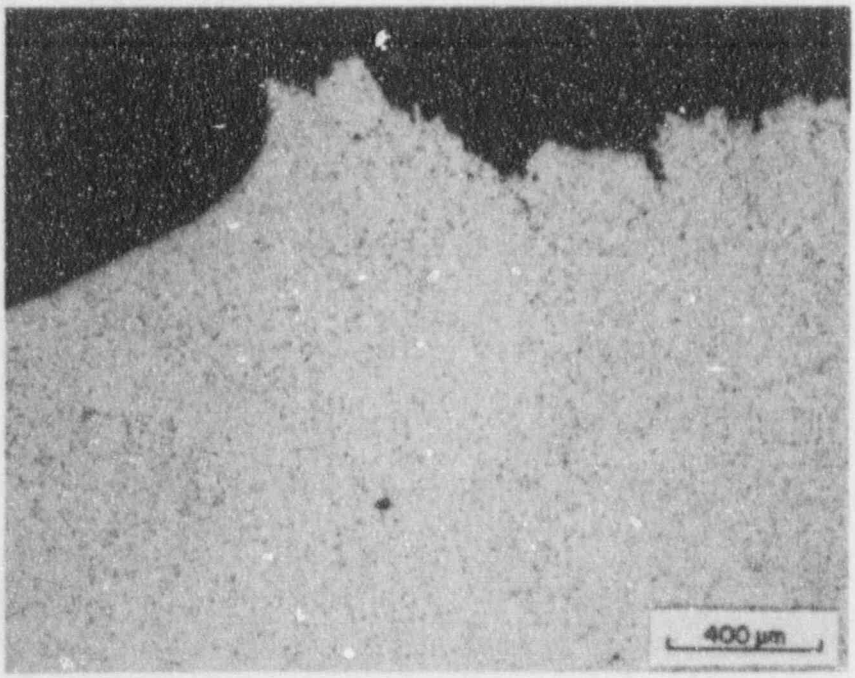

Fig. 3.5. The profile of the fracture surface of three-wire stainless-steel, weld overlay, clad metal, L-T orientation, CVN specimen WC10-C tested at 200° C reveals a dimple rupture mode. The specimen was sectioned longitudinally, and normal to the machined notch which is visible is in the upper-left side of the micrograph (Murakami's etch).

Figures 3.6 and 3.7 show the appearance of the fracture profiles of L-T and L-S orientation specimens, respectively, at higher magnifications than used in Fig. 3.5. Each figure contains profiles of specimens tested at -100 and 200° C. There does not seem to be much difference in the fracture profile between L-T and L-S orientation specimens that were tested at the same temperature. There is, however, a difference in the fracture paths followed: the fracture paths of specimens tested at -100° C, Figs. 3.6(a) and 3.7(a), have followed the δ-ferrite present, more specifically, the γ-δ boundary, whereas the fracture in the specimens tested at 200° C, Figs. 3.6(b) and 3.7(b), proceeded primarily through the austenitic matrix in a dimple rupture mode. This is the same mode of failure that was observed in the single-wire cladding mentioned above. At -100° C, the CVN impact energy of the δ-ferrite is less than that of the austenitic matrix, whereas, at the upper-shelf temperatures of 200° C, the reverse holds.

Two J-R tests of the cladding were conducted at room temperature using 12.5-mm-thick [0.5TC(T)] compact specimens, one each in the L-T and L-S orientation (with respect to the base plate). The data were examined using the linear analysis specified in the ASTM Test for J_{Ic}, a Measure of Fracture Toughness (E 813) edition current at the time, as well as a power law fit.

Y212744

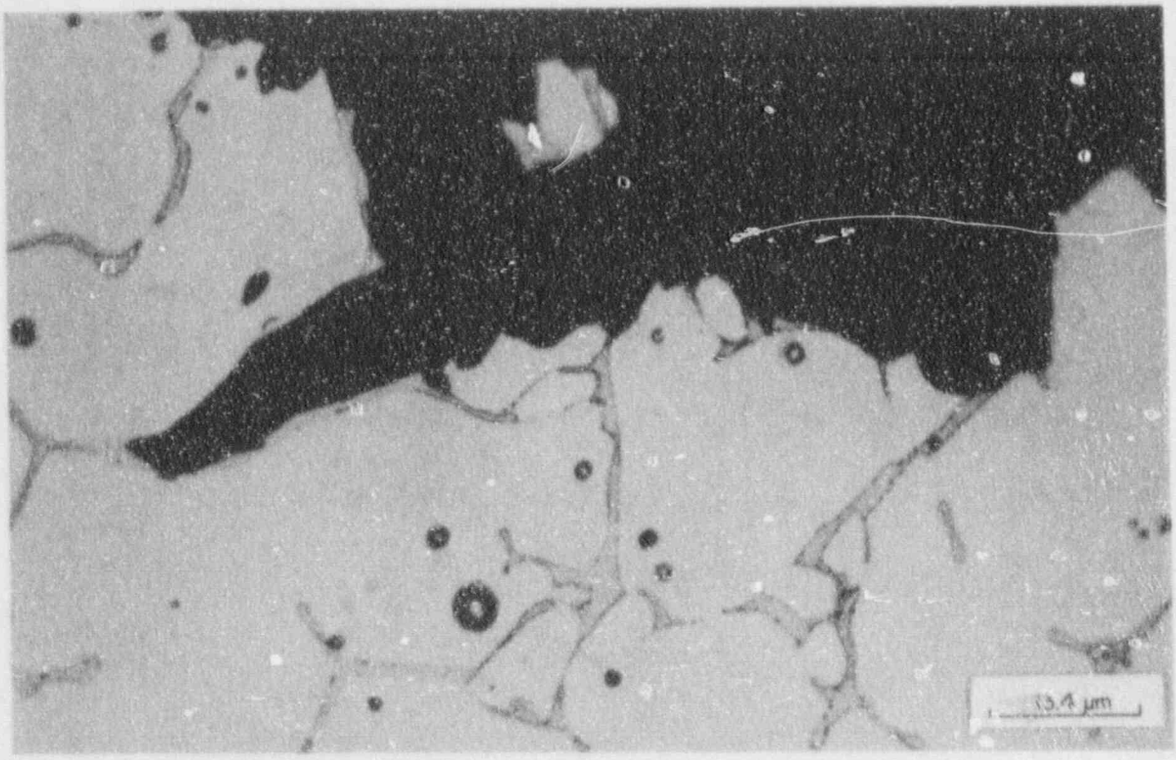

(a)

Y212666

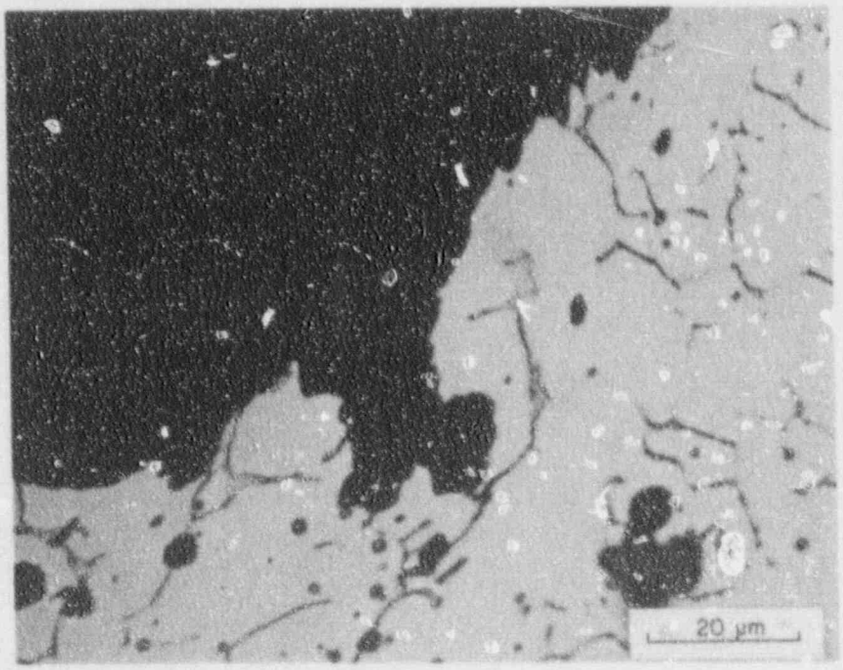

(b)

Fig. 3.6. Profiles of the fracture surfaces of three-wire stainless steel weld overlay, clad metal, L-T orientation, CVN specimens. (a) in specimen WC09-E tested at -100°C the fracture path follows the δ-ferrite. (b) specimen WC10-C tested at 200°C reveals a dimple rupture mode (Murakami's etch).

Y213059

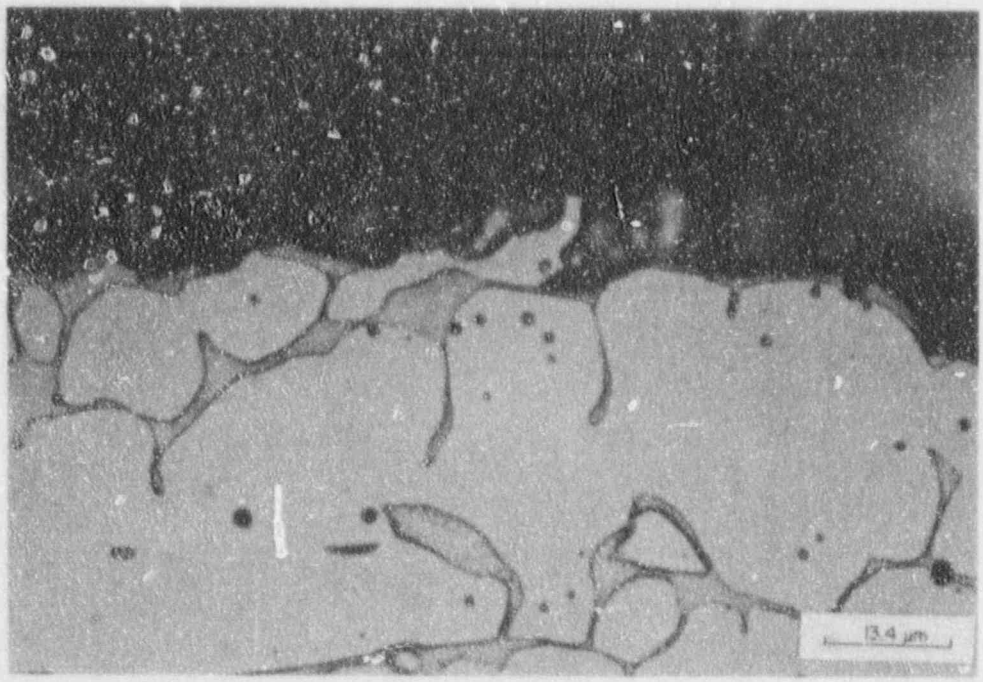

(a)

Y213062

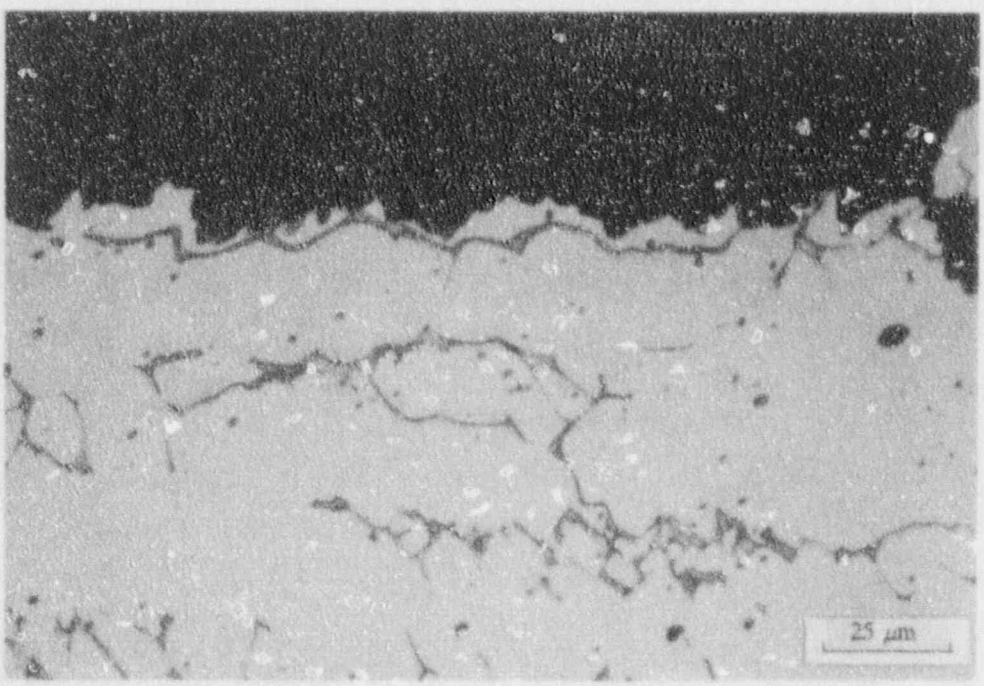

(b)

Fig. 3.7. Profiles of the fracture surfaces of three-wire stainless steel, weld overlay, clad metal, L-S orientation, CVN specimens. (a) in specimen WC02-E tested at -100°C the fracture path follows the δ-ferrite. (b) specimen WC03-C tested at 200°C reveals a dimple rupture mode (Murakami's etch).

The intersections of the regression fits with the 0.15-mm exclusion line were used as measures of J_{Ic}. The results (Fig. 3.8 and Table 3.10) show that both J_{Ic} and the tearing modulus in the L-T orientation were higher than those in the L-S orientation, but that the differences are relatively small. Note that the values of J_{Ic} are not strictly valid because the differences between the final measured and calculated values of crack extension of about 22% for both specimens exceeded the 15% limit allowed in E 813.

3.2. POSTTEST MATERIAL EXAMINATION OF CLAD PLATE MATERIALS

It should be recalled that the plates were clad with a single layer of stainless steel and given a slightly milder postweld heat treatment (593°C for 10 h) than typical for a clad reactor pressure vessel (607-635°C for 40 h). The HAZ from the single-layer clad plates has not received the additional tempering from the subsequent weld layers that occurs in the case of three-layer clad material. The HAZ from single-layer clad material is, therefore, expected to have higher yield and ultimate strengths than HAZ material from the three-layer characterization block. In order to confirm this, tensile tests were performed with specimens machined from the HAZ of one of the broken halves of the clad plates. Crack-arrest and T-L orientation CVN specimens were also manufactured from the large clad plate specimens after their testing was completed. The T-L orientation CVN specimens are required in order to determine the reference nil-ductility transition temperature (RT_{NDT}). A metallographic examination of the various zones across the plate was also performed.

3.2.1 Tensile tests performed

Tensile tests at room temperature have been performed on the base metal, HAZ, and 308 stainless steel weld overlay clad metal. Besides confirming the higher tensile properties expected of the HAZ as discussed earlier, another purpose was to obtain stress-strain curves and Young's modulus for future elastic-plastic finite-element analyses of the clad plate experiments. All tests were performed on L-orientation specimens, where L refers to the main rolling direction of the base metal. For convenience, "L" is also used to designate the tensile specimens oriented along the weld direction of the stainless steel clad metal. The weld direction is also parallel to the rolling direction of the underlying base metal.

The clad and base material tensile specimens were machined from the three-layer clad block used for pretest material characterization. The tensile test results are, therefore, expected to exhibit only small differences from the previously given values. The sizes of the clad and HAZ specimens used for both the stress-strain curves and Young's modulus (E) were limited by the available material. The clad and base metal specimens were 4.55 and 12.5 mm in diameter, respectively. Although the base metal specimens were machined from the three-layer characterization block, their tensile properties should not be affected by the number of weld layers because of distance from the weld zone. Tensile specimens from the HAZ of one of the broken halves of clad plate CP-15 were machined such that the 6.35-mm-gage diameter of the specimens was just below the single-layer cladding.

The results of the tensile tests are given in Table 3.11. Also included are the averages of values from the pretest material characterization from Table 3.3. As expected, the average yield and ultimate strengths of the HAZ of single-layer cladding are approximately 20 and 15% higher, respectively, than HAZ of the three-layer clad characterization block. The base metal and cladding reflect the small scatter associated with tensile testing of a single batch of material.

ORNL-DWG 86-4104A ETDR

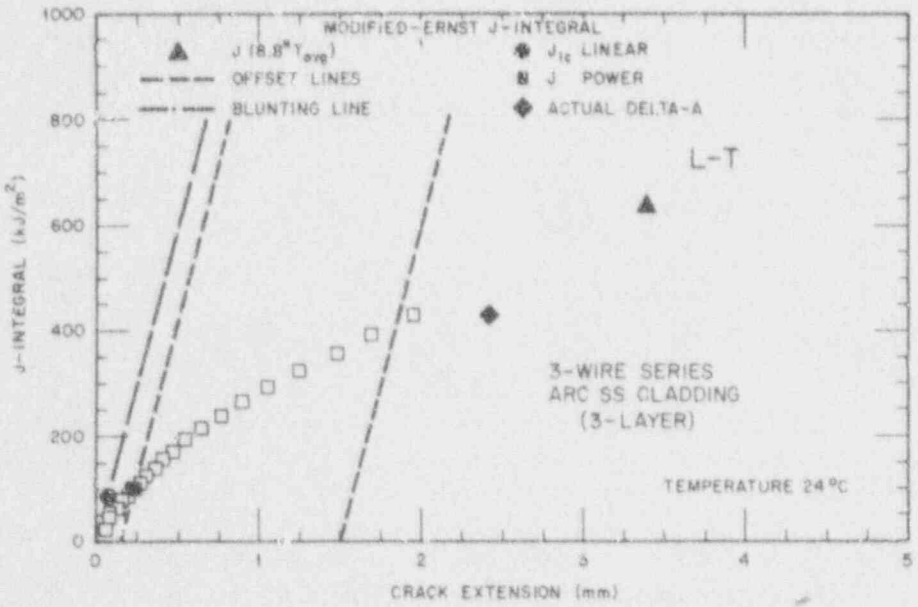

ORNL-DWG 86-4103A ETDR

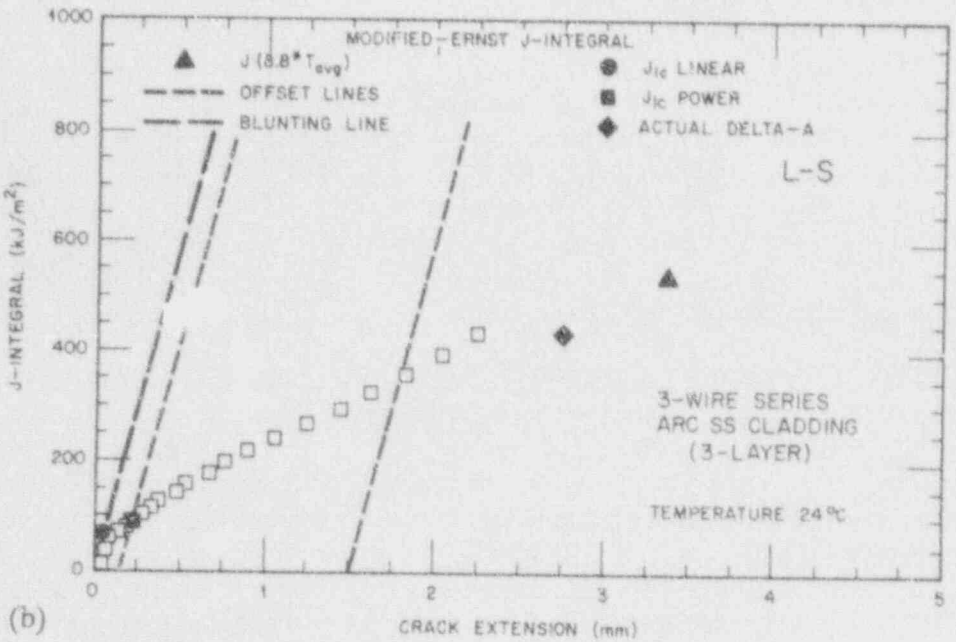

(b)

Fig. 3.8. J-R curves of the stainless steel weld overlay clad metal from the three-layer characterization block obtained using 0.5TC(T) compact specimens in the (a) L-T orientation, and (b) L-S orientation, with respect to the base plate rolling direction and weld direction.

Table 3.10. Results of J-R testing of three-wire series arc weld overlay cladding using 0.5T compact tension specimens

Specimen	Orientation[a]	J_{Ic} (kJ/m^2)		Tearing modulus	J (kJ/m^2)
		Power law	Linear		
WC16A	L-S	91	68	96	531
WC17C	L-T	95	83	113	645

[a]With respect to base metal and welding direction.

Table 3.11. Posttest room temperature tensile properties of heat-affected zone from single-layer clad plate CP-15 and additional results from later tests on base metal and cladding from characterization block [average values from pretest characterization have also been included; all specimens in L-orientation (rolling direction of base metal and welding direction of clad metal)]

Specimen	Test temperature (°C)	Strength (MPa)		Total elongation (%)	Reduction of area (%)
		0.2% yield	Ultimate		
Heat-affected zone posttest from clad plate CP-15					
CP-3	26	674	793	19	66
CP-6	26	720	820	20	63
Pretest average[a]	22	572	700	16	62
Tests on specimens machined from characterization block					
Quarter-thickness base metal					
3UAE5	26	575	708	20	58
3UAE6	24	575	710	19	58
Pretest average[a]	22	589	727	16	59
Stainless steel weld overlay clad metal[b]					
A26A	24	301	574	46	53
A26B	26	297	577	48	57
Pretest average[a]	22	308	561	52	50

[a]Average values from characterization block material, see Table 3.3.

[b]Material also from characterization block, but with extra postweld heat treatment.

Posttest hardness measurements on the HAZ of one of the broken halves of the clad plates showed a hardness of about 101 Rockwell B-hardness (HRB). Although hardness measurements on the Rockwell B scale are not recommended for materials with values greater than 100 HRB, this value is higher than the values measured on the material characterization block (97-98 HRB). A UTS of approximately 820 MPa estimated using this hardness measurement has been confirmed on one of the specimens machined from the HAZ of the plates clad with a single layer.

3.2.2 Determination of Young's modulus

Two L-orientation specimens each from the quarter-thickness depth in base metal, HAZ, and cladding (and of the same dimensions as those used in the tensile tests described above) were instrumented with electric resistance strain gages in order to measure Young's modulus, E, and Poisson's ratio, ν. There were two axial and two circumferential gages on each specimen connected in series, and placed diametrically opposite to each other to eliminate by averaging any bending strains due to misalignment. The measurements were performed at room temperature, approximately 25°C. The specimens were first subjected to three loading and unloading cycles between 0 and approximately 25% of the 0.2% yield strength.

Table 3.12 shows the E and ν values for the clad plate materials. Strain measurements were performed at loads corresponding to the stress ranges shown for each material in Table 3.12, and E calculated as the secant modulus between the upper and lower stresses. The values reported here are the average of four measurements: two each during loading and unloading. Also given are the standard deviations calculated from each set of four measurements. The accuracy of the E and ν values reported is estimated to be about 5 and 10%, respectively, because the strains were about 500 $\mu\epsilon$ for the axial direction and 140 $\mu\epsilon$ for the circumferential direction.

Table 3.12. Young's modulus, E, and Poisson's ratio, ν, for clad plate material at room temperature for L-orientation specimens (rolling direction of base metal and welding direction of clad metal)

Specimen	Specimen diameter (mm)	Stress range (MPa)	Young's modulus (GPa)		Poisson's ratio	
			E	S[a]	ν	S[a]
Quarter-thickness base metal						
3UAE2	12.8	17–138	205	0.7	0.26	0.01
3UAE3	12.8	17–138	210	0.6	0.26	0.002
3UAE5	12.8	17–138	206			
3UAE6	12.8	17–138	204			
Heat-affected zone, posttest from single layer clad plate CP-15						
CP-1	5.08	11–109	205	2	0.27	0.01
CP-2	5.08	11–109	205	1	0.26	0.01
Cladding						
WC04E	4.55	13–68	152	0.4	0.47	0.06
WC15E	4.55	13–68	144	1.4	0.43	0.01

[a]Standard deviation of four values measured with each specimen.

Young's modulus for base metal was also estimated from autographic records made using an averaging liner variable displacement transformer (LVDT) placed over a 50-mm-gage length on specimens 3UAE5 and 3UAE6, see Table 3.12. The averaging LVDT consists of two LVDT gages mounted diametrically opposite each other in order to eliminate by averaging the bending strains. The E values obtained using the LVDTs are in close agreement with those obtained using electric resistance strain gages. Other elastic modulus determinations on low-upper-shelf 2.25Cr-1Mo material using the averaging, 50-mm-gage length LVDT also gave close agreement with elastic moduli determined with electric resistance strain gages [5]. Young's modulus determination is much simpler with a 50-mm LVDT than with electric resistance strain gages, and the use of a 50-mm LVDT would, therefore, be recommended if sufficient material is available for machining 50-mm-gage length specimens.

The lower than expected value of Young's modulus for cladding was initially thought to be incorrect because of specimen misalignment. However, steps to improve the alignment of the load train with the specimen centerline by remachining the ends of the specimen and using dead loads, still gave essentially the same results. A literature search for the elastic constants of 308 stainless steel weld cladding was unsuccessful, but Ref. 6 gives the plane-orthotropic elastic constants of type 308 stainless steel electroslag weld. Young's modulus and Poisson's ratio in the same metallographic direction as in this case gave E-values of 142 GPa and 0.53, respectively. It is assumed that the values reported for cladding are reasonable.

Figures 3.9 through 3.11 are "composite" stress-strain curves produced for base metal, HAZ and cladding, respectively. In the case of the HAZ and stainless steel clad metal, the linear-elastic slopes of the HAZ and cladding stress-strain curves have been adjusted to the average values of E reported above, and then merged with a stress-strain curve deduced from an X-Y plotter record of load vs displacement. The linear portion of the original load-displacement curves for both cladding and HAZ were inaccurate, a reflection of the insufficient accuracy of the small gage lengths of the specimens and the corresponding 12.7-mm-gage length mechanical extensometers. As previously mentioned, tests on base metal with a 50-mm LVDT extensometer gave an initial slope that was in good agreement with E-values determined using electric resistance strain gages and no adjustment was necessary. These curves have also been digitized and are given in Table 3.13.

3.2.3 Determination of RT_{NDT} for base metal

In accordance with Subarticle NB-2330 of the *ASME Boiler and Pressure Vessel Code*, Section III, 1986 Edition, RT_{NDT} is the higher of the drop-weight NDT and (T - 33)°C, where T is defined as the higher of the temperatures at which T-L orientation Charpy specimens attain a 68-J (50-ft-lb) impact energy ***and*** a lateral expansion of 0.89 mm (35 mils).

As presented earlier, the drop-weight NDT of the base metal is 36°C. Full Charpy V-notch impact curves have been developed for the T-L orientation and the results are given in Table 3.14. The CVN specimens were machined from the broken half of clad plate CP-15. They were machined from a location close to the surface of the clad plate that corresponds to approximately the 0.4t depth of the original 178-mm thick HSST Plate 012. Figure 3.12 shows the CVN impact energy, lateral expansion and percent shear fracture appearance. The temperature, T, as defined in NB-2330 has been determined to be 105°C, so the RT_{NDT} of the material is 72°C. Thus, it is the Charpy V-notch energy of the T-L orientation that controlled the RT_{NDT} determination.

The results of the T-L CVN tests have been fitted with a hyperbolic tangent curve. The form of the equation and the regression parameters are given in Table 3.15. The average CVN upper-shelf energy (USE) in the T-L orientation is about 80 J, and the 68-J criterion for the RT_{NDT} was met with only a very small margin. For comparison, the USE in both the L-T and L-S orientations was about 105 J.

3.2.4 Crack-arrest toughness of clad plate base metal

Weld-embrittled (WE) crack-arrest specimens in the L-T orientation were fabricated from the base metal of broken clad plates CP-18 and CP-20. The L-T orientation corresponds to the EB-induced flaw propagating along the surface. Beside characterizing the crack-arrest toughness properties, the specimens were also used to check a special fixture that will be used in the hot cells. The specimens to be tested in the hot cells are from the Sixth Irradiation Series [7], and are in three sizes, 25 × 76 × 76, 25 × 152 × 152, and 33 × 152 × 152 mm. Special jigs will be used with each size, and thus crack-arrest specimens of each of these sizes were fabricated.

As described above, NDT and RT_{NDT} temperatures are 36 and 72°C, respectively, with the T-L orientation CVN values controlling the RT_{NDT} determination. However, the orientation for surface crack propagation in the clad plates is L-T (which, incidentally, fulfills both the 68J and 0.89-mm requirements). Accordingly, the results of the crack-arrest tests have been normalized using the NDT temperature rather than RT_{NDT}.

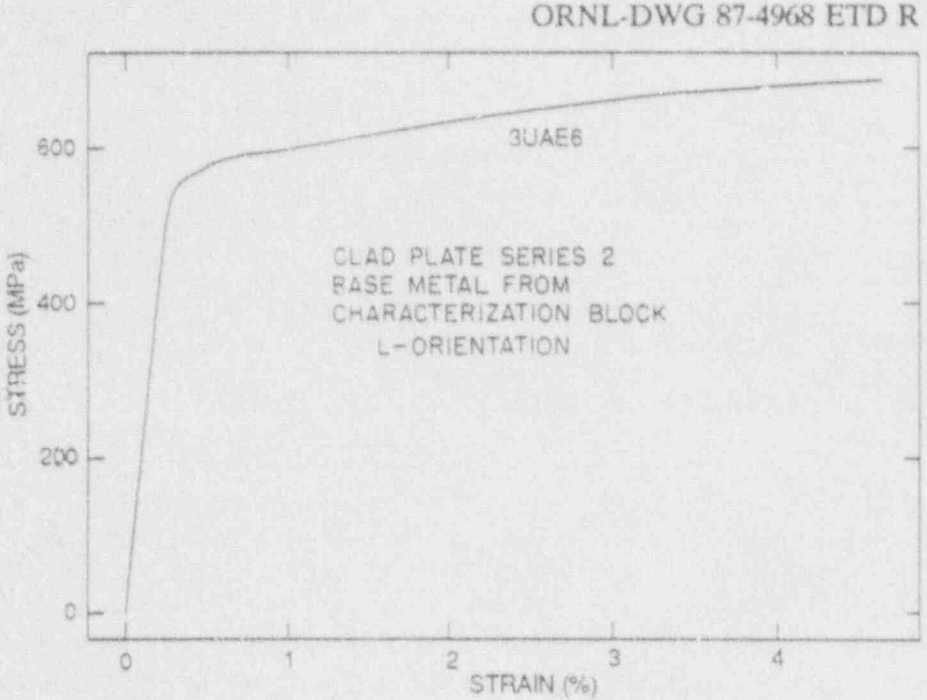

Fig. 3.9. The stress-strain curve for the specially heat-treated (normalized and PWHT) A 533 grade B base metal of clad plates. Specimens were longitudinally oriented with respect to the plate rolling direction.

ORNL-DWG 87-4969 ETD R

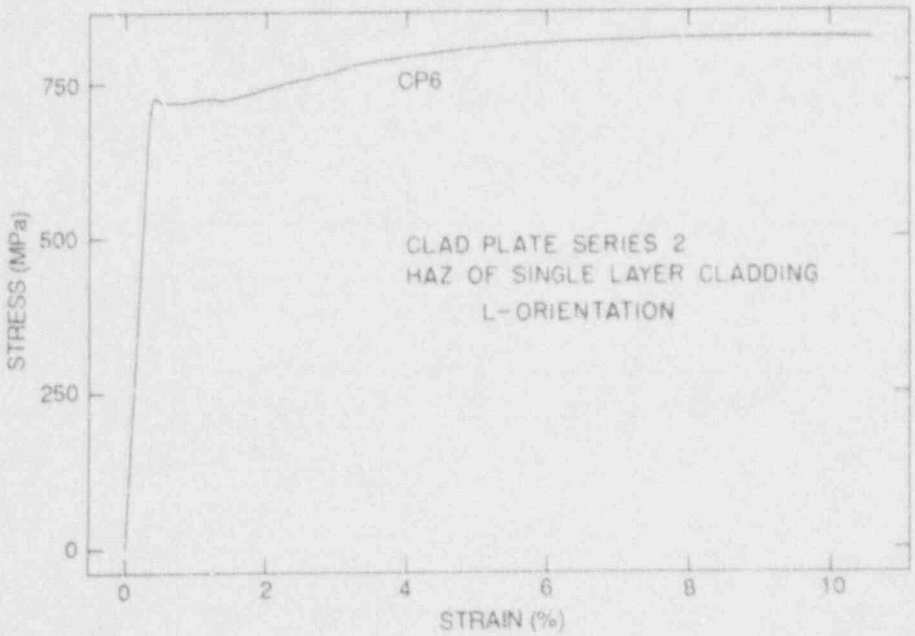

Fig. 3.10. The stress-strain curve for HAZ of single-layer clad plates. Specimens were longitudinally oriented with respect to the plate rolling direction.

ORNL-DWG 87-4970 ETD R

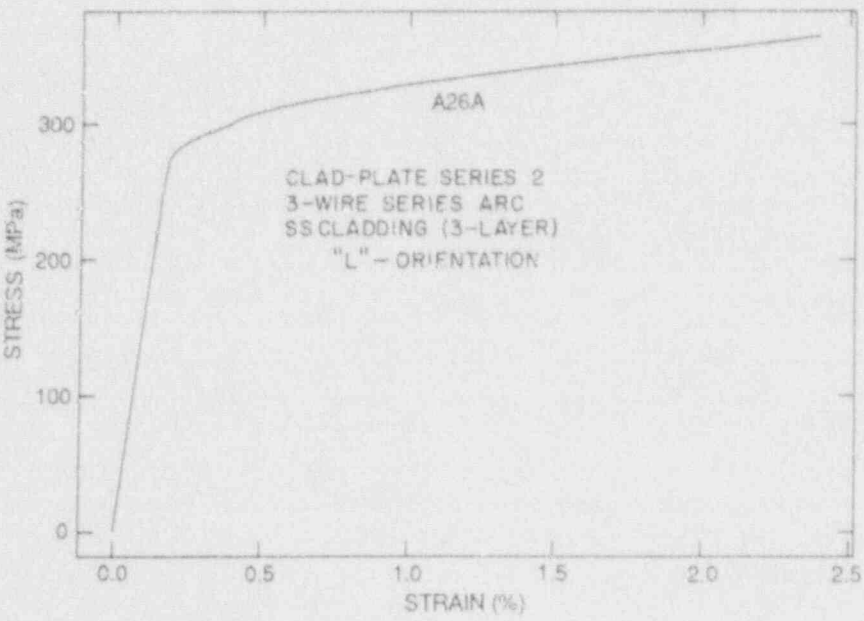

Fig. 3.11. The stress-strain curve for stainless steel weld overlay cladding. Specimens were longitudinally oriented with respect to the rolling direction of the base metal of the clad plate specimen as well as the weld direction.

Table 3.13. Stress and strain values generated by digitizing the load-displacement curves obtained during tensile testing of the clad plate materials: specially heat treated A 533 grade B base metal (specimen 3UAE6-1), heat-affected zone obtained posttest from the one-layer clad plate CP-15 (specimen CP6-1), and three-wire series-arc stainless steel weld overlay cladding (specimen A26A-1) (linear elastic portion was corrected to values obtained during Young's modulus measurements)

3UAE6-1		CP6-1		A26A-1	
Strain (%)	Stress (MPa)	Strain (%)	Stress (MPa)	Strain (%)	Stress (MPa)
0	0	0.004	2	0	0
0.199	409	0.319	644	0.172	263
0.201	413	0.32	655	0.175	266
0.206	422	0.325	663	0.178	269
0.213	436	0.329	670	0.18	271
0.219	447	0.335	678	0.182	273
0.225	458	0.342	686	0.186	275
0.233	473	0.346	692	0.191	277
0.239	483	0.352	698	0.196	278
0.244	492	0.359	704	0.201	280
0.249	499	0.366	709	0.206	281
0.25	500	0.372	713	0.21	282
0.255	507	0.384	719	0.217	283
0.261	515	0.392	722	0.225	284
0.267	522	0.407	725	0.234	285
0.274	528	0.424	726	0.245	287
0.281	533	0.436	726	0.258	288
0.289	538	0.451	726	0.273	289
0.298	543	0.468	724	0.289	292
0.309	547	0.484	723	0.31	293
0.32	550	0.508	720	0.327	295
0.33	553	0.531	719	0.348	296
0.345	556	0.551	719	0.369	298

Table 3.13. (continued)

3UAE6-1		CP5-1		A26A-1	
Strain (%)	Stress (MPa)	Strain (%)	Stress (MPa)	Strain (%)	Stress (MPa)
0.36	559	0.586	719	0.386	300
0.374	560	0.622	718	0.4	301
0.384	562	0.651	719	0.413	303
0.398	563	0.722	719	0.424	304
0.418	566	0.762	719	0.44	306
0.432	567	0.782	719	0.462	307
0.449	570	0.812	718	0.485	308
0.468	571	0.839	719	0.519	310
0.481	572	0.879	719	0.55	312
0.531	580	0.912	720	0.599	314
0.631	586	0.96	721	0.674	318
0.681	589	1.034	723	0.763	321
0.732	592	1.086	725	0.833	324
0.907	595	1.161	724	0.905	326
1.157	604	1.245	725	0.947	328
1.407	613	1.263	725	1	330
1.654	622	1.277	724	1.057	331
1.904	630	1.294	723	1.139	333
2.152	639	1.335	723	1.193	335
2.4	646	1.364	723	1.251	337
2.648	653	1.416	723	1.364	340
2.897	659	1.502	726	1.434	342
3.146	666	1.573	728	1.641	347
3.395	671	1.727	732	1.843	352
3.602	674	1.818	735	2.042	355
3.985	680	1.96	740	2.223	360
4.258	684	2.158	745	2.399	365
4.646	688	2.261	749		

Table 3.13. (continued)

3UAE6-1		CP6-1		A26A-1	
Strain (%)	Stress (MPa)	Strain (%)	Stress (MPa)	Strain (%)	Stress (MPa)
		2.359	752		
		2.563	756		
		2.763	762		
		2.952	767		
		3.262	779		
		3.572	785		
		3.767	789		
		4.061	793		
		4.275	796		
		4.483	799		
		4.78	804		
		5.081	806		
		5.277	808		
		5.64	812		
		5.784	812		
		6.286	815		
		6.785	817		
		7.083	818		
		7.293	819		
		7.626	820		
		7.788	822		
		8.111	821		
		8.527	822		
		9.164	823		
		9.619	823		
		9.689	823		
		9.792	822		
		9.949	822		

Table 3.13. (continued)

3UAE6-1		CP6-1		A26A-4	
Strain (%)	Stress (MPa)	Strain (%)	Stress (MPa)	Strain (%)	Stress (MPa)
		10.128	822		
		10.321	821		
		10.598	820		

Table 3.14. Charpy V-notch impact test results in the T-L orientation (0.4t depth) for the heat-treated A 533 grade B material removed posttest from clad plate CP-15 (normalized at 1032°C for 2 h, air cooled, postweld heat treated at 593°C for 10 h)

Specimen	Test temperature (°C)	Energy (J)	Lateral expansion (mm)	Fracture appearance (% shear)
CP-02	0	5	0.051	6
CP-03	0	5	0.025	5
CP-09	21	29	0.432	21
CP-10	21	24	0.356	15
CP-11	50	49	0.762	39
CP-12	50	36	0.533	30
CP-22	66	40	0.660	40
CP-23	66	37	0.635	40
CP-24	66	36	0.660	35
CP-08	80	36	0.787	52
CP-13	80	48	0.813	44
CP-14	80	53	0.914	57
CP-15	100	77	1.321	99
CP-16	100	67	1.092	73
CP-17	100	67	1.118	70
CP-18	105	72	1.092	90
CP-19	105	77	1.194	95
CP-20	105	81	1.295	100
CP-21	120	74	1.245	98
CP-01	120	69	1.245	100
CP-04	200	66	1.168	100
CP-07	200	81	1.359	100
CP-05	300	81	1.524	100
CP-06	300	83	1.397	100

ORNL-DWG 87-4971 ETD R

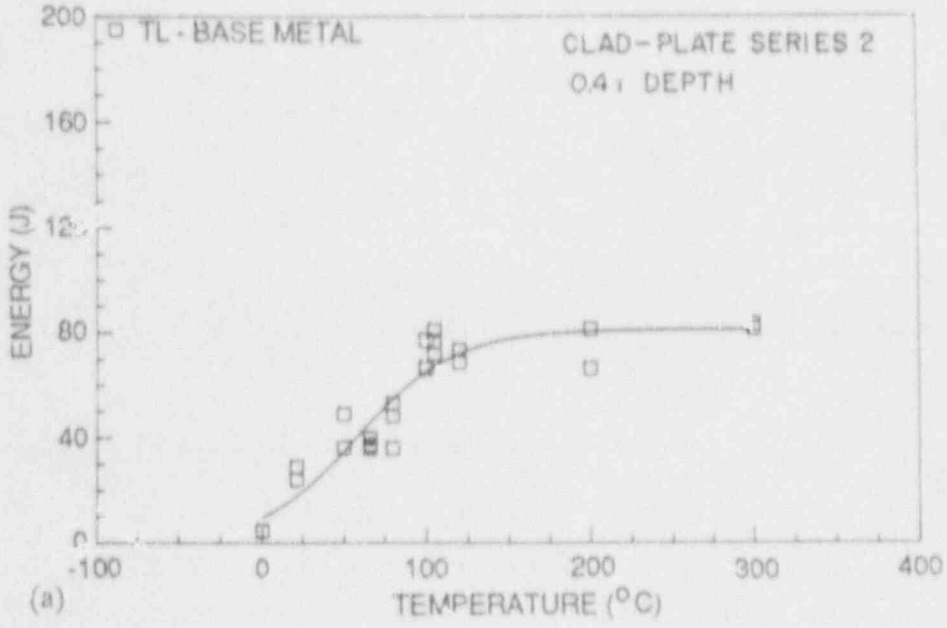

ORNL-DWG 87-4972 ETD R

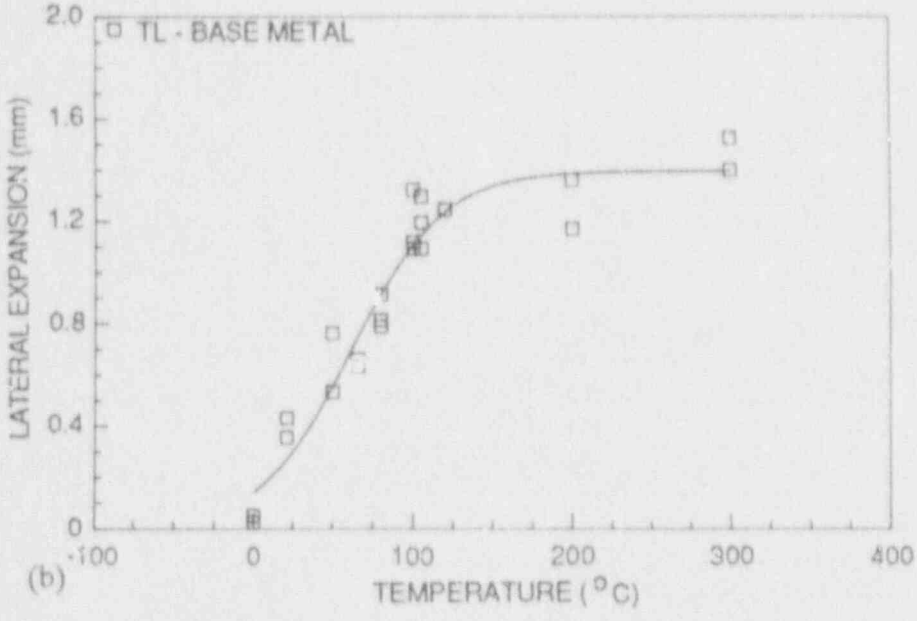

Fig. 3.12. Results of Charpy V-notch impact testing A 533 grade B, quarter-thickness depth material in the T-L orientation from the broken half of clad plate CP-15. (a) impact energy. (b) lateral expansion. (c) percent shear fracture appearance.

ORNL-DWG 87-4973 ETDR

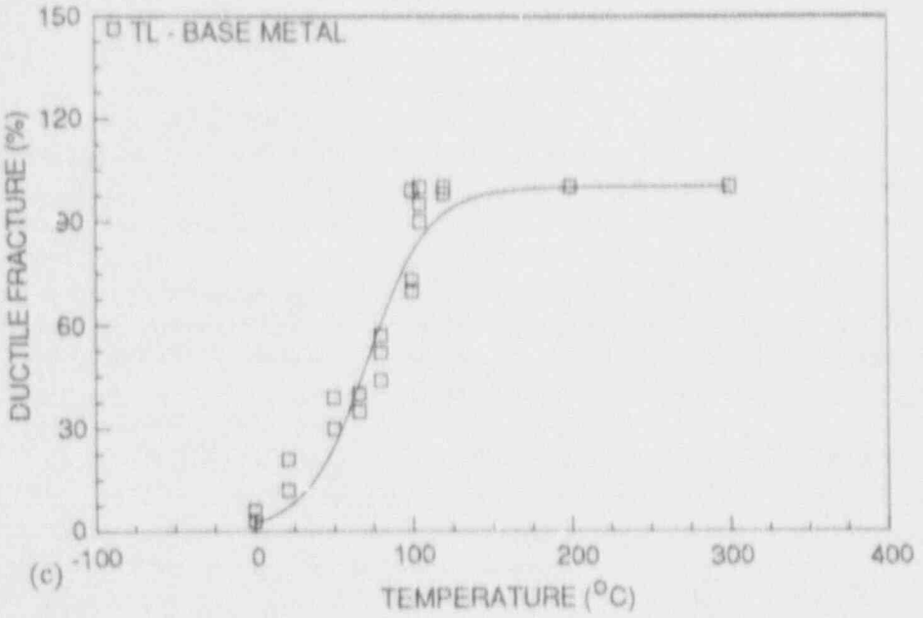

Fig. 3.12. (Continued)

Table 3.15. Form of hyperbolic tangent equation and curve fit parameters resulting from regression analysis for the clad plate base metal Charpy V-notch specimens in various orientations, nil-ductility transition temperature, 36°C

Specimen orientation[a]	$E = (A/2)\{1 + \tanh[B(T - C)]\}^b$			E at NDT (J)	Temperature (°C)	
	A (J)	B (°C^{-1})	C (°C)		41 J	68 J
T-L	81	0.01695	59	26	59	107
L-T	104	0.01964	41	46	31	58
L-S	102	0.02308	48	37	40	64

[a]Specimens for the L-T and L-S orientations were machined from quarter-thickness Jepth material, while those for the T-L orientation were from the 0.4t depth.

[b]T = temperature (°C).

The crack-arrest toughness K_{Ia} was measured according to ASTM Standard Test Method for Determining the Plane-Strain Crack-Arrest Toughness (E 1221-88). The results are shown in Table 3.16. Figure 3.13 shows K_{Ia} plotted vs the test temperature, T. Also plotted on the same figure is the ASME Section XI K_{IR} curve, indexed to the NDT. The results from the smallest specimen size used, 25 × 76 × 76 mm, were all invalid according to ASTM E 1221-88 because the remaining ligament was too small. This specimen size has been used successfully with a WE notch in the control specimens of Sixth HSST Irradiation Series [7]. Therefore, it appears that for this material and this specimen size, a fatigue sharpened notch is required.

Table 3.16 gives the ratio of K_{Ia}/K_{IR}, the mean and standard deviation for the two groups of specimen sizes giving valid results, as well as for all usable results. The two data points below the K_{IR} curve are for specimens with a remaining ligament less than 5% of the nominal specimen width. Such a small ligament has experienced gross plastic deformation and is well beyond the validity range of the compliance expression in ASTM E 1221-88 that is used to calculate K_a. They are obviously outliers and have been disregarded in the analysis of the data. Two other "invalid" values were included in the computations since previous studies have shown that the validity criteria of E 1221-88 may be too restrictive [8]. Although the number of test results in this case is too small to enable definite conclusions, it is instructive to compare the average K_{Ia}/K_{IR} ratios to those obtained in the characterization of the A 533 grade B class 1 steel (HSST Plate 13A) used in Series 1 of the wide-plate tests. The average and standard deviations from the wide plate tests [9] are 1.5 and 0.2, respectively, while the corresponding values from a Battelle Columbus Laboratory (BCL) study on the same HSST Plate 13A are 1.6 and 0.2, respectively [10]. Thus, the mean of the K_{Ia}/K_{IR} ratio and standard deviation from the present study (1.8 and 0.4, respectively), at first glance, may seem to be higher than those obtained in the two previous investigations on the same material. However, in the Battelle study, unusually high K_{Ia}/K_{IR} ratios (2.3 to 2.9) were not included in the averages as they were considered outliers. Also, considering the standard deviation exhibited by the clad plate material, the other two batches of results are within the scatter band of the clad plate data. On the basis of the limited number of results, it seems that K_{Ia} for this material in the temperature range -25 to 75°C is only mildly dependent on temperature.

3.2.5 Metallographic examination of clad plate material

Samples of the base metal from Plate CP-15 were polished and etched to allow the microstructure to be examined. Sections were made parallel to the L, S, and T planes of the plate (Fig. 3.14). Unetched samples allowed the inclusions to be examined, and etching revealed the microstructure. The HAZ resulting from cladding the plates was examined on sections from Plate CP-15 taken parallel to the fracture surface (L) and also perpendicular to the fracture surface, in one of the directions of crack growth (T). A piece of the cladding from Plate CP-15 was also sectioned along the L, S, and T planes, and examined in the etched and unetched conditions.

The microstructure of the base metal (Fig. 3.15) consists of coarse ferrite grains with large grains of fine upper bainite. As the cladding is approached, the HAZ consists of the coarse ferrite grains with a decoration of fine bainite around the edges, which is the result of these grains being heated only slightly into the austenite region. Closer to the cladding, the material is heated further during the cladding application, so more of the ferrite is transformed to austenite, which then forms a fine bainite on recooling. Eventually, the entire structure is heated into the

Table 3.16. Crack arrest test results from L-T orientation specimens fabricated from base material of broken half of clad plate CP-18 (specially heat-treated A 533 grade B chemistry plate, nil-ductility transition temperature, 36°C)

Nominal specimen size (mm)	Specimen number	Test temperature (°C)	K_{Ia} (MPa√m)	K_{Ia}/K_{IR}
33 × 152 × 152	CP9[a]	23	66	1.7
	CP9	23	75	1.9
	CP7	50	61	1.7
	CP10	75	83	1.2
	CP11	75	86	1.3
33 × 152 × 152		K_{Ia}/K_{IR} (mean) ± 1σ = 1.5 ± 0.3		
25 × 152 × 152	CP1	23	80	2.0
	CP2	23	87	2.2
	CP3	-25	80	2.5
	CP4	-25	52[a]	1.6[a]
25 × 152 × 152		K_{Ia}/K_{IR} (mean) ± 1σ = 2.1 ± 0.4		
25 × 76 × 76	CP13	-25	24[b]	0.8
	CP15	-25	23[b]	0.7
	CP18	23	79[a]	2.0
For all valid specimens		K_{Ia}/K_{IR} (mean) ± 1σ = 1.8 ± 0.4		

[a]Invalid according to ASTM E 1221-88 (remaining ligament too small, but used in analysis of data, not included in calculation of K_{Ia}/K_{IR} (mean)).

[b]No test, gross plastic deformation in the entire remaining ligament, and not included in any analysis of the data.

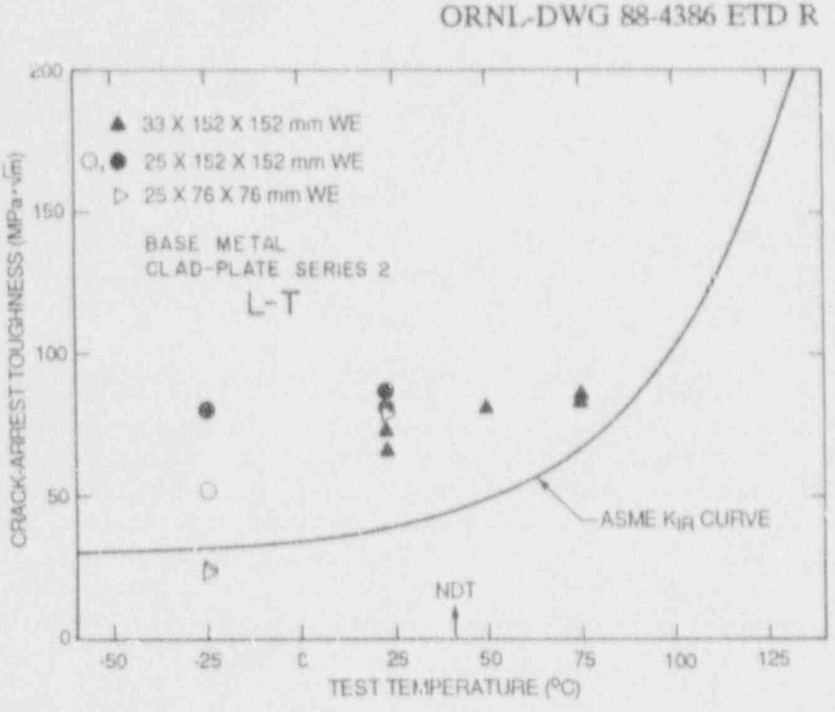

Fig. 3.13. Results of crack-arrest tests on special heat-treated clad plate A 533B base material compared to ASME K_{IR} curve. Open symbols are invalid according to ASTM E 1221-88. The material for the specimens was obtained from the broken half of clad plate CP-18.

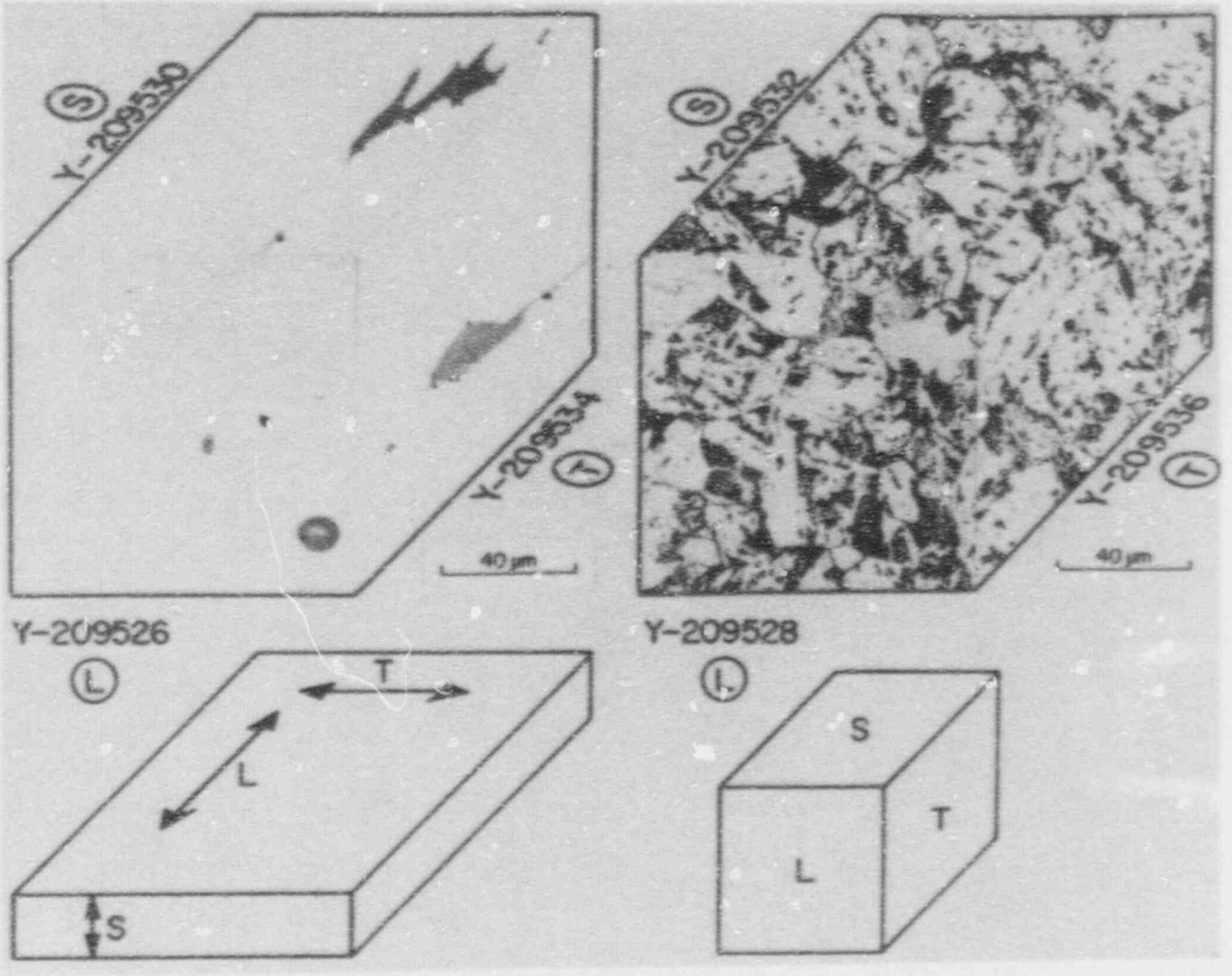

Fig. 3.14. Microstructure of the normalized A 533 grade B, showing the orientation of the L, S, and T planes with respect to the clad plate specimen. (a) unetched. (b) etched.

ORNL-PHOTO 6357-87A

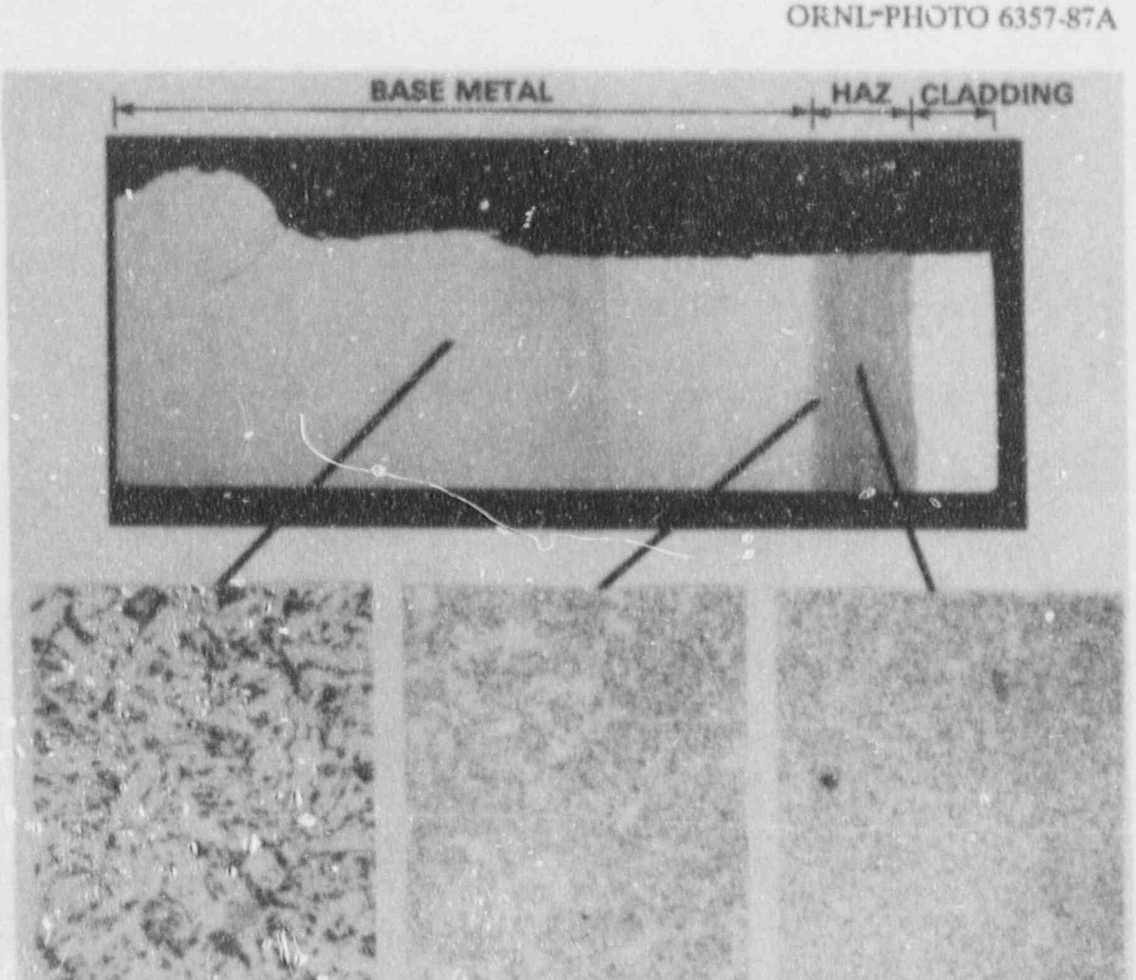

Fig. 3.15. Microstructure of the normalized and tempered A 533 grade B base metal and the heat-affected zone.

austenite region transforming it into fine grains of ferrite and bainite as it cools. Close to the fusion line, the material is heated to higher temperatures, and forms coarse austenite grains, which transform to an acicular bainitic structure on cooling. All of these microstructures are then tempered somewhat during the application of subsequent passes of cladding, with the amount of tempering depending on the location of the material. The cladding on the plate was applied by means of the three-wire process resulting in a deposit 20 mm wide and 4 to 5 mm thick. The HAZ beneath each pass is "scallop-shaped," Fig. 3.16. The HAZ material at the edge of the scallop subjected to subsequent welding passes during the cladding operation will be reheated and tempered significantly, while the HAZ material at the other edge of that scallop will be unaffected. Thus, there will be a gradient in the microstructure and the mechanical properties both through the thickness and across each segment of the HAZ.

YP3823A

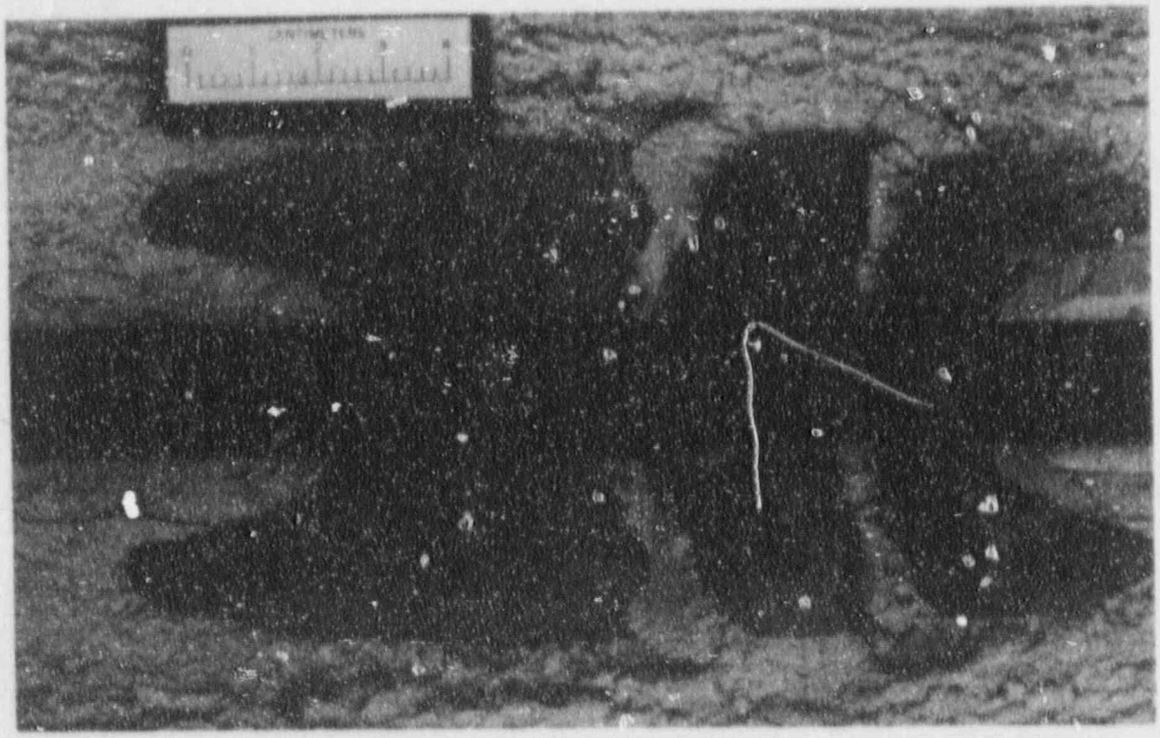

Fig. 3.16. Closeup of the fracture surface from clad plate CP-17 showing the scalloped shape of the HAZ resulting from each weld pass.

The cladding consists of three types of stainless steel wires, deposited simultaneously. This weld metal will also be diluted with some amount of the base metal. The three types of stainless steel wire used were 312, 308, and 309. The cladding microstructure is shown in Fig. 3.17. The bulk of the cladding consists of thin networks of ferrite dispersed within the austenite. The ferrite number (FN) of CVN specimens machined from the three-layer cladding characterization block was measured by a Ferrite Scope, and the results ranged from 4 to 6 FN.

3.2.6 Hardness variation across plate thickness

A microhardness traverse was made across the thickness of the plate on a section taken perpendicular to the final fracture surface (plane T). The result of this traverse is shown in Fig. 3.18. There is some scatter in the data, which is the result of the small indenter sampling different regions in the inhomogeneous microstructure. In spite of this, several features can be noted from the traverse. The cladding and HAZ have the lowest and the highest hardness, respectively. The base metal has a lower hardness than the HAZ, and there seems to be a gradient in the base metal, with the hardness tending to increase toward the "back" of the plate. The "back" of the clad plate specimens originated at the center of the 178-mm plate from which they were fabricated.

To confirm these results, a second traverse was made using the much larger (1.6-mm-diam) indenter of the Rockwell B hardness tester. In order to achieve a fine spacing of the hardness measurements, yet prevent interference between adjacent measurements, the readings were staggered across the specimen surface. These data are also plotted in Fig. 3.18 for comparison with the microhardness data. The same trends are shown by the second set of hardness data, confirming the microhardness results.

3.3 SUMMARY

The results of the material characterization show that plate specimen cladding is significantly weaker in tensile strength than either HAZ or base metal, but the ductility (as measured by the percent total elongation) of the cladding is higher than that of the other two materials. The toughness of the HAZ, as measured by the CVN impact energy at 25°C, and the tensile strength are both higher than those of either the cladding or the base metal. The tough HAZ arrested running flaws and prevented their propagation to the surface (as described in the following chapters). Thus, the HAZ contributed significantly to the enhanced load-bearing capacity of clad plates as compared to unclad ones and has played a dominant role in the behavior of flaws propagating in the vicinity of cladding.

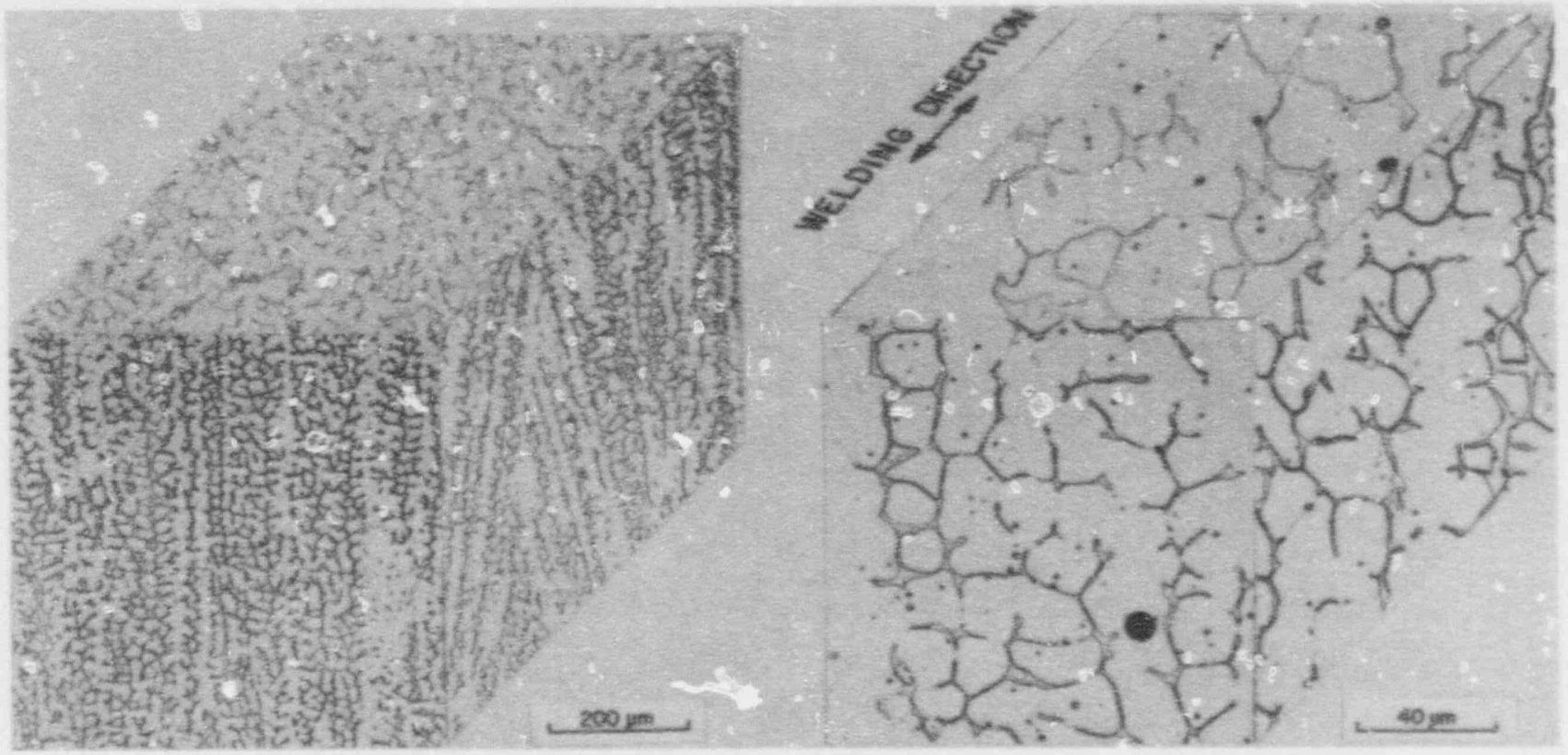

Fig. 3.17. Microstructure of the three-wire series-arc stainless steel cladding.

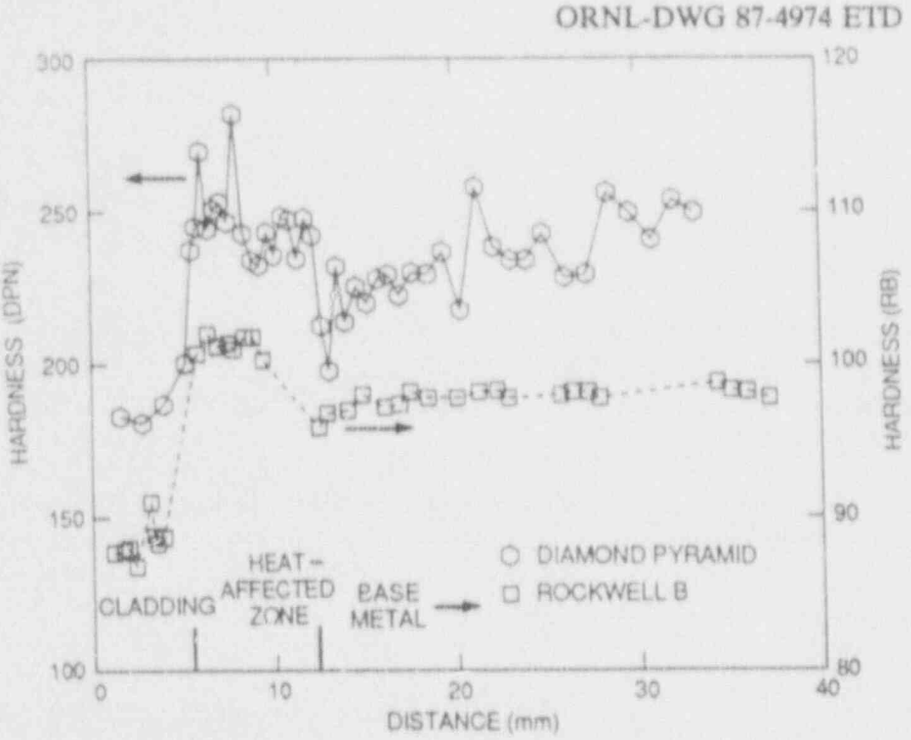

Fig. 3.18. Hardness traverse through cladding, heat-affected zone, and base metal of clad plate CP-15.

REFERENCES

1. G. D. Whitman, G. C. Robinson, Jr., and A. W. Savolainen, "A Review of Current Practice in Design, Analysis, Materials, Fabrication, Inspection, and Test," pp. 553 in *Technology of Steel Pressure Vessels for Water-Cooled Nuclear Reactors*, ORNL-NSIC-21, Union Carbide Corp. Nuclear Div., Oak Ridge Natl. Lab., Oak Ridge, Tenn., December 1967.*

2. J. J. McGowan, R. K. Nanstad, and K. R. Thoms, *Characterization of Irradiated Current-Practice Welds and A 533 Grade B Class 1 Plate for Nuclear Pressure Vessel Service*, USNRC Report NUREG/CR-4880, Vol. 1, (ORNL-6484/V1), Martin Marietta Energy Systems, Inc., Oak Ridge Natl. Lab., Oak Ridge, Tenn., July 1988.*

3. D. A. Canonico, "Significance of Reheat Cracks to the Integrity of Pressure Vessels for Light-Water Reactors," *Weld. J. Research Supplement*, 57(5), 127-s-142-s (May 1979).†

4. W. R. Corwin, R. G. Berggren, R. K. Nanstad, and R. J. Gray, "Fracture Behavior of a Neutron-Irradiated Stainless Steel Submerged Arc Weld Cladding Overlay," pp. 199-221 in *Nucl. Eng. Des.* 89, 1985.†

---

*Available for purchase from National Technical Information Service, Springfield, VA 22161.
†Available in public technical libraries.

5. R. K. Nanstad et al., "Low-Upper-Shelf Material Characterization", pp. 86 in *Heavy-Section Steel Technology Program Semiannual Progress Report for April-September 1987*, USNRC Report NUREG/CR-4219, Vol. 4, No. 2 (ORNL/TM-9593/V4&N2), Martin Marietta Energy Systems, Inc., Oak Ridge Natl. Lab., Oak Ridge, Tenn., April 1988.*

6. B. R. Dewey, L. Adler, R.T. King and K. V. King, "Measurements of Anisotropic Elastic Constants of Type 308 Stainless Steel Electroslag Welds," pp. 420-26 in *Experimental Mechanics*, 17(11), November 1977.†

7. S. K. Iskander, W. R. Corwin, and R. K. Nanstad, *Results of Crack-Arrest Tests on Two Irradiated High-Copper Welds*, USNRC Report NUREG/CR-5584 (ORNL/TM-11575), Martin Marietta Energy Systems, Inc., Oak Ridge Natl. Lab, Oak Ridge, Tenn., December 1990.*

8. R. K. Nanstad et al., "Low-Upper-Shelf Material Characterization," pp. 51-54 in *Heavy-Section Steel Technology Program Semiannual Progress Report for October 1986-March 1987*, USNRC Report NUREG/CR-4219, Vol. 4, No. 1 (ORNL/TM-9593/V4&N1), Martin Marietta Energy Systems, Inc., Oak Ridge Natl. Lab., Oak Ridge, Tenn., August 1987.*

9. W. R. Corwin et al., "Crack-Arrest Test Results in Support of Wide Plate Testing," pp. 54-56 in *Heavy-Section Steel Technology Program Semiannual Progress Report for April-September 1985*, USNRC Report NUREG/CR-4219, Vol. 2 (ORNL/TM-9593/V2), Martin Marietta Energy Systems, Inc., Oak Ridge Natl. Lab., Oak Ridge, Tenn., January 1986.*

10. A. R. Rosenfield et al., "Crack-Arrest Studies at Battelle Columbus," pp. 102-9 in *Heavy-Section Steel Technology Program Semiannual Progress Report for April-September 1984*, USNRC Report NUREG/CR-3744, Vol. 2 (ORNL/TM-9154/V2), Martin Marietta Energy Systems. Inc., Oak Ridge Natl. Lab., Oak Ridge, Tenn., December 1984.*

---

*Available for purchase from National Technical Information Service, Springfield, VA 22161.
†Available in public technical libraries.

4. EXPERIMENTAL OBSERVATIONS FROM TESTS ON PLATES

In Chap. 2, the types of tests performed were designated as either "arrest" or "initiation" tests depending on whether or not the plates contained a preexisting flaw. The type of tests performed on the plates and the loads and strains at which various events took place are summarized in Table 4.1. The tests will be described in detail in this chapter in the order in which the tests were performed, and the results will be discussed further in Chap. 5. Six *initially unflawed* plates were loaded to induce a specified strain level on the surface of the base metal. The EB weld was then hydrogen charged, while the load was maintained constant using stroke control, until a flaw initiated. This type of test on an *initially unflawed* plate is thus essentially an *arrest* experiment, the purpose of which is to study the effect of cladding on a running flaw. In the remaining two plates, a flaw was induced in the EB weld by hydrogen charging with no load applied. Each plate was then mounted in the testing machine and the load increased at a uniform rate under stroke control until this preexisting flaw either popped-in and arrested, or the entire plate ruptured. Thus, the difference between the initial tests on these two plates and the six mentioned above is the presence of a flaw, when the plates were first mounted in the test machine. The tests of the second type, as well as those performed on plates with an arrested flaw, are designated as *initiation* tests. The objective of the "initiation" tests was to determine the load-bearing capacity of the flawed plates.

Table 4.1. Test conditions and results for the eight plates tested

Plate	Condition	Type of test[a]	Test Temperature (°C)	Load (kN)		Surface strain (%)
				Initiation	Postarrest	
CP-15	Clad	A	25	676	654	0.31
		I	-25	759	709	
		I	-100	600	b	
CP-17	Clad[c]	A	25	890	823	0.45
		I	-25	756/725	b	
CP-19	Clad	A	25	987	689	0.65
		I	-50	703	b	
CP-21	Unclad	A	25	676	b	0.27
CP-18	Clad	A	-25	823	649	0.39
		I	-25	698	b	
CP-20	Clad	A	-25	868	b	0.41
CP-16	Clad	I	21	703	694	0.3
		I	21	890	738	
		I	-25	698	b	
CP-22	Unclad	I	21	685	b	0.3

[a]A = arrest, I = initiation.

[b]Plate ruptured in two pieces.

[c]Several pop-ins occurred before rupture.

The first three clad plates (CP-15, -17 and -19) were initially tested in the "arrest" mode at room temperature. Plate CP-15 was loaded to a target strain level of 0.31%, which approximated yield in the base metal on the surface of the plate. At that strain, the crack arrested and the plate did not rupture; therefore, the initial load on the next two plates, CP-17 and -19, was increased to higher strain levels in order to increase the energy available for crack propagation. They did not rupture either; and, since we had almost attained the maximum loading capacity of the machine, the remaining two clad plates, CP-18 and -20, were initially tested at lower temperatures. The unclad plate, CP-21, was tested at room temperature at a target strain that corresponded to yield of the base metal on the surface of the plate, the same as the first plate tested. The unclad plate ruptured, which indicated that the cladding had contributed considerably to the load carrying capacity of the clad plates as compared to that of the unclad plate.

The remaining two plates, CP-16 and -22, were tested in the "initiation" mode in which an initially flawed plate was loaded at room temperature. The load was monotonically increased until the flaw popped or the plate ruptured. The flaw in clad plate CP-16 popped and then arrested, whereas, in the case of the unclad plate CP-22, the plate ruptured in two. The load in initiation type tests may be termed the "critical" load for the existing flaw, in contrast to the "hypercritical" loads to which the plates were loaded during the "arrest" experiments.

4.1 TESTING OF CLAD PLATE CP-15

Clad plate CP-15 was loaded at room temperature to 676 kN. This load was calculated to induce a stress in the uniform moment span of the plate equal to the yield strength of the base metal (596 MPa). The measured surface strain in the base metal was 0.31%. The EB weld zone was then hydrogen charged while the load was maintained constant using machine ram stroke control. Pop-in occurred within about 1 h, the load dropping about 3% and arresting* at 654 kN. The plate was removed from the testing machine and heat-tinted at 325°C. The plate was reinstalled, cooled to -25°C, and loaded at a constant machine ram displacement rate. A second pop-in occurred at a load of 759 kN, with arrest occurring at 709 kN (a load drop of 7%). The plate was removed from the testing machine and heat-tinted at 250°C. The plate was re..stalled in the testing machine, cooled to -100°C, and the load increased at a uniform rate until the plate broke completely at 600 kN. Figure 4.1 shows the two broken halves of the 150-kg test specimen with heat-tinted shapes of the first and second pop-ins. The fracture surface has been examined in detail and is described in a later section.

After the first pop-in event, a surface crack in the HAZ of the EB weld could be discerned, but it did not appear to have extended on the surface. Instead, a small concave dimple extended transversely from the ends of the flaw, indicating that the flaw extended under the surface. The extension of the transverse dimple stopped short of the cladding. The crack had actually propagated in the base metal just below the surface until it encountered the HAZ. A very thin layer of metal covered the flaw.

---

*The load at arrest is more accurately termed the "post-arrest" load for reasons discussed in Chap. 5. For brevity, it will be termed the arrest load in this chapter.

YP3768

Fig. 4.1. The broken halves of the 150-kg clad test specimen CP-15 with heat-tinted shapes of the first and second pop-ins.

During the second pop-in, the flaw *appeared* to have extended in the base metal along the previously dimpled surface just a few millimeters on either side of the previous flaw. The resulting 70-mm flaw length on the surface was still quite short of the 114-mm flaw length needed to reach the cladding. As will be described later, the flaw had in fact propagated beneath the cladding and its HAZ on both sides and had been prevented by the HAZ or the cladding from becoming a surface crack. The dimple extended into the cladding about 5 to 10 mm. The surface extension of the flaw in the base metal was merely the rupturing of the thin layer mentioned above. Figure 4.2 shows the surface crack in the HAZ of the EB weld after the second pop-in (top center), extending as very shallow troughs or dimples into the cladding on either side. The crater on the left of the crack was formed during EB welding and not during testing. Note the buckled weldable strain gages, indicating the large COD to which they had been subjected.

After the second pop-in, due to the lack of observable flaw extension along the surface, the plate was X-rayed, and examined ultrasonically and with dye penetrant. The X-ray and ultrasonic examinations indicated a subsurface flaw about 27 cm long. The dye penetrant failed to reveal any extensions of the flaw on the surface beyond those observed visually, see Fig. 4.3. The thin surface layer over the portion of the flaw residing in the base metal had only partially ruptured, thus blocking the dye penetrant from indicating that portion of the flaw. The details of the dye penetrant and ultrasonic examination are given in a later section.

YP3755

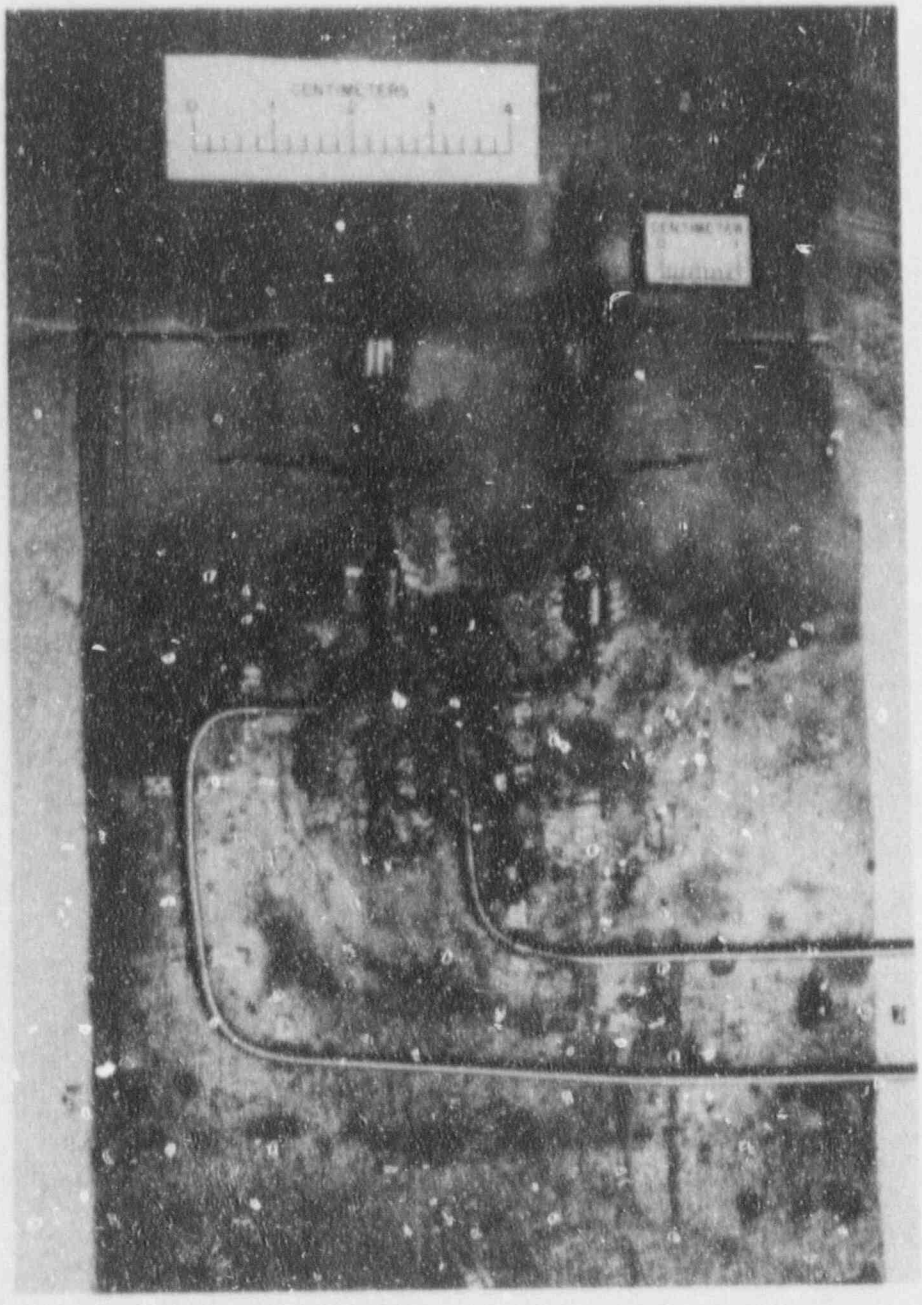

Fig. 4.2. Surface crack in the heat-affected zone of the electron beam weld of clad plate CP-15 after the second pop-in (top center), extending as dimples into the cladding on either side. The crater on the left of the crack was formed during electron beam welding and not during testing.

YP3754

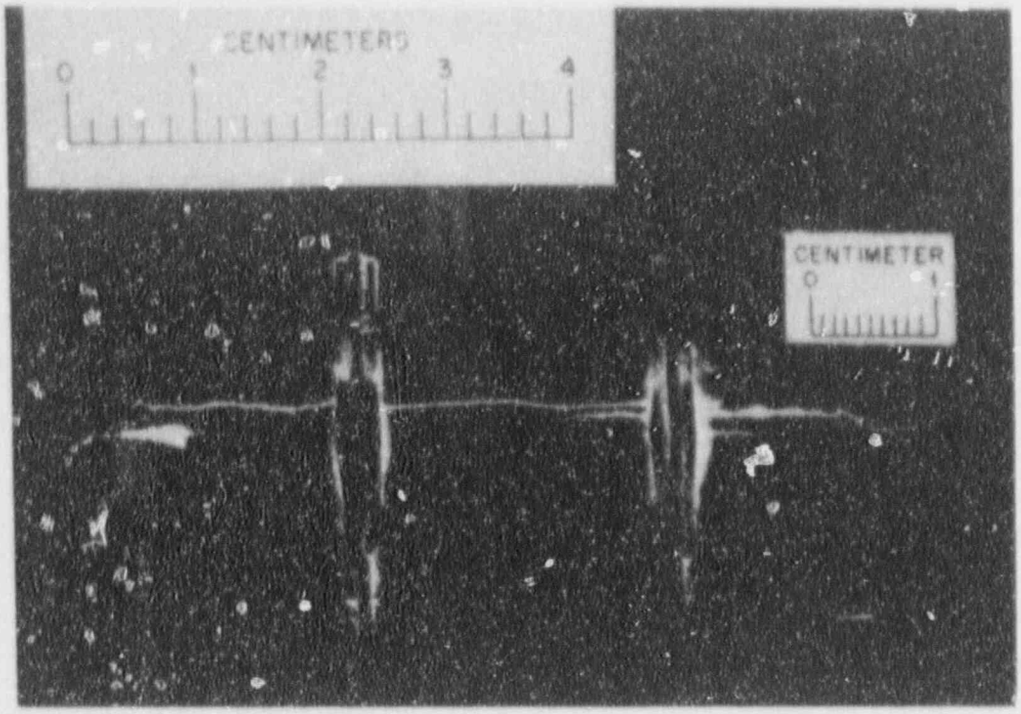

Fig. 4.3. Dye penetrant examination of clad plate CP-15 after the second pop-in failed to reveal any extensions of the flaw on the surface beyond those observed visually.

4.1.1 Fractography of clad plate CP-15

The fracture surface of plate CP-15 was examined to determine the profile of the crack front at the arrest events. For this specimen, the initial fracture and arrest occurred at room temperature, the second fracture and arrest occurred at -25°C, and the final fracture of the plate was at -100°C. Heat-tinting was used to mark the crack front after the two arrest events.

After the final fracture, examinations and optical micrographs were made of the fracture surface. The fracture surfaces were then cut from both of the fractured specimen halves. One was then cut into smaller sections to allow further examination using a SEM.

4.1.2 First pop-in event

The initial event, which occurred at room temperature, initiated in the HAZ of the EB weld and propagated down into the plate as well as extending out to either side. Near the surface, the crack was arrested on either end by the HAZ associated with the cladding. The result was the bowed-out shape shown in Fig. 4.4. The fracture mode during this event was cleavage, all the way to the arrest location. There is no evidence of ductile fracture at the arrest point, as is shown in Fig. 4.5.

YP3763

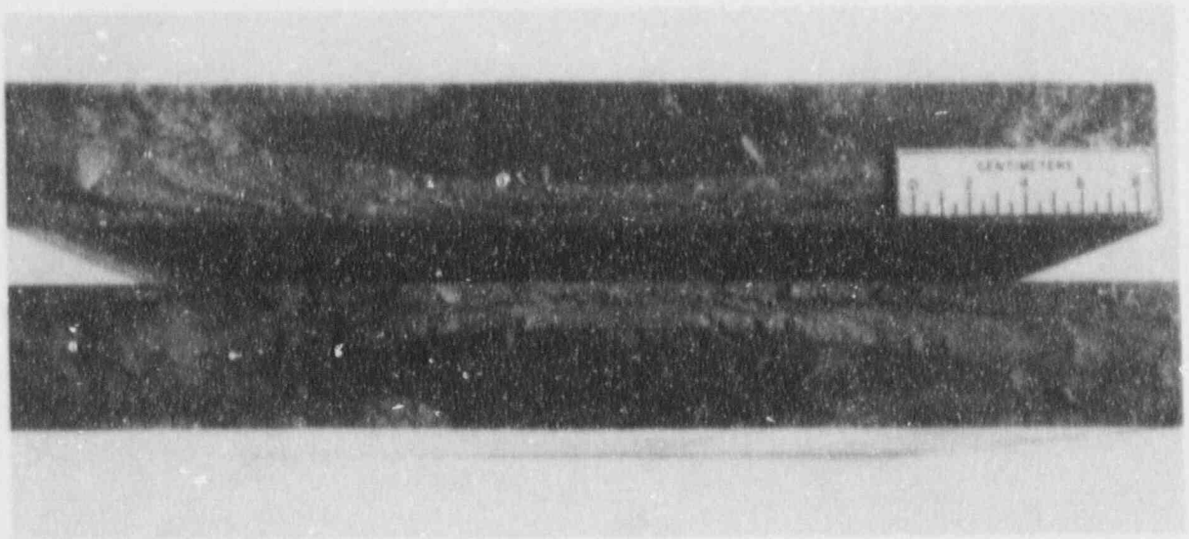

Fig. 4.4. Macrograph of the fracture surface of clad plate CP-15.

ORNL-PHOTO 6356-87

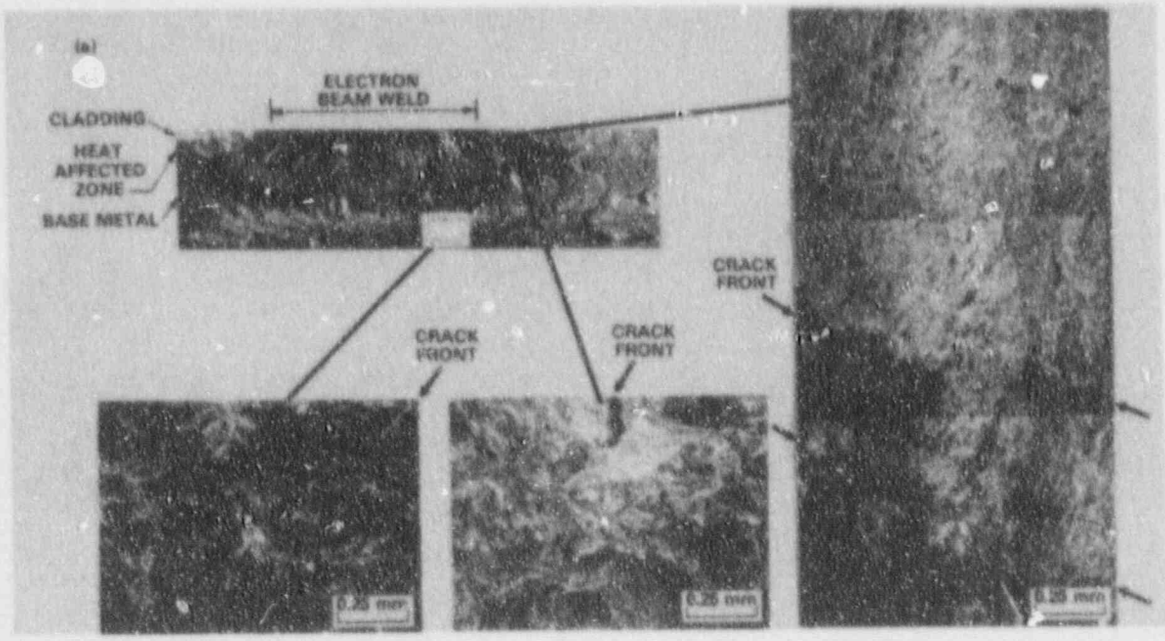

Fig. 4.5. Fractography of clad plate CP-15. There is no evidence of ductility at the arrest locations. The second event resulted in crack arrest in the cladding on the right side of the flaw.

4.1.3 Second pop-in event

The second fracture and arrest occurred at -25°C. The crack extended from the first arrest point into the plate, extending much further to either side and also penetrating somewhat deeper. SEM examination showed that the crack was again arrested by the HAZ boundary on one end of the crack, here termed the "left-hand side." Again, in this case, the fracture mode was cleavage, all the way to the arrest point. In the center of the plate, the crack also extended by cleavage to its arrest location. However, at the other end of the flaw, here referred to as the "right-hand side," the flaw was able to penetrate the HAZ and did actually come into contact with the cladding. In this case, the HAZ was fractured over a distance of roughly 25 mm, at which point the flaw deviated and returned to follow the HAZ boundary. The distance over which the HAZ was penetrated matched the width of the initial weld pass of the single-layer cladding. The crack front deflection occurred at the point where the HAZ of the second weld pass of cladding encountered the HAZ from the first pass. The crack grew through the first segment of HAZ by a cleavage mechanism until it encountered the stainless steel cladding. Near the edge of the cladding, the flaw penetrated into the cladding for 0.8 mm. The amount of penetration decreased further from the edge of the cladding until the flaw followed the cladding/base metal interface. Fracture of the stainless steel cladding occurred primarily by a ductile mechanism, as the austenitic material will not cleave. Occasionally the fracture path seeks out the δ-ferrite, resulting in localized cleavage.

4.1.4 Final fracture

The final fracture at -100°C resulted in the complete fracture of the plate. Fracture occurred by cleavage through the remaining areas of base metal and HAZ. At this temperature, which is well into the lower transition segment of the Charpy impact energy curve of the cladding, fracture in the cladding tends to follow the brittle ferrite phase,* resulting in a relatively brittle fracture appearance. In this case, however, there was no indication that the crack had stopped at the interface between the cladding and the HAZ, or at the HAZ/base metal boundary.

4.2 TESTING OF CLAD PLATE CP-17

The initial test temperature of the second clad plate (CP-17) was also 25°C and surface strains were about 0.45% during hydrogen charging. The loads were 890 and 823 kN at pop-in and arrest, respectively. Figure 4.6 shows the crack in the HAZ of the EB weld on the surface of plate CP-17. As in plate CP-15, the crater on the right side of the crack was formed during EB welding and not during testing. Figure 4.7 shows the same area as Fig. 4.6 during dye examination.

The plate was heat-tinted, then reloaded at -25°C until it ruptured. An audible pop-in occurred at 756 kN followed by other pop-ins before complete rupture at 725 kN. Figure 4.8 shows the load displacement record of these events.

---

*See discussion of the Charpy tests in Chap. 3, "Pretest Material Characterization."

YP3828

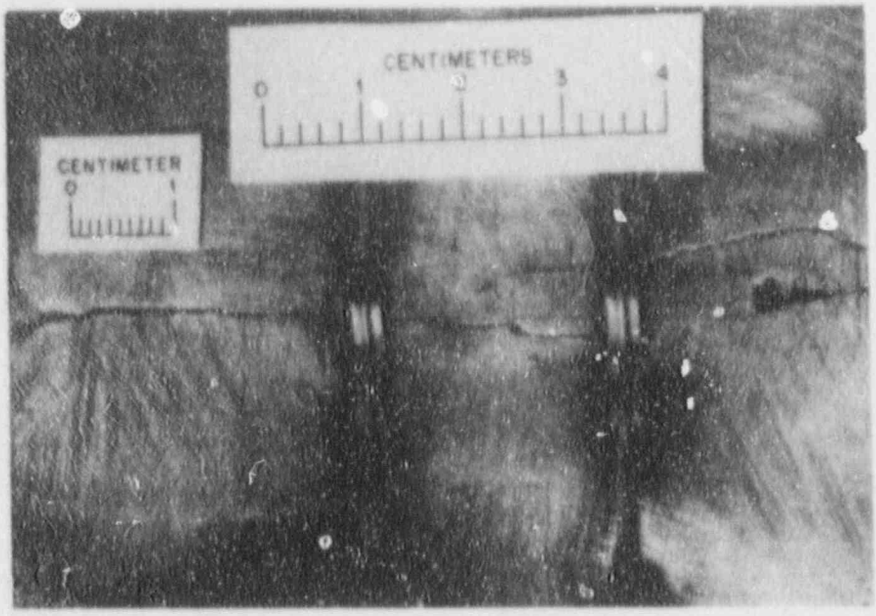

Fig. 4.6. Crack in the heat-affected zone of the electron beam weld on the surface of clad plate CP-17.

YP3827

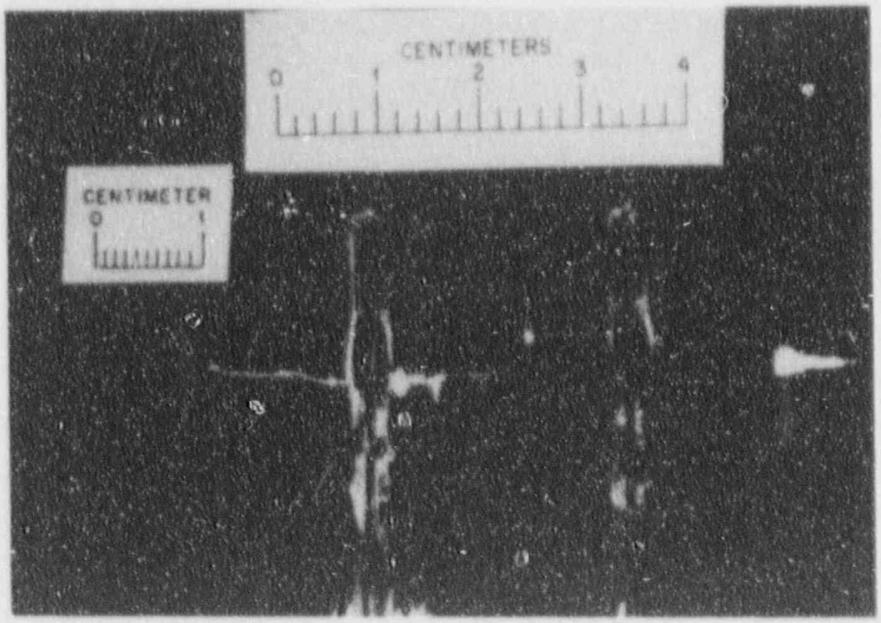

Fig. 4.7. The same area of clad plate CP-17 shown in Fig. 4.6 during dye penetrant examination.

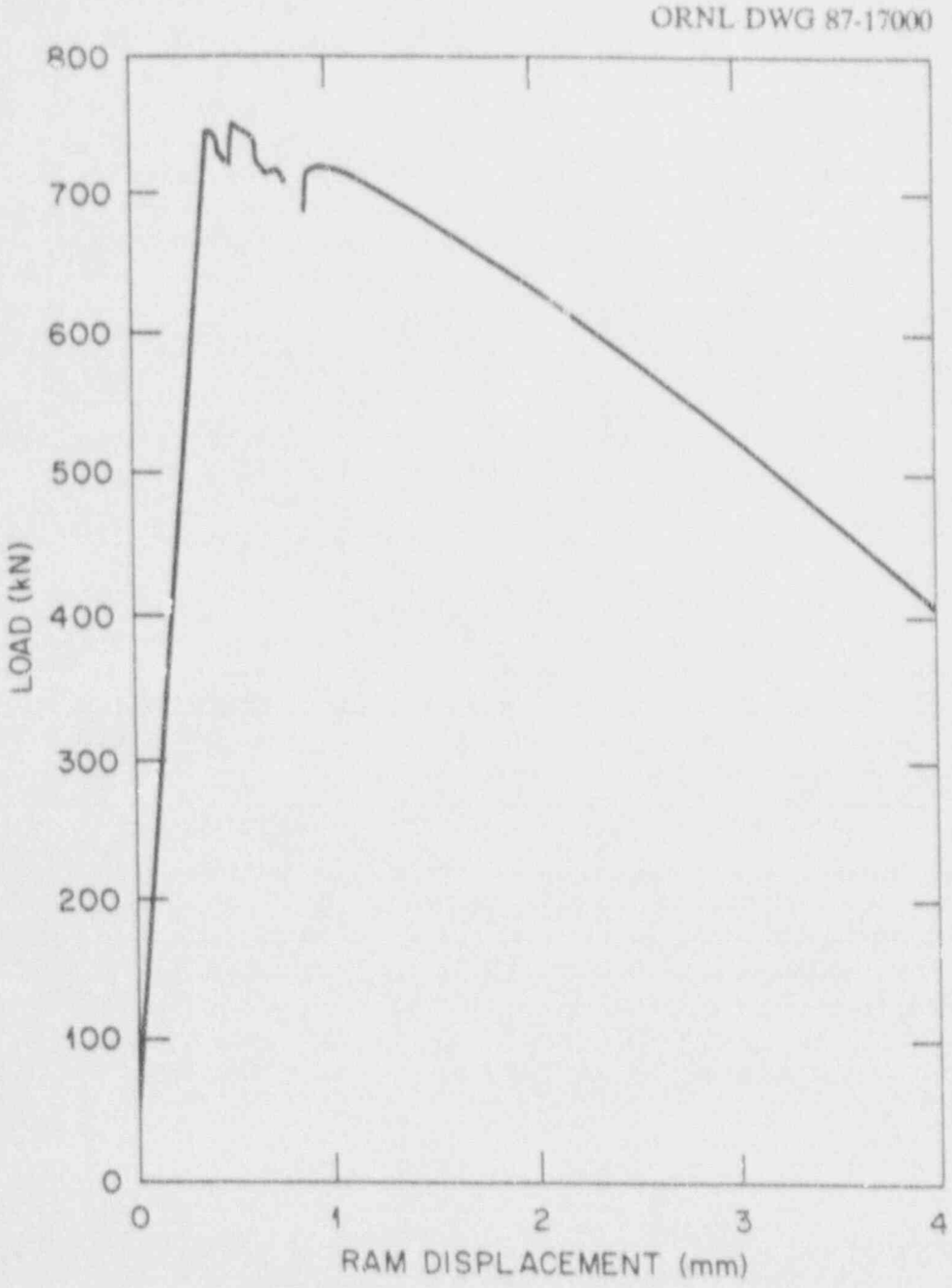

Fig. 4.8. Load-displacement record of events during the rupture of clad plate CP-17.

Figure 4.9 shows the fracture surfaces of the broken halves of plate CP-17. Figure 4.10 is a close-up of the heat-tinted, arrested flaw shape of plate CP-17 and six data points from the ultrasonic examination (see Sect. 4.3.1). The HAZ of each weld pass is clearly visible, and it appears that the HAZ of the first pass has deflected the "wing tips" of the flaw toward the middle thickness of the plate before arresting. The two lighter colored bands appearing across the dark heat-tinted flaw area are unbroken ligaments that are deeply undercut. The pop-ins observed during the final stages of loading, before rupture, may have been the breaking of these ligaments.

4.2.1 Dye penetrant and ultrasonic examination of clad plates CP-15 and CP-17

Plate CP-15 was examined after the second pop-in of the flaw, while plate CP-17 was examined after the first pop-in. Both penetrant and ultrasonic techniques were applied. The penetrant technique used Zyglo™ ZL-22A material (a Magnaflux Corporation product). This fluorescent dye penetrant is viewed with an ultraviolet light and is considered a high-sensitivity indicator for surface-breaking flaws. Results of the penetrant tests are documented in Figs. 4.3 and 4.7.

The ultrasonic examination was performed with a 5-MHz search unit with a contact wedge to produce a 45° shear wave in steel. The measurements depend on the detection of the tip-diffracted signals from the crack. Scanning was performed from the unclad surface and in two directions (perpendicular to the crack surface) to detect the maximum through-wall crack depth as referenced to plate thickness and centerline. Initial attempts on CP-15 estimated the maximum flaw depth to be about one-half the thickness, t.

Crack tip measurements on CP-17 indicted a maximum crack depth of approximately 60% (30 mm) of the thickness at a position approximately 25 mm to one side of the centerline. This data point and five others are shown superimposed on the fracture surface in Fig. 4.10. The maximum extension under the clad was indicated to be on the same side as the 0.6t data point. The estimate of maximum flaw depth at each end was essentially the same (0.38t or 19 mm). The accuracy of the tip estimates depends on the detection of the extreme crack extension. The tendency is to underestimate the depth if the tip is closed or highly stressed.

YP3826

Fig. 4.9. Fracture surfaces of the broken halves of clad plate CP-17.

ORNL-DWG 87-17001R

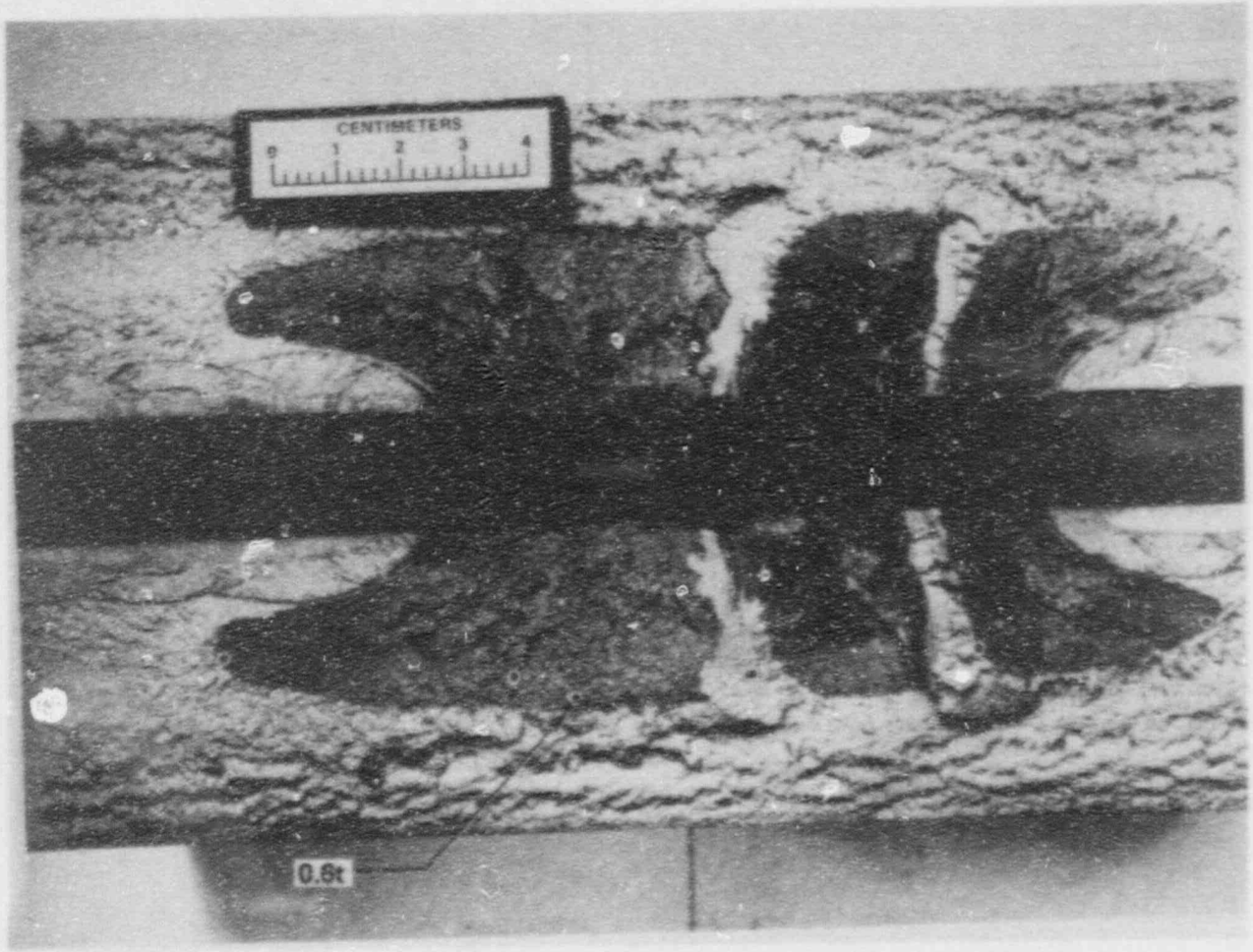

Fig. 4.10. Closeup of the heat-tinted, arrested flaw shape of clad plate CP-17 and six data points from the ultrasonic examination, one point highlighted by the 0.6t arrow.

4.3 TESTING OF CLAD PLATE CP-19

This plate was loaded to a surface strain of about 0.65%, which corresponded to a load of 987 kN. The flaw popped-in and arrested at a load of 689 kN. Figure 4.11 shows the fairly wide but shallow crater formed on the surface of plate CP-19 as the flaw tunneled below. The flaw ran the entire width of the plate until it penetrated the side. Figure 4.12 shows the location on the side of plate CP-19 where the propagating flaw emerged and the acid used for hydrogen charging ran out of this crevice.

After heat-tinting at approximately the same temperature as in previous tests, the plate was reloaded until it fractured at 703 kN.

Figure 4.13(a) shows the interesting arrested flaw shape formed in plate CP-19. The flaw ran parallel to and almost symmetrically about the centerline of the plate cross-section! The flaw can only propagate in tensile stresses, and in the *original* plate, compressive stresses occur below the neutral axis which is located approximately at midthickness of the plate. A possible explanation of such a flaw shape is that the neutral axis of the plate must have shifted simultaneously with the propagation of the crack to some location in the unbroken ligament on the compressive side. Figure 4.13(b) shows schematically the displacements (after the flaw arrested), through the thickness of the plate in the plane of the flaw with the neutral axis near the bottom of the plate (assuming plane sections remain plane). These displacements have been converted into stresses (see Chap. 5), and since the sum of in-plane axial forces is zero, the location of the neutral axis with respect to the plate thickness has been determined.

4.4 TESTING OF UNCLAD PLATE CP-21

To provide a comparison with the clad plate tests, unclad plate CP-21 was tested at the same 676-kN load used initially on clad plate CP-15. The surface strain was 0.27%, some 13% less than the strain at the same load in the case of a clad plate (see below), reflecting perhaps the greater stiffness of the unclad plate. The test was performed at room temperature. The plate fractured in two pieces approximately 2.5 h after the start of hydrogen charging. Figure 4.14 shows the fractured surfaces of the two broken halves of unclad plate CP-21. The differing "textures" of the fracture surface seem to indicate that the crack front first propagates below the surface, leaving an unbroken ligament. This ligament then cleaves when the stresses become sufficiently high thus reestablishing a through-crack configuration. The crack front propagates again below the surface, and the process repeats. A similar sequence of events appeared to have occurred in unclad plate CP-22 tested in the initiation mode and will be described later. The dark discoloration was formed by the acid and should be disregarded.

4.5 TESTING OF CLAD PLATE CP-18

This plate was tested at -25°C with pop-in and arrest occurring at 823 and 649 kN, respectively. Figure 4.15 shows the fracture surface of clad plate CP-18. Note the similarity to the fracture surface of plate CP-19 shown in the previous figure. The tunneling of this flaw was also accompanied by the formation on the surface of a shallow crater similar to the one in clad plate CP-19 (Fig. 4.12). The 649-kN arrest load is only 4% below the 676-kN load that ruptured the unclad plate CP-21. It provides another indication of the enhanced crack-arrest capability of clad plates even at a temperature 50 K below the temperature at which unclad plate CP-21 ruptured (see Sect. 4.4).

YP3891

Fig. 4.11. Fairly wide but shallow crater formed on the surface of clad plate CP-19 as the flaw tunneled below.

YP3893

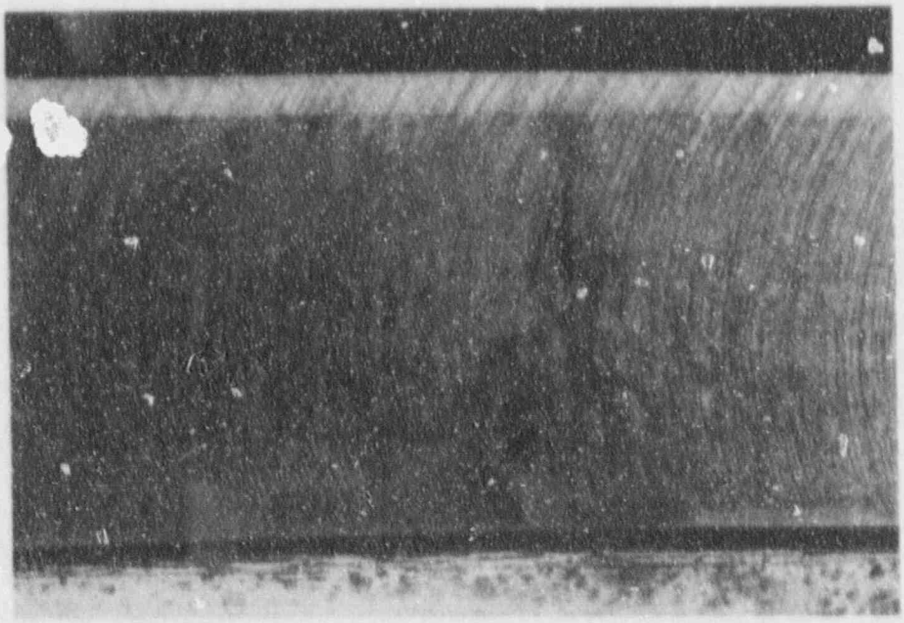

Fig. 4.12. Location on the side of clad plate CP-19 where the propagating flaw emerged and the acid used for hydrogen charging ran out of this crevice.

ORNL-PHOTO 10141-91

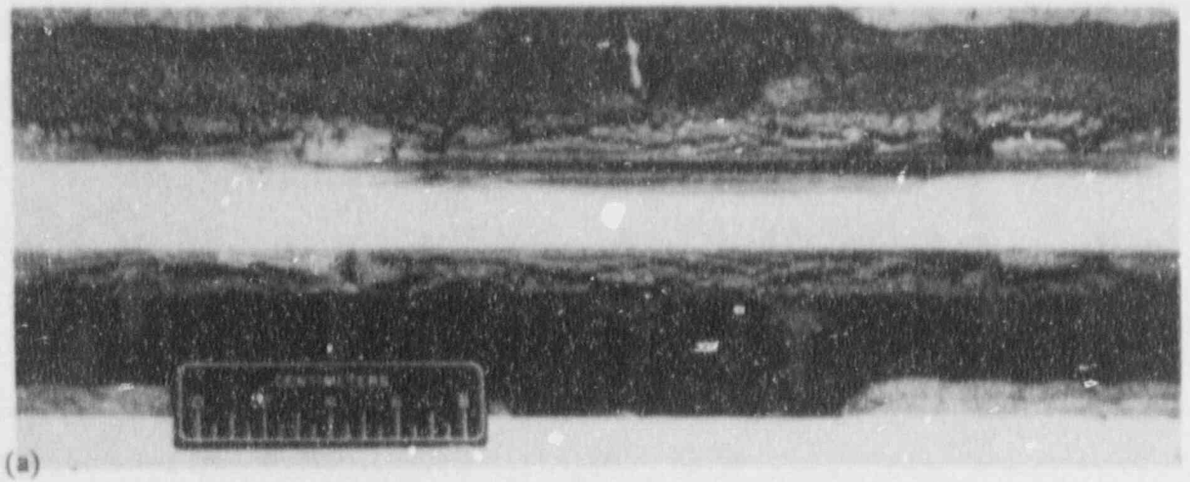

(a)

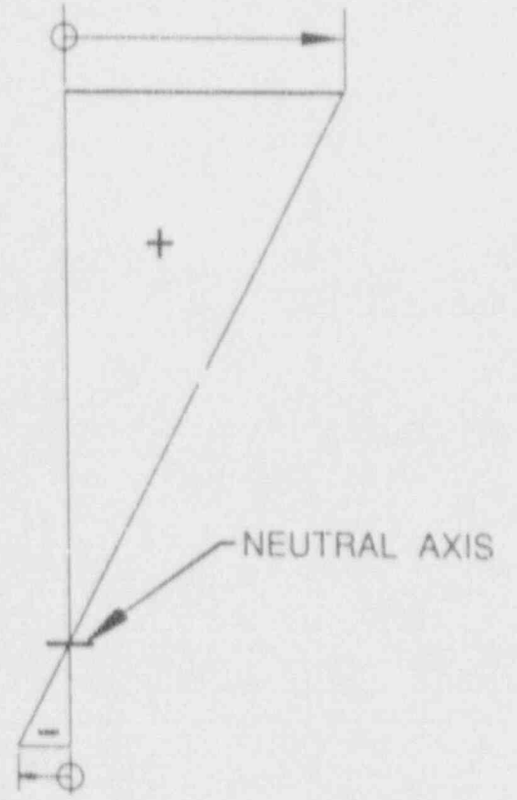

(b) COMPRESSIVE SURFACE DISPLACEMENT

Fig. 4.13. (a) Interesting arrested flaw shape formed in clad plate CP-19. (b) surface displacement after arrest of the flaw.

YP4123

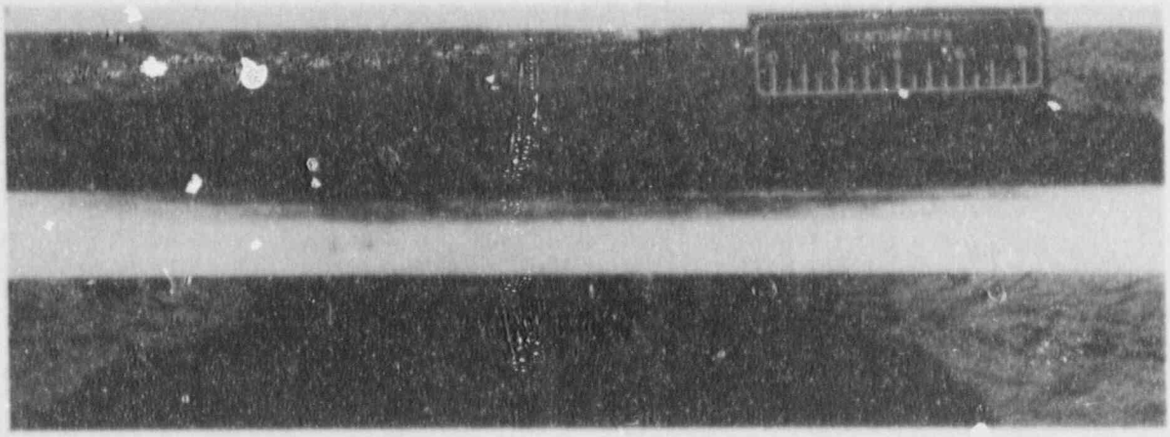

Fig. 4.14. Fracture surfaces of the two broken halves of unclad plate CP-21. The plate ruptured approximately 2.5 h after the start of the hydrogen charging.

YP4122

Fig. 4.15. Fracture surface of clad plate CP-18. Note the similarity to the fracture surface of clad plate CP-19 shown in Fig. 4.13(a).

The sulfuric acid used during hydrogen charging of this plate at -25°C froze and the test had to be discontinued until a more suitable concentration was substituted. After thawing, the acid was removed, but it was the following day before the test was resumed. Just as the plate reached the target load of 823 kN, and before any acid was added and the hydrogen charging current switched on, the flaw initiated. It is not clear whether a smaller flaw had already initiated in the EB weld region (triggered by the remnants of the acid in the EB weld region).

After the heat-tinting, the plate was loaded at -25°C until it ruptured at 698 kN.

4.6 TESTING OF CLAD PLATE CP-20

This clad plate was tested at the same temperature as clad plate CP-18, -25°C. The target strain of 0.41% corresponded to a load of 868 kN, about 5% higher than that used initially in testing clad plate CP-18. The plate ruptured approximately 4.5 h after the start of the hydrogen charging. The fracture surfaces of clad plate CP-20 are shown in Fig. 4.16.

Recall that, in the case of clad plate CP-18, tested at the same temperature, but at a slightly lower load, the cladding arrested the propagation of the flaw. Thus, the strain and load levels for clad plate CP-18 seem to form an upper bound to the load-bearing arresting capability of the clad plates at -25°C.

4.7 "INITIATION" MODE TESTS ON CLAD PLATE CP-16 AND UNCLAD PLATE CP-22

Plates CP-16 and CP-22 were precracked by hydrogen charging the EB flaw before loading was applied. After mounting the specimens in the test machine, the loads were increased monotonically until pop-in occurred. The loading rate was also the same as that used in the series of tests described above, as well as being within the range specified in ASTM E 399-83, namely 0.55 to 2.75 MPa$\sqrt{m}$s^{-1}.

Clad plate CP-16 and unclad plate CP-22 were both tested at room temperature (approximately 21°C). The flaws produced in both plates by the EB weld/hydrogen charging technique were approximately semielliptic in shape, 16 mm deep. The lengths of the flaws along the surface were 58 and 67 mm for the clad and unclad plate, respectively. The shapes of the EB weld induced flaws are apparent on the fracture surfaces shown later in this section. The flaws were difficult to detect on the surface before testing.

In the test on plate CP-16, pop-in occurred at a load of 703 kN, and the drop-in load to the arrest point was less than 1% (Fig. 4.17). It is believed that the earlier pop-in which occurred at 632 kN, as shown in Fig. 4.17, is associated with the joining of initial flaws lying in different planes on either side of the EB weld heat-affected zone (HAZ). On the basis of an approximately 1500 $\mu\epsilon$ increase observed with strain gage* XD-3, indicating a sizeable crack jump, the plate was unloaded.

The flaw induced by hydrogen charging the EB weld HAZ was now more easily observable, Fig. 4.18, but no evidence of propagation along the surface could be seen. However, dimpling that extended from the crack ends to the cladding (Fig. 4.18), indicated the presence of a subsurface crack. The flaw area was examined with dye penetrant, Fig. 4.19, but no surface crack other than that in the EB weld HAZ could be detected. In Fig. 4.19, the two parallel lines normal to the flaw were added to mark the start of the cladding.

*The location of all gages used on clad plate CP-16 are shown in Fig. 2.8.

YP4128

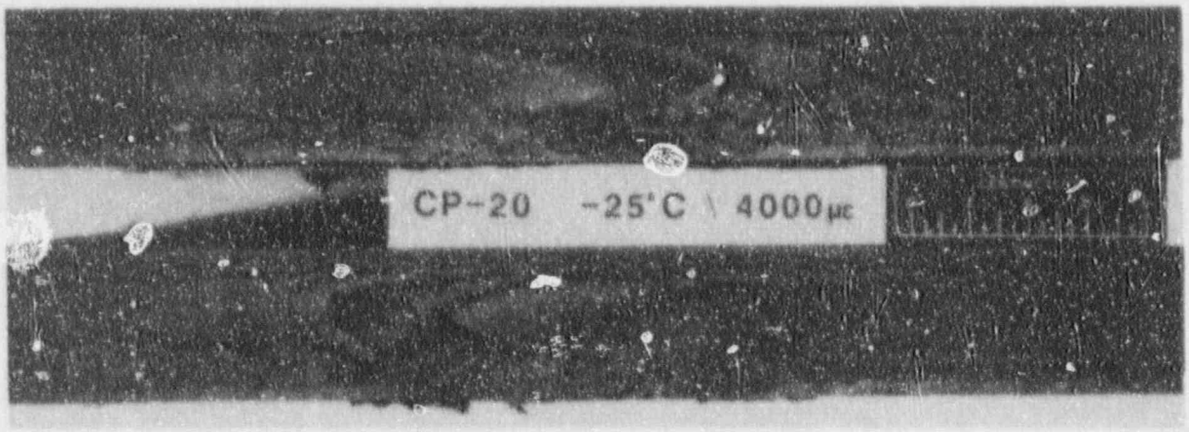

Fig. 4.16. Fracture surfaces of clad plate CP-20.

ORNL-DWG 88-7422

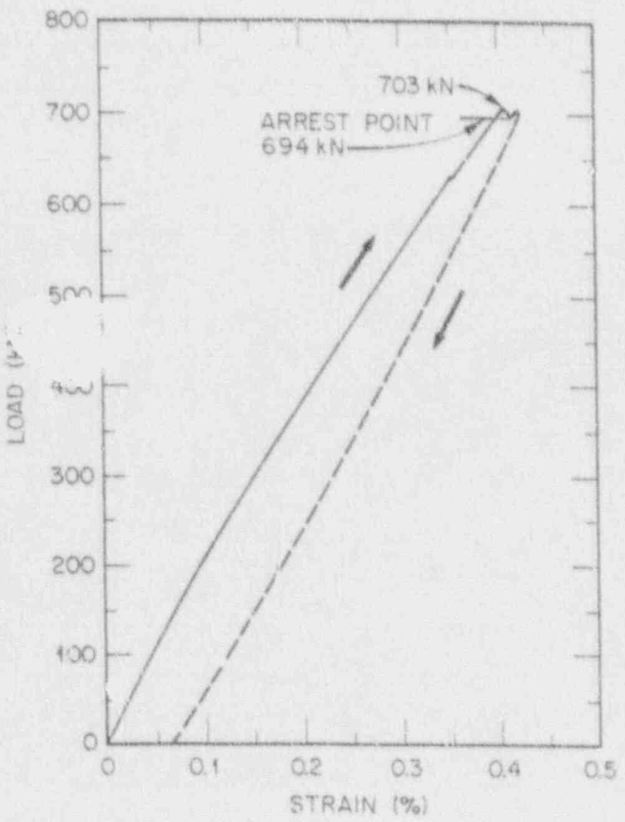

Fig. 4.17. Load vs strain measured by gage XE-1, recorded on X-Y chart during the test of clad plate CP-16, showing main pop-in at load of 703 kN, and a less than 1% drop in load to the arrest point. Note earlier pop-in. Strain gage locations have been indicated in Section 2.

YP5202

Fig. 4.18. The flaw in the electron beam weld heat-affected zone after the first event during the test of clad plate CP-16. No evidence of propagation along the surface can be seen. Note the dimpling that extends from the crack ends to the cladding.

YP5201

Fig. 4.19. Dye penetrant indication of flaw in clad plate CP-16 after first event. This is the same area as shown in Fig 4.18, but no surface crack other than that in the electron beam weld heat-affected zone could be detected. The two parallel lines normal to the flaw were added to mark the start of the cladding.

After heat-tinting the plate, it was reinstalled in the test machine and reloaded again at the same constant stroke rate and at room temperature. A second pop-in event occurred at a load of 890 kN, with an arrest occurring after a 17% load drop, Fig. 4.20. From the dimple on the top surface of the cladding, it was apparent that the second-event flaw had run beneath the entire width of the cladding to the edge of the plate. A second heat-tint was performed, and the plate was reloaded at -25°C until it broke into two halves at 698 kN.

The fracture surface of clad plate CP-16 is shown in Fig. 4.21. The HAZ has arrested the flaw in both the first and second events. Figure 4.22 shows a close-up of the EB flaw and its arrested shape at the end of the first event in which it tunneled slightly below the HAZ without penetrating the HAZ. A very thin ligament, less than 0.5 mm thick, remained intact in the base metal on the tensile side of the plate in between the EB weld and the cladding, and prevented dye penetrant detection of the flaw beneath. During the second event, the flaw propagated along the mid-thickness of the plate with intact ligaments approximately 10 and 16 mm deep along the top and bottom surfaces of the plate respectively, see Fig. 4.21. The flaw geometry of this plate confirmed the observation made previously that the dimple on the clad surface of the plate indicates tunnelling of the flaw beneath the cladding. Such indications of tunnelling have been observed several times before in all of the previous clad plate tests. The profiles of the EB flaw in CP-16 as well as that of the flaw at the end of the first event in plate CP-16 are shown in Fig. 4.23.

Unclad plate CP-22, also tested at room temperature, ruptured at a load of 685 kN, within 1% of the initial pop-in load of clad plate CP-16, except that in this case no arrest occurred and the plate broke into two halves. A general view of the fracture surface is shown in Fig. 4.24, and a closeup of the EB flaw is presented in Fig. 4.25. The differing "textures" of the fracture surface seem to indicate that the crack front first propagates below the surface, leaving an unbroken ligament. This ligament then cleaves when the stresses become sufficiently high, thus reestablishing a through-crack configuration. The crack front propagates again below the surface, and the process repeats. A similar sequence of events appeared to have occurred in the other unclad plate CP-21 as described earlier. The initial EB flaw profile in unclad plate CP-22 is presented in Fig. 4.26.

It may be recalled that unclad plate CP-21 was loaded to 676 kN and then a running flaw was triggered by hydrogen charging with no arrest occurring. The loads prior to fracture in both unclad plates differ by 2%. Allowing for scatter and the differences in the EB flaws, a load of approximately 676 kN (corresponding to a surface yield stress of the base metal at room temperature) is the critical load for this geometry and at this temperature. This is further confirmed by the similar crack shapes resulting from the tests on these two clad plates: CP-15 (which did not have an initial flaw) and CP-16 (which was initially flawed). The rupture load at a temperature 10 K below the drop-weight NDT for both unclad plates CP-21 and CP-22 was the load that caused yielding on the surface, in agreement with the concepts of the drop-weight test. Almost the same load at the same temperature initiated pop-in in clad plates CP-15 and -16, but the propagating flaw was arrested by the surface layers of HAZ or cladding.

ORNL-DWG 88-7423

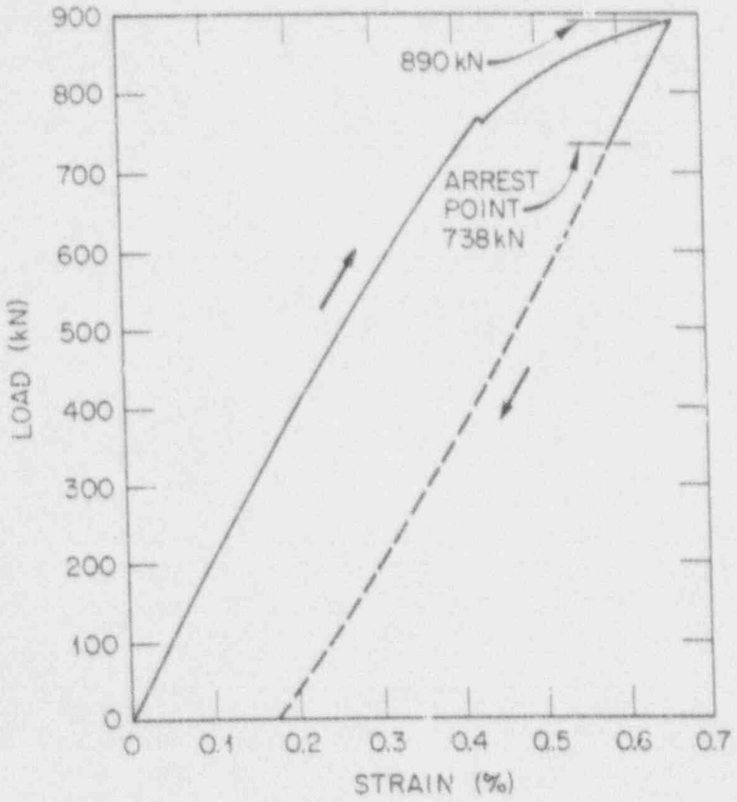

Fig. 4.20. Plot of load vs strain measured by gage XE-1, for second event during the test of clad plate CP-16, showing pop-in at load of 890 kN, with an arrest occurring after a 17% load drop. An earlier pop-in occurred at 760 kN.

YP5228

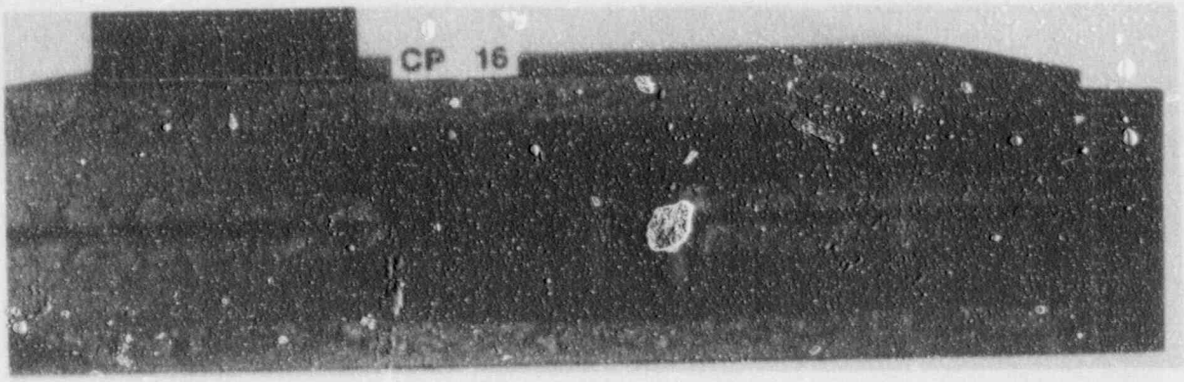

Fig. 4.21. The fracture surface of clad plate CP-16. During the second event the flaw propagated along the central portion of the plate thickness, with intact ligaments approximately 10 and 16-mm-thick along the top and bottom surfaces of the plate, respectively.

YP5227

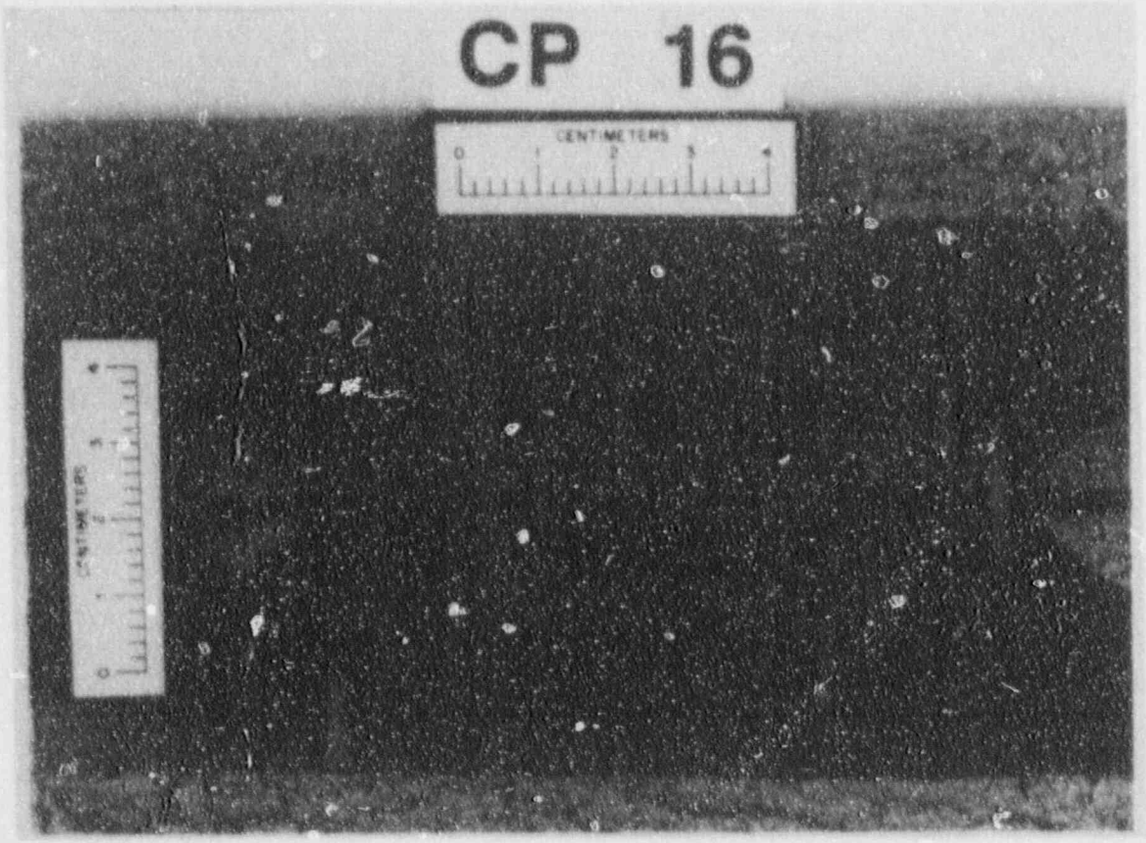

Fig. 4.22. Closeup of the electron beam weld flaw and its arrested shape in clad plate CP-16 at the end of the first event.

ORNL-DWG 88-8212

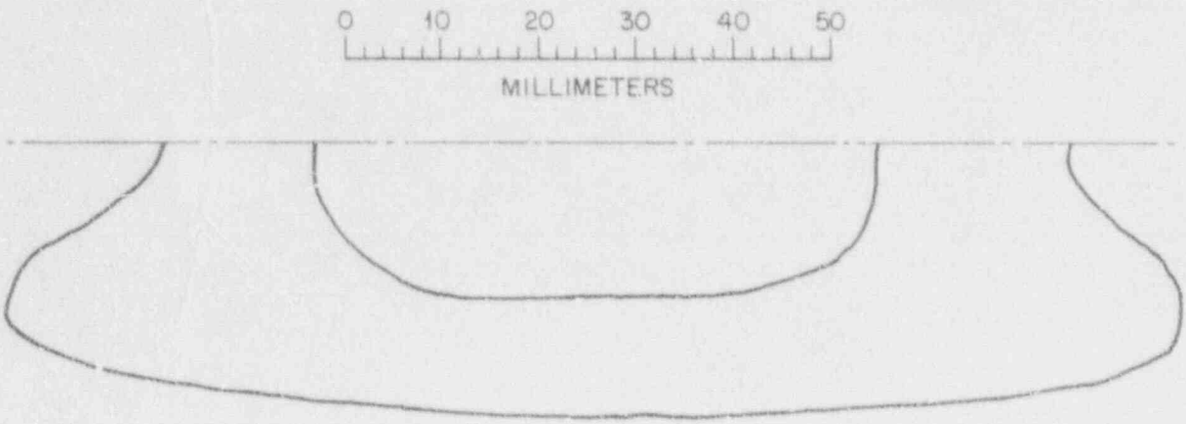

Fig. 4.23. General view of the fracture surface in unclad plate CP-22.

YP5204

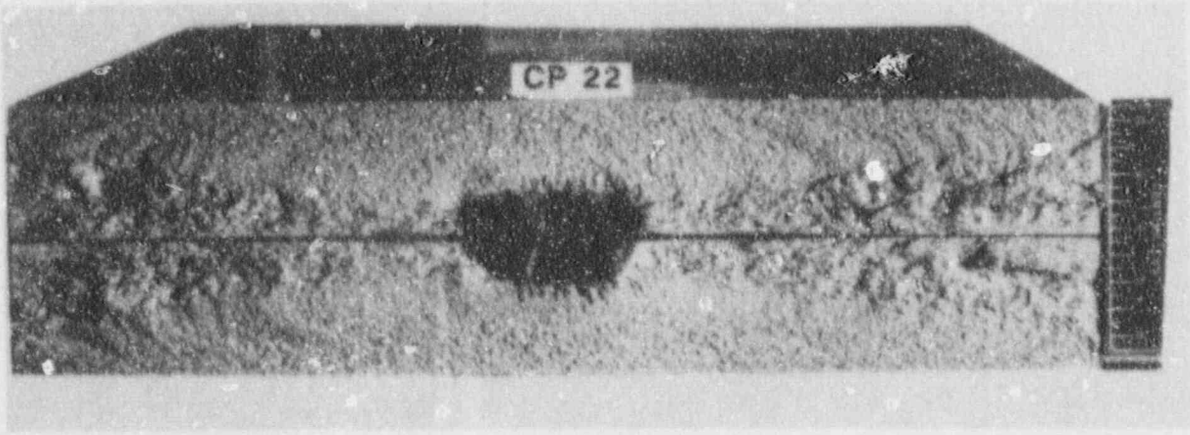

Fig. 4.24. Closeup of the electron beam weld flaw in unclad plate CP-22.

YP5203

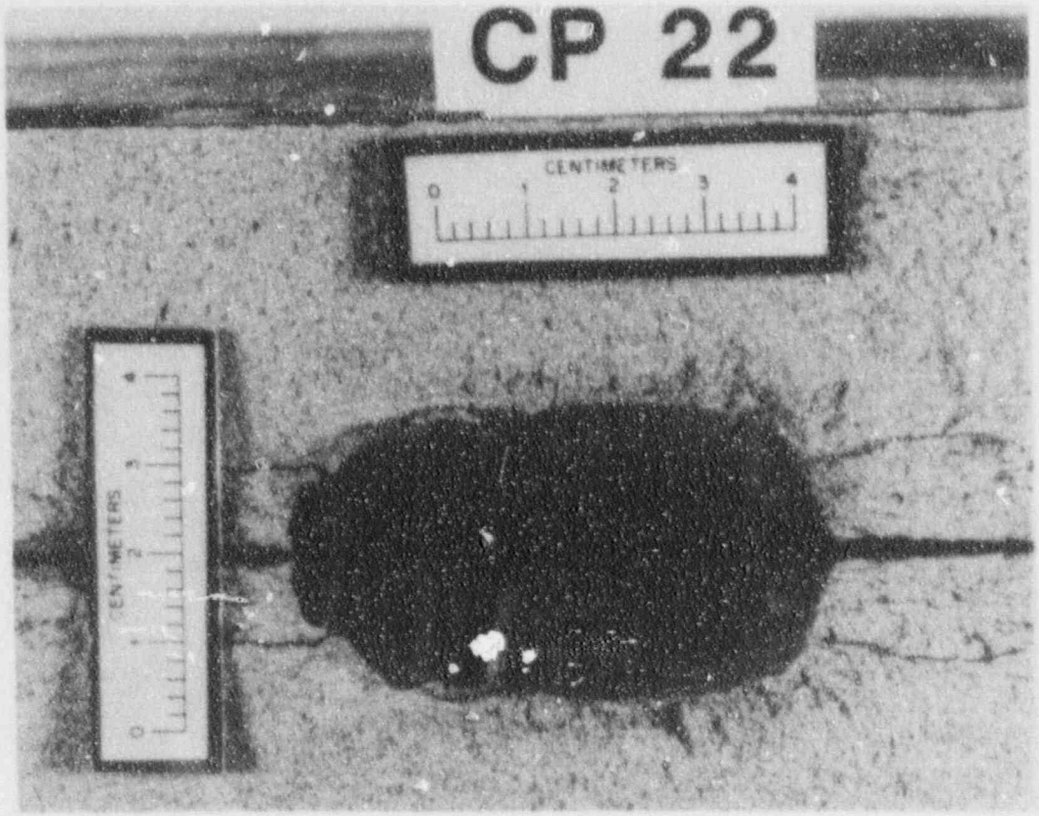

Fig. 4.25. Profiles of the electron beam weld and arrested flaws at the end of the first event in clad plate CP-16.

ORNL-DWG 88-8213

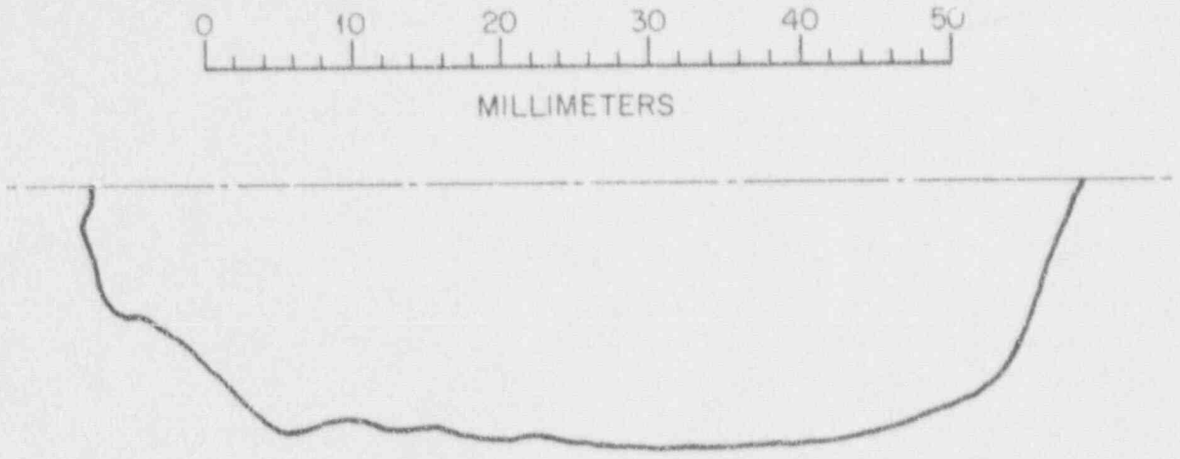

Fig. 4.26. Initial electron beam weld flaw in unclad plate CP-22.

4.8 DATA RECORDED BY STATIC AND DYNAMIC INSTRUMENTATION

The purpose of the static instrumentation was to monitor and record strain levels, COD, temperature distribution, test machine load, and ram displacement. During the time the load was being held constant and the EB weld was being hydrogen charged to initiate a flaw, a data scan was performed every 6 min. This is, of course, too slow to capture any of the dynamic events associated with crack propagation events, since this was not the aim of this program. During the testing of the plates, crack tunneling was observed, and an attempt was made to gain insight into the sequence of events associated with this phenomenon. Toward this end, dynamic instrumentation was included in the test of clad plate CP-16. For convenience, the layout of the gages previously shown in Chap. 2 is presented again in Fig. 4.27.

Some of the data recorded for CP-16 by the static data acquisition system (DAS) during one scan just before crack initiation and one just after are shown in Table 4.2. The strains in the base metal, gages XE-5 to XE-8, are slightly above the yield strain* before crack initiation and drop to slightly below yield afterward. Note that the large strain increase in gage XE-9, which is directly in the crack path and near the base/clad interface, reflects the propagation and arrest of the crack in its vicinity. The strain increase in gages XE-10, XE-11, and XE-12 are less than those in XE-9, reflecting their greater distance from the tip of the arrested crack.

*Approximately 2870 $\mu\epsilon$ for the base metal.

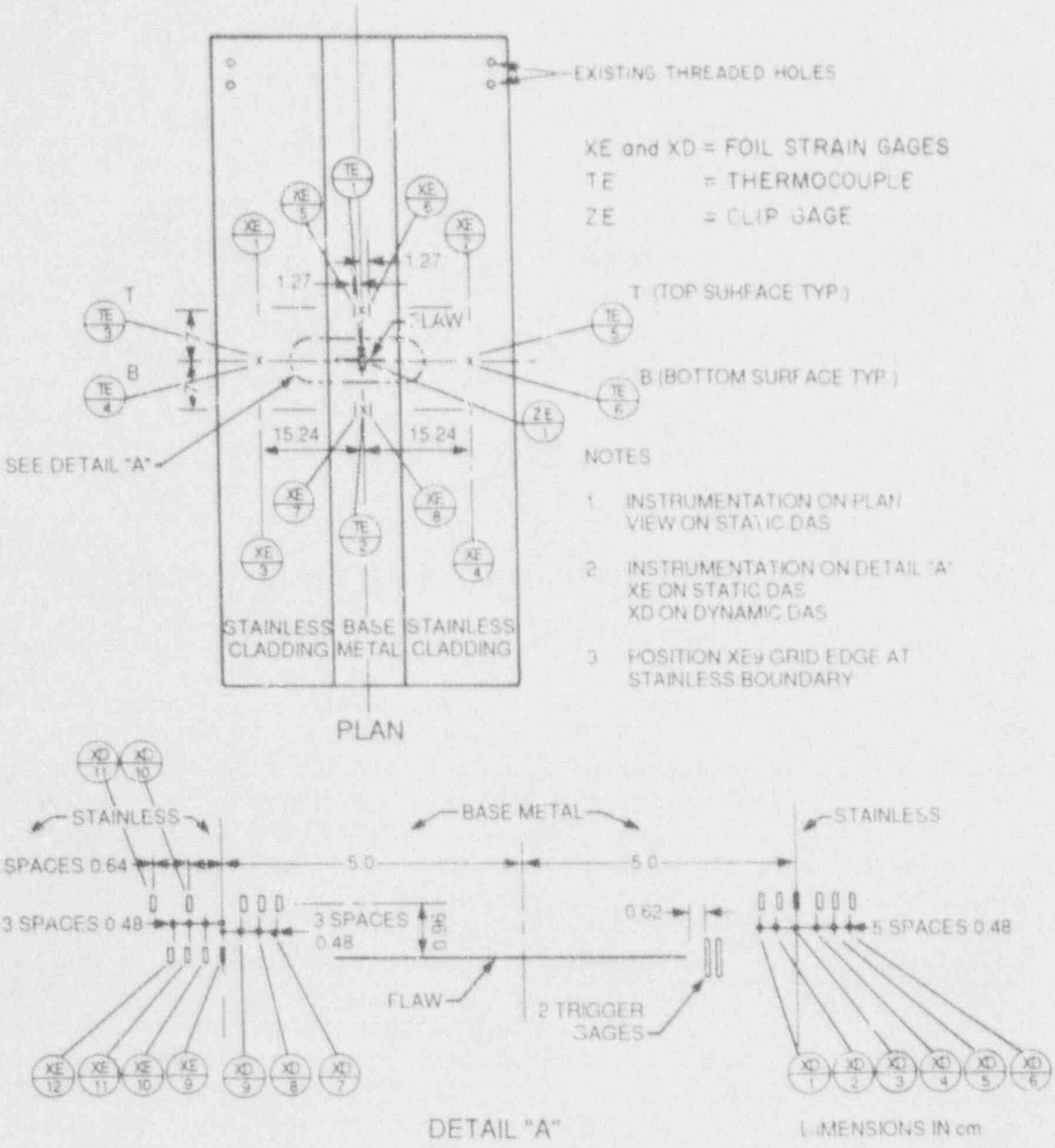

Fig. 4.27. Layout of instrumentation used for tests on plates CP-16 and CP-22 (repeated from Chap. 2).

Table 4.2. Data recorded for plate CP-16 by the static DAS during one scan just before crack initiation and the one just after arrest

Signal	Just before initiation	Just after arrest
Load	708 kN	703 kN
Stroke	9.2 mm	9.4 mm
COD gage	0.58 mm	0.81 mm
XE-1	4055 $\mu\epsilon$	4240 $\mu\epsilon$
XE-2	3554 $\mu\epsilon$	3746 $\mu\epsilon$
XE-3	4020 $\mu\epsilon$	4202 $\mu\epsilon$
XW-4	3805 $\mu\epsilon$	3970 $\mu\epsilon$
XE-5	2940 $\mu\epsilon$	2715 $\mu\epsilon$
XE-6	3059 $\mu\epsilon$	2759 $\mu\epsilon$
XE-7	2987 $\mu\epsilon$	2769 $\mu\epsilon$
XE-8	3094 $\mu\epsilon$	2802 $\mu\epsilon$
XE-9	4268 $\mu\epsilon$	5404 $\mu\epsilon$
XE-10	3710 $\mu\epsilon$	4391 $\mu\epsilon$
XE-11	3775 $\mu\epsilon$	4029 $\mu\epsilon$
XE-12	3634 $\mu\epsilon$	3809 $\mu\epsilon$

Figures 4.28 and 4.29 show the data recorded by the dynamic DAS. Figure 4.28 shows strain data for gages on the right of the flaw, while Fig. 4.29 shows data on the left (see also Fig. 4.27). Time zero refers to the time the trigger gage broke due to the large strain caused by the underlying crack. Some of these figures were available immediately after the main pop-in, and were invaluable in aiding the interpretation of the load drop as being a significant propagation event and not a small pop-in of the EB weld. In particular, the 1600-$\mu\epsilon$ increase in gage XD-3 led to the decision that a significant crack propagation event had occurred, thus the test was discontinued and the flaw surface heat-tinted.

It may be observed from the response of gage XD-1 that the strain peaked while the crack passed in its vicinity, then dropped about 200 $\mu\epsilon$, indicating a relief of the surface strains. The behavior of gage XD-2 is similar, but the strains were slightly higher than their level prior to pop-in because the crack arrested in its vicinity. This elevation of strains after arrest is more apparent in gages XD-3 to XD-6. The strain gages on the other side of the flaw have all registered an increase in strain during the event. It is not known what caused the dip in strain at time zero observed in gages XD-6 through XD-11; it could be an electric transient precipitated by the triggering system.

ORNL-DWG 88-4365 ETD

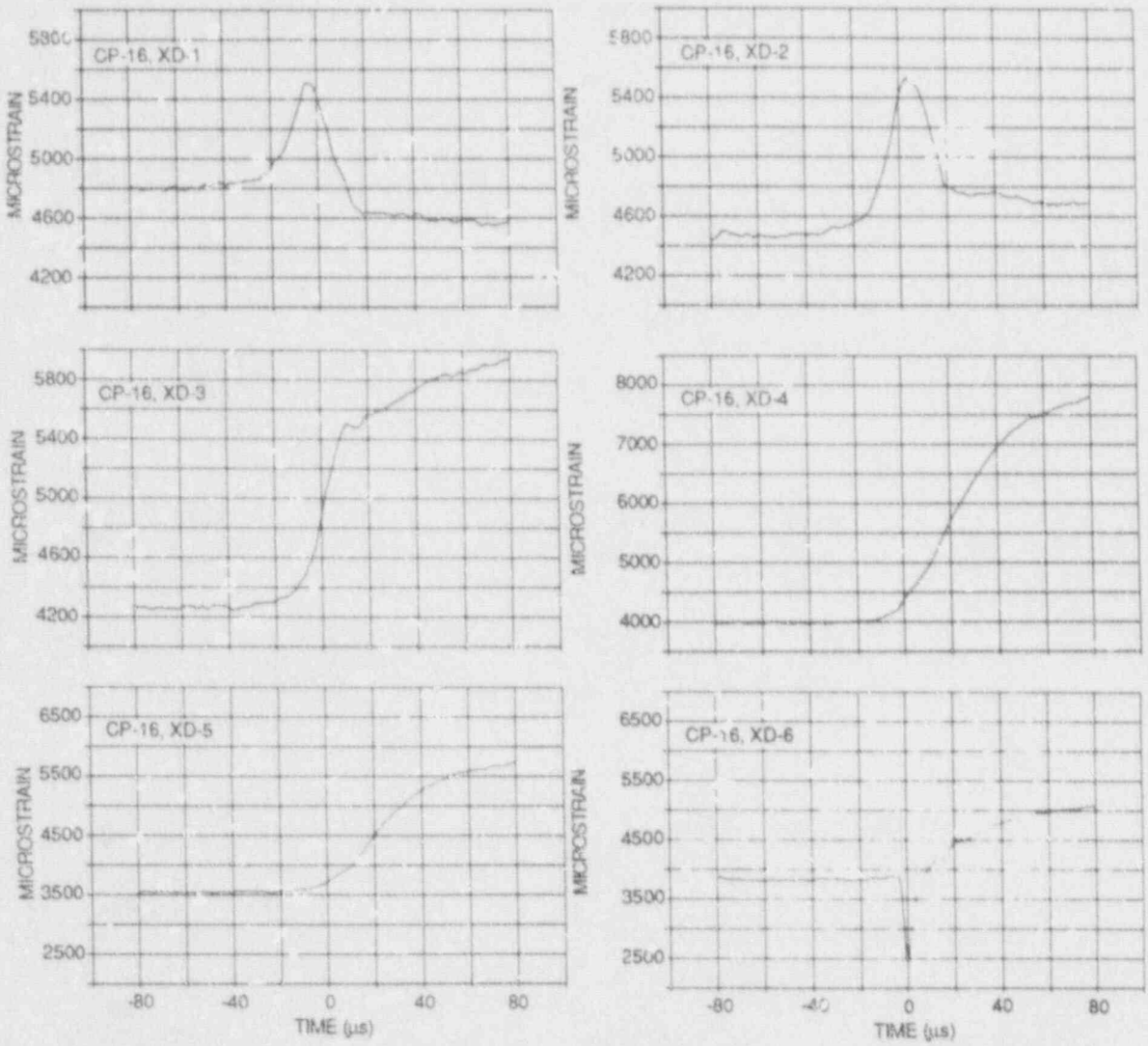

Fig. 4.28. Data recorded by the dynamic data acquisition system from gages on "right hand" of flaw during the first major crack propagation and arrest event for clad plate CP-16.

ORNL-DWG 88-4366 ETD

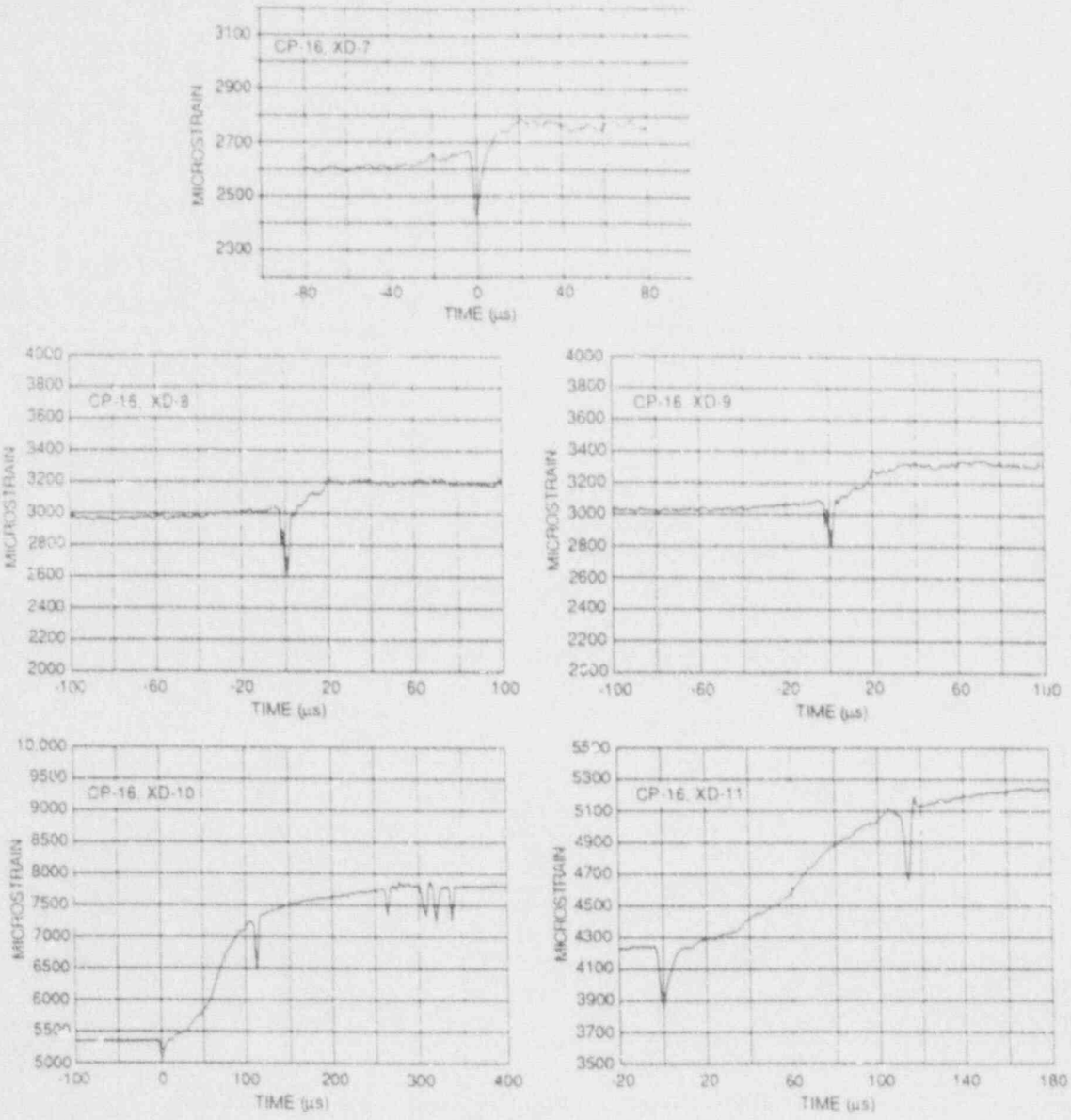

Fig. 4.29. Data recorded by the dynamic data acquisition system from gages on "left hand" of flaw during the first major crack propagation and arrest event for clad plate CP-16.

The velocity of a transient wave registered by peaks in strain gages XD-1 and XD-2 was estimated to be about 480 m/s. This is within the range measured for brittle mode crack propagation velocities for the same steel in the Wide-Plate Series 1 experiments, 200 to 1000 m/s [1]. It should be noted that strain gages XD-3, XD-4, and XD-5 showed only an increase in strain but no decrease as did the XD-1 or XD-2. Recall that the strain normal to the plane of the crack is a maximum [2] at an angle* of 70°. The crack arrested before it reached the cladding, which is a possible explanation of the difference in behavior registered by the two sets of gages located before and after the arrest point.

It was not possible to confirm from these measurements that the crack first tunnels, then propagates to the surface, as indicated by the markings on the fracture surfaces of several plates (see discussion of tests on unclad plates CP-21 and CP-22).

REFERENCES

1. D. J. Naus et al., p. 129 in *Crack Arrest Behavior in SEN Wide Plates of Quenched and Tempered A 533 Grade B Steel Tested Under Nonisothermal Conditions,* USNRC Report NUREG/CR-4930 (ORNL-6388), Martin Marietta Energy Systems, Inc., Oak Ridge Natl. Lab., Oak Ridge, Tenn., August 1987.†

2. G. R. Irwin, "Analysis of Stresses and Strains Near the End of a Crack Traversing a Plate," *J. Appl. Mech.* 24, 361-64 (September 1957).‡

---

*Measured counterclockwise from the plane of the crack, with the origin located at the crack tip.

†Available for purchase from National Technical Information Service, Springfield, VA 22161.

‡Available in public technical libraries.

5. RESULTS, ANALYSIS, AND DISCUSSION

Eight plates were tested in this program, and Table 5.1 summarizes the test conditions and results. This table shows in chronological order of testing, the type of test (whether "arrest" or "initiation"), test temperature, initiation (or pop-in) load and surface strain, and, if applicable, the postarrest load. The postarrest load is the load registered by the test machine after pop-in, and not necessarily the load at arrest of the flaw. The initiation and postarrest loads are discussed below.

In this report, the terms "initiation" and "arrest" refer to the first test to which a plate is subjected. An "initiation" test is one in which a plate specimen with a preexisting flaw is loaded until the flaw propagates. In an "arrest" experiment, a plate with an EB weld site is loaded to a target load and the load maintained constant under machine ram stroke control. The EB flaw site is then hydrogen charged until the flaw initiates from the EB flaw site. The purpose of this mode of testing is to load the specimen to a higher load than would be possible with a preexisting flaw. This method challenges the cladding with a propagating flaw the driving force for which is larger than would be possible with an initially cracked plate. All subsequent tests on plates with an arrested flaw are, of course, "initiation" tests.

Table 5.1. Test conditions and results for the eight plates tested

Plate	Condition	Type of test[a]	Test Temperature (°C)	Load (kN)		Surface strain (%)
				Initiation	Postarrest	
CP-15	Clad	A	25	676	654	0.31
		I	-25	759	709	
		I	-100	600	[b]	
CP-17	Clad[c]	A	25	890	823	0.45
		I	-25	756/725	[b]	
CP-19	Clad	A	25	987	689	0.65
		I	-50	703	[b]	
CP-21	Unclad	A	25	676	[b]	0.27
CP-18	Clad	A	-25	823	649	0.39
		I	-25	698	[b]	
CP-20	Clad	A	-25	868	[b]	0.41
CP-16	Clad	I	21	703	694	0.3
		I	21	890	738	
		I	-25	698	[b]	
CP-22	Unclad	I	21	685	[b]	0.3

[a]A = arrest, I = initiation.

[b]Plate ruptured in two pieces.

[c]Several pop-ins occurred before rupture.

5.1 RESULTS OF THE ARREST-TYPE EXPERIMENTS

Six of these plates were tested in the "arrest" mode at either -25 or 25°C. In the arrest experiments, the surface strain in the uniform bending moment span of the plate was used as a guide in the selection of the target load. Figure 5.1 shows approximately the points on the load vs surface strain curve at which the six plates have been tested in the arrest mode. Plates for which designations are shown on the left side of the curve were tested at -25°C, and those with designations shown on the right hand side were tested at 25°C. The loads (and strains) were maintained constant under stroke control during the period of hydrogen charging and are a measure of the crack-driving force acting (or the potential energy stored in the plate) at the instant the flaw initiated in the EB weld.

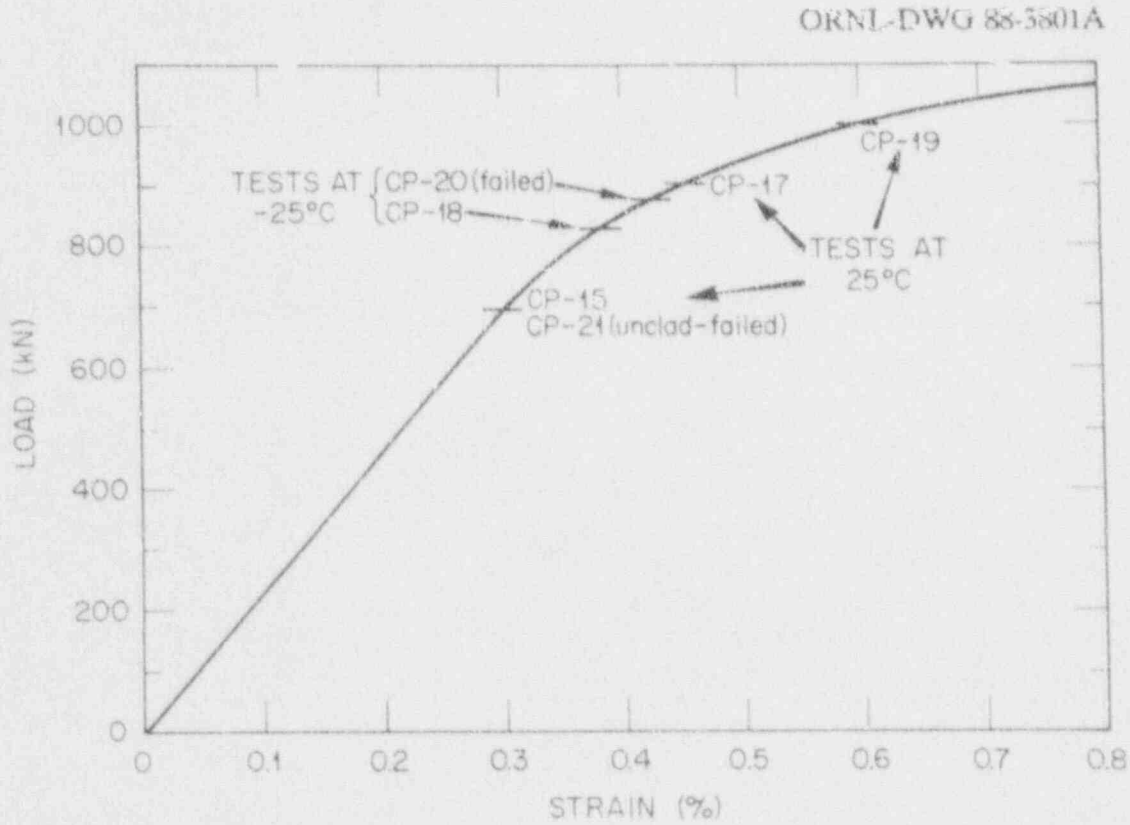

Fig. 5.1. Point on load vs surface strain curve at which the six plates were tested in the "arrest" mode. All plates designated on the left-hand side of the curve were tested at -25°C, while those designated on the right-hand side were tested at 25°C.

Four plates were tested at room temperature and for the first plate tested, CP-15, the surface strain was chosen to be approximately the yield strain of the base metal. The crack arrested and the plate did not rupture. The target surface strain was increased for both plates CP-17 and CP-19. An unclad plate, CP-21, fractured when loaded to approximately the base metal yield strain on the surface. Thus, in all three cases, by arresting propagating cracks, the cladding enhanced the load-carrying capacity of a clad plate compared to that of an unclad one.

In each case, the flaw initiated and arrested after propagating beneath the cladding a distance that increased with increasing target strain. The pop-in, postarrest loads and corresponding crack lengths for the four plates tested at room temperature are shown schematically in Fig. 5.2. It may be noted that as the potential energy stored in the plate increased, the length of the arrested flaw also increased as shown schematically by the shaded flaw shape in Fig. 5.2. The actual flaw shapes can be discerned from the photographs of the fracture surfaces shown in Fig. 5.3. Drawings of all the crack shapes are given in Appendix C, and may be used as a guide in discerning the crack shape on the photographs.

The remaining two clad plates, CP-18 and CP-20, were tested at -25°C in order to provide data at a second temperature besides room temperature. Clad plate CP-18 maintained its integrity and the 649-kN postarrest load of clad plate CP-18 is just 4% lower than the load that led to complete fracture of unclad plate CP-21, even though the temperature was 50 K lower, an indication of the contribution of cladding to an enhanced load-carrying capacity of clad plates when compared to the unclad one.

The 868-kN rupture load of clad plate CP-20 at -25°C is only 5% higher than the corresponding 823-kN pop-in load that led to arrest in the experiment on clad plate CP-18. Thus, the maximum load to which these clad plates can be loaded and still produce arrest at -25°C is between 823 and 868 kN. At 25°C, it is greater than 987 kN, but the upper bound could not be determined because the machine capacity is 1000 kN.

The four plates (CP-15, CP-17, CP-18, and CP-19) did not rupture after the EB-flaw initiated but the propagating flaw arrested, and because the machine was under stroke control,

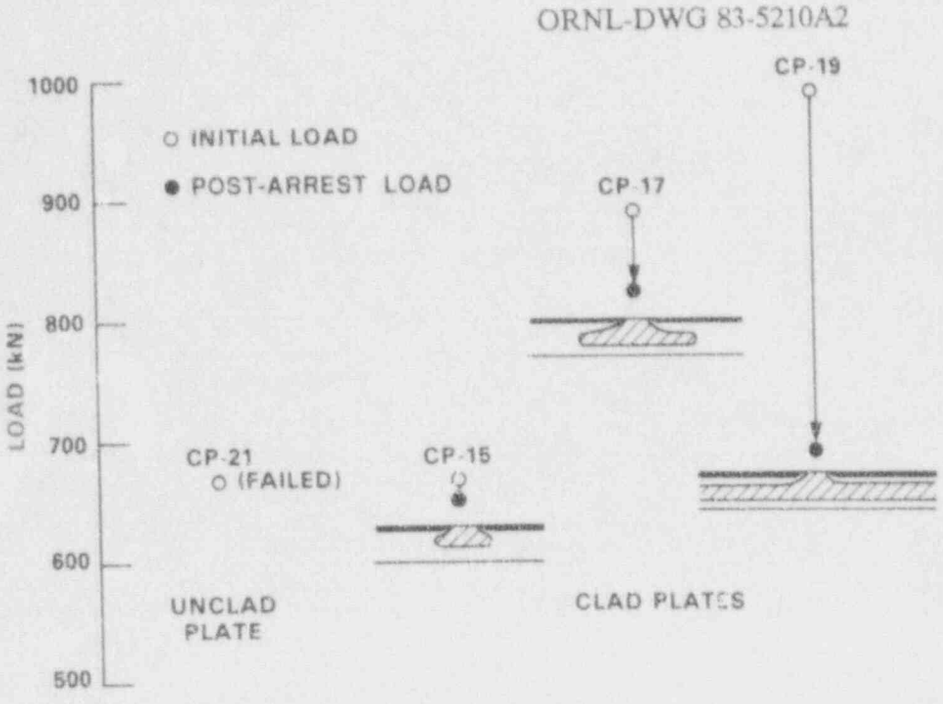

Fig. 5.2. Pop-in, postarrest loads, and corresponding crack lengths for the four plates tested at room temperature.

YP3767

(a)

YP3823A

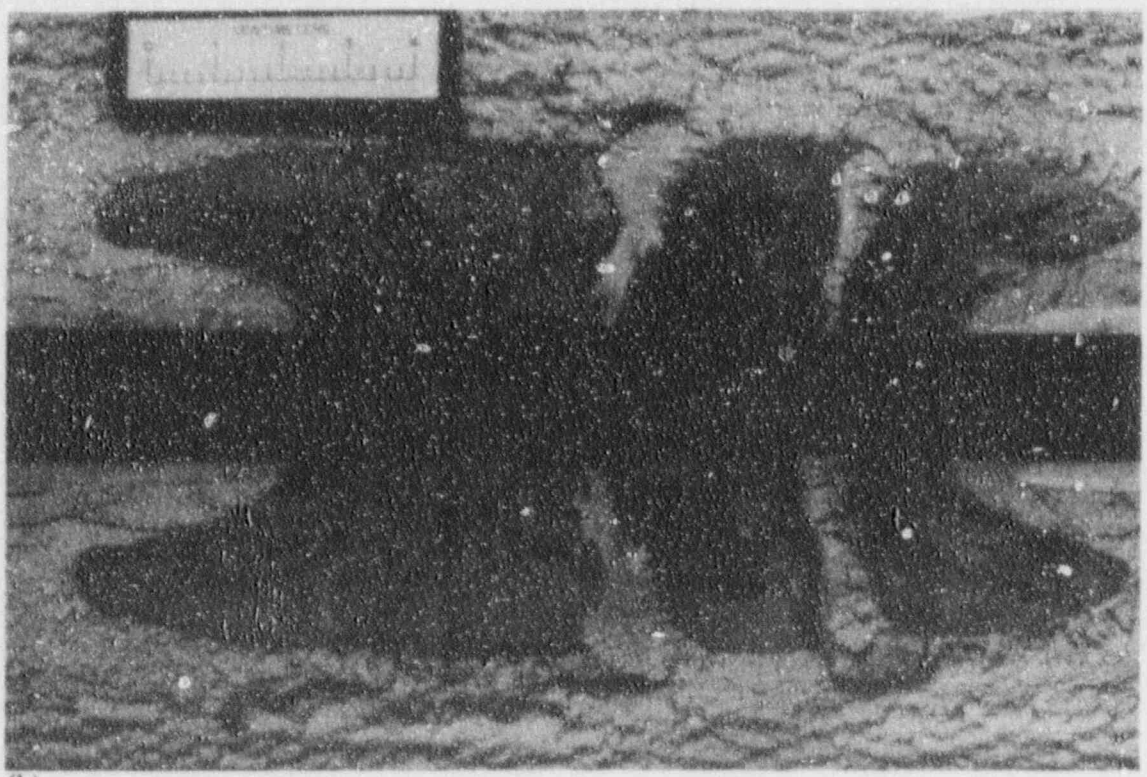

(b)

Fig. 5.3. The heat-tinted appearance of arrested flaw shapes after the first major pop-in can be discerned on the fracture surfaces of clad plates. (a) CP-15. (b) CP-17. (c) CP-19.

YP4121

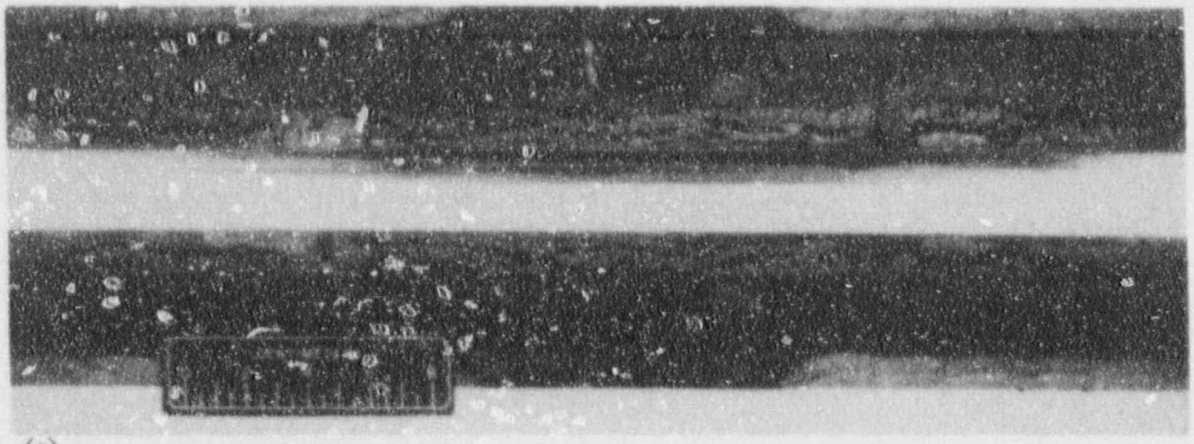

(c)

Fig. 5.3. (Continued)

the plates were able to sustain loads that were dependent upon the crack size, material properties, etc. As mentioned earlier, the specimens were removed from the test-machine and heat tinted to define the arrested flaw shapes. The heat tinting temperatures ranged from about 250 to 350° C and the application times were approximately 1 h.* At these temperatures and time, it is not expected that the material properties at the crack tip would have been affected. The plates were then re-mounted into the test machine and reloaded until further pop-ins occurred or the plates ruptured. The process was then repeated with plates that had arrested the propagating flaw. The purpose of these tests was to generate data on the load carrying capacity of clad plates with different sizes of flaws at little or no additional cost.

The loads measured at pop-in and arrest in plates with various sizes of flaws are also presented in Table 5.1. As can be seen from Table 5.1, with one exception, the load-carrying capacity (both the pop-in and arrest loads) of clad plates with fairly large preexisting flaws, was about equal to or exceeded that of an unclad plate. It should be noted that in many cases the test temperatures of these plates with preexisting flaws was 50 K below that which broke the unclad plate. The only case in which a clad plate with a preexisting flaw ruptured at a load lower than the rupture load of an unclad plate was the retest of CP-15 at a temperature of 125 K *lower* than that of the unclad plate.

The combined toughness of the surface layer of cladding and HAZ seemed to have contributed significantly to the load-bearing capacity of the clad plates by arresting flaws at loads and temperatures that have ruptured unclad plates. In fact, the clad plate CP-19 arrested a flaw subjected to a driving force (as measured by the target load), almost 50% higher than that which broke an unclad plate. Moreover, the residual load-bearing capacity of plates, as measured by

*Since the required time at temperature depends strongly on the thermal conditions during heat tinting, the coloration of one of the external machined surfaces of the plate is also a good indicator of the fracture surface color. When the color of one of the external machined surfaces becomes a hay or a light blue, the heating can be discontinued.

the critical loads in initiation experiments with fairly large flaws, was generally greater than required to break the unclad plate, even though the test temperatures were lower by 50 K.

5.2 RESULTS OF INITIATION--TYPE TESTS ON PLATES CP-16 AND CP-22

Two plates, CP-16 and CP-22, were tested in the "initiation" mode. The loads at various events during this type of test for clad plate CP-16 and unclad plate CP-22 are shown in Table 5.1. Recalling that these two plates were tested with preexisting flaws, the initiation or pop-in loads may be termed the "critical" loads for these plates. It is interesting to note that the pop-in load for plate CP-16 is within 5% of the target load of unflawed plate CP-15. The arrested crack shapes for CP-15 and CP-16 are also very similar.

With regard to the two unclad plates, one with and one without a preexisting flaw, approximately the same loads have led to rupture. Unclad plate CP-21 was loaded to 676 kN. Then a running flaw was triggered by hydrogen charging, and no arrest occurred. In the case of the other unclad plate, CP-22, which had a preexisting flaw, it ruptured at a load of 689 kN. Thus, the loads prior to fracture in both unclad plates differ by 2%. The loads at flaw initiation for these four plates are summarized in Table 5.2. Allowing for scatter and the differences in geometry of the EB flaws, the small differences in load indicates that the loads chosen for the two unflawed plates, CP-15 and CP-21, tested in the arrest mode were coincidentally the critical initiation loads of the plates at room temperature. Moreover, the critical loads do not seem to be sensitive to the range of EB flaw geometry variation exhibited by these plates. Noteworthy in all four plates, the surface stress was approximately equal to the yield strength of the base material. The test temperature of 25°C is some 10 K below the NDT temperature of the base metal, and flaw propagation in a brittle mode in these cases is in agreement with the underlying concepts of the drop weight test used to determine the NDT temperature.

Table 5.2. Comparison of loads at flaw initiation in tests at room temperature on four plates tested with and without initial flaws (flaw propagation led to arrest in the clad plates and rupture in the unclad plates)

Plate surface condition	Tests on plates with initial flaws		Tests on plates without initial flaws	
	Plate designation	Load (kN)	Plate designation	Load (kN)
Clad	CP-16	703	CP-15	676
Unclad	CP-22	685	CP-21	676

5.3 PRELIMINARY ANALYTICAL RESULTS

Fracture mechanics analysis of the experimental results is complicated by the presence of the heat-affected zone, the cladding, and the arrested crack shapes. Analytical methods are being developed and will be applied to analyze the experimental results. In the meantime, preliminary analyses have been performed using closed-form expressions, limit-load analysis, and finite-element methods.

5.3.1 Closed form and limit load analysis

The maximum stress intensity factor K_I at initiation of plate CP-16 is estimated to be about 108 MPa$\sqrt{m}$, and occurred at the surface. A crack length (measured along the surface), and a crack depth of 64 and 18 mm, respectively, together with a load of 703 kN, were used in the calculation. The estimation was performed using the approximate, closed-form expression for semielliptic flaws due to Merkle [1], which is also given in Appendix A. The K_{Ic} value for a test temperature of 25° C and an NDT temperature of 36° C obtained from the ASME K_{Ic} curve is about 52 MPa$\sqrt{m}$. The ASME K_{Ic} curve is a lower-bound one, thus, a K_{Ic} of 108 MPa$\sqrt{m}$ at the test temperature seems to be a reasonable value for the specially heat-treated A 533 grade B material used.

In the four clad plates, CP-16, CP-17, CP-18, and CP-19, the flaw, by extending the entire width of the plate, had become essentially a "long" flaw. The cross section of the plate in the plane of the flaw resembles a box section and a photograph of a typical fracture surface of one of the four plates is shown in Fig. 5.3(c). A schematic of this fracture surface is shown in Fig. 5.4(a). The stress intensity factor for this case may be estimated by assuming that the geometry is approximately that of a centrally located crack in a finite-width strip loaded by end-moments [2]. The load that ruptured the four plates with such a flaw is approximately 700 kN. The rupture loads for all four plates differ from their average by only 3%. The stress intensity factor corresponding to this load is 60 MPa$\sqrt{m}$ assuming that linear elastic fracture mechanics is still applicable.

In conjunction with the estimate of K_I for this long flaw, it is of interest to calculate the average stress at the instant of rupture in the ligament on the tensile side of the clad plates. Figure 5.4 gives the nomenclature used in a free-body analysis of the forces acting on the plate at the instance of rupture. Figure 5.4(a) schematically shows a remaining ligament typical of the four plates tested (CP-16, CP-17, CP-18, and CP-19). The moment of the resultant internal forces acting on the clad plate at the instant of rupture, with a flaw extending the entire plate width, is given in the small box in Fig. 5.4(b) as

$$M = \sigma c r d \tag{5.1}$$

The moment of the externally applied machine forces acting on the plate in four-point bending is

$$M = \frac{P\,l}{2} \tag{5.2}$$

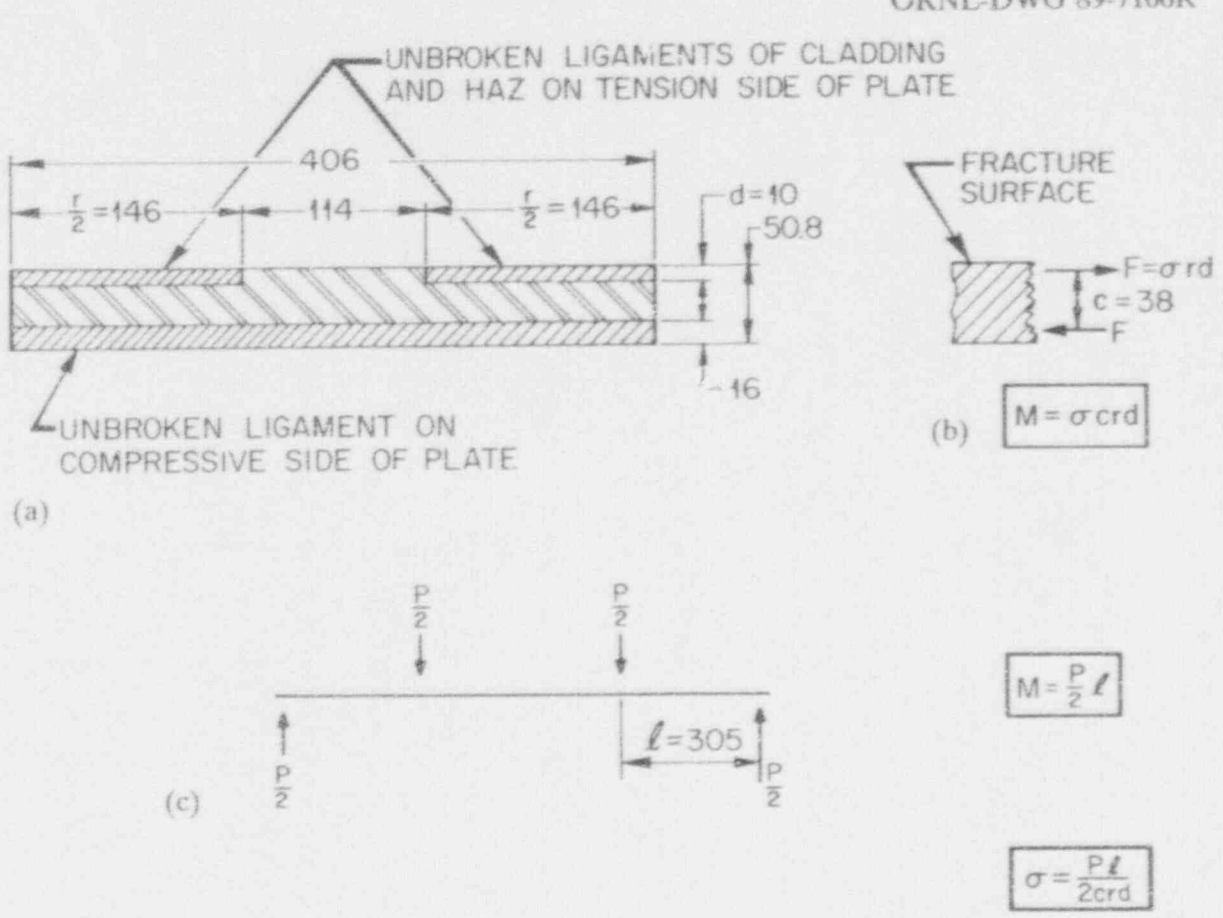

Fig. 5.4. Rigid plastic collapse analysis of stresses required to rupture the four plates, CP-16, CP-17, CP-18, and CP-19. (a) idealized, typical remaining ligaments. (b) forces acting on the fracture surface. (c) forces and pertinent dimensions of the four-point bend load train.

as shown in Fig. 5.4(c). Equating the two moments, the average stresses in the unbroken tensile ligament just before rupture is

$$\sigma = \frac{Pl}{2crd} \tag{5.3}$$

By using the loads recorded at the moment of rupture during the tests on these plates, the average stresses in the unbroken ligaments have been estimated, and are given in Table 5.3. It may be seen that in every case the average stress at rupture is 9 to 30% higher than the average ultimate tensile strength of the composite layer of both cladding and HAZ at the test temperature. It is not known why the average tensile stress at rupture is 9 to 30% greater than the combined UTS of the cladding and HAZ. The UTS of the cladding (see Chap. 3) were measured on a three-layer clad characterization block, whereas the plate specimens had a single layer. Perhaps the single layer cladding has a higher UTS than that of three-layer cladding.

Table 5.3. Comparison of tensile stress at rupture of several plates with large flaws to the average ultimate tensile strength of the composite layer of cladding and heat-affected zone

Plate	Test temperature (°C)	Load P (kN)	Average rupture stress (MPa)	Ultimate[a] tensile strength (MPa)
CP-19	-50	703	965	885
CP-17	-25	725	996	760
CP-18	-25	698	959	760
CP-16	-25	698	959	760

[a]Average of the ultimate tensile strength (UTS) of three-layer cladding and heat-affected zone (HAZ). The UTS of HAZ was obtained by increasing values obtained by testing HAZ from the three-layer characterization block by 15% to account for higher UTS of single-layer HAZ. Average values of UTS for cladding and HAZ at -50°C are 870 and 900 MPa, respectively, and at 0°C are 640 and 860 MPa. The values at -25°C were obtained by linear interpolation.

A K_{Ic}-CVN correlation* in the transition-temperature region given by Rolfe and Barsom [3] can be used to estimate the values of the K_{Ic} at -25°C for HAZ in the L-S orientation [Fig. 3.4(b)]. Using lower- and upper-bound values of 55 and 85 J for the HAZ CVN impact energy, respectively, K_{Ic} values ranging from 86 to 107 MPa$\sqrt{m}$ were estimated. Thus, at the rupture load the K_I of 60 MPa$\sqrt{m}$ estimated above is less than the K_{Ic} estimated from the CVN correlation, which may explain why, in order to rupture these four plates, the load on the plate had to be increased to a level that would result in the failure of the remaining ligament when the stresses exceed its ultimate tensile strength.

The postarrest loads shown in Fig. 5.2 and Table 5.1 are controlled by the compliance of the specimen, and are not necessarily the loads at the moment of arrest of the flaw. The crack initiates, propagates and arrests in a time interval that is smaller than that required for the specimen (because of its inertia) to deflect. The crack velocity, measured in one of the plate tests, is approximately 500 m/s. The flaw can, therefore, propagate the full half-width of the plate, a distance of 0.2 m, in 400 μs. In all cases the flaw propagates less than 0.2 m. The first natural period of vibration of the plate [4], approximated as a simply supported beam is approximately 1000 μs. Thus, only after arrest does the new and smaller stiffness of the flawed plate have an effect. Because the tests were performed under machine ram stroke control, the load drops to a value controlled by the new stiffness of the specimen. The actual load at arrest of the flaw can be higher than the final load shown.

5.3.2 Finite-element analyses performed

Some preliminary finite element analyses have been made [5], but more will be performed using methods that are under development. The results of the preliminary finite-element analysis of a flaw in plate CP-15 are shown in Fig. 5.5. The flaw, 16.9-mm-deep and 96.4-mm-long, is an idealization of the one assumed to have existed at the end of the first event, i.e., at the time the crack arrested when it encountered the cladding. The purpose of the analysis is to estimate the stress intensity factors at the end of the first event.

Figure 5.5 also shows the variation of the stress intensity factor around the crack front estimated using two other different methods. One of these methods is the Merkle expression mentioned above in Sect. 5.3.1. The other method is an equation due to Newman and Raju [6]. The various parameters in the Newman and Raju equation for K_I were obtained by curve fitting finite-element results. The Merkle expression indicates that the maximum value of K_I occurs at $\beta = 30°$, whereas both other finite-element based methods indicate that the maximum occurs near the surface. The values of the maximum K_I also vary from approximately 90 to 110 MPa$\sqrt{m}$ depending on the method used. Thus, the value of 103 MPa$\sqrt{m}$ estimated previously (Sect. 5.3.1) for CP-16, using the Merkle expression, is in this range. The location of the maximum K_I obtained by finite-element methods indicates that the flaw has a tendency to initiate from the surface, although as discussed in the next section, experimental evidence seems to show that flaws tend to tunnel, and thus the maximum K_I is below the surface. An investigation of the conditions leading to initiation of finite length surface flaws requires some assumptions to be made regarding whether the state of stress is plane strain or plane stress for both the calculation of K_I and the critical material parameters. On the surface it is plane stress, and "away" from the surface it is plane strain. This is due to constraint, a subject which is currently under investigation.

---

*This correlation is $(K_{Ic}/E)^2 = A(CVN)$, using units of ft-lb for CVN impact energy, psi$\sqrt{in.}$ and psi for K_{Ic} and E, respectively. The value of A = 5 (psi·in.)/(ft-lb) given by Rolfe and Barsom was used

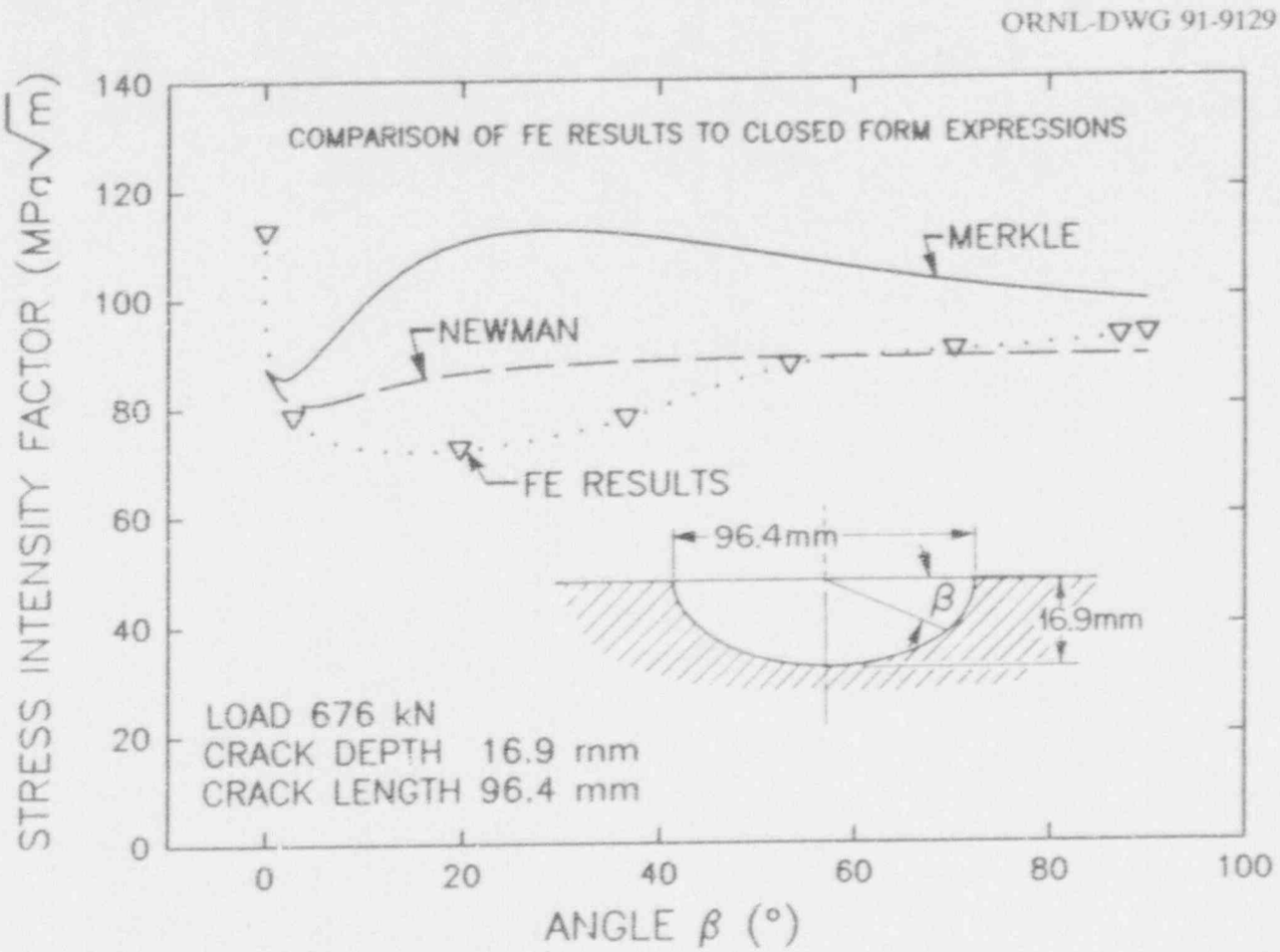

Fig. 5.5. Variation of the stress intensity factor along the crack front. The angle β is measured from the surface toward the deepest point. The finite-element results are from Ref. 5.

5.4 TUNNELING BEHAVIOR OF FINITE-LENGTH SURFACE FLAWS

Examination of the fracture surfaces of the unclad plates indicates a propensity of propagating flaws to tunnel, *even in the absence of the tough surface layer* composed of cladding and HAZ. Tunneling was observed in the finite-length flaw used in the V8-A experiment [7] even though it was not subjected to a bending-load stress distribution. In Ref. 7, Appendix N shows photographs of the tunneled flaw, and pp. 95-106 and 142-51 of Ref. 7 give posttest examination and analytical results, respectively. It is believed that tunneling also occurred in the TSE-2 experiment [8].

In the case of the two unclad plates tested, the differing "textures" of the fracture surfaces of both plates seem to indicate that the crack first propagates below the surface. This leaves a sharp pointed, wedge-shaped, unbroken ligament between the tunneled flaw and the surface. This increases the stresses in the wedge-shaped ligament, causing it to cleave, thus reestablishing a surface crack, approximately semielliptic in shape. The crack propagates again below the surface, and the process repeats. This sequence of events appeared to have occurred in both unclad plates CP-21 and CP-22.

The value of K_I at the surface of a finite-length flaw is difficult to calculate. Nonetheless, qualitative arguments can be developed for providing some insight for the reasons that flaws show tendencies to tunnel. The variation of the stress intensity factor along the crack front was calculated by means of the Merkle expression (Ref. 1 and Appendix A). Figures 5.6(a) through (c) show, for various crack depths, the variation of the stress intensity factor K_I with depth position (a') along the crack front of a semielliptic flaw in a plate in bending. The depth (a') in Fig. 5.6 has been normalized with respect to the crack depth (a), so that 0 is the surface and 1 is the deepest point in the crack, respectively. The geometry of the plate and the loading conditions are those used in the clad plate experiments, but the plate is assumed to be homogeneous and the elastic material properties of base metal, HAZ, and cladding are assumed equal.

The stress intensity factors were calculated for three crack depths, a = 16, 25, and 34 mm. The smallest and largest values of crack depth correspond approximately to the initial depth of an EB weld and the deepest arrested flaw depth respectively, with the 25-mm depth added as an intermediate value. The stress intensity factors were also calculated for three aspect ratios (b/a) = 2, 5, and 10. A ratio (b/a) of 2 and a crack depth of 16 mm correspond approximately to the initial EB weld. The other ratios represent an idealized flaw shape as the flaw grows longer for a constant crack depth.

For the initial flaw, the stress intensity factors vary only slightly along the crack front. Thus, when this flaw initiates, it may initially propagate below the surface because the critical stress intensity factor K_{Ic} is apt to be lower below the surface because of higher constraint. This will leave an unbroken, wedge shaped, ligament between the flaw and the surface. This ligament then breaks, creating a new semielliptic flaw. This process then repeats itself for the new crack, perhaps for a somewhat deeper flaw. But as Fig. 5.6 shows, except for the values of the stress intensity factors, there is little difference between the shapes of the curves, so the above arguments still hold for the various crack depths and the process keeps repeating itself. As mentioned above, the appearance of fracture surfaces appears to support the idea of alternate tunneling followed by a rupture of the remaining ligament.

ORNL-DWG 89-7107R2

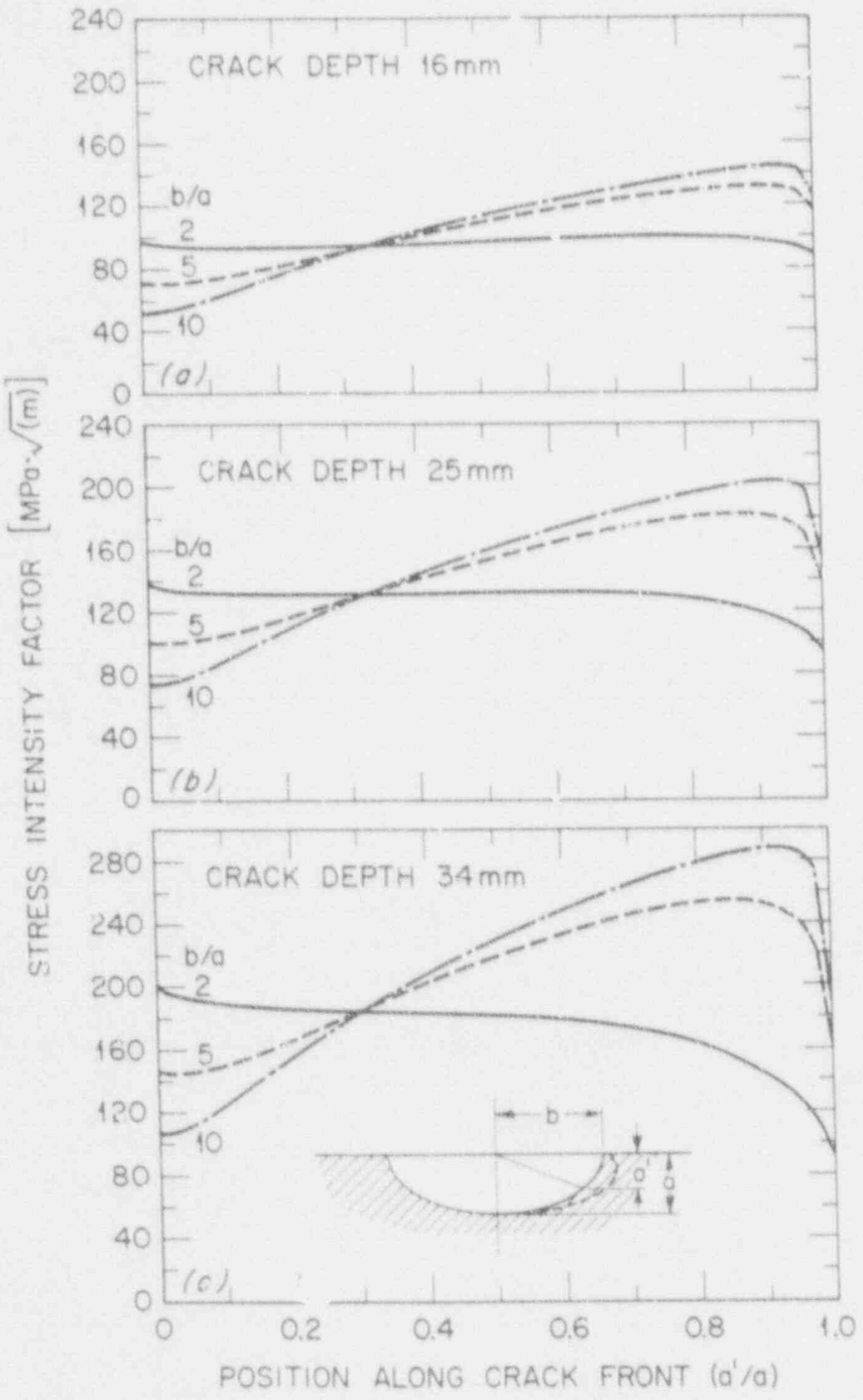

Fig. 5.6. Variation of stress intensity factor along the crack front of an elliptic flaw with b/a ratios of 2, 5, and 10 and for crack depths of (a) 16 mm, (b) 25 mm, and (c) 34 mm. The plates were subjected to a 700-kN load, and a value of a'/a = 0 and 1 correspond to the surface and deepest point, respectively.

As the flaw increases in depth and length, the maximum value of K_I for surface flaws is below the surface, Fig. 5.6(c). These values are considerably in excess of the expected values of the arrest toughness for the temperature ranges encountered in these tests. This indicates that the cladding by preventing the tunneled flaws from becoming surface flaws, must have decreased K_I considerably. In the case of many of the tests, a strong, tough surface layer of cladding and HAZ did not allow the remaining ligament to rupture. The cladding and HAZ also provided a force that tended to close the crack, thus reducing the levels of K_I in the base metal considerably and thereby enhancing the load-carrying capacity of the plates.

The position of a point along the crack front can be given either in terms of the angle β as in Fig. 5.5, or as the fractional crack depth (a'/a) where (a') and (a) are the depth of the point and the crack depth, respectively, measured from the surface of the crack, as in Fig. 5.6. The angle β was used in Fig. 5.5 in order to provide a direct comparison to the results given in Ref. 5. The fractional crack depth was used in the above discussion about tunneling behavior for direct comparison to the investigations by Cheverton et al. [8]. Each method of indicating position along the crack front has advantages and disadvantages. A small change in crack depth could mean a relatively large change in the angle β for b/a ratios > 2. For example, for ratios of half crack length to crack depth (b/a) that correspond to those of the initial flaw in CP-16, the range of the angle β = 0 to 30° covers fractional crack depths of 0 to approximately 70%, while the remaining 60° of the crack front correspond to the remaining 30% of the crack depth. This topic is discussed in Appendix B, and an equation to convert β to the fractional crack depth (a'/a) is given. Also, the variation of (a'/a) is plotted as a function of β for a range of values of b/a.

5.5 SUMMARY AND CONCLUSIONS

The tough, strong surface layer of cladding and HAZ seemed to have contributed significantly to the load-bearing capacity of the plates tested by arresting flaws at loads and temperatures that have fractured unclad plates. Moreover, the residual load-bearing capacity of clad plates, as measured by the critical loads in initiation experiments with fairly large flaws, was generally greater than those required to break unclad plates, even though the test temperatures were lower by 50 K.

The tests indicate a propensity of propagating flaws to tunnel, even without the aid of the tough surface layer composed of cladding and HAZ, as has occurred in the base metal portion of the clad plates and in the unclad plates. This potential for tunneling is probably due to the maximum value of K_I/K_{Ic} occurring below the surface.

It is not clear at this time whether cladding alone, without benefit of a tough HAZ, which played a pronounced role in arresting propagating flaws in the plates tested, would also have elevated the load-bearing capacity of these plates. In case of radiation embrittled reactor pressure vessels, the HAZ will undergo toughness degradation similar to that of the base metal, because the chemistries are the same. Therefore, it may not play such a prominent role in arresting propagating flaws.

In order to clarify the role played by the HAZ in enhancing the load carrying capacity of the plates, it is possible to perform tests similar to those already performed in this program with plates the cladding of which is removed, leaving only HAZ as a strong surface layer. It should be noted that the thickness of each of the cladding and HAZ is approximately 5 mm each. Such plates could be reconstituted from the broken pieces of the clad plates already tested.

The strength of clad plates with flaws extending the entire width of the plate seems to be governed by the ultimate tensile strength of cladding and HAZ, since the values of K_I for tunneled cracks were insufficient to cause failure.

An important factor that contributed to the enhanced load-bearing capacity of the clad plates was the presence of compressive stresses due to bending. This limited the depth to which the flaw could propagate. In the case of an RPV, a severe thermal shock could initiate a flaw and it may propagate beneath the cladding. The integrity of the vessel could then be challenged by the purely tensile stresses created during repressurization. Nonetheless, the results of this program indicate that if cladding is sufficiently tough, it could prevent flaws from propagating on the surface. The flaws could still tunnel, but if the cladding does not rupture, it reduces K_I somewhat. Considerable analytical work still remains to be performed in order to quantify the reduction of K_I by the relatively thin but tough surface layer. A limited amount of analysis has been performed in this study, but considerably more is yet to be performed, using methods that are still under development.

REFERENCES

1. J. G. Merkle, "Stress-Intensity Factor Estimates for Part-Through Surface Cracks in Plates Under Combined Tension and Bending," pp. 3-22 and 31-32 in *Quarterly Progress Report on Reactor Safety Programs Sponsored by the Division of Reactor Safety Research for July-September 1974, Vol. II Heavy-Section Steel Technology*, ORNL-TM-4729, Union Carbide Corp. Nuclear Div., Oak Ridge Natl. Lab., Oak Ridge, Tenn., November 1974.*

2. H. Tada, P. C. Paris, and G. R. Irwin, *The Stress Analysis of Cracks Handbook*, 2nd ed., Paris Productions, Inc., St. Louis, 1985, pp. 11.3.†

3. S. T. Rolfe and J. M. Barsom, *Fracture and Fatigue Control in Structures, Applications of Fracture Mechanics*, Prentice-Hall, New Jersey, 1977, pp. 180.†

4. S. Timoshenko, *Vibration Problems in Engineering*, 2 ed., D. Van Nostrand, 1937, pp. 342.†

5. J. S. Parrott and B. A. Owens, "Finite-Element Analyses of Plates CP-15, -17, -18, and -19," pp. 248-62 in *Heavy-Section Steel Technology Program Semiannual Progress Report for April-September 1987*, USNRC Report NUREG/CR-4219, Vol. 4, No. 2 (ORNL/TM-9593/V4&N2), Martin Marietta Energy Systems, Inc., Oak Ridge Natl. Lab., Oak Ridge, Tenn., April 1988.*

---

*Available for purchase from National Technical Information Service, Springfield, VA 22161.

†Available in public technical libraries.

6. J. C. Newman, Jr., and I. S. Raju, "Analysis of Surface Cracks in Finite Plates Under Tension or Bending Loads," NASA Technical Paper 1578, December 1979.†

7. R. H. Bryan et al., *Test of 6-in.-Thick Pressure Vessels. Series 3: Intermediate Test Vessel V-8A - Tearing Behavior of Low-Upper-Self Material*, USNRC Report NUREG/CR-4760 (ORNL-6187), Martin Marietta Energy Systems, Inc., Oak Ridge Natl. Lab., Oak Ridge, Tenn., May 1987.*

8. R. D. Cheverton, D. G. Ball, S. E. Bolt, S. K. Iskander, and R. K. Nanstad, *Pressure Vessel Fracture Studies Pertaining to the PWR Thermal-Shock Issue: xperiment TSE-7,"* USNRC Report NUREG/CR-4304 (ORNL-6177), Martin Marietta Energy Systems, Inc., Oak Ridge Natl. Lab., Oak Ridge, Tenn., July 1985.*

---

*Available for purchase from National Technical Information Service, Springfield, VA 22161.

†Available in public technical libraries.

APPENDIX A

SUMMARY OF THE MERKLE EXPRESSION USED TO CALCULATE THE STRESS INTENSITY FACTOR ALONG THE CRACK FRONT FOR SURFACE SEMIELLIPTIC FLAWS

The variation of the stress intensity factor along the crack front of semielliptic flaws was calculated by means of an approximate, closed-form expression due to Merkle [1]. This expression is:

$$K_I = \frac{M_1 M_2}{\Phi} \sigma_s \sqrt{\pi a}\, F(\theta) \ , \tag{A.1}$$

where

$$M_1 = \psi_0(\theta) - (1 - \frac{\sigma_0}{\sigma_s})(2\frac{a}{w})\psi_1(\theta) \ , \tag{A.2}$$

$$M_2 = \sqrt{\frac{\tan(\frac{\pi a}{2w})}{\frac{\pi a}{2w}}} \left[1 + (\frac{a}{w})^{\frac{5}{2}} \sin\theta \right] , \tag{A.3}$$

$$\psi_0(\theta) = 1.211 - 0.186 \sqrt{\cos\theta} \ , \tag{A.4}$$

$$\psi_1(\theta) = 0.18 + 0.54 \ (\frac{a}{b}) \cos\theta \ , \tag{A.5}$$

$$F(\theta) = \left[1 - (\frac{b^2 - a^2}{b^2}) \left(\frac{r_c}{b} \right)^2 \sin^2\theta \right]^{\frac{1}{4}} , \tag{A.6}$$

and

$$\phi^2 = 1 + 4.593 \left(\frac{a}{2b}\right)^{1.65} \qquad (A.7)$$

The variables a, b, r, w, σ_0, σ_b, and θ are defined in Fig. A.1.

Comparisons of stress intensity factors using both the Merkle solution and the finite element method have been previously performed, and some of which will be reproduced here for convenience. For example, Fig. A.2 shows the agreement between the two methods for a semicircular flaw [2]. The flaw was subjected to a stress gradient similar to that produced by a bending load. The excellent agreement between the two solution methods for a semicircular flaw is not surprising since the Merkle solution is a generalization of the solution for a semicircular flaw. However, the closed form solution seems to overestimate K_I at the deepest point for $b' > 1$, Fig. A.3 [3]. Similarly, as shown in Fig. A.4, K_I is overestimated for points along the crack front deeper than about 30% of the total crack depth (also from Ref. 3).

Nonetheless, the closed-form solution has been valuable to the HSST Program for many years [3,4,5] since it allows a very large number of parametric studies to be done very simply.

REFERENCES

1. J. G. Merkle, "Stress-Intensity Factor Estimates for Part-Through Surface Cracks in Plates Under Combined Tension and Bending," pp. 3-22 and 31-32 in *Quarterly Progress Report on Reactor Safety Programs Sponsored by the Division of Reactor Safety Research for July-September 1974*, Vol. II Heavy Section Steel Technology, ORNL-TM-4729, Union Carbide Corp. Nuclear Div., Oak Ridge Natl. Lab., Oak Ridge, Tenn., November 1974.*

2. S. K. Iskander et al., "Calculation of Stress Intensity Factors in Three Dimensions," pp. 97-104 in *Heavy-Section Steel Technology Program Quarterly Progress Report for January-March 1979*, USNRC Report NUREG/CR-0818 (ORNL/NUREG/TM-324), Union Carbide Corp. Nuclear Div., Oak Ridge Natl. Lab., Oak Ridge, Tenn., August 1979.*

3. R. D. Cheverton et al., *Pressure Vessel Fracture Studies Pertaining to the PWR Thermal-Shock Issue: Experiment TSE-7*, USNRC Report NUREG/CR-4304 (ORNL-6177), Martin Marietta Energy Systems, Inc., Oak Ridge Natl. Lab., Oak Ridge, Tenn., July 1985.*

4. R. H. Bryan et al., *Test of 6-in.-Thick Pressure Vessels. Series 3: Intermediate Test Vessel V-8*, USNRC Report NUREG/CR-0675 (ORNL/NUREG-58), Union Carbide Corp., Oak Ridge Natl. Lab., Oak Ridge, Tenn., December 1979.*

5. R. H. Bryan et al., *Test of 6-in.-Thick Pressure Vessels. Series 3: Intermediate Test Vessel V-84 - Tearing Behavior of Low-Upper-Self Material,* USNRC Report NUREG/CR-4760 (ORNL-6187), Martin Marietta Energy Systems, Inc., Oak Ridge Natl. Lab., Oak Ridge, Tenn., May 1987.*

*Available for purchase from National Technical Information Service, Springfield, VA 22161.

ORNL-DWG 74-10460R

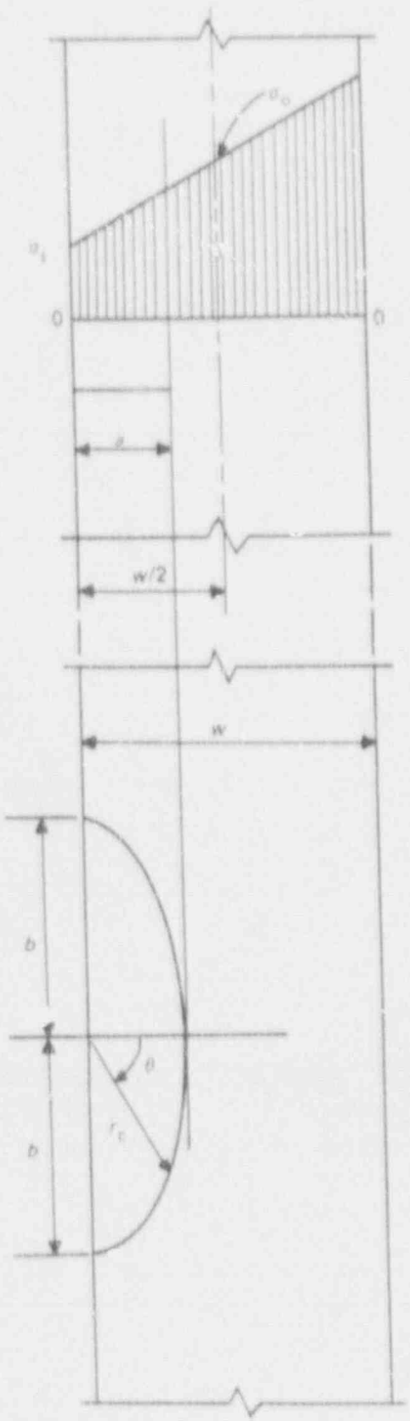

Fig. A.1. Definition of terms associated with the analysis of a semielliptical surface crack.

ORNL-DWG 79-5919A ETD

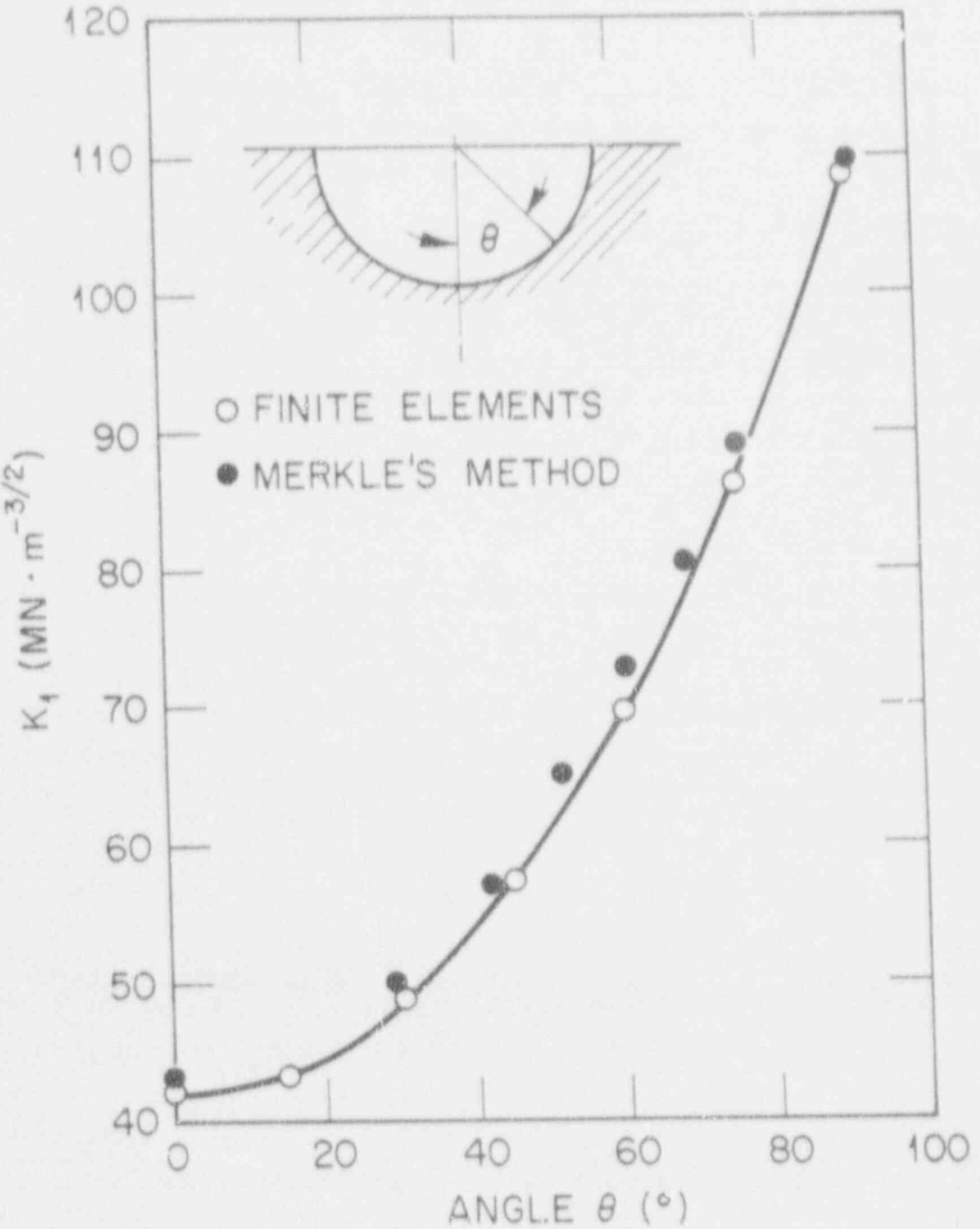

Fig. A.2. Comparison of the stress intensity factor K_I for a semicircular flaw calculated by two methods. The angle θ is measured from the deepest point on crack front. The flaw is 19 mm deep and is subjected to a steep thermal stress gradient, see Ref. 2.

ORNL-DWG 89-7108R

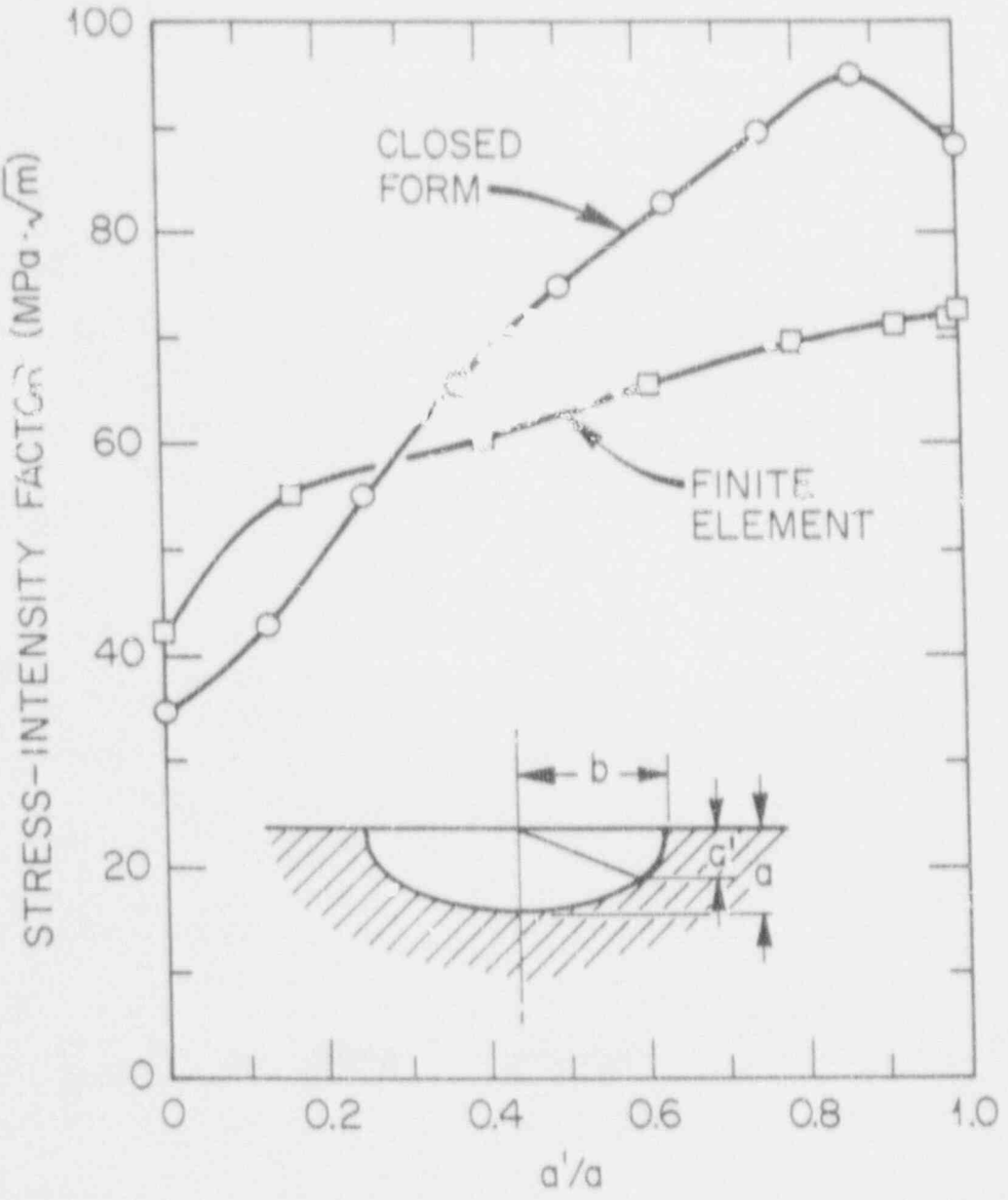

Fig. A.3. Comparison of the variation of K_I along the crack front as calculated by two methods for a semielliptic flaw. The crack is 19 mm deep, b/a = 10 (from Ref. 3).

ORNL-DWG 89-7109R

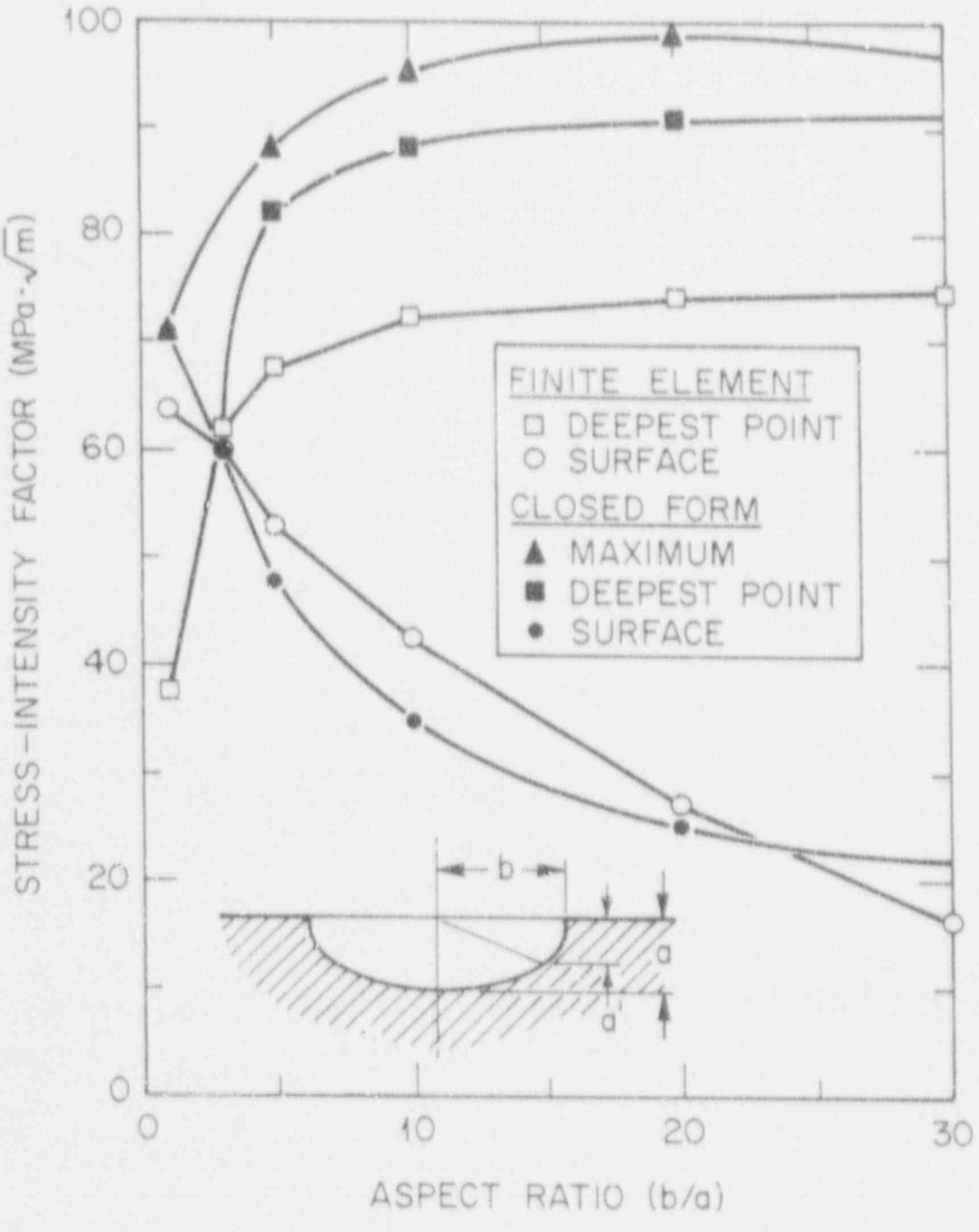

Fig. A.4. Comparison of K_I calculated by two methods for semielliptic flaws as function of b/a. The crack is 19 mm deep (from Ref. 3).

APPENDIX B

RELATIONSHIP BETWEEN THE FRACTIONAL CRACK DEPTH OF A POINT ON THE CRACK FRONT OF A SEMIELLIPTICAL CRACK AND THE ANGLE β

In the main body of the report, the stress intensity factor K_I was plotted as a function of its position along the crack front of a semielliptic crack. The position along the crack front of a semielliptic crack was given as either the fractional crack depth (a'/a), where (a') and (a) are the depth of the point and the crack depth, respectively, measured from the surface of the crack, or as a function of the angle β, measured from the surface toward the deepest point, see Fig. B.1. Each method of indicating position along the crack front has advantages and disadvantages.

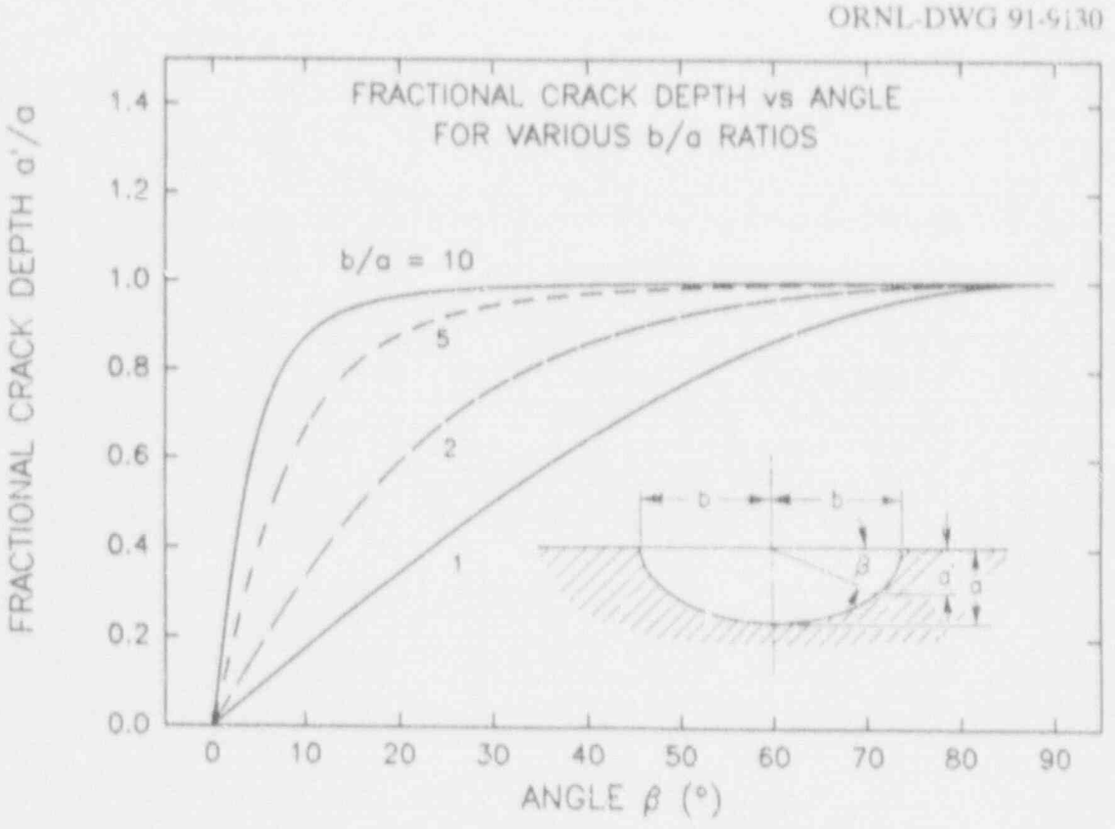

Fig. B.1. The variation of the fractional crack depth (a'/a) with angle β of a point on the crack front of a semiellipse whose major and minor axes are a and b, respectively.

The relationship between (a'/a) and β is not linear, which makes the direct comparison of variations of K_I difficult if different methods of representing the position along the crack front are used. For example, it is not immediately apparent where the maximum value of K_I is located with respect to its position along the crack front as a function of the fractional crack depth if the data were presented as a function of the angle β, and *vice versa*.

The relationship between (a') and β depends on the values of the major and minor axes (b) and (a), respectively, of the semielliptic crack:

$$a' = \sqrt{\frac{1}{\frac{1}{(b\,\tan\beta)^2} + \frac{1}{a^2}}} \qquad \text{(B.1)}$$

or if expressed as in terms of the fractional crack depth (a'/a)

$$\frac{a'}{a} = \sqrt{\frac{1}{\frac{1}{(\frac{b}{a}\,\tan\beta)^2} + 1}} \qquad \text{(B.2)}$$

A plot of the variation of (a'/a) as a function of β for various values of the ratio b/a (Eq. B.2) is given in Fig. B.1. It may be seen that for values of b/a > 1, either method of representing position along the crack front becomes very sensitive to small changes.

APPENDIX C

DRAWINGS OF INITIAL AND ARRESTED CRACK SHAPES FOR CLAD AND UNCLAD PLATE SPECIMENS TESTED

ORNL-DWG 90-16518

CP-15

(1) EVENT 1, H_2 POP-IN OF EB WELD, DYNAMIC FLAW INITIATION

(2) EVENT 2, FIRST ARREST PROFILE

(3) EVENT 3, STATIC FLAW INITIATION

(4) EVENT 4, SECOND ARREST PROFILE

ALL DIMENSIONS IN cm

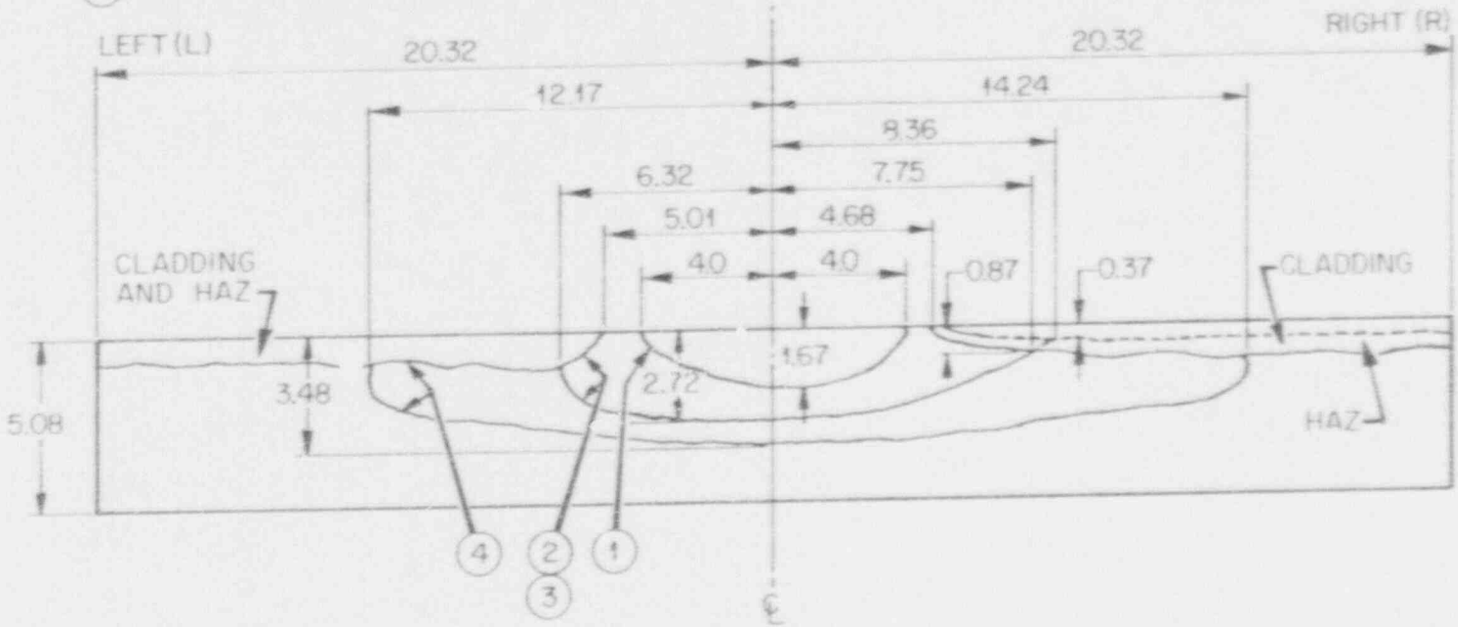

ORNL-DWG 90-16519

CP-16

(1) EVENT 1, H_2 POP-IN OF EB WELD AND ARREST, STATIC FLAW INITIATION

(2) EVENT 2, FIRST ARREST PROFILE

(3) EVENT 3, STATIC FLAW INITIATION

(4) EVENT 4, SECOND ARREST PROFILE

ALL DIMENSIONS IN cm

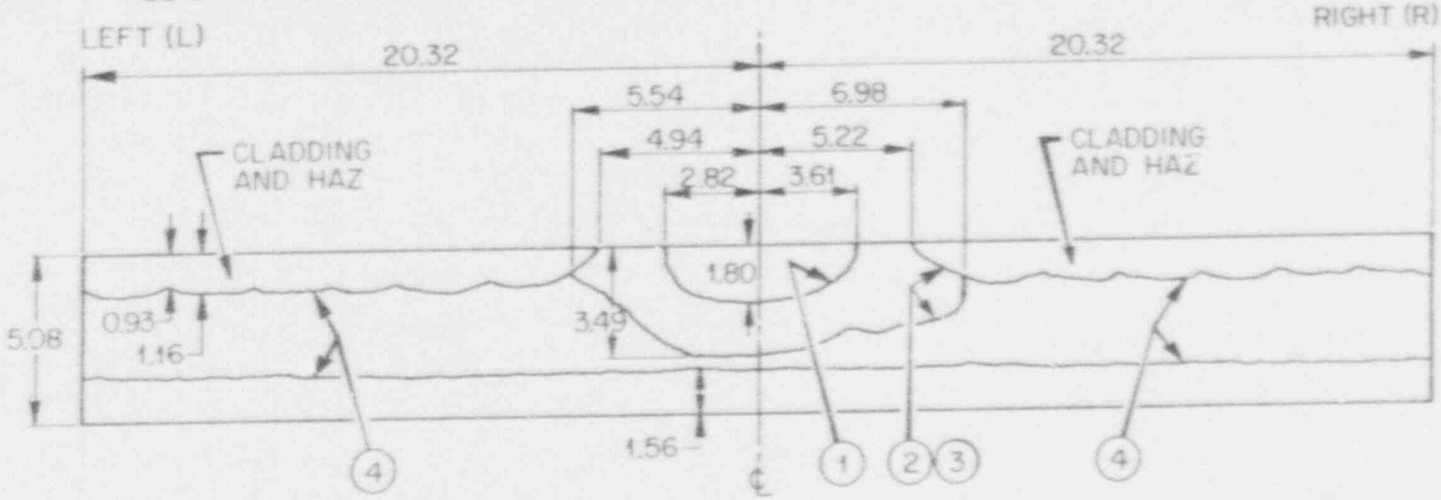

ORNL-DWG 91-9127

CP-17

① EVENT 1, FIRST ARREST PROFILE OF POP-IN OF FB WELD; INITIATION OF FLAW PROFILE OF 2nd EVENT

② EVENT 2, "BOX-BEAM" ARREST PROFILE OF 2nd EVENT; FLAW INITIATION PROFILE PRIOR TO RUPTURE

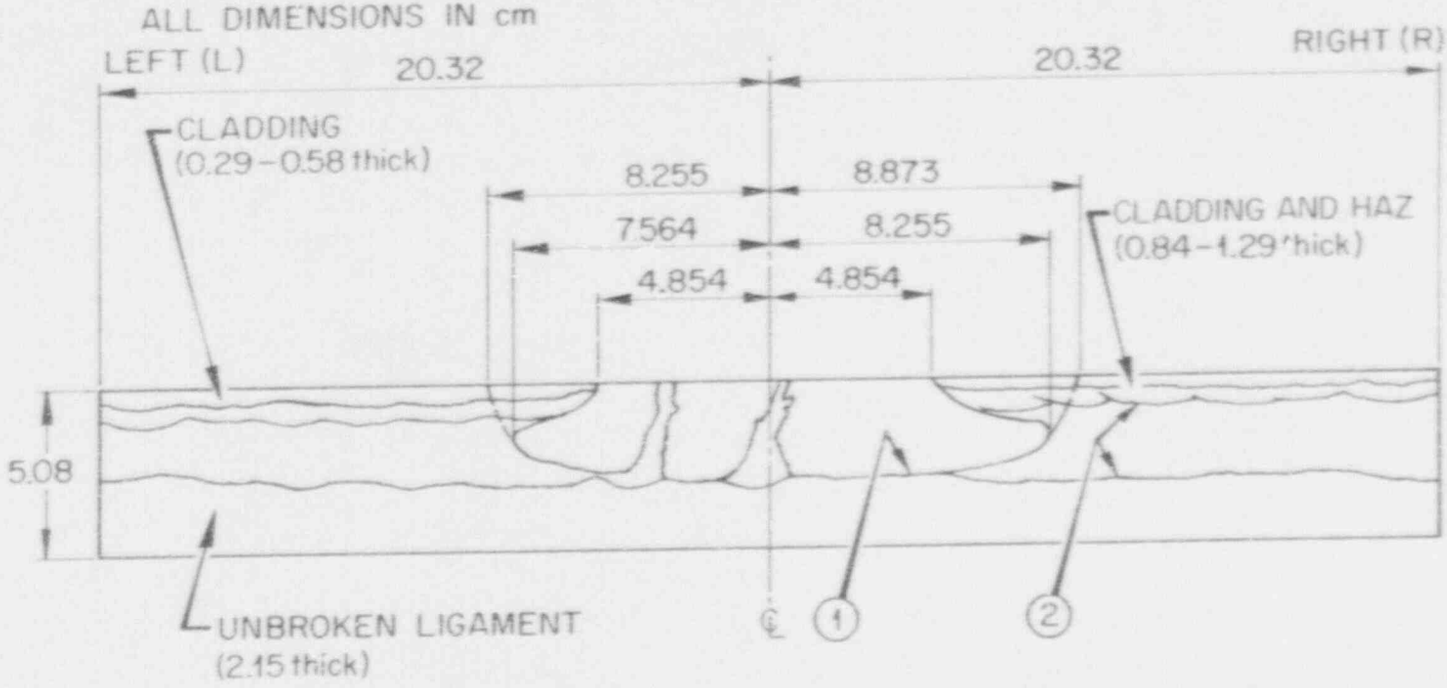

ORNL-DWG 90-16520

CP-18

(1) EVENT 1, H_2 POP-IN OF EB WELD, DYNAMIC FLAW INITIATION

(2) EVENT 2, ARREST PROFILE

ALL DIMENSIONS IN cm

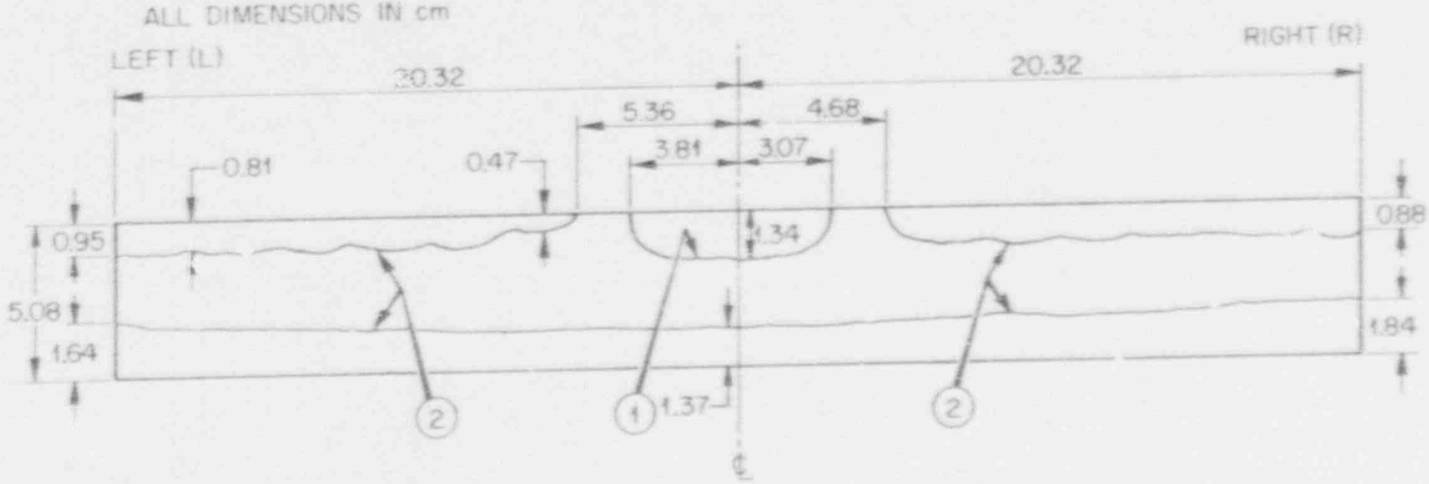

ORNL-DWG 91-9128

CP-19

(1) EVENT 1, FIRST ARREST PROFILE OF POP-IN OF EB-WELD;
INITIATION OF FLAW PROFILE FOR 2nd EVENT PRIOR TO RUPTURE

ALL DIMENSIONS ARE IN cm

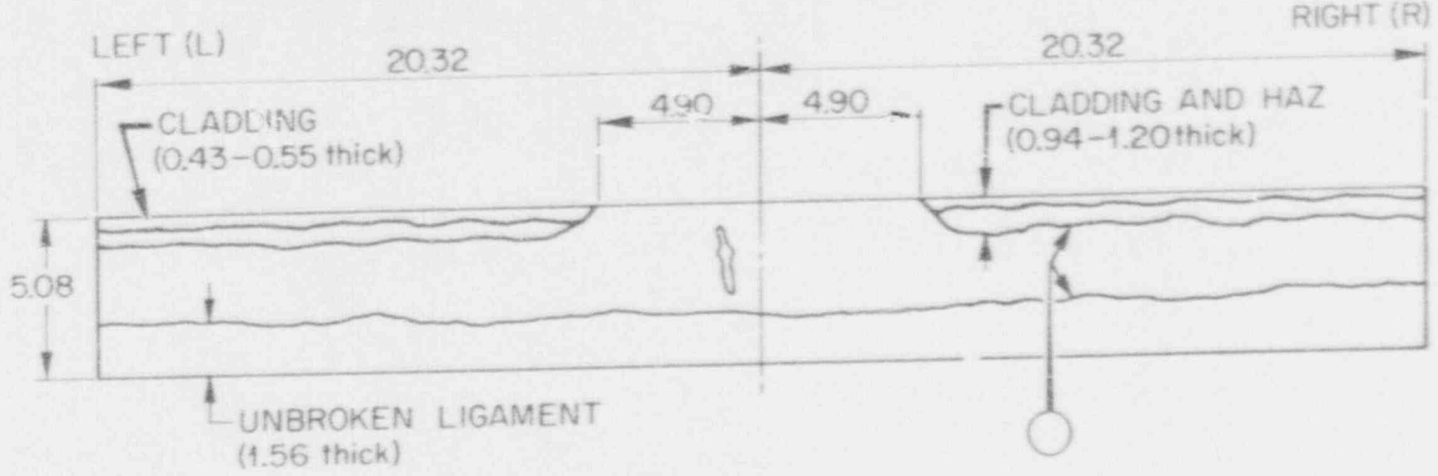

ORNL-DWG 90-16521

CP-20

(1) EVENT 1, H_2 POP-IN OF EB WELD, DYNAMIC FLAW INITIATION

ALL DIMENSIONS IN cm

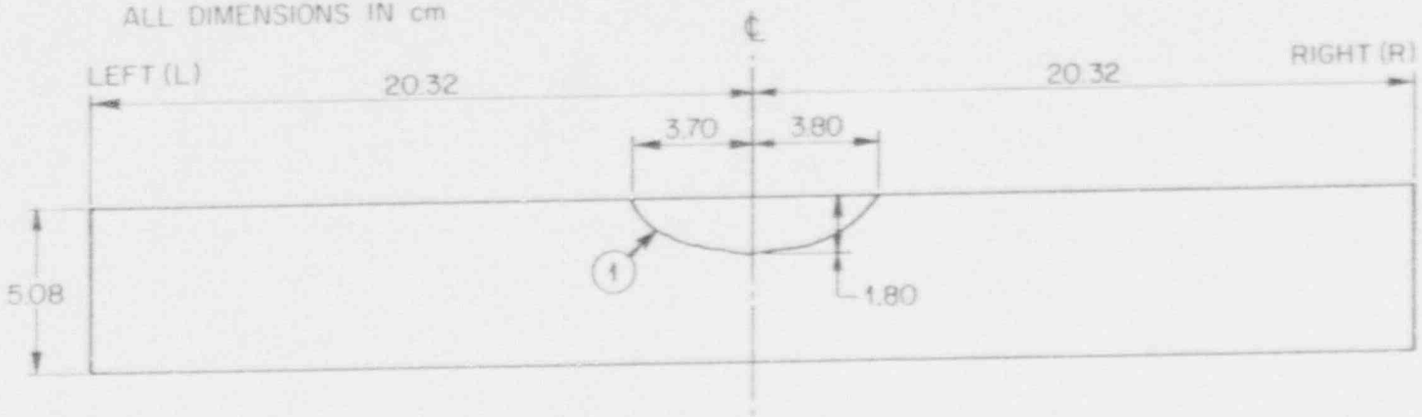

ORNL-DWG 90-16522

CP-21

(1) EVENT 1, H_2 POP-IN OF EB WELD

ALL DIMENSIONS IN cm

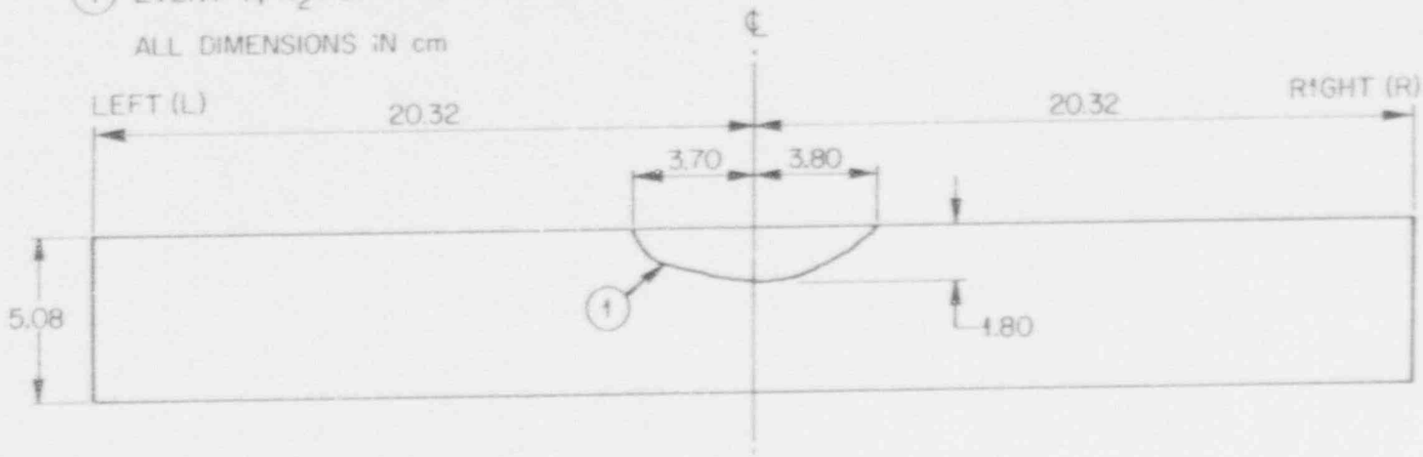

ORNL-DWG 90-16523

CP-22

(1) EVENT 1, H_2 POP-IN OF EB WELD

ALL DIMENSIONS IN cm

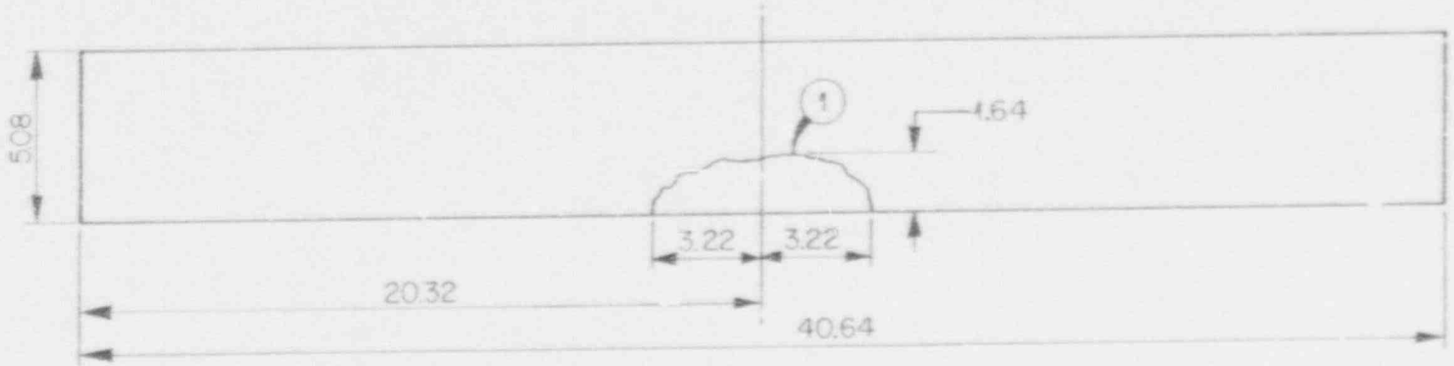

APPENDIX D

FINAL REPORT SUBMITTED BY COMBUSTION ENGINEERING ABOUT THE HEAT TREATMENT OF THE PLATE MATERIAL AND THREE-WIRE CLADDING OF THE PLATES

HEAT TREATMENT AND WELD OVERLAY

CLADDING OF HSST PLATE 012B

FOR MARTIN MARIETTA ENERGY SYSTEMS, INC.
SPECIFICATION MET-PV/-WRCO 21883
SUBCONTRACT 76X-72185V

FINAL REPORT: MAY 13, 1985

MML-85-100

Prepared By: _____
C. D. Hackett

_____
C. T. Ward

C-E Contract 8583
Project No. 90C588
Shop Order 98130469

Heat Treatment and Weld Overlay Cladding of HSST Plate 012B

For Martin Marietta Energy Systems, Inc.

Specification MET-PVT-WRCO 21883

Subcontract 76X-72185V

1.0 INTRODUCTION

Under this subcontract C-E supplied a number of test specimens which were cut from the subject plate and fabricated per customer specifications and drawings. Activity by C-E included heat treatment, weld overlay cladding, mechanical property tests, and preliminary machining. Specimens were then delivered to the customer for final machining and testing as part of a program to assess the effect of weld overlay cladding on fracture behavior of pressure vessels.

The base material, HSST 012B, was supplied by the customer as a 7 inch thick plate of A533B composition, 64 inches wide and 273 inches long. Work at C-E used 115 inches of plate length to make the delivered specimens, additional trial welds and mechanical property tests.

To represent older pressure vessels the customer specified that weld overlay cladding be made by the three wire series arc process, a method now replaced by newer practice. Hence it was necessary for C-E to reconstitute a suitable welding equipment system and to obtain the special welding filler metals for the series arc process. Most of the subcontract effort and span time was directed to compliance with the Charpy-V notch (CVN) impact test properties specified for the cladding deposit. After acceptable properties were demonstrated, the fabrication of the delivered test specimens was performed in about 10 weeks.

This report and Attachments 1 and 2 provide a record of the fabrication and testing performed under the subcontract.

2.0 HEAT TREATMENT AND MECHANICAL PROPERTIES OF BASE METAL

After receipt of HSST 012B, all of the material used by C-E was oxygen cut from the plate into three pieces as shown in Figure 1. At this time, the fabrication base plate (95 X 64 inches) was oriented, laid out and identified as shown in Drawing C-SK-GCR 111082-001. Until the austenitizing heat treatment was completed as described below, the fabrication base plate was kept intact as a single 95 X 64 inch piece. The 20 X 33 inch piece, identified as initial heat treatment block in Figure 1, was used to determine heat treatment procedures and resultant mechanical properties. Subsequently the remainder of the initial heat treatment block was consumed as base metal for the series arc cladding tests as was the 20 X 31 inch block identified for cladding tests in Figure 1.

2.0 HEAT TREATMENT AND MECHANICAL PROPERTIES OF BASE METAL - CONTINUED

Initially the grain coarsening response of HSST 012B was determined by heat treating a number of small specimens taken from a 20 X 1 inch slice, saw cut as shown in Figure 1 from the lower edge of the initial heat treatment block. Results indicated that austenitizing above 1900°F would risk excessive grain coarsening. Therefore a nominal austenitizing treatment of 1890°F for two hours was selected, with cooling in still air to minimize gradients in mechanical properties and to further raise the ductile/brittle transition temperature. This treatment was then applied to the remainder of the initial heat treatment block (now 20 X 32 inches) in a gas fired lab furnace after fitting a seal welded buffer plate, 7 X 7 inches, around the entire periphery as a picture frame. Buffer plate material was from another heat of A533B. Cooling was in nominally still air with plate suspended vertically above floor level, thickness direction being horizontal.

Later, the same normalizing treatment, 1890°F two hours, was applied to the 95 X 64 inch fabrication base plate in a gas fired shop furnace, also with plate suspended vertically for cooling above floor level, but with A533B buffer material of 8 inch thickness and 5 inch width fillet welded around the plate edge. Temperature and cooling rates were measured during normalizing at midpoint and plate edges by thermocouples implanted at the 1/4T. Variation from edge to midpoint during cooling was negligible, due to the edge buffer, and was smaller in the case of the larger fabrication base plate. Uniformity of temperature during cooling was verified by visual observation of temperature "color" and by optical pyrometer readings over the entire plate surfaces. When a need arose later for additional test material, this uniformity of heat treatment, edge to edge, allowed mechanical tests to be made in the 7 inch wide edge allowance material shown in Figure 1 adjacent to the heat treatment verification block.

Cooling time of 2.5 hours from austenitizing temperature to 900°F was the same for both plates. However, during the temperature interval of 1300°F to 975°, the larger fabrication base plate cooled faster than the initial heat treatment block due to natural air currents and lower ambient temperature in the shop area than in the lab.

mpering after normalizing was combined with post weld heat treatment (PWHT), to be performed as one step after the completion of any welding. This practice is in accordance with paragraph NB2170 of Section III, ASME Boiler and Pressure Vessel Code.

After normalizing, a series of mechanical tests were made, first from the initial heat treatment block within the lower right quadrant as shown in Figure 1, and later from the heat treatment verification block and the adjacent 7 inch wide edge allowance block. All test data sheets are

2.0 HEAT TREATMENT AND MECHANICAL PROPERTIES OF BASE METAL - CONTINUED

included in Attachment 1, identified by a laboratory test code symbol as listed in Table 1 below. During this period of testing, the portion of the fabrication test block to the left of the heat treatment verification block was kept intact and in the as-normalized condition.

Table 1. Mechanical Test Locations and Identification Test Code

LAB TEST CODE	LOCATION	PWHT
GK	Initial Heat Treatment Block Lower Right Quadrent in Figure 1.	1125°F 40 Hrs.
GO	Initial Heat Treatment Block Lower Right Quadrant in Figure 1.	1125°F 40 Hrs.
HR Tensile Tests	Heat Treatment Verification Block at Midwidth of Plate	1130°F 40 Hrs.
HR CVN Tests PA-PI	Heat Treatment Verification Block at Midwidth of Plate	1130°F 40 Hrs.
HP Tensile Tests	Heat Treatment Verification Block at Midwidth of Plate	1115°F 40 Hrs.
HP CVN Tests PA-PI	Heat Treatment Verification Block at Midwidth of Plate	1115°F 40 Hrs.
HR CVN Tests PI-P18	Heat Treatment Verification Block Near Plate Edge	1130°F 40 Hrs.
HP CVN Tests PI-P18	Heat Treatment Verification Block Near Plate Edge	1115°F 40 Hrs.
IX	Heat Treatment Verification Block Near Plate Edge	1130°F 40 Hrs.
IW	Heat Treatment Verification Block Near Plate Edge	1115°F 40 Hrs.
KZ	7-Inch Edge Allowance Block Adjacent to Heat Treatment Verification Block at Midwidth of Plate	1100°F 10 Hrs.
KY	7-Inch Edge Allowance Block Adjacent to Heat Treatment Verification Block at Midwidth of Plate	As Normalized

2.0 HEAT TREATMENT AND MECHANICAL PROPERTIES OF BASE METAL - [illegible]

The heat treatment verification block and adjacent edge allowance block had been removed by oxygen cutting across the full 64 inch width of the plate. However the mechanical test locations were confined to the 30 inch section shown in Figure 1.

Results of all mechanical tests are summarized below in Table 2. The large amount of scatter in CVN impact test results from the heat treatment verification block was investigated but the cause was not proven. No difference could be seen by light microscopy between broken CVN specimens representing extreme limits of the scatter band, nor could the microstructure of the heat treatment verification block be distinguished from that of the initial heat treatment block, which displayed less scatter. Specimens with scatter had been machined at a different time period and the extent of machining cold work at the notch tip was considered. An improved lubricant was adopted for notch machining before specimens from the edge allowance block were made. These displayed less scatter than specimens from the verification block.

Table 2. Mechanical Properties of HSST 012B

Location	Temper PWHT °F Hrs.	Yield Strength KSI	Tensile Strength KSI	DWT NDTT °F	20 Ft. Lb. CVN Temperature °F
Initial Heat Treatment Block	1125 40	79.8 79.1	99.0 98.7	70	25
Heat Treatment Verification Block	1130 40	76.7 76.7	96.5 96.7	75	10 to 110
Heat Treatment Verification Block	1115 40	81.2 80.9	101.3 100.9	80	10 to 110
7-Inch Edge Allowance Block	1100 10	87.2 86.1	107.5 105.7	120	60
7-Inch Edge Allowance Block	NONE	83.3 82.4	111.5 110.1	130	100

3.0 WELDING CONDITIONS AND WELD PROPERTIES:

3.1 Weld Metal CVN Impact Test Requirements and Procedures

Using Standard 10 x 10 mm specimens, a CVN energy value of 40 foot pounds minimum was specified for the clad deposit when tested at or below the ductile-brittle transition temperature of the base metal, defined as the lesser of:

- The 20 foot pound CVN transition temperature of the base metal
- Or that temperature which is 20°F below the drop weight test nil-ductility temperature (NDTT) of the base metal.

To examine variation of properties as influenced by the reheating or hot straining effects in multilayer deposits, the specification also included 10 x 5 mm subsize CVN tests in each layer, broken at the base metal ductile-brittle transition temperature, both with and without application of the next layer. Amount of cladding to be applied to the delivered test specimens ranged from one to three layers. Therefore, subsize CVN tests were required for each of the following five conditions:

- First layer alone
- First layer after applying second layer
- Second layer
- Second layer after applying third layer
- Third layer

To be acceptable, each of these five test conditions must display an average CVN energy value within ± 20% of the mean energy of all specimens from all five conditions.

The CVN specimens were oriented parallel to the welding direction with the notch base normal to the weld face. Standard 10 x 10 mm specimens were made from two layer deposits since the deposited thickness (buildup) is about 0.3 inches per layer. Most of the cross section area of the 10 x 10 mm specimens was from second layer deposit which would then largely govern the properties. A 5 mm height for the subsize specimen was the largest size that could be sandwiched between layers because of the irregular fusion boundary surfaces. In several cases some of the adjacent layer was found to be unintentionally present on a 10 mm face of subsize specimens.

3.2 Welding Procedure, Filler Metals and Deposit Composition

3.2.1 All submerged arc flux used on the subcontract was from a single lot of Arcosite S-4, Lot number OD 2F. This grade has not been produced for years, but enough was obtained as surplus material from another fabricator. To reduce the

effect of any variability of the flux, the material was homogenized by reblending in a Patterson Kelly Blender. As a further precaution during all first layer welding on the delivered specimens, vacuum recycling of the flux was avoided and only virgin flux was used.

3.2.2 Preheat and interpass temperature was controlled within the range of 300°F - 350°F for all welding during the subcontract.

3.2.3 Arrangement of welding filler wires is shown in Figure 2 as they enter the arc zone, looking in the weld travel direction. Identification and chemical check analysis results for filler wires are listed in Table 3 below.

Table 3. Filler Wires Used on Subcontract.

Lab No.	R6193	R5713	R5714	R6172
Size	5/32" ϕ	5/32" ϕ	5/32" ϕ	5/32" ϕ
Type	312	308	309	304
Heat No.	3F428L	9667	775568	646093
C	.054	.024	.018	.063
Mn	1.55	1.69	1.57	1.06
P	.016	.019	.007	.022
S	.007	.012	.011	.016
Si	.34	.49	.14	.55
Ni	8.88	9.66	12.84	8.71
Cr	30.45	20.70	24.31	18.46
Mo	.06	.19	.05	.29
V	.08	.04	.03	.09
Cb	< .01	< .01	< .01	< .01
Ti	< .01	< .01	.08	< .01
Co	.05	.04	.03	.11
Cu	.06	.09	.02	.64
N	.063	.039	.060	.062

For all welds on the subcontract, the vertical hot wire label[illegible] (for vertical) in Figure 2 was Type 308, listed unde[illegible] in Table 3. Various combinations of Type 308, T304 [illegible]d T304 were employed during the series of weld tests for the angled hot wire "A" and the cold wire "C", as labeled in Figure 2.

At the left side of Figure 2 a stationary cold wire is shown tack welded at the 135° corner detail present on the delivered specimens identified as beam specimen fabrication slabs. Labeled "S" for stationary, this fourth wire was used only at this location for the initial pass or "corner pass".

The stationary cold wire "S" was Type 312 listed under R6193 in Table 3. A second layer corner pass was not needed since the beam fabrication slabs had only one layer of clad. Initial weld passes for all other delivered test specimens were made on an attached side bar extension which was discarded, hence not subject to testing.

Combination of filler wires used for the three weld layers on the delivered test specimens is listed in Table 4 along with welding conditions. Table 4 is also applicable to the final test weld to determine weld metal CVN properties, which was found acceptable, and is identified as test code "00". Note that layers two and three are identical, both as to filler wire selection and welding conditions.

Table 4. Filler Wire and Welding Conditions for Delivered Test Specimens and for Laboratory Test Code "00".

		Layer Number			Corner
		1st	2nd	3rd	Pass
	Amps	480	480	480	480
	Volts	25	25	25	26
	Travel IPM	8	8	8	7.5
V	Type	308	308	308	308
	Feed IPM	47	47	47	47
A	Type	309	304	304	309
	Feed IPM	47	47	47	47
C	Type	308	304	304	309
	Feed IPM	18	18	18	18
S	Type				312
	Feed IPM	-	-	-	7.5

During cladding of the delivered test specimens, delta ferrite content was monitored with a Fischer Ferritscope calibrated in accordance with AWS A4.2. Readings observed are as follows:

- Corner Pass on Beam Fabrication Slabs ..... 8 to 9 FN
- First Layer..... 7.5 to 10 FN
- Second and Third Layers..... 8 to 10 FN

Chemical check analysis of first and third layers was taken from the runout tab attached to the end of the delivered

Multilayer Clad Block. Results are listed below in Table 5. Item D41083 is the first layer check and D41084 is the third layer. Additional check analysis results taken from separate test welds using the same set of welding conditions in Table 4 are also listed in Table 5.

Table 5. Check Analysis of Weld Layers Listed in Table 4. D41083 and D41084 are from Delivered Test Specimens. Others from Separate Test Welds.

Lab No.	D41083	D41084	D40950	D40954	D40955	D40956	D41050
Layer	1	3	1	1	2	3	Corner Pass
C	.051	.049	.055	.049	.049	.049	.056
Mn	1.51	1.26	1.59	1.53	1.28	1.34	1.47
P	.015	.022	.016	.016	.023	.023	.013
S	.016	.019	.014	.013	.017	.017	.012
Si	.67	.81	.63	.66	.78	.82	.69
Ni	9.91	9.08	9.75	9.97	9.18	9.04	9.39
Cr	20.11	19.38	19.75	20.21	19.38	19.34	19.85
Mo	.17	.23	.18	.16	.23	.23	.18
V	.03	.07	.03	.03	.06	.06	.03
Cb	<.01	<.01	<.01	<.01	<.01	<.01	<.01
Ti	.01	<.01	<.01	<.01	<.01	<.01	<.01
Co	.03	.07	.03	.03	.07	.08	.03
Cu	.06	.40	.07	*	.36	.39	.06
N	.049	.057	.051	.047	.054	.055	.051

*Cu contamination during button remelting of chips. All other samples were solid pieces and not remelted.

In addition to the delivered specimens and Test Code "00", the second and third layer procedure listed in Table 4 was used for all preceding test welds, except for the first two made which are identified as test codes GP and IK. Filler metals for 1st and 2nd layers of these two initial test welds are as follows:

	FIRST LAYER			SECOND LAYER		
	V	A	C	V	A	C
GP	308	308	309	308	308	308
IK	308	308	309	308	304	308

All subsequent weld tests from test code IL through OC utilized Table 4 conditions for the second and for the third layer where applied. It was believed important to maintain carbon content of the second and third layers at 0.05% which

is the lowest carbon content consistently achievable in the first layer due to carbon gain from base metal dilution. The Table 4 combination for second layer represented the only filler wire heats available at the time which would provide 0.05% carbon in second and third layers and, at the same time, a relatively low level of delta ferrite and chromium content to minimize intermetallic phases during PWHT. Practice for the first layer of the other test welds was varied as listed below in the order they were made and tested:

Test Code Identification	V	A	C
IL, LE, LF LG, LM, MS	308	308	304
NH	308	308	309
OC	308	309	309

Typical compositions of first layer deposits are listed in Table 6. Second and third layer compositions are in Table 7.

Table 6. Compositions of First Layer Deposits. Test Codes GP through OC.

Test Code	GP	IK	IL Through MS			NH	OC
Lab No.	D40668	D40672	D40618	D40684	D40762	D40952	D40948
C	.047	.060	.049	.058	.057	.048	.042
Mn	1.59	1.60	1.46	1.45	1.47	1.57	1.62
P			.023	.023	.022	.017	.013
S			.015	.014	.016	.015	.016
Si	.77	.73	.76	.71	.72	.71	.74
Ni	9.69	8.88	8.73	8.53	8.41	9.00	10.63
Cr	19.64	17.95	18.87	18.35	18.02	18.93	21.63
Mo	.20	.23	.22	.23	.23	.20	.13
V	.04	.04	.04	.04	.04	.03	.03
Cb	<.01	<.01	<.01	<.01	<.01	<.01	<.01
Ti	.02	.02	<.01	<.01	<.01	<.01	.01
Co	.05	.06	.04	.04	.04	.03	.02
Cu	.10	.10	.16	.16	.15	.07	.05
N	.047	.046	.044	.044	.046	.045	.055

Table 7. Compositions of Second and Third Layer Deposits. Test Codes GP through OC.

Test Code	GP	IK	IL Through NH			OC
Lab No.	D30667	D40671	D40764	D40665	D40812	D40949
Layer No.	2	2	2	2	3	2
C	.040	.046	.052	.053	.052	.047
Mn	1.63	1.45	1.23	1.30	1.23	1.34
P			.024	.023	.024	.021
S			.019	.018	.019	.020
Si	.76	.80	.74	.75	.78	.79
Ni	9.66	9.15	8.99	8.97	8.87	9.22
Cr	20.54	19.59	19.18	19.18	19.27	19.60
Mo	.18	.22	.23	.24	.24	.22
V	.04	.05	.06	.06	.07	.06
Cb	< .01	< .01	< .01	< .01	< .01	< .01
Ti	.02	.02	< .01	< .01	< .01	< .01
Co	.04	.07	.07	.07	.07	.07
Cu	.10	.29	.36	.35	.40	.36
N	.047	.052	.059	.058	.057	.056

3.3 CVN Impact Tests of Weld Deposits.

3.3.1 All of the test data is included in Attachment 2 as separate sheets for Test Codes, GP, IK, IL, LE, LF, LG, LM, MS, NH, OC, and OO. Also in Attachment 2 are data sheets listing check chemical analysis of selected broken CVN specimens. Location analyzed by XRF was the 10 mm wide face and root surface, as close as possible to the fractured end. However, with the 10 mm diameter XRF mask size the distance from the broken end to the beam center was at least 6 mm. Therefore the compositions may not be representative of the fracture face, particularly in first layer specimens where base metal dilution effects can vary significantly over a weld travel distance of 6 mm. Correlation of check analysis with CVN results indicates that a lean alloy content approaching the martensite line on the DeLong diagram is detrimental. In the case of Test Code MS, and others, the lean alloy content was caused by an unintended increase of base metal dilution in first layer passes. Other results in Attachment 2, notably from the first layer of Code "OC", suggest that a very high content of Cr, Ni and delta ferrite is beneficial to CVN properties.

3.3.2 Figures 3, 4 and 5 show the standard CVN specimen energy level versus test temperature for test codes GP, IK, IL, LE, LF, LG and LM, made and tested as two layer deposits. Of these, IL, LE, LF, LG and LM are identical to test code OO

and the delivered specimens with regard to the second layer procedure and chemical composition. The subsize CVN results further indicate that the first layer properties of OO and the delivered specimens should be better than the first layer of these earlier specimens. Figures 3 and 4 indicate that the 40 foot pound temperature is about 50°F. In Figure 4 there is no obvious difference between specimens postheated at 1125°F 40 hours and those at 1100°F 10 hours, nor is there an obvious effect of reheating. As seen in Figure 5 reheating does have embrittling effect in the as-welded condition.

3.3.3 The subsize CVN specimens from test code "OO" meet the criteria for ± 20% maximum variation from the mean energy value. Data from "OO" suggests that high base metal dilution during the first layer is detrimental and may be the cause of scatter in CVN energy observed in first layer results. For this reason, the flux was not recycled during first layer cladding of delivered specimens.

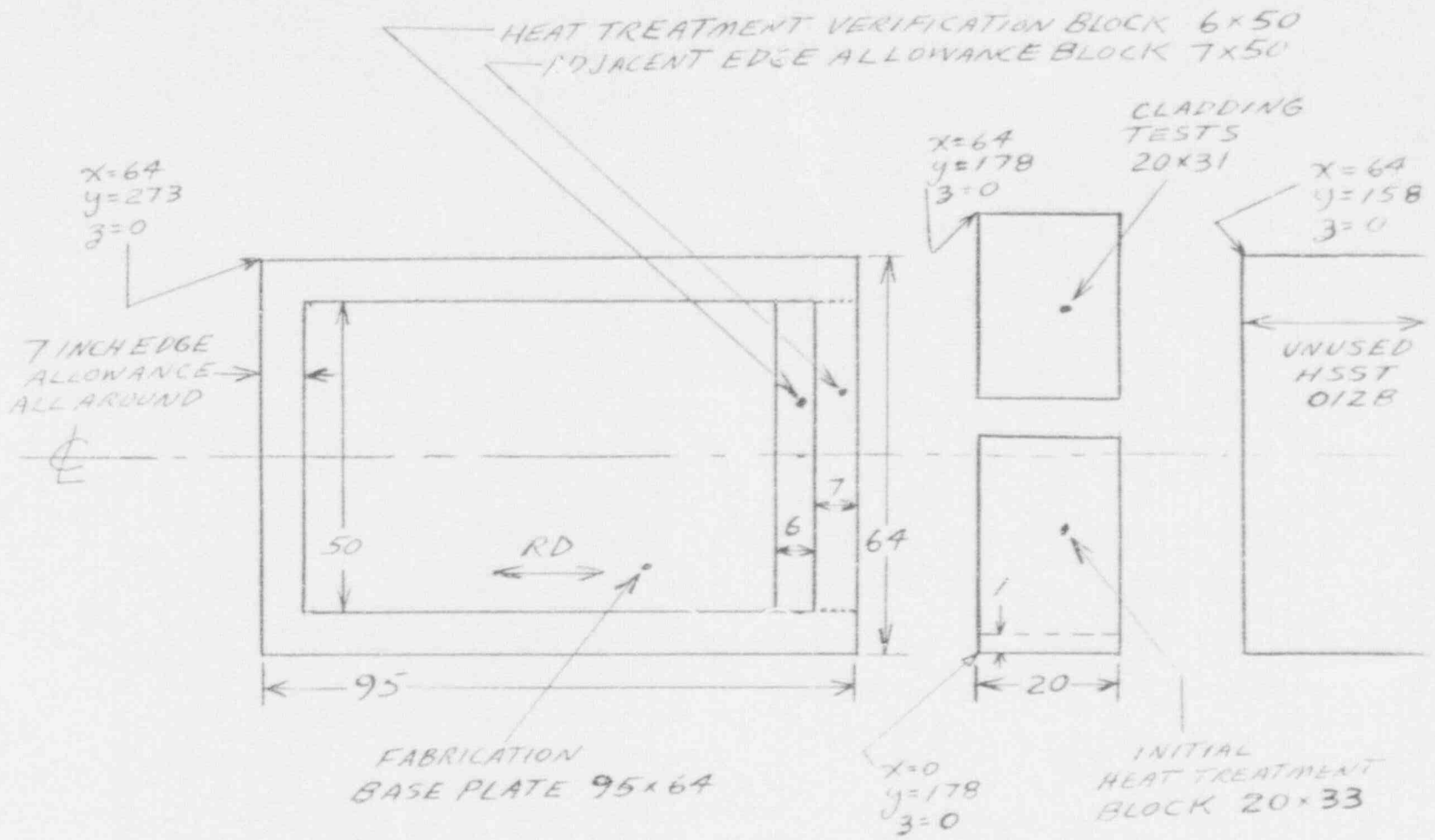

FIGURE 1. LAYOUT AND CUTTING OF HSST 012B

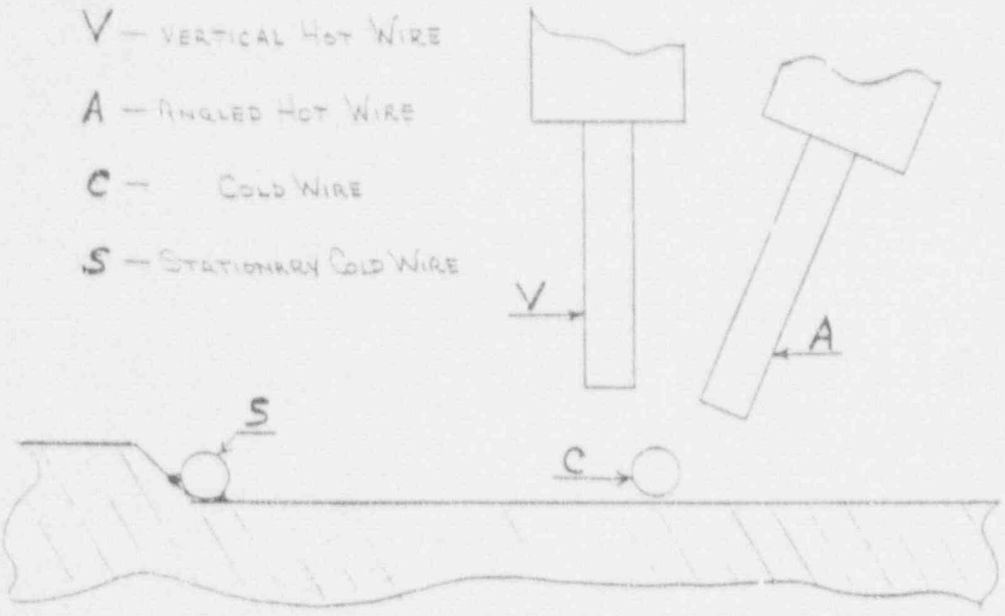

FIGURE 2. ARRANGEMENT OF HOT WIRES COLD WIRE, AND A STATIONARY WIRE FOR CORNER PASS

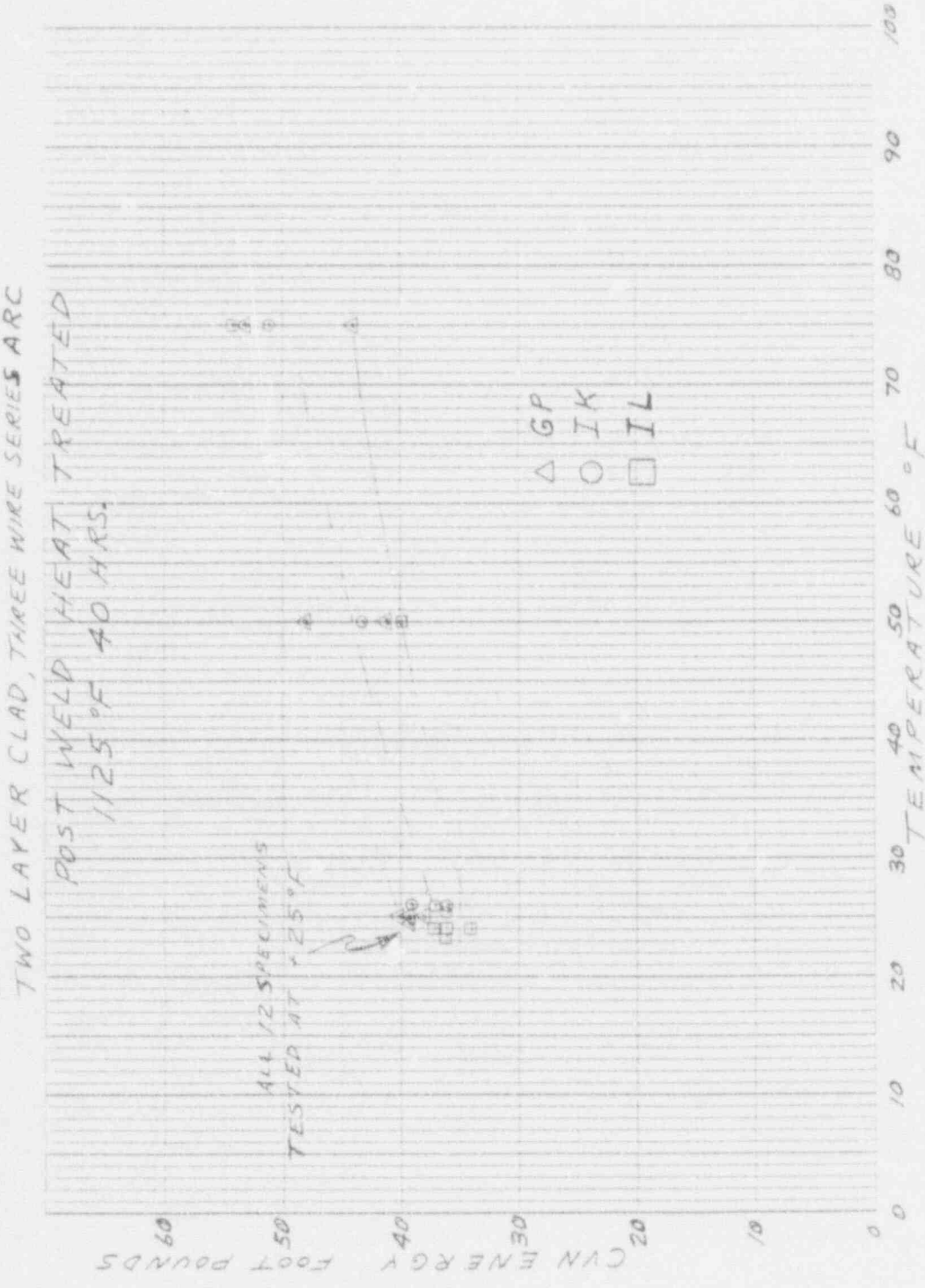

FIGURE 3. CVN RESULTS FOR GP, IK, IL

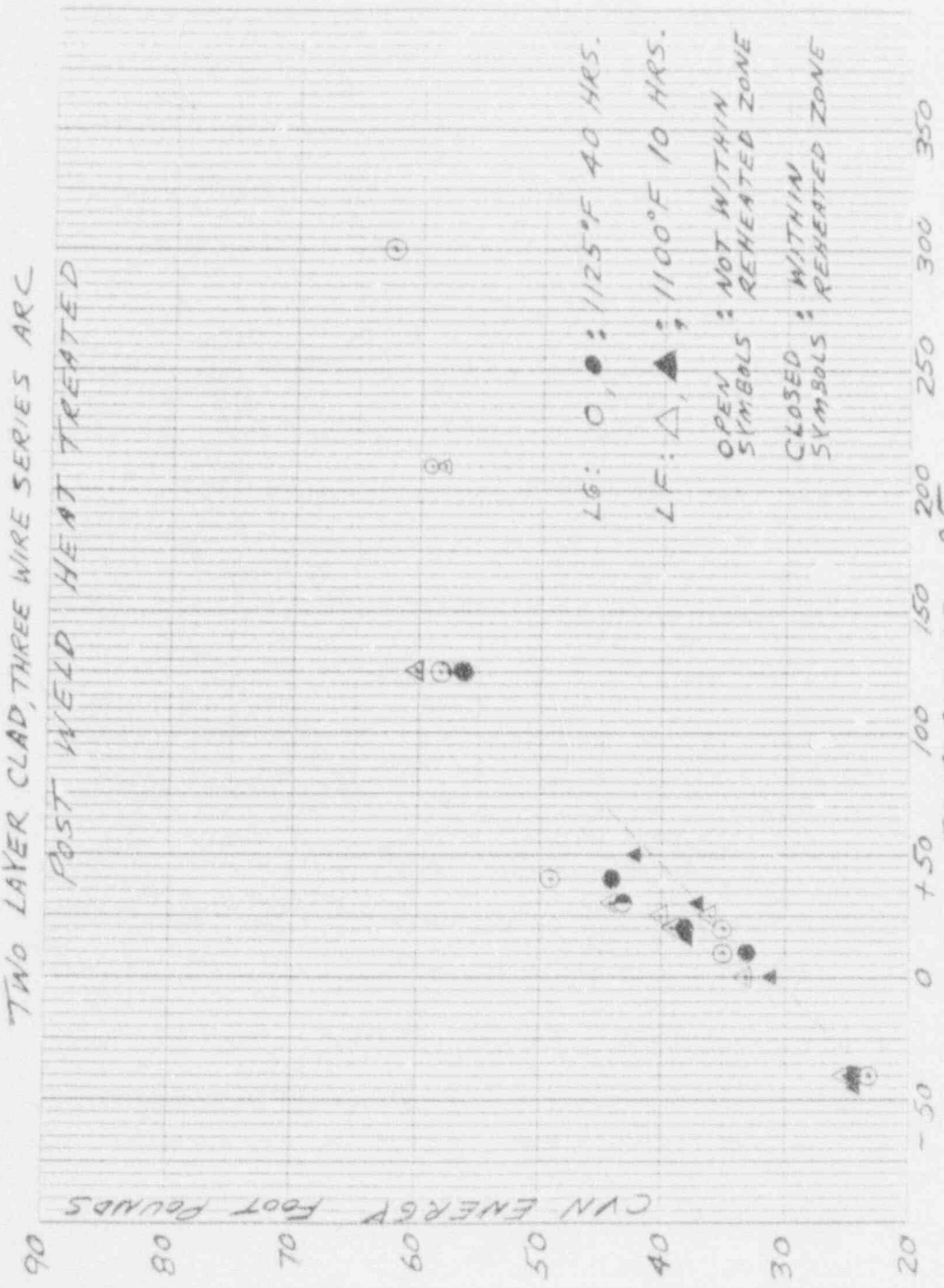

FIGURE 4. CVN RESULTS FOR LG, LF

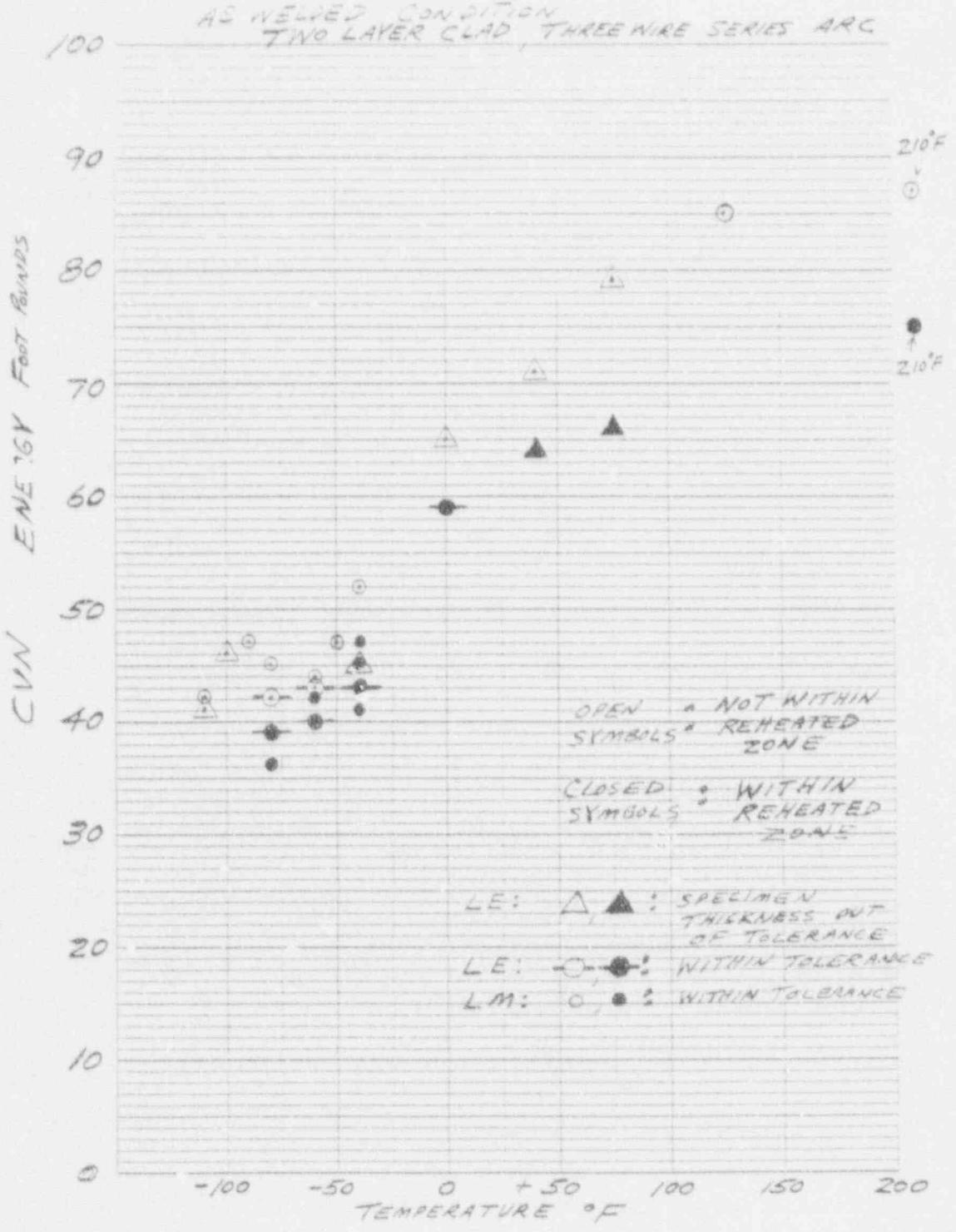

FIGURE 5. CVN RESULTS FOR LE, LM

ATTACHMENT 1

MML-85-100

BASE METAL PROPERTIES

COMBUSTION ENGINEERING, INC.
METALLURGICAL & MATERIALS LABORATORY

E-880 (5-83)

JOB NO. _____ IMPACT TEST DATA SHEET 1 OF 10

PROJECT NO. _____ CO SAMPLES CONTRACT NO. _____ DATE _____

TEST MATERIAL HSST Plate 012B
Initial Heat Treatment Block

HEAT TREATMENT 1890°F 2 Hrs. AC + 1125°F 40 Hrs. FC
100°F/Hr. Rate above 600°F.

TYPE OF TEST SPECIMEN CHARPY V NOTCH LINEAR VELOCITY IN FT. PER SECOND 17
ENERGY OF BLOW 240 FT. LBS. LOCATION AND ORIENTATION CVN and DWT
From 1/4T Parallel to Rolling Direction.

TYPE SATEC MODEL SI-1 CAPACITY OF MACHINE 240 FT. LBS.

SAMPLE NO.	WIDTH INCHES	THICKNESS INCHES	DEPTH BELOW NOTCH INCHES	TEST TEMP. F	ENERGY ABSORPTION FT. LBS.	% SHEAR	MILS LATERAL EXPANSION	REMARKS DROP WEIGHT TESTS: °F	RESULTS
CO-PA	.394	.394	.315	+ 75	40	20	29	+40	1F
B	.394	.394	.315	+ 75	44	20	31	+50	1F
C	.395	.394	.316	+ 75	41	20	28	+60	1F
D	.395	.394	.315	+ 50	36	10	24	+70	1NF,1F
E	.394	.394	.315	+ 50	35	10	23	+75	2NF
F	.395	.394	.315	+ 50	35	10	22		
G	.394	.393	.315	+ 10	10	0	2	NDTT:	
H	.394	.394	.315	+ 10	12	0	5	+20°F	
I	.394	.394	.315	+ 10	13	0	4		
J	.395	.394	.315	+120	75	60	51		
K	.395	.393	.315	+120	63	50	42		
L	.394	.395	.315	+120	58	40	39		
M	.394	.393	.315	+160	102	100	64		
N	.394	.393	.314	+160	88	90	57		
O	.395	.395	.316	+160	100	95	63		
P	.394	.395	.315	+212	98	95	64		
R	.396	.394	.314	+212	107	100	66		
S	.394	.394	.315	+212	88	90	59		
T	.394	.394	.315	+300	107	100	72		
U	.394	.392	.315	+300	102	100	64		
V	.394	.394	.316	+300	108	100	70		
W	.394	.393	.314	+ 25	19	5	6		
X	.394	.395	.316	+ 25	22	5	7		
Y	.394	.393	.315	+ 25	27	5	13		

COMBUSTION ENGINEERING, INC.
METALLURGICAL & MATERIALS LABORATORY

E-880 (5-63)

JOB NO. _____ IMPACT TEST DATA SHEET 2 OF 10

PROJECT NO. _____ HR SAMPLES CONTRACT NO. _____ DATE _____

TEST MATERIAL HSST Plate 01?B, Heat Treatment Verification Block, Mid Width of Plate

HEAT TREATMENT 1890°F 2 Hrs. AC + 1130°F 40 Hrs. FC, 100°F/Hr. Rate above 600°F.

TYPE OF TEST SPECIMEN CHARPY V NOTCH LINEAR VELOCITY IN FT PER SECOND 17

ENERGY OF BLOW 240 FT. LBS LOCATION AND ORIENTATION CVN and Dw. From 1/4T. Parallel to Rolling Direction.

TYPE SATEC MODEL S1-1 CAPACITY OF MACHINE 240 FT. LBS

SAMPLE NO.	WIDTH INCHES	THICKNESS INCHES	DEPTH BELOW NOTCH INCHES	TEST TEMP. F	ENERGY ABSORPTION FT. LBS	% SHEAR	MILS LATERAL EXPANSION	REMARKS DROP WEIGHT TESTS: °F RESULTS
HR-PA	.396	.394	.316	+55	24	5	18	+1[illegible] 1F.
B	.396	.395	.316	+60	10	0	3	+80 .NF
C	.395	.395	.316	+50	10	5	12	+90 1NF
D	.395	.395	.316	+40	11	0	9	
E	.395	.395	.316	+50	12	0	9	NDTT:
F	.395	.395	.316	+60	32	10	21	+75°F
G	.395	.395	.316	+75	32	10	20	
H	.395	.395	.316	+50	19	5	10	
I	.395	.395	.316	+50	10	0	4	

COMBUSTION ENGINEERING, INC.
METALLURGICAL & MATERIALS LABORATORY

S-880 (5-83)

JOB NO. _____ IMPACT TEST DATA SHEET 3 OF 10

PROJECT NO. _____ HP SAMPLES CONTRACT NO. _____ DATE _____

TEST MATERIAL HSST Plate 012B. Heat Treatment Verification Block.
Mid Width of Plate.

HEAT TREATMENT 1890°F 2 Hrs. AC + 1115°F 40 Hrs. FC.
100°F/Hr. Rate Above 600°F

TYPE OF TEST SPECIMEN CHARPY V NOTCH LINEAR VELOCITY IN FT. PER SECOND 17
ENERGY OF BLOW 240 FT · LBS LOCATION AND ORIENTATION CVN and DWT
From 1/4T. Parallel to Rolling Direction.

TYPE SATEC MODEL SI-1 CAPACITY OF MACHINE 240 FT · LBS

SAMPLE NO.	WIDTH INCHES	THICKNESS INCHES	DEPTH BELOW NOTCH INCHES	TEST TEMP. F	ENERGY ABSORPTION FT. LBS.	% SHEAR	MILS LATERAL EXPANSION	REMARKS DROP WEIGHT TESTS: °F	RESULTS
HP-PA	.395	.394	.316	+55	27	5	14	+75	1F
B	.395	.395	.316	+60	25	5	15	+80	1F
C	.395	.395	.316	+50	29	10	18	+90	2NF
D	.395	.395	.316	+40	12	0	4		
E	.395	.395	.316	+50	34	10	23	NDTT:	
F	.396	.395	.316	+60	20	5	12	+80°F	
G	.395	.395	.316	+75	40	20	27		
H	.395	.395	.316	+45	21	5	14		
I	.396	.395	.316	+45	21	5	12		

COMBUSTION ENGINEERING, INC.
METALLURGICAL & MATERIALS LABORATORY

E 680 (5-83)

JOB NO. _____ IMPACT TEST DATA SHEET 4 OF 10

PROJECT NO. _____ HR SAMPLES CONTRACT NO. _____ DATE _____

TEST MATERIAL HSST Plate 012B . Heat Treatment Verification Block.
Near Plate Edge.

HEAT TREATMENT 1890°F 2 Hrs. AC + 1130°F 40 Hrs. FC.
100°F/Hr. Rate above 600°F.

TYPE OF TEST SPECIMEN CHARPY V NOTCH LINEAR VELOCITY IN FT PER SECOND 12

ENERGY OF BLOW 240 FT - LBS LOCATION AND ORIENTATION CVN From 1/4T.
Parallel to Rolling Direction.

TYPE SATEC MODEL S1:1 CAPACITY OF MACHINE 240 FT - LBS

SAMPLE NO.	WIDTH INCHES	THICKNESS INCHES	DEPTH BELOW NOTCH INCHES	TEST TEMP. F	ENERGY ABSORPTION FT - LBS	% SHEAR	MILS LATERAL EXPANSION	REMARKS
HR-P1	.394	.394	.315	+75	12	0	9	
2	.395	.394	.315	+75	16	0	10	
3	.395	.394	.315	+75	11	0	8	
4	.394	.394	.315	+50	21	5	14	
5	.394	.394	.315	+50	39	10	23	
6	.395	.394	.315	+50	28	5	15	
7	.395	.394	.315	+25	11	0	6	
8	.395	.394	.315	+25	12	0	5	
9	.395	.394	.315	+25	6	0	2	
10	.395	.394	.315	+125	64	35	43	
11	.395	.394	.315	+125	58	30	39	
12	.395	.394	.315	+125	51	25	36	
13	.395	.394	.315	+100	21	5	17	
14	.395	.395	.316	+100	42	20	34	
15	.395	.395	.315	+100	39	15	29	
16	.395	.394	.315	+210	97	80	66	
17	.395	.394	.313	+250	110	100	70	
18	.395	.394	.315					

COMBUSTION ENGINEERING, INC.
METALLURGICAL & MATERIALS LABORATORY

E 880 (5-83)

JOB NO. _____ IMPACT TEST DATA SHEET 5 OF 10

PROJECT NO. _____ HP SAMPLES CONTRACT NO. _____ DATE _____

TEST MATERIAL HSST Plate 012B, Heat Treatment Verification Block.
Near Plate Edge.

HEAT TREATMENT 1890°F 2 Hrs. AC + 1115°F 40 Hrs. FC.
100°F/Hr. Rate above 600°F.

TYPE OF TEST SPECIMEN CHARPY V NOTCH LINEAR VELOCITY IN FT. PER SECOND 17
ENERGY OF BLOW 240 FT. LBS LOCATION AND ORIENTATION CVN From 1/4T,
Parallel to Rolling Direction.

TYPE SATEC MODEL SI-1 CAPACITY OF MACHINE 240 FT. LBS

SAMPLE NO.	WIDTH INCHES	THICKNESS INCHES	DEPTH BELOW NOTCH INCHES	TEST TEMP. F	ENERGY ABSORPTION FT. LBS.	% SHEAR	MILS LATERAL EXPANSION	REMARKS
HP-P 1	.395	.394	.316	+ 75	27	5	20	
2	.395	.395	.316	+ 75	33	10	21	
3	.395	.393	.315	+ 75	14	0	8	
4	.394	.394	.315	+ 50	8	0	2	
5	.395	.395	.316	+ 50	16	0	9	
6	.395	.394	.315	+ 50	25	5	16	
7	.395	.394	.315	+ 25	5	0	1	
8	.395	.394	.315	+ 25	11	0	4	
9	.395	.394	.315	+ 25	16	0	7	
10	.395	.394	.316	+125	69	40	53	
11	.395	.394	.315	+125	53	10	39	
12	.395	.394	.315	+125	44	25	32	
13	.395	.394	.315	+100	38	20	28	
14	.395	.394	.315	+100	17	5	11	
15	.395	.395	.315	+100	39	20	26	
16	.395	.394	.315	+210	91	90	60	
17	.395	.394	.315	+250	98	100	62	
18	.395	.394	.315					

COMBUSTION ENGINEERING, INC.
METALLURGICAL & MATERIALS LABORATORY

E-880 (5-83)

JOB NO. _____ IMPACT TEST DATA SHEET 6 OF 10

PROJECT NO. _____ IX SAMPLES CONTRACT NO. _____ DATE _____

TEST MATERIAL HSST Plate 02B. Heat Treatment Verification Block.
Near Plate Edge and Adjacent to HR-P1 through HR-P1B.

HEAT TREATMENT 1890°F 2 Hrs. AC + 1130°F 40 Hrs. FC.
100°F/HR Rate above 600°F.

TYPE OF TEST SPECIMEN CHARPY V NOTCH LINEAR VELOCITY IN FT. PER SECOND 17
ENERGY OF BLOW 240 FT. LBS. LOCATION AND ORIENTATION CVN From 1/4T.
Parallel to Rolling Direction.

TYPE SATEC MODEL SI-1 CAPACITY OF MACHINE 240 FT. LBS.

SAMPLE NO.	WIDTH INCHES	THICKNESS INCHES	DEPTH BELOW NOTCH INCHES	TEST TEMP. F	ENERGY ABSORPTION FT. LBS.	% SHEAR	MILS LATERAL EXPANSION	REMARKS
IX-PA	.395	.395	.315	+ 75	38	10	24	
B	.395	.395	.316	+ 75	21	5	11	
C	.394	.394	.316	+ 75	27	10	25	
D	.394	.395	.316	+ 50	32	10	18	
E	.395	.394	.31[illegible]	+ 50	24	5	13	
F	.395	.395	.316	+ 50	9	0	4	
G	.395	.395	.316	+ 25	11	0	2	
H	.395	.395	.316	+ 25	15	0	7	
I	.395	.395	.316	+ 25	6	0	1	
J	.395	.394	.316	+100	55	25	36	
K	.395	.395	.316	+100	42	20	29	
L	.395	.394	.316	+100	41	15	20	
M	.395	.395	.316	+125	34	15	25	
N	.395	.395	.316	+125	54	25	38	
O	.395	.395	.316	+125	65	40	43	
P	.395	.395	.316	+210	92	80	70	
R	.395	.395	.316	+250	103	100	68	
S	.395	.39[illegible]	.31[illegible]6					
T	.395	.395	.31[illegible]					
U	.395	.395	.315					
V	.395	.395	.316					
W	.395	.395	.316					
X	.395	.395	.316					
Y	.395	.395	.316					

COMBUSTION ENGINEERING, INC.
METALLURGICAL & MATERIALS LABORATORY

E-880 (5-63)

JOB NO. _____ IMPACT TEST DATA SHEET 7 OF 10

PROJECT NO. _____ IW SAMPLES CONTRACT NO. _____ DATE _____

TEST MATERIAL HSST Plate 012B. Heat Treatment Verification Block.
Near Plate Edge and Adjacent to HP-P1 through HP-P18.

HEAT TREATMENT 1890°F 2 Hrs. AC + 1115°F 40 Hrs. FC.
100°F/Hr. Rate above 600°F.

TYPE OF TEST SPECIMEN CHARPY V NOTCH LINEAR VELOCITY IN FT. PER SECOND 17
ENERGY OF BLOW 240 FT. LBS. LOCATION AND ORIENTATION CVN from 1/4T,
Parallel to Rolling Direction.

TYPE SATEC MODEL SI-1 CAPACITY OF MACHINE 240 FT. LBS

SAMPLE NO.	WIDTH INCHES	THICKNESS INCHES	DEPTH BELOW NOTCH INCHES	TEST TEMP. °F	ENERGY ABSORPTION FT. LBS.	% SHEAR	MILS LATERAL EXPANSION	REMARKS
IW-PA	.395	.394	.315	+ 75	32	10	17	
B	.395	.395	.316	+ 75	19	10	25	
C	.395	.395	.316	+ 75	24	5	13	
D	.395	.395	.316	+ 50	31	10	18	
E	.395	.395	.316	+ 50	33	5	10	
F	.395	.395	.316	+ 50	25	5	13	
G	.395	.395	.316	+ 25	15	0	7	
H	.395	.395	.316	+ 25	8	0	2	
I	.395	.395	.316	+ 25	17	0	6	
J	.395	.395	.316	+100	46	20	28	
K	.395	.395	.316	+100	14	0	8	
L	.395	.395	.316	+100	20	0	13	
M	.395	.395	.316	+125	42	20	28	
N	.395	.395	.316	+125	45	45	30	
O	.395	.395	.316	+125	48	25	31	
P	.395	.395	.316	+210	87	80	61	
R	.395	.394	.315	+250	72	70	50	
S	.395	.395	.316	+250	95	100	62	
T	.395	.395	.316					
U	.395	.395	.316					
V	.395	.395	.316					
W	.395	.395	.316					
X	.395	.395	.316					
Y	.395	.395	.316					

COMBUSTION ENGINEERING, INC.
METALLURGICAL & MATERIALS LABORATORY

E-1785 (5-83)

MECHANICAL PROPERTIES
DATA SHEET

PROJECT NO. _____
CONTRACT _____
JOB _____

GK Samples

SHEET 8 OF 10
DATE _____

MATERIAL HSST Plate 012B, Initial Heat Treatment Block.

HEAT TREATMENT 1890°F 2 HRS. AC + 1125°F 40 Hrs. FC.
100°F /Hr. Rate Above 600°F.

Tensile Tests from 1/4T. Parallel to Rolling Direction.

IDENTIFICATION		GK-1A	GK-1B				
TEST TEMPERATURE		+75°F	+75°F				
DIMENSIONS	WIDTH						
	~~THICKNESS~~/DIAMETER	.506	.506				
	AREA						
YIELD STRENGTH	KSI	79.8	79.1				
	LBS.	16,050	15,900				
TENSILE STRENGTH	KSI	99.0	98.7				
	LBS.	19,900	9,850				
ELONG. IN 2 INCHES		2.46	2.45				
	PERCENT	23.0	22.5				
REDUCTION IN AREA	~~WIDTH~~/DIAMETER	.314	.313				
	~~THICKNESS~~/DIAMETER	.312	.312				
	AREA						
	% REDUCTION	61.7	61.7				
LOCATION OF FRACTURE							
BEND TESTS	FACE						
	% ELONG.						
	ROOT						
	% ELONG.						
	SIDE						
REMARKS							

E-1785 (5-83)

COMBUSTION ENGINEERING, INC.
METALLURGICAL & MATERIALS LABORATORY

MECHANICAL PROPERTIES
DATA SHEET

HR Samples

PROJECT NO. _____
CONTRACT _____
JOB _____

SHEET 9 OF 10
DATE _____

MATERIAL HSST Plate 012B. Heat Treatment Verification Block. Mid Width of Plate.

HEAT TREATMENT 1890°F 2 Hrs. AC + 1130°F 40 Hrs. FC, 100°F/Hr. Rate Above 600°F.

Tensile Tests from 1/4T. Parallel to Rolling Direction.

IDENTIFICATION		HR-PA	HR-PB				
TEST TEMPERATURE		+75°F	+75°F				
DIMENSIONS	WIDTH						
	THICKNESS/DIAMETER	.504	.504				
	AREA						
YIELD STRENGTH	KSI	76.7	76.7				
	LBS.	15,300	15,300				
TENSILE STRENGTH	KSI	96.5	96.7				
	LBS.	19,250	19,300				
ELONG. IN ____	INCHES	2.45	2.48				
	PERCENT	22.5	24.0				
REDUCTION IN AREA	WIDTH/DIAMETER	.308	.307				
	THICKNESS/DIAMETER	.307	.307				
	AREA						
	% REDUCTION	62.6	63.0				
LOCATION OF FRACTURE							
BEND TESTS	FACE						
	% ELONG.						
	ROOT						
	% ELONG.						
	SIDE						
REMARKS							

COMBUSTION ENGINEERING, INC.
METALLURGICAL & MATERIALS LABORATORY

E-1785 (5-83)

MECHANICAL PROPERTIES
DATA SHEET
HP Samples

PROJECT NO. _____
CONTRACT _____
JOB _____

SHEET 10 OF 10
DATE _____

MATERIAL HSST Plate 012B. Heat Treatment Verification Block. Mid Width of Plate.

HEAT TREATMENT 1890°F 2 Hrs. AC + 1115°F 40 Hrs FC, 100°F/Hr. Rate above 600°F.

Tensile Tests from 1/4T. Parallel to rolling direction.

IDENTIFICATION		HP-PA	HP-PB				
TEST TEMPERATURE		+75°F	+75°F				
DIMENSIONS	WIDTH						
	~~THICKNESS~~/DIAMETER	.504	.505				
	AREA						
YIELD STRENGTH	KSI	81.2	80.9				
	LBS.	16,200	16,200				
TENSILE STRENGTH	KSI	101.3	100.9				
	LBS.	20,200	20,200				
ELONG. IN ____	INCHES	2.45	2.44				
	PERCENT	22.5	22.0				
REDUCTION IN AREA	~~WIDTH~~/DIAMETER	.319	.319				
	~~THICKNESS~~/DIAMETER	.317	.318				
	AREA						
	% REDUCTION	60.2	60.4				
LOCATION OF FRACTURE							
BEND TESTS	FACE						
	% ELONG.						
	ROOT						
	% ELONG.						
	SIDE						
REMARKS							

COMBUSTION ENGINEERING, INC.
METALLURGICAL & MATERIALS LABORATORY

F 1785 (5-83)

MECHANICAL PROPERTIES
DATA SHEET

PROJECT NO. _____
CONTRACT _____ K2 Samples SHEET ____ OF ____
JOB _____ DATE 1o1-88

MATERIAL HSST Plate 012B. Fabrication Base Plate. From 7 inch edge allowance block adjacent to Heat Treatment Verification Block. Mid-width of Plate.

HEAT TREATMENT 1890°F 2 Hrs. AC + 1100°F 10 Hrs. FC
100°F/Hr. Rate above 600°F
Tensile Tests from 1/4T. Parallel to Rolling Direction

IDENTIFICATION		K2-PA	K2-PB
TEST TEMPERATURE			
DIMENSIONS	WIDTH		
	THICKNESS/DIAMETER	.504	.503
	AREA	.200	.199
YIELD STRENGTH	KSI	87.7	86.2
	LBS.	17,600	17,100
TENSILE STRENGTH	KSI	107.5	106.2
	LBS.	21,620	21,050
ELONG. IN 1 INCHES		2.54	2.68
	PERCENT	27.0	27.2
REDUCTION IN AREA	WIDTH/DIAMETER		.318
	THICKNESS/DIAMETER	.323	.5
	AREA		
	% REDUCTION	58.7	60.1
LOCATION OF FRACTURE			
BEND TESTS	FACE		
	% ELONG.		
	POOT		
	% ELONG.		

REMARKS

COMBUSTION ENGINEERING, INC.
METALLURGICAL & MATERIALS LABORATORY

E-680 (5-83)

JOB NO. _____ IMPACT TEST DATA SHEET ____ OF ____

PROJECT NO. _____ KZ SAMPLES CONTRACT NO. _____ DATE _____

TEST MATERIAL HSST Plate 012B, Fabrication Base Plate. From 7 inch edge allowance block adjacent to Heat Treatment Verification Block. Mid-Width of Plate.

HEAT TREATMENT 1890°F 2 Hrs. AC + 1100°F 10 Hrs. FC
100°F/Hr. Rate above 600°F

TYPE OF TEST SPECIMEN CHARPY V NOTCH _____ LINEAR VELOCITY IN FT. PER SECOND 12
ENERGY OF BLOW 240 FT. LBS LOCATION AND ORIENTATION CVN and DWT from 1/4T
Parallel to rolling direction.

TYPE SATEC MODEL SI-1 CAPACITY OF MACHINE 240 FT. LBS

SAMPLE NO.	WIDTH INCHES	THICKNESS INCHES	DEPTH BELOW NOTCH INCHES	TEST TEMP. F	ENERGY ABSORPTION FT. LBS	% SHEAR	MILS LATERAL EXPANSION	REMARKS
KZ-P1	.394	.394	.315	+75	23	5	15	°F Results
KZ-P2	.394	.394	.315	+75	26	5	18	+100 1F
KZ-P3	.393	.394	.316	+75	25	5	16	+120 1NF,1F
KZ-P4	.393	.394	.315	+40	17	0	11	+130 2NF
KZ-P5	.393	.394	.315	+40	22	5	12	
KZ-P6	.394	.393	.315	+40	20	0	12	NDTT: +120°F
KZ-P7	.394	.393	.315	+140	38	15	28	
KZ-P8	.394	.394	.316	+200	57	35	39	
KZ-P9								
KZ-P10	.395	.394	.315	+300	91	100	67	
KZ-P11	.395	.393	.315	+250	81	95	58	
KZ-P12	.395	.394	.316	+400	83	100	63	
KZ-P13	.395	.393	.315	+300	80	100	57	
KZ-P14	.395	.394	.315	+60	24	5	15	
KZ-P15	.395	.394	.316	+105	40	20	30	
KZ-P16	.395	.394	.315	+20	19	0	10	
KZ-P17	.395	.394	.315					

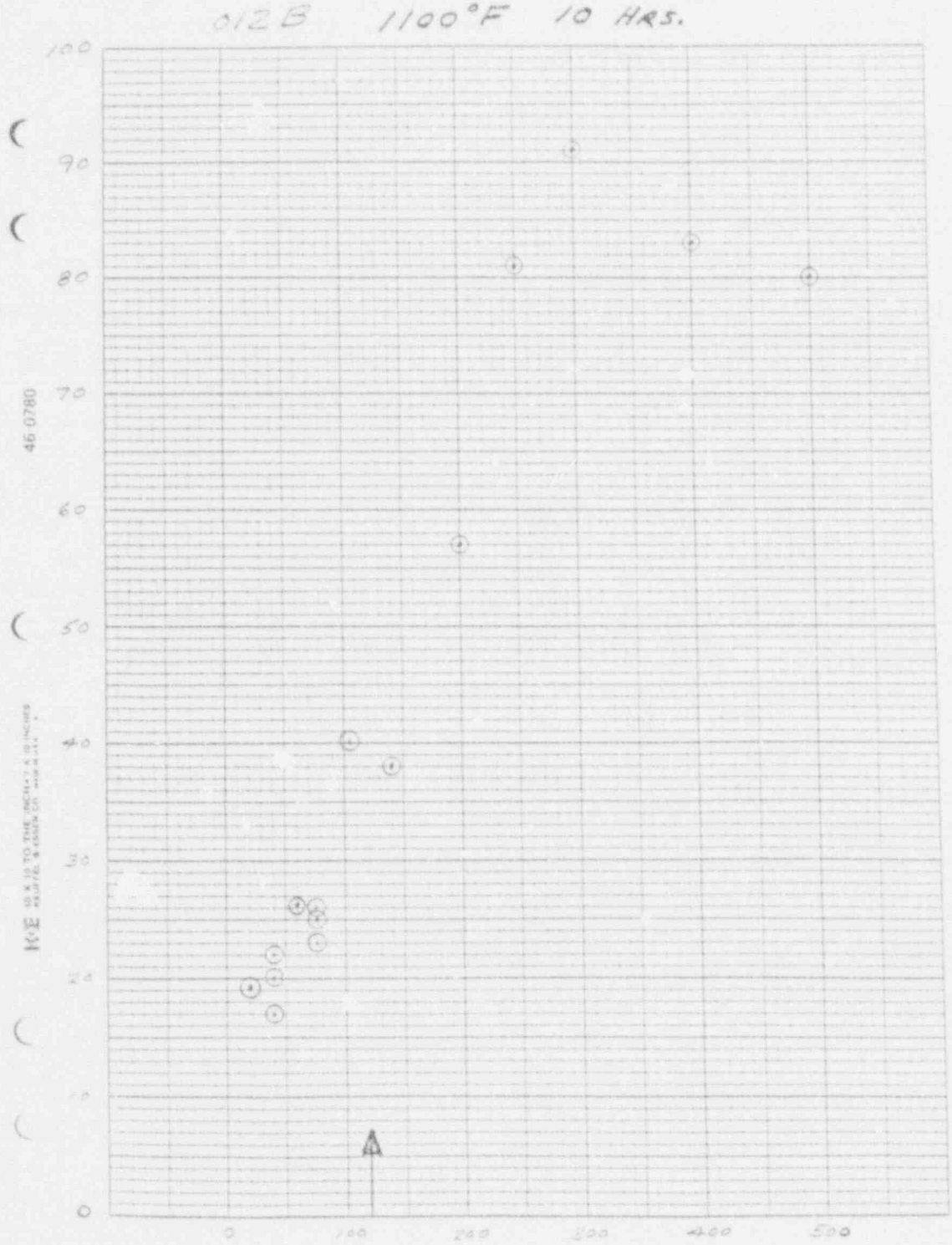
012B 1100°F 10 HRS.
100
90
80
70
60
50
40
30
20
10
0
0
100
200
300
400
500
46 0780

COMBUSTION ENGINEERING, INC.
METALLURGICAL & MATERIALS LABORATORY

E-1785 (5-83)

MECHANICAL PROPERTIES
DATA SHEET

PROJECT NO. _____ SHEET ____ OF ____
CONTRACT _____ KY Samples DATE 7-13-84
JOB _____

MATERIAL HSST Plate 012B. Fabrication Base Plate. From 7 inch edge allowance block adjacent to Heat Treatment Verification Block. Mid-width of Plate.

HEAT TREATMENT 1890°F 2 Hrs. AC
Tensile Tests from 1/4T. Parallel to Rolling Direction

IDENTIFICATION		KY-PA	KY-PB
TEST TEMPERATURE			
DIMENSIONS	WIDTH		
	THICKNESS/DIAMETER	.503	.502
	AREA	.199	.198
YIELD STRENGTH	KSI	83.3	82.4
	LBS.	16,650	16,300
TENSILE STRENGTH	KSI	111.5	110.1
	LBS.	22,150	21,800
ELONG. IN 2 INCHES		2.40	2.39
	PERCENT	20.0	19.5
REDUCTION IN AREA	WIDTH/DIAMETER	.329	.314
	THICKNESS/DIAMETER	.325	.313
	AREA		
	% REDUCTION	57.7	61.1
LOCATION OF FRACTURE			
BEND TESTS	FACE		
	% ELONG.		
	ROOT		
	% ELONG.		
	SIDE		

REMARKS

COMBUSTION ENGINEERING, INC.
METALLURGICAL & MATERIALS LABORATORY

E-880 (5-83)

JOB NO. _____ IMPACT TEST SHEET ___ OF ___

PROJECT NO. _____ KY SAMPLES CONTRACT NO. _____ DATE _____

TEST MATERIAL HSST Plate 02B, Fabrication Base Plate. From 7 inch edge allowance block adjacent to Heat Treatment Verification Block. Mid-Width of Plate.

HEAT TREATMENT 1890°F 2 Hrs. AC

TYPE OF TEST SPECIMEN CHARPY V NOTCH LINEAR VELOCITY IN FT. PER SECOND 17
ENERGY OF BLOW 240 FT. LBS. LOCATION AND ORIENTATION CVN and DWT from 1/4T. Parallel to rolling direction.

TYPE SATEC MODEL SI-1 CAPACITY OF MACHINE 240 FT. LBS.

SAMPLE NO.	WIDTH INCHES	THICKNESS INCHES	DEPTH BELOW NOTCH INCHES	TEST TEMP. F	ENERGY ABSORPTION FT. LBS.	% SHEAR	MILS LATERAL EXPANSION	REMARKS
KY-P1	.393	.394	.316	+40	14	0	5	°F Results
KY-P2	.393	.394	.316	+40	12	0	4	+75 1F
KY-P3	.393	.394	.316	+40	11	0	4	+90 1F
KY-P4	.393	.394	.316	+75	14	0	4	+110 1F
KY-P5	.393	.394	.316	+75	15	0	5	+130 1NF,1F
KY-P6	.394	.394	.316	+75	17	0	8	+140 2NF
KY-P7	.393	.394	.316	+100	23	5	14	NDTT: +130°F
KY-P8	.393	.394	.316	+100	20	0	13	
KY-P9	.393	.394	.316	+100	22	5	15	
KY-P10	.394	.394	.316	+200	42	25	32	
KY-P11	.394	.394	.317	300	78	90	56	
KY-P12	.395	.394	.316	+250	52	50	35	
KY-P13	.393	.394	.316	+400	88	100	65	
KY-P14	.393	.394	.316	+500	82	100	63	
KY-P15	.395	.393	.316	+130	30	25	22	
KY-P16	.393	.394	.316	+120	35	10	25	
KY-P17	.393	.394	.316	+125	28	10	19	
KY-P18	.393	.393	.316	00	79	100	55	

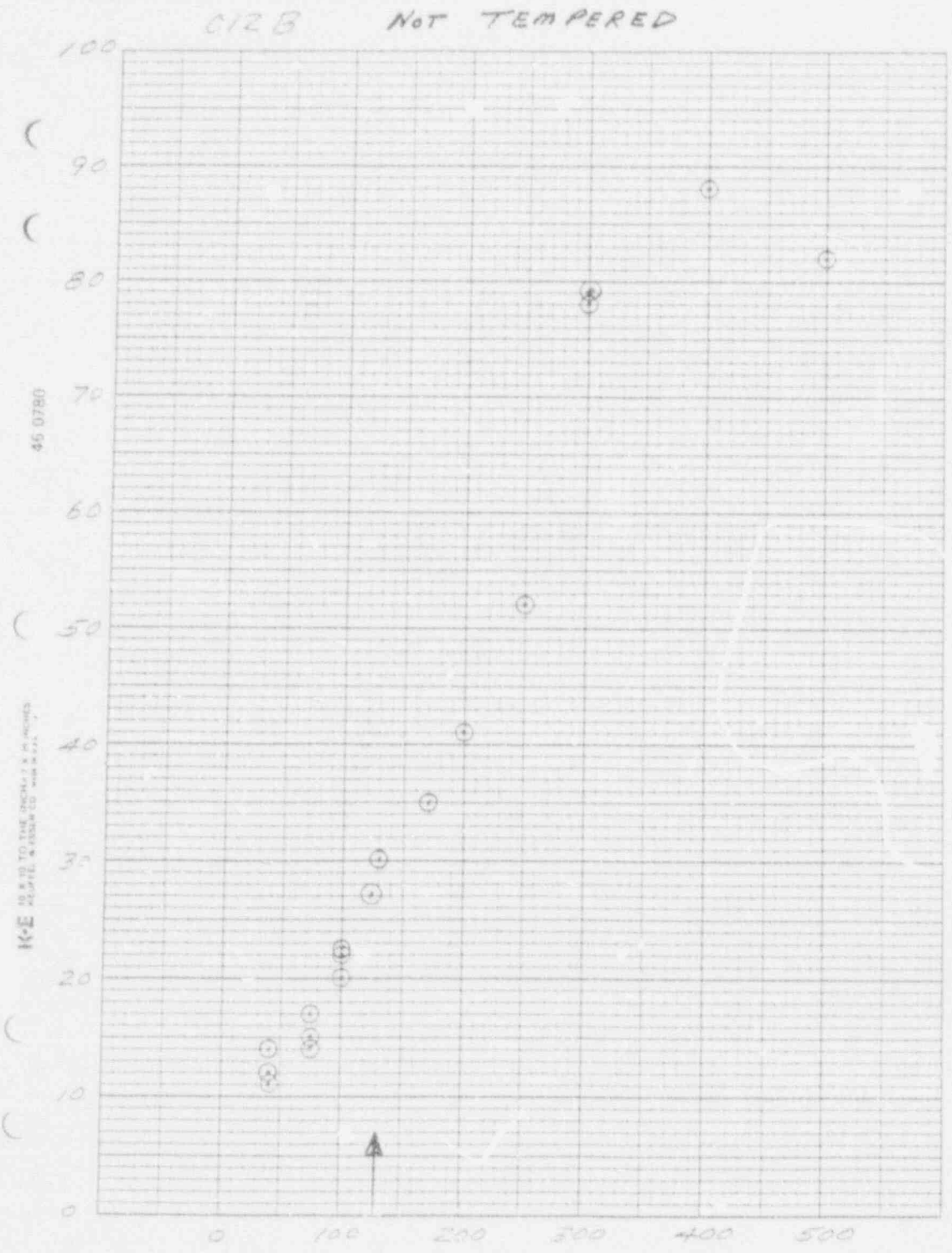
C12B NOT TEMPERED
100
90
80
70
60
50
40
30
20
10
0
0
100
200
300
400
500
46 0780
K+E

C-E Power Systems
Combustion Engineering, Inc.
911 W. Main Street
Chattanooga, Tennessee 37402
Tel: 615/265-4631

C-E POWER SYSTEMS

Metallurgical and Materials
Laboratory - Chattanooga

May 23, 1984

Dr. W. R. Corwin
Metals and Ceramics Division
Oak Ridge National Laboratory
P. O. Box X
Oak Ridge, Tennessee 37830

Dear Bill:

Subject: Mechanical Property Data - Purchase Order 76X-72185V
Job No. 98130469/Project 900588
MML-84-109

Enclosed are all property data so far from the series arc cladding deposit and from HSST plate 012B. CVN properties of three different clad samples, after PWHT at 1125°F, are listed in data sheets 1 - 3, identified as GP, IK and IL. These are two layer deposits made with Arcos S-4 flux, and tested as full size CVN specimens spanning both layers. Energy values are unexpectedly low, indicating a 40 foot pound temperature of +50°F or higher, and it is not yet apparent how the energy value below +50°F can be increased to a desired level without deviating from the welding practice applicable to older vessels. However, as you suggested in our conversation, another approach is to increase the transition temperature of the base metal above the level observed so far.

Base metal properties, listed in data sheets 1 through 10, are tabulated below:

Austenitized at 1890°F, 2 Hrs., Air Cool

	Heat Treatment Verification Block From Fabrication Base Plate.		Initial Heat Treatment Block
Temper/PWHT*	1115°F, 40 Hrs.	1130°F, 40 Hrs.	1125°F, 40 Hrs.
Yield Strength	81.2	76.7	79.8
KSI	80.9	76.7	79.1
Tensile Strength	101.3	96.5	99.0
KSI	100.9	96.7	98.7
DWT NDTT	+80°F	+75°F	+70°F
20 Foot Pound CVN Temperature	Data indicates a scatter band extending from +10°F to 110°F.		

*Temper and PWHT combined in one step per paragraph NB2170, Section 3, ASME B and PVC.

Presently the fabrication base plate to the left of the heat treatment verification block location is intact and is still in the as normalized condition. Only the 6 X 64 inch heat treatment verification block has been subjected to tempering. Although none of the mechanical property tests were located within the 7 inch wide "quenched edge" zone of the fabrication base plate, this material was buffered during normalizing by an 8 inch thick, 5 inch wide picture frame around the entire periphery. While being cooled in still air from austenitizing temperature, the plate was suspended in a vertical plane and held above floor level. Thermocouples imbedded at 1/4T indicated the cooling rate was uniform from plate edge to midpoint throughout the cooling cycle. Uniform cooling was confirmed also by visual observation of temperature "color" over the entire surface. Therefore the 7 inch wide edge material should be suitable for additional mechanical tests. All of this 7 inch wide zone is now in the as normalized condition.

Light Microscpoy of broken CVN specimens shows uniform, equiaxed structure of about ASTM 4 to 5 transformation product grain size. Differences in light microstructure are not now apparent between specimens representing extremi of the CVN scatterband.

Several questions arise. Could the objectives of the program be met if tempering/PWHT temperature is less than 1100°F? Could tempering/PWHT be omitted?

Yours Very truly,

C. T. Ward

C. T. Ward

CTW:bs

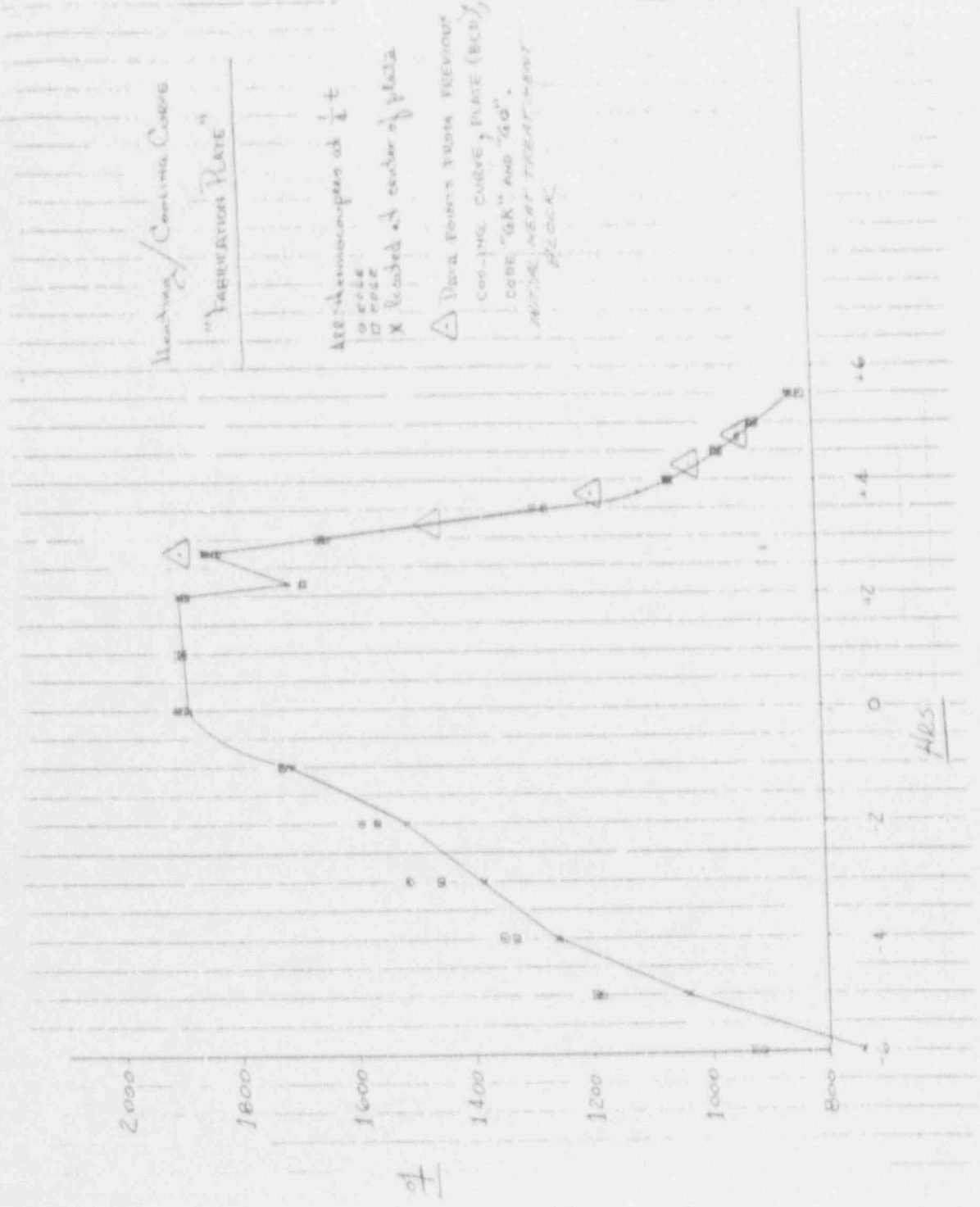
Hardness / Cooling Curve
"Fabrication Plate"
Hardness Impressions at 1/4 t
Edge
Edge
Quarter of plate
Data Points from previous cooling curve, Plate (BCD), Code "GK" and "GO". Normalized treatment block
2000
1800
1600
1400
1200
1000
800
1/4 t
-6
-4
-2
0
+2
+4
+6
Abs.

ATTACHMENT 2

MML-85-100

CLADDING PROPERTIES

COMBUSTION ENGINEERING, INC.
METALLURGICAL & MATERIALS LABORATORY

E-680 (5-83)

JOB NO. _____ IMPACT TEST DATA SHEET 1 OF 1

PROJECT NO. _____ GP SAMPLES CONTRACT NO. _____ DATE _____

TEST MATERIAL Two Layer Clad, Three Wire Series Arc Process. Base Metal - HSST-01TR

HEAT TREATMENT PWHT: 1125°F 40 Hrs. FC. 100°F/Hr. Rate Above 600°F

TYPE OF TEST SPECIMEN CHARPY V NOTCH LINEAR VELOCITY IN FT. PER SECOND ___ '?___

ENERGY OF BLOW 240 FT. LBS. LOCATION AND ORIENTATION CVN Parallel to Welding

Direction. Base of notch no. 1 to weld face.

TYPE SATEC MODEL SI-1 CAPACITY OF MACHINE 240 FT. LBS.

	SAMPLE NO.	WIDTH INCHES	THICKNESS INCHES	DEPTH BELOW NOTCH IN INCHES	TEST TEMP. °F	ENERGY ABSORPTION FT. LBS.	% SHEAR	MILS LATERAL EXPANSION	REMARKS
	GP-WA	.393	.393	.315	+75	53		57	
	B	.393	.394	.315	+50	48		49	
	C	.393	.393	.315	+25	39		34	
	D	.393	.393	.315	+25	38		36	
	E	.393	.393	.315	+50	41		38	
	F	.393	.394	.315	+25	39		33	
	G	.393	.393	.314	+25	40		39	
	H	.393	.393	.315	+75	44		52	
	I	.393	.394	.315					

COMBUSTION ENGINEERING, INC.
METALLURGICAL & MATERIALS LABORATORY

E 690 (5-83)

JOB NO. _____ IMPACT TEST DATA SHEET 2 OF 3

PROJECT NO. _____ IK SAMPLES CONTRACT NO. _____ DATE _____

TEST MATERIAL Two Layer Clad. Three Wire Series Arc Process. Base Metal - A533T-Cl2F

HEAT TREATMENT PWHT: 1125°F 60 Hrs. F.C. 100°F/Hr. rate Above 600°F.

TYPE OF TEST SPECIMEN CHARPY V NOTCH LINEAR VELOCITY IN FT. PER SECOND 17
ENERGY OF BLOW 240 FT - LBS. LOCATION AND ORIENTATION CVN Parallel to Welding Direction. Base of Notch Normal to Weld Face.

TYPE SATEC MODEL SI-1 CAPACITY OF MACHINE 240 FT - LBS.

	SAMPLE NO.	WIDTH INCHES	THICKNESS INCHES	DEPTH BELOW NOTCH INCHES	TEST TEMP. F	ENERGY ABSORPTION FT. - LBS.	% SHEAR	MILS LATERAL EXPANSION	REMARKS
	IK-VA	.395	.395	.315	+75	37		33	
	B	.395	.395	.315	+25	39		35	
	C	.395	.395	.315	+25	36		32	
	D	.395	.395	.315	+50	43		41	
	E	.394	.395	.315	+25	36		34	
	F	.394	.394	.315	+75	51		50	

COMBUSTION ENGINEERING, INC.
METALLURGICAL & MATERIALS LABORATORY

F 880 (5-83)

JOB NO. _____ IMPACT TEST DATA SHEET 1 OF 1

PROJECT NO. _____ 11 SAMPLES CONTRACT NO. _____ DATE _____

TEST MATERIAL Two Layer Clad. Three Wire Series Arc Process. Base Metal - A533GR1CB

HEAT TREATMENT PWHT: 1125°F 40 Hrs. FC. 100°F/Hr. Rate Above 600°F.

TYPE OF TEST SPECIMEN CHARPY V NOTCH LINEAR VELOCITY IN FT. PER SECOND 17

ENERGY OF BLOW 240 FT. - LBS LOCATION AND ORIENTATION CVN Parallel To Welding Direction. Base of Notch Normal to Weld Face.

TYPE SATEC MODEL SI-1 CAPACITY OF MACHINE 240 FT LBS

SAMPLE NO.	WIDTH INCHES	THICKNESS INCHES	DEPTH BELOW NOTCH INCHES	TEST TEMP. F	ENERGY ABSORP. TION FT. LBS.	% SHEAR	MILS LATERAL EXPANSION	REMARKS
TL-LA	.394	.391	.314	+25	34		29	
B	.392	.391	.313	+25	36		32	
C	.393	.391	.313	+25	37		30	
D	.395	.393	.315	+50	40		37	
E	.393	.392	.314	+25	36		36	
F	.394	.392	.313	+75	54		52	

COMBUSTION ENGINEERING, INC.
METALLURGICAL & MATERIALS LABORATORY

E 680 (5-82)

JOB NO. _____ IMPACT TEST DATA SHEET ____ OF ____

PROJECT NO. _____ LE SAMPLES CONTRACT NO. _____ DATE _____

TEST MATERIAL Two Layer Clad. Three Wire Series Arc Process. Base Metal - A8ST 8128

HEAT TREATMENT As Welded Condition.

TYPE OF TEST SPECIMEN CHARPY V NOTCH LINEAR VELOCITY IN FT. PER SECOND 12
ENERGY OF BLOW 240 FT - LBS LOCATION AND ORIENTATION CVN Parallel to welding direction. Base of notch normal to weld face.

TYPE SATEC MODEL SI-1 CAPACITY OF MACHINE 240 FT LBS

	SAMPLE NO.	WIDTH INCHES	THICKNESS INCHES	DEPTH BELOW NOTCH INCHES	TEST TEMP. F	ENERGY ABSORPTION FT. LBS.	% SHEAR	MILS LATERAL EXPANSION	REMARKS
*	LE-WA	.393	.391	.314	+75	79		82	Specimens not
*	LE-WB	.393	.388	.314	+40	71		72	within reheated
	LE-WC	.395	.394	.315	-60	43		38	zone.
*	LE-WD	.393	.387	.315	0	65		62	
*	LE-WE	.393	.392	.315	-40	45		43	
*	LE-WF	.393	.390	.315	-100	46		41	
	LE-WG	.394	.393	.315	-80	42		38	
*	LE-WH	.394	.391	.315	-110	41		39	
	LE-ZA	.394	.394	.315	0	59		58	Specimens
*	LE-ZB	.394	.391	.315	+75	66		67	within
	LE-ZC	.394	.394	.315	-40	43		38	reheated
	LE-ZD	.394	.394	.315	-60	40		35	zone
	LE-ZE	.394	.394	.315	-80	39		34	
*	LE-ZF	.394	.389	.315	+40	64		65	

*Specimen thickness dimension is out of tolerance.

COMBUSTION ENGINEERING, INC.
METALLURGICAL & MATERIALS LABORATORY

E 680 (5-83)

JOB NO. _____ IMPACT TEST DATA SHEET ____ OF ____

PROJECT NO. _____ LF SAMPLES CONTRACT NO. _____ DATE _____

TEST MATERIAL Two Layer Clad, Three Wire Series Arc Process. Base Metal - HOST 012B

HEAT TREATMENT 1100°F 10 Hrs. FC 100°F/Hr. Rate above 600°F

TYPE OF TEST SPECIMEN CHARPY V NOTCH LINEAR VELOCITY IN FT. PER SECOND 17
ENERGY OF BLOW 240 FT. LBS LOCATION AND ORIENTATION CVN Parallel to welding direction. Base of notch normal to weld face.

TYPE SATEC MODEL S1:1 CAPACITY OF MACHINE 240 FT. LBS

SAMPLE NO.	WIDTH INCHES	THICKNESS INCHES	DEPTH BELOW NOTCH INCHES	TEST TEMP. F	ENERGY ABSORP. TION FT. LBS.	% SHEAR	MILS LATERAL EXPANSION	REMARKS
LF-WA	.394	.394	.315	-40	25		20	Specimens not
LF-WB	.395	.394	.315	0	33		31	within reheated
LF-WC	.393	.393	.315	+20	39		37	zone.
LF-WD	.394	.394	.315	+30	44		43	
LF-WE	.395	.394	.315	+25	40		39	
LF-WF	.394	.394	.315	+25	36		36	
LF-WG	.394	.394	.315	+210	58		79	
LF-WH	.393	.394	.315	+175	60		72	
LF-ZA	.394	.394	.315	-40	24		20	Specimens
LF-ZB	.395	.394	.315	0	31		30	min
LF-ZC	.395	.394	.314	+20	38		37	reheated
LF-ZD	.395	.394	.314	+30	37		36	zone
LF-ZE	.393	.394	.315	+50	42		45	

COMBUSTION ENGINEERING, INC.
METALLURGICAL & MATERIALS LABORATORY

E-880 (5-63)

JOB NO. _____ IMPACT TEST DATA SHEET ____ OF ____

PROJECT NO. _____ LG SAMPLES CONTRACT NO. _____ DATE _____

TEST MATERIAL Two Layer Clad, Three Wire Series Arc Process. Base Metal - A533T-01TB

HEAT TREATMENT 1125°F 40 Hrs. F.C. 100°F/Hr. Rate Above 600°F

TYPE OF TEST SPECIMEN CHARPY V NOTCH LINEAR VELOCITY IN FT. PER SECOND 12
ENERGY OF BLOW 240 FT. LBS. LOCATION AND ORIENTATION CVN Parallel to welding Direction. Base of notch normal to weld face.

TYPE SATEC MODEL SI-1 CAPACITY OF MACHINE 240 FT. LBS.

SAMPLE NO.	WIDTH INCHES	THICKNESS INCHES	DEPTH BELOW NOTCH INCHES	TEST TEMP. °F	ENERGY ABSORPTION FT. LBS.	% SHEAR	MILS LATERAL EXPANSION	REMARKS
LG-WA	.393	.393	.315	-40	23		20	Specimens not
LG-WB	.393	.393	.314	+10	35		32	within reheated
LG-WC	.393	.393	.315	+40	49		53	zone.
LG-WD	.393	.393	.314	+20	35		31	
LG-WE	.393	.393	.314	+30	43		37	
LG-WF	.393	.393	.315	+210	59		73	
LG-WG	.393	.393	.315	+300	62		82	
LG-WH	.393	.393	.314	+125	58		71	
LG-ZA	.393	.393	.315	-40	24		23	Specimens
LG-ZB	.393	.393	.315	+10	33		34	within
LG-ZC	.393	.393	.315	+40	44		45	reheated
LG-ZD	.394	.393	.315	+20	38		38	zone
LG-ZE	.393	.393	.315	+30	43		45	
LG-ZF	.393	.393	.315	+125	56		67	

COMBUSTION ENGINEERING, INC.
METALLURGICAL & MATERIALS LABORATORY

E-680 (5-63)

JOB NO. _____ IMPACT TEST DATA SHEET ____ OF ____

PROJECT NO. _____ LM SAMPLES CONTRACT NO. _____ DATE _____

TEST MATERIAL Two Layer Clad, Three Wire Series Arc Process. Base Metal = MEST D12B.

HEAT TREATMENT As Welded Condition.

TYPE OF TEST SPECIMEN CHARPY V NOTCH LINEAR VELOCITY IN FT. PER SECOND 17
ENERGY OF BLOW 240 FT. LBS LOCATION AND ORIENTATION CVN Parallel to welding Direction. Base of notch normal to weld face.

TYPE SATEC MODEL SI-1 CAPACITY OF MACHINE 240 FT. LBS.

SAMPLE NO.	WIDTH INCHES	THICKNESS INCHES	DEPTH BELOW NOTCH INCHES	TEST TEMP. F	ENERGY ABSORPTION FT. LBS	% SHEAR	MILS LATERAL EXPANSION	REMARKS
LM-WA	.395	.394	.315	-40	52		46	Specimens not
LM-WB	.395	.394	.315	-50	47		40	within reheated
LM-WC	.395	.394	.315	-60	44		41	zone.
LM-WD	.395	.394	.315	-80	45		39	
LM-WE	.395	.394	.315	-90	47		41	
LM-WF	.395	.393	.315	-110	42		39	
LM-WG	.394	.393	.315	+210	87		95	
LM-WH	.394	.394	.315	+125	85		86	
LM-ZA	.395	.394	.315	-40	41		37	Specimens
LM-ZB	.395	.394	.315	-40	45		41	within
LM-ZC	.395	.394	.315	-40	47		47	reheated
LM-ZD	.395	.394	.315	-60	42		39	zone
LM-ZE	.394	.394	.316	-80	38		31	
LM-ZF	.394	.394	.315	+210	75		90	

COMBUSTION ENGINEERING, INC.
METALLURGICAL & MATERIALS LABORATORY

I-880 (5-83)

JOB NO. _____ IMPACT TEST DATA SHEET ____ OF ____

PROJECT NO. _____ MS SAMPLES CONTRACT NO. _____ DATE 9/4/84

TEST MATERIAL Three Layer Clad, Three Wire Series Arc Process. Base Metal - HSST-01?B

HEAT TREATMENT PWHT: 110F ∠ 10 Hrs. FC 100°F/Hr. Rate above 600°F

TYPE OF TEST SPECIMEN CHARPY V NOTCH LINEAR VELOCITY IN FT PER SECOND 12

ENERGY OF BLOW 240 FT. LBS. LOCATION AND ORIENTATION CVN Parallel to welding direction. Base of notch normal to weld face.

TYPE SATEC MODEL SI-1 CAPACITY OF MACHINE 240 FT. LBS.

SAMPLE NO.	WIDTH INCHES	THICKNESS INCHES	DEPTH BELOW NOTCH INCHES	TEST TEMP. F	ENERGY ABSORP. TION FT. LBS.	% SHEAR	MILS LATERAL EXPANSION	REMARKS
MS-A	.198	.395	.314	+60	11		26	1st Layer
MS-B	.197	.395	.314	+60	12		28	
MS-C	.198	.395	.314	+60	11		27	
MS-D	.198	.395	.314	+60	11		20	
MS-E	.197	.395	.314	+60	15		29	1st Layer
MS-F	.198	.395	.314	+60	12		26	after 2nd
MS-G	.198	.395	.314	+60	16		31	
MS-H	.198	.395	.314	+60	16		29	
MS-I	.198	.395	.314	+60	17		31	2nd Layer
MS-J	.197	.395	.314	+60	17		36	
MS-K	.198	.395	.314	+60	16		37	
MS-L	.198	.395	.314	+60	17		37	
MS-M	198	.395	.314	+60	19		41	2nd layer
MS-N	.198	.395	.314	+60	20		40	after 3rd
MS-O	.197	.395	.314	+60	19		42	
MS-P	.198	.395	.314	+60	20		41	
MS-R	.198	.394	.314	+60	20		42	3rd Layer
MS-S	.198	.395	.314	+60	20		40	
MS-T	.198	.395	.314	+60	20		42	
MS-U	.198	.395	.314	+60	23		46	
MS-V	.197	.393	.314	+60	13		37	1st Layer
MS-W	.197	.394	.314	+60	13		36	
MS-X	.197	.394	.314	+60	13		36	

COMBUSTION ENGINEERING, INC.
METALLURGICAL & MATERIALS LABORATORY

E 680 (5-63)

JOB NO. _____ IMPACT TEST DATA SHEET ____ OF ____

PROJECT NO. _____ NH SAMPLES CONTRACT NO. _____ DATE 9/20/84

TEST MATERIAL Two Layer Clad, Three Wire Series Arc Process. Base Metal - HSST 01A

HEAT TREATMENT PWHT: 1100°F 10 Hrs FC 100°F/Hr. Rate above 600°F

TYPE OF TEST SPECIMEN CHARPY V NOTCH LINEAR VELOCITY IN FT PER SECOND 17
ENERGY OF BLOW 240 FT - LBS LOCATION AND ORIENTATION CVN Parallel to welding direction. Base of notch normal to weld face.

TYPE SATEC MODEL 51-1 CAPACITY OF MACHINE 240 FT. LBS

SAMPLE NO.	WIDTH INCHES	THICKNESS INCHES	DEPTH BELOW NOTCH INCHES	TEST TEMP. F	ENERGY ABSORPTION FT. LBS.	% SHEAR	MILS LATERAL EXPANSION	REMARKS
NH-A	.197	.395	.314	+60	14		32	Corner Pass
NH-B	.197	.395	.314	+60	16		34	1st Layer
NH-C	.197	.395	.315	+60	14		31	
NH-D	.197	.394	.314	+60	15		34	
NH-E	.197	.395	.314	+60	17		37	
NH-F	.393	.395	.314	+60	41		48	Standard CVN
NH-G	.393	.395	.315	+60	41		46	2nd and 1st
NH-H	.393	.395	.314	+60	42		47	Layers
NH-I	.393	.395	.314	+60	37		43	
NH-K	.197	.395	.314	+60	17		38	2nd Layer
NH-L	.197	.395	.314	+60	19		41	
NH-M	.197	.395	.314	+60	19		43	
NH-N	.197	.395	.314	+60	17		37	

COMBUSTION ENGINEERING, INC.
METALLURGICAL & MATERIALS LABORATORY

E-800 (5-83)

JOB NO. _____ IMPACT TEST DATA SHEET ____ OF ____

PROJECT NO. _____ OC SAMPLES CONTRACT NO. _____ DATE 10/11/84

TEST MATERIAL Two Layer Clad, Three Wire Series Arc Process, Base Metal - HSST #12B

HEAT TREATMENT PWHT: 1100°F 10 Hrs. FC 100°F/Hr. Rate above 600°F

TYPE OF TEST SPECIMEN CHARPY V NOTCH LINEAR VELOCITY IN FT. PER SECOND 17

ENERGY OF BLOW 240 FT. LBS LOCATION AND ORIENTATION: CVN Parallel to weld line direction. Base of notch normal to weld face.

TYPE SATEC MODEL S1.1 CAPACITY OF MACHINE 240 FT. LBS

SAMPLE NO.	WIDTH INCHES	THICKNESS INCHES	DEPTH BELOW NOTCH INCHES	TEST TEMP. °F	ENERGY ABSORPTION FT. LBS.	% SHEAR	MILS LATERAL EXPANSION	REMARKS
OC-A	.197	.395	.314	+60	21		48	Corner Pass
OC-B	.196	.394	.314	+60	21		46	
OC-C	.197	.394	.314	+60	23		47	
OC-E	.197	.394	.314	+60	18		40	2nd Layer
OC-G	.197	.394	.314	+60	24		50	1st Layer
OC-H	.197	.394	.314	+60	24		49	
OC-I	.197	.395	.314	+60	25		49	
OC-J	.197	.394	.314	+60	25		56	
OC-L	.197	.395	.314	+60	21		43	2i . Layer
OC-M	.197	.395	.314	+60	19		40	
OC-N	.197	.394	.314	+60	23		58	
OC-O	.394	.395	.314	+60	43		50	Standard CVN
OC-P	.395	.395	.314	+60	42		51	2nd and 1st
OC-R	.394	.394	.314	+60	44		52	Layers
OC-S	.394	.394	.314	+60	44		46	

COMBUSTION ENGINEERING, INC.
METALLURGICAL & MATERIALS LABORATORY

E 680 (5 83)

JOB NO. _____ IMPACT TEST DATA SHEET ____ OF ____

PROJECT NO. _____ 00 SAMPLES CONTRACT NO. _____ DATE 10/24/84

TEST MATERIAL Three Layer Clad. Three Wire Series Arc Process. Base Metal - HSST-012B

HEAT TREATMENT PWHT: 1100°F 10 Hrs. FC 100°F/Hr. Rate above 600°F

TYPE OF TEST SPECIMEN CHARPY V NOTCH LINEAR VELOCITY IN FT. PER SECOND 17

ENERGY OF BLOW 240 FT LBS LOCATION AND ORIENTATION CVN Parallel to welding direction. Base of notch normal to weld face.

TYPE SATEC MODEL SI-1 CAPACITY OF MACHINE 240 FT - LBS

SAMPLE NO.	WIDTH INCHES	THICKNESS INCHES	DEPTH BELOW NOTCH INCHES	TEST TEMP. F	ENERGY ABSORPTION FT. LBS.	% SHEAR	MILS LATERAL EXPANSION	REMARKS
00-A	.197	.394	.316	+60	20		39	1st. Layer
00-B	.197	.394	.316	+60	22		43	
00-C	.197	.394	.316	+60	14		28	
00-D	.197	.395	.316	+60	14		26	1st Layer
00-E	.197	.394	.316	+60	15		29	after 2nd
00-F	.197	.395	.316	+60	16		30	
00-G	.197	.394	.316	+60	15		28	
00-H	.197	.393	.316	+60	14		25	
00-I	.197	.394	.316	+60	22		38	1st Layer
00-J	.197	.395	.316	+60	14		30	
00-K	.197	.394	.316	+60	20		37	2nd Layer
00-L	.197	.395	.316	+60	19		35	
00-M	.197	.395	.316	+60	19		35	
00-N	.197	.395	.316	+60	16		32	2nd Layer
00-O	.197	.395	.316	+60	15		29	after 3rd
00-P	.197	.394	.316	+60	21		35	2nc Layer
00-R	.197	.394	.316	+60	19		35	
00-S	.197	.395	.316	+60	17		34	
00-T	.197	.394	.316	+60	19		34	3rd Layer
00-U	.197	.394	.316	+60	19		32	
00-V	.197	.394	.316	+60	22		39	
00-W	.197	.394	.316	+60	17		27	

Chemical Analysis of Broken CVN Specimens, Location Near Fracture on Face and Root Sides

CVN Specimen Test ID	LF-WD		LF-ZE		MS-A		MS-B	
Lab No.	D40841		D40840		D40820		D40821	
Specimen Side (A or B)	A	B	A	B	A	B	A	B
Mn	1.27	1.52	1.52	1.27	1.57	1.61	1.64	1.64
Si	.77	.71	.70	.75	.74	.75	.80	.76
Ni	9.00	8.31	8.13	8.85	8.35	8.44	8.30	8.25
Cr	19.10	18.00	17.31	19.07	17.91	18.12	17.75	17.84
Mo	.24	.23	.24	.23	.23	.23	.23	.23
V	.06	.04	.04	.06	.04	.04	.04	.04
Cb	< .01	.01	< .01	< .01	< .01	< .01	< .01	< .01
Ti	< .01	.01	< .01	.01	.01	.02	.01	< .01
Co	.07	.05	.06	.07	.06	.05	.06	.05
Cu	.36	.17	.16	.36	.17	.17	.17	.16
CVN Energy Ft. Lbs.	44*		42*		11		12	

*Indicates Standard CVN specimen, 10 x 10 mm. All others 10 x 5 mm.

Chemical Analysis of Broken CVN Specimens, Location Near Fracture on Face and Root Sides

CVN Specimen Test ID	MS-C		MS-D		MS-E		MS-F	
Lab No.	D40822		D40823		D40824		D40825	
Specimen Side (A or B)	A	B	A	B	A	B	A	B
Mn	1.56	1.52	1.64	1.63	1.62	1.62	1.56	1.55
Si	.72	.73	.79	.78	.75	.78	.69	.71
Ni	8.17	8.13	8.34	8.20	8.68	8.75	8.08	8.14
Cr	17.39	17.37	17.99	17.91	18.68	19.03	17.24	17.54
Mo	.24	.24	.23	.23	.22	.21	.24	.23
V	.04	.04	.04	.04	.04	.04	.04	.04
Cb	< .01	< .01	< .01	< .01	< .01	< .01	< .01	< .01
Ti	.01	.02	< .01	.01	< .01	.01	< .01	.01
Co	.06	.05	.05	.05	.05	.05	.05	.06
Cu	.17	.16	.17	.16	.16	.17	.16	.16
CVN Energy Ft. Lbs.	11		11		15		12	

Chemical Analysis of Broken CVN Specimens, Location Near Fracture on Face and Root Sides

CVN Specimen Test ID	MS-G		MS-H		MS-I		MS-J	
Lab No.	D40826		D40827		D40828		D40829	
Specimen Side (A or B)	A	B	A	B	A	B	A	B
Mn	1.62	1.57	1.57	1.45	1.33	1.34	1.32	1.33
Si	.74	.71	.70	.73	.73	.78	.76	.80
Ni	8.63	8.10	8.07	8.48	8.93	8.88	8.87	8.86
Cr	18.72	17.41	17.36	18.14	18.90	18.95	18.88	19.02
Mo	.22	.23	.23	.23	.23	.23	.23	.23
V	.04	.04	.04	.05	.06	.06	.06	.06
Cb	< .01	< .01	< .01	< .01	< .01	< .01	< .01	< .01
Ti	.01	.01	.01	.01	< .01	.01	.01	.01
Co	.05	.05	.05	.06	.08	.07	.07	.08
Cu	.16	.16	.16	.24	.34	.36	.37	.36
CVN Energy Ft. Lbs.	16		16		17		17	

Chemical Analysis of Broken CVN Specimens, Location Near Fracture on Face and Root Sides

CVN Specimen Test ID	MS-K		MS-L		MS-M		MS-N	
Lab No.	D40830		D40831		D40832		D40833	
Specimen Side (A or B)	A	B	A	B	A	B	A	B
Mn	1.33	1.30	1.35	1.31	1.30	1.53	1.34	1.32
Si	.75	.75	.75	.79	.74	.76	.75	.76
Ni	9.00	8.72	8.91	8.74	8.94	8.55	8.93	8.83
Cr	19.00	18.81	18.98	18.98	19.11	18.43	19.06	19.05
Mo	.23	.24	.23	.24	.24	.22	.23	.23
V	.06	.06	.06	.06	.06	.04	.06	.06
Cb	< .01	< .01	< .01	< .01	< .01	< .01	< .01	< .01
Ti	.01	.01	< .01	.01	.01	.01	.01	.01
Co	.07	.07	.07	.07	.07	.06	.07	.07
Cu	.34	.37	.34	.36	.37	.20	.34	.36
CVN Energy Ft. Lbs.	16		17		19		20	

Chemical Analysis of Broken CVN Specimens, Location Near Fracture on Face and Root Sides

CVN Specimen Test ID	MS-O		MS-P		MS-R		MS-S	
Lab No.	D40834		D40835		D40836		D40837	
Specimen Side (A or B)	A	B	A	B	A	B	A	B
Mn	1.31	1.31	1.40	1.32	1.32	1.28	1.28	1.34
Si	.73	.75	.74	.77	.80	.80	.80	.81
Ni	8.85	8.88	8.62	8.92	9.09	8.95	9.04	9.01
Cr	19.01	18.87	18.68	19.11	19.32	19.31	19.35	19.35
Mo	.23	.24	.23	.23	.23	.24	.23	.23
V	.05	.06	.05	.06	.06	.06	.06	.06
Cb	< .01	< .01	< .01	< .01	< .01	< .01	< .01	< .01
Ti	.01	.01	< .01	.01	.01	.01	.01	.01
Co	.07	.07	.06	.07	.08	.08	.08	.07
Cu	.33	.36	.28	.36	.38	.40	.39	.38
CVN Energy Ft. Lbs.	19		20		20		20	

Chemical Analysis of Broken CVN Specimens, Location Near Fracture on Face and Root Sides

CVN Specimen Test ID	MS-T		MS-U		MS-V		MS-W	
Lab No.	D40838		D40839		D40843		D40844	
Specimen Side (A or B)	A	B	A	B	A	B	A	B
Mn	1.30	1.28	1.30	1.32	1.56	1.58	1.55	1.52
Si	.81	.80	.80	.82	.76	.74	.76	.74
Ni	9.06	8.92	9.09	9.01	8.59	8.49	8.40	8.24
Cr	19.29	19.28	19.45	19.26	18.18	17.99	17.57	17.77
Mo	.23	.23	.23	.24	.22	.23	.24	.23
V	.06	.06	.06	.06	.04	.04	.04	.04
Cb	<.01	<.01	<.01	<.01	<.01	<.01	<.01	<.01
Ti	.01	.01	<.01	.01	<.01	<.01	.01	.02
Co	.08	.08	.08	.08	.05	.05	.05	.06
Cu	.39	.40	.38	.39	.17	.17	.17	.17
CVN Energy Ft. Lbs.	20		23		13		13	

Chemical Analysis of Broken CVN Specimens, Location Near Fracture on Face and Root Sides

CVN Specimen Test ID	MS-X		NH-C		NH-E		NH-H	
Lab No.	D40845		D40863		D40864		D40865	
Specimen Side (A or B)	A	B	A	B	A	B	A	B
Mn	1.60	1.58	1.59	1.62	1.67	1.60	1.44	1.61
Si	.76	.77	.67	.70	.72	.68	.78	.70
Ni	8.30	8.34	8.84	8.82	9.04	8.70	9.04	8.86
Cr	17.45	17.85	18.50	18.76	19.13	18.50	19.27	18.69
Mo	.24	.23	.20	.20	.19	.20	.22	.20
V	.04	.04	.03	.03	.03	.03	.06	.03
Cb	< .01	< .01	< .01	< .01	< .01	< .01	< .01	< .01
Ti	.01	.02	.02	.01	.01	.02	.01	.01
Co	.05	.05	.04	.04	.04	.04	.08	.04
Cu	.16	.16	.09	.09	.09	.08	.34	.09
CVN Energy Ft. Lbs.	13		14		17		42*	

*Indicates Standard CVN specimen, 10 x 10 mm. All others 10 x 5 mm.

Chemical Analysis of Broken CVN Specimens, Location Near Fracture on Face and Root Sides

CVN Specimen Test ID	NH-I		NH-M		NH-N		OC-A	
Lab No.	D40866		D40867		D40868		D40937	
Specimen Side (A or B)	A	B	A	B	A	B	A	B
Mn	1.43	1.54	1.42	1.38	1.38	1.41	1.61	1.64
Si	.79	.66	.78	.78	.77	.80	.70	.72
Ni	9.07	8.86	9.07	9.04	9.10	9.00	9.86	9.89
Cr	19.32	18.47	19.29	19.29	19.27	19.33	20.60	20.77
Mo	.23	.21	.23	.22	.23	.22	.15	.14
V	.06	.03	.06	.05	.06	.06	.03	.03
Cb	< .01	< .01	< .01	< .01	< .01	< .01	< .01	< .01
Ti	.01	.01	.01	.01	< .01	.01	.02	.02
Co	.07	.04	.07	.08	.08	.08	.03	.03
Cu	.34	.09	.34	.34	.35	.34	.06	.06
CVN Energy Ft. Lbs.	37*		19		17		21	

*Indicates Standard CVN specimen, 10 x 10 mm. All others 10 x 5 mm.

Chemical Analysis of Broken CVN Specimens, Location Near Fracture on Face and Root Sides

CVN Specimen Test ID	OC-B		OC-C		OC-E		OC-G	
Lab No.	D40938		D40939		D40940		D40941	
Specimen Side (A or B)	A	B	A	B	A	B	A	B
Mn	1.60	1.63	1.60	1.58	1.41	1.44	1.62	1.62
Si	.69	.69	.69	.70	.77	.78	.72	.72
Ni	10.01	9.98	10.05	10.02	9.33	9.24	10.40	10.54
Cr	20.73	20.84	20.92	20.91	19.73	19.65	21.55	21.63
Mo	.14	.14	.14	.14	.21	.20	.13	.12
V	.03	.03	.03	.03	.05	.05	.03	.03
Cb	< .01	< .01	< .01	< .01	< .01	< .01	< .01	< .01
Ti	.03	.03	.02	.02	.01	.02	.01	.01
Co	.03	.03	.03	.03	.0(	.06	.03	.03
Cu	.06	.06	.06	.06	.29	.29	.07	.06
CVN Energy Ft. Lbs	21		23		18		24	

Chemical Analysis of Broken CVN Specimens, Location Near Fracture on Face and Root Sides

CVN Specimen Test ID	OC-H		OC-I		OC-J		OC-L	
Lab No.	D40942		D40943		D40944		D40945	
Specimen Side (A or B)	A	B	A	B	A	B	A	B
Mn	1.62	1.58	1.57	1.58	1.57	1.59	1.40	1.40
Si	.72	.68	.70	.68	.70	.66	.77	.77
Ni	10.66	10.61	10.60	10.58	10.63	10.59	9.22	9.12
Cr	21.63	21.54	21.60	21.54	21.57	21.53	19.71	19.50
Mo	.13	.12	.12	.12	.12	.13	.21	.22
V	.03	.03	.03	.03	.03	.03	.05	.05
Cb	< .01	< .01	< .01	< .01	< .01	< .01	< .01	< .01
Ti	.02	.03	.02	.01	.02	.01	.01	.01
Co	.02	.02	.02	.03	.03	.03	.06	.07
Cu	.06	.06	.06	.06	.06	.06	.31	.34
CVN Energy Ft. Lbs.	24		25		25		21	

Chemical Analysis of Broken CVN Specimens, Location Near Fracture on Face and Foot Sides

CVN Specimen Test ID	OC-M		OC-N		OO-B		OO-C	
Lab No.	D40946		D40947		D40963		D40964	
Specimen Side (A or B)	A	B	A	B	A	B	A	B
Mn	1.38	1.38	1.34	1.41	1.62	1.62	1.64	1.64
Si	.78	.78	.79	.79	.68	.71	.64	.70
Ni	9.23	9.16	9.22	9.12	9.86	9.91	9.52	9.87
Cr	19.68	19.54	19.54	19.54	20.03	20.03	19.49	19.99
Mo	.21	.22	.21	.21	.17	.16	.18	.17
V	.05	.06	.06	.06	.03	.03	.03	.03
Cb	< .01	< .01	< .01	< .01	< .01	< .01	< .01	< .01
Ti	< .01	< .01	.01	< .01	.02	.01	.03	.02
Co	.07	.07	.07	.07	.03	.03	.04	.04
Cu	.33	.35	.35	.35	.08	.08	.08	.08
CVN Energy Ft. Lbs.	19		23		22		14	

Chemical Analysis of Broken CVN Specimens, Location Near Fracture on Face and Root Sides

CVN Specimen Test ID	00-D		00-F		00-I		00-J	
Lab No.	D40965		D40966		D40967		D40968	
Specimen Side (A or B)	A	B	A	B	A	B	A	B
Mn	1.63	1.63	1.61	1.43	1.60	1.62	1.64	1.63
Si	.72	.65	.65	.78	.66	.69	.67	.65
Ni	9.51	9.63	9.48	9.27	9.87	10.00	9.61	9.83
Cr	19.41	19.57	19.30	19.50	19.94	20.25	19.69	20.03
Mo	.18	.18	.18	.22	7	.17	.18	.17
V	.03	.03	.03	.05	.03	.03	.03	.03
Cb	< .01	< .01	< .01	< .01	< .01	< .01	< .01	< .01
Ti	.02	.02	.02	.02	.01	.02	.03	.03
Co	.04	.04	.04	.06	.03	.04	.03	.04
Cu	.08	.08	.08	.30	.08	.08	.08	.08
CVN Energy Ft. Lbs.	14		16		22		14	

Chemical Analysis of Broken CVN Specimens, Location Near Fracture on Face and Root Sides

CVN Specimen Test ID	00-O		00-P		00-S		00-V	
Lab No.	D40969		D40970		D40971		D40972	
Specimen Side (A or B)	A	B	A	B	A	B	A	B
Mn	1.39	1.43	1.33	1.35	1.38	1.35	1.42	1.39
Si	.84	.82	.77	.78	.81	.80	.84	.83
Ni	9.19	9.15	9.16	9.16	9.11	9.20	9.10	9.03
Cr	19.49	19.54	19.38	19.41	19.37	19.45	19.65	19.45
Mo	.22	.23	.22	.23	.22	.22	.22	.24
V	.06	.06	.06	.06	.06	.06	.06	.06
Cb	<.01	<.01	<.01	<.01	<.01	<.01	<.01	<.01
Ti	.02	.02	.02	.02	.01	.02	<.01	.01
Co	.08	.08	.07	.08	.07	.07	.07	.08
Cu	.35	.37	.34	.35	.33	.36	.34	.39
CVN Energy Ft. Lbs.	15		21		17		22	

Chemical Analysis of Broken CVN Specimens, Location Near Fracture on Face and Root Sides

CVN Specimen Test ID	OO-W	
Lab No.	D40′	
Specimen Side (A or B)	A	B
Mn	1.39	1.38
Si	.83	.84
Ni	9.15	9.13
Cr	19.57	19.56
Mo	.23	.23
V	.06	.06
Cb	<.01	<.01
Ti	.02	.02
Co	.08	.08
Cu	.36	.39
CVN Energy Ft. Lbs.	17	

	MS	NH	OC	OO
First Layer Sample No 2nd La[illegible]	11 12 11 11	16 14 15 17	24 24 25 25	20 22 14 22 14
First Layer Sample With 2nd Layer Deposited	15 12 16 16			14 15 16 15 14
Second Layer Sample No 3rd Layer	17 17 16 17	17 19 19 17	21 19 23 18	20 19 19 21 19 17
Second Layer Sample With 3rd Layer Deposited	19 20 19 20			16 15
Third Layer Sample	20 20 20 23			19 19 22 17

3 Wire Series Arc Clad - Charpy Data (Ft-lb)

3 Wire Series Arc Clad - First Layer

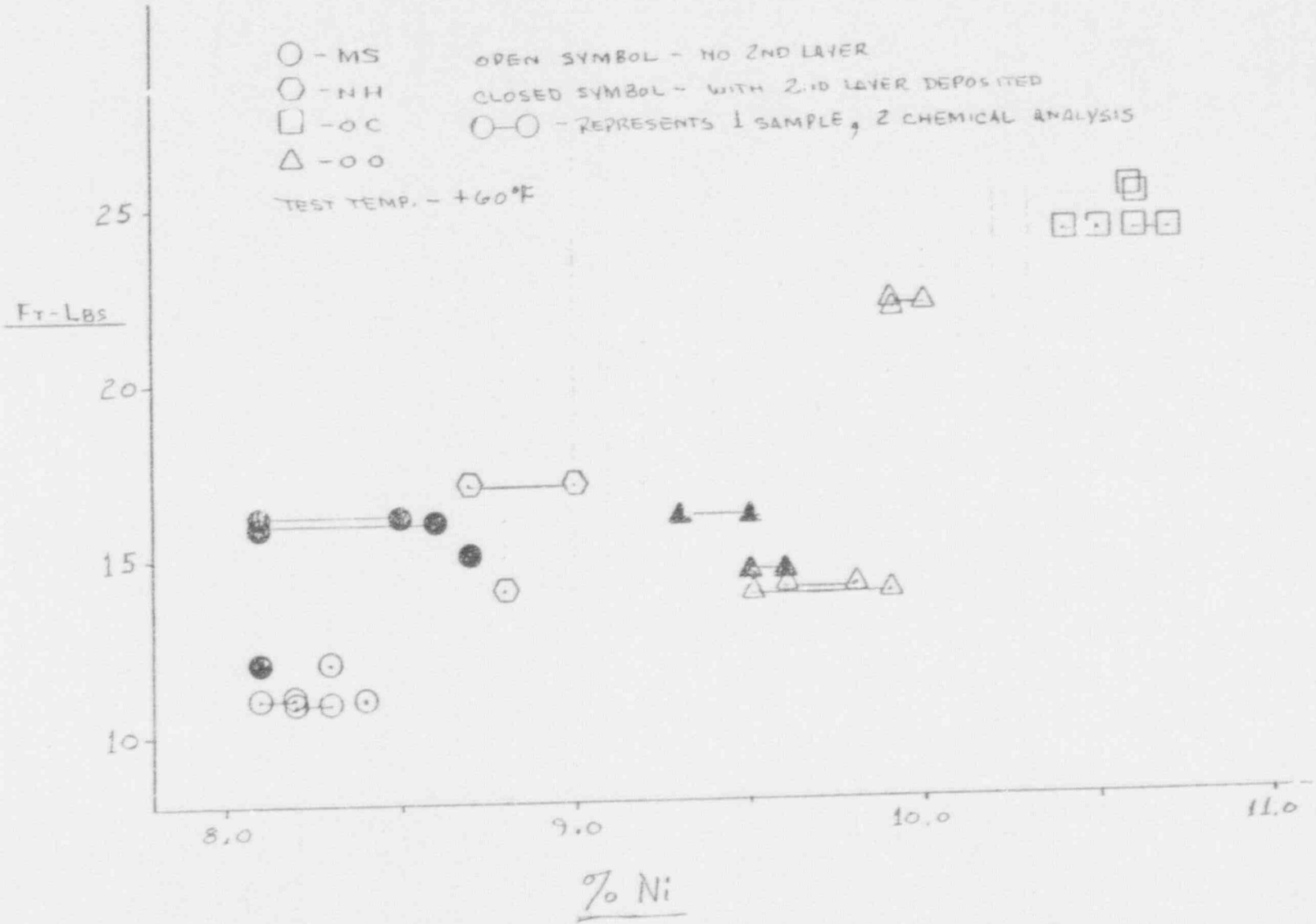

3 WIRE SERIES ARC CLAD - SE

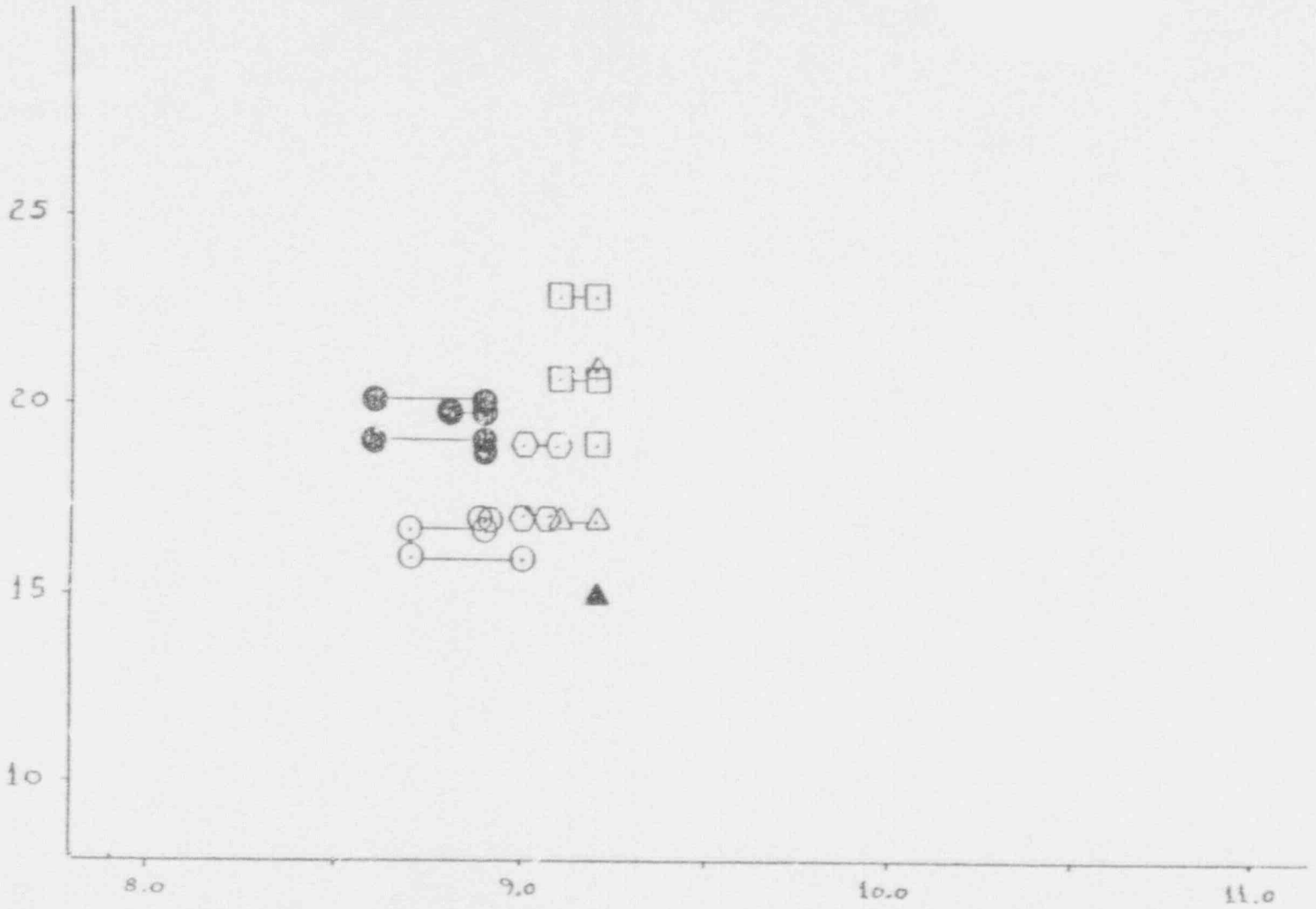

APPENDIX E

MATERIAL CERTIFICATIONS FOR THE A 533 GRADE B CLASS 1 BASE MATERIAL USED IN THE CLAD PLATE SPECIMENS

Chicago Tube & Iron Co.
Mr. B.E. Higgin, Buyer
P.O. Box 277
Birmingham, Ala. 35202

(7B)

CONSIGNEE: Chicago Tube & Iron Co.
Dayton, Ala. 35202

TEST CERTIFICATE

MILL ORDER NO.	CUSTOMER P.O.	
78522-2	7004 SHEET 4	MP 92074 DC

THIS MATERIAL HAS BEEN MANUFACTURED AND TESTED IN ACCORDANCE WITH PURCHASE ORDER REQUIREMENTS AND SPECIFICATION(S):

SA-533 GR. B CL. 1
CEMX MP-51.0 Rev. 6 1973 Except Para. 6.0 QAS-51 Rev. 4/ASME Code Sect. 2 & 3 CL. 1 1971 Edition Thru Summer 1973 Addenda

BEND TEST O.K. HOMOGENEITY TEST

Sheet #1 of 3

CHEMICAL ANALYSIS

MELT NO.	C	Mn	P	S	Cu	Si	Ni	Cr	Mo	V	Ti	Al	X		Grain Size
B3112	22	1.32	007	013		27	63		55				VIP STEEL		7-8
B3112														Slab #1	7-8

HSST-12

PHYSICAL PROPERTIES

MELT NO.	SLAB NO.	YIELD PSI X100	TENSILE PSI X100	% ELONG. IN 2"	% R.A.	BHN	IMPACTS				DESCRIPTION
B3112	1	668	891	25							1- 7" x 128-1/2 x 273
		651	854	25							

LOC. TEMP.	TRANS. V-NOTCH IMPACTS			LATERAL EXPANSION IN INCHES			FRACTURE APPEARANCE % SHEAR
TC +30°F.	54	53	46	.044	.040	.042	40-40-40
TC +60°F.	51	63	69	.052	.053	.042	50-50-50
TC +30°F.	74	60	66	.048	.059	.056	50-50-50

We hereby certify the above information is correct.

SUPERVISOR TESTING: L. H. Kline

PURCHASED

Chicago Bridge & Iron Co.
8 Mr. S.E. Wiggin, Buyer

LUKENS STEEL COMPANY
COATESVILLE, PA 19320
TEST CERTIFICATE

DATE 9-16-74 FILE NO 1540-02-04

MILL ORDER NO 78522-2 CUSTOMER P.O. 7004 SHEET 4

Chicago Bridge & Iron Co.
Boyles, Ala. 35202

THIS MATERIAL HAS BEEN MANUFACTURED AND TESTED IN ACCORDANCE WITH PURCHASE ORDER REQUIREMENTS AND SPECIFICATIONS

SAME

Sheet #2 of 2

CHEMICAL ANALYSIS

HEAT NO	C	MN	P	S	CU	SI	N	CR	MO	V	TI	AL	B

PHYSICAL PROPERTIES

HEAT NO	SIZE	YIELD	TENSILE	ELONG	R.A.	BEND	IMPACT	DESCRIPTION

U.T. Procedure - LS-102 DTD 8/21/69 Rev. 13 DTD 4/16/73 & Spec. Rev. DTD 6/12/73

Plate and tests heated to 1630-1660°F., held 7 hrs. and 25 minutes and water quenched (time in quench tank - 28 minutes), then tempered 1225-1250°F., held 7 hrs. and water quenched (time in quench tank - 28 minutes).

Plate and tests stress relieved by heating to 1040-1060°F., held 3 hrs. and 30 minutes and air cooled.

Tests stress relieved by heating within a rate of 100°F. per hr. to 1150°F., held 50 hrs. and furnace cooled within a rate of 100°F. per hr. to 600°F.

U.T. Testing was not performed by LUKENS STEEL CO.

We hereby certify the above information is correct.

H.C. Clark

199

NUREG/CR-5785
ORNL/TM-11950
Dist. Category RF

Internal Distribution

1. D. J. Alexander
2. B. R. Bass
3. J. W. Bryson
4-5. R. D. Cheverton
6. K. V. Cook
7-9. W. R. Corwin
10. T. L. Dickson
11. F. M. Haggag
12-23. S. K. Iskander
24. J. E. Jones, Jr.
25. J. Keeney-Walker
26. W. J. McAfee
27. D. E. McCabe
28. J. G. Merkle
29-31. R. K. Nanstad
32. D. J. Naus
33. C. B. Oland
34-35. W. E. Pennell
36. C. E. Pugh
37. G. C. Robinson
38. D. K. Shum
39. G. M. Slaughter
40. R. L. Swain
41. T. J. Theiss
42. ORNL Patent Office
43. Central Research Library
44. Document Reference Section
45-46. Laboratory Records
47. Laboratory Records (RC)
48-50. M&C Records Office

External Distribution

51. L. C. Shao, Director of Engineering, U.S. Nuclear Regulatory Commission, Washington, DC 20555

52. C. Z. Serpan, Jr., Division of Engineering, U.S. Nuclear Regulatory Commission, Washington, DC 20555

53. M. Vagins, NRC, Division of Engineering, U.S. Nuclear Regulatory Commission, Washington, DC 20555

54. A. Hiser, NRC, Division of Engineering, U.S. Nuclear Regulatory Commission, Washington, DC 20555

55. R. L. Johnson, Division of Safety Issue Resolution, Engineering Issues Branch, NL/-302, U.S. Nuclear Regulatory Commission, Washington, DC 20555

56. M. E. Mayfield, Division of Engineering, U.S. Nuclear Regulatory Commission, Washington, DC 20555

57. A. Taboada, Division of Engineering, U.S. Nuclear Regulatory Commission, Washington, DC 20555

58. W. L. Fourney, Department of Mechanical Engineering, University of Maryland, College Park, MD 20742

59. J. D. Landes, The University of Tennessee, Knoxville, TN 37996-2030

60. C. W. Schwartz, Civil Engineering Dept., The University of Maryland, College Park, MD 20742

61. A. R. Rosenfield, Battelle Columbus Division, Columbus, OH 43201

62. E. T. Wessel, 312 Wolverine, Haines City, FL 33844

63. Office of Assistant Manager for Energy Research and Development, DOE-OR, P. O. Box 2001, Oak Ridge, TN 37831-6269

64-65. Office of Scientific and Technical Information, P. O. Box 62, Oak Ridge, TN 37831

66-315. Given distribution as shown in category RF (NTIS-10)

NRC FORM 335 (2-89) NRCM 1102, 3201, 3202

U.S. NUCLEAR REGULATORY COMMISSION

BIBLIOGRAPHIC DATA SHEET

(See instructions on the reverse)

1. REPORT NUMBER (Assigned by NRC, Add Vol., Supp., Rev., and Addendum Numbers, if any.)

NUREG/CR-5785
ORNL/TM-11950

2. TITLE AND SUBTITLE

Experimental Results of Tests to Investigate Flaw Behavior of Mechanically Loaded Stainless Steel Clad Plates

3. DATE REPORT PUBLISHED

MONTH: April YEAR: 1992

4. FIN OR GRANT NUMBER

B0119

5. AUTHOR(S)

S. K. Iskander, G. C. Robinson, W. R. Corwin, B. C. Oland, D. J. Alexander, and K. V. Cook

6. TYPE OF REPORT

Technical

7. PERIOD COVERED (Inclusive Dates)

8. PERFORMING ORGANIZATION – NAME AND ADDRESS (If NRC, provide Division, Office or Region, U.S. Nuclear Regulatory Commission, and mailing address; if contractor, provide name and mailing address.)

Oak Ridge National Laboratory
Oak Ridge, TN 37831

9. SPONSORING ORGANIZATION – NAME AND ADDRESS (If NRC, type "Same as above"; if contractor, provide NRC Division, Office or Region, U.S. Nuclear Regulatory Commission, and mailing address.)

Division of Engineering
Office of Nuclear Regulatory Research
U. S. Nuclear Regulatory Commission
Washington, DC 20555

10. SUPPLEMENTARY NOTES

11. ABSTRACT (200 words or less)

A small crack near the inner surface of clad nuclear reactor pressure vessels is an important consideration in the safety assessment of the structural integrity of the vessel. Four-point bend tests on large plate specimens, six clad and two unclad, were performed to determine the effect of stainless steel cladding upon the propagation of small surface cracks subjected to stress states similar to those produced by pressurized thermal shock conditions. Results of tests at temperatures 10 and 60°C below the nil-ductility transition temperature have shown that a tough surface layer composed of cladding and heat-affected zone has arrested running flaws in clad plates under conditions where unclad plates have ruptured. Furthermore, the load-bearing capacity of clad plates with large subclad flaws significantly exceeded that of an unclad plate with a much smaller flaw. More testing is necessary to unambiguously single out whether it is the cladding or the heat-affected zone that is primarily responsible for the observed enhanced load-bearing capacity of plates. The compressive stresses that limited the depth to which the flaw could propagate are absent in a repressurization event. Nonetheless, the experiments show that if the surface layer is sufficiently tough, it could prevent a flaw, near the surface, from propagating along the surface. The flaw could tunnel below the surface, but a sufficiently tough surface layer would reduce the maximum stress intensity factor.

12. KEY WORDS/DESCRIPTORS (List words or phrases that will assist researchers in locating the report.)

cladding
crack arrest
crack initiation
finite length flaws
fracture mechanics
fracture toughness
heat-affected zone
irradiation
light-water reactors
pressurized thermal shock
reactor pressure vessel
stainless steel
surface flaws
weld-overlay cladding

13. AVAILABILITY STATEMENT

unlimited

14. SECURITY CLASSIFICATION

(This Page) unclassified

(This Report) unclassified

15. NUMBER OF PAGES

16. PRICE

UNITED STATES
NUCLEAR REGULATORY COMMISSION
WASHINGTON, D.C. 20555